

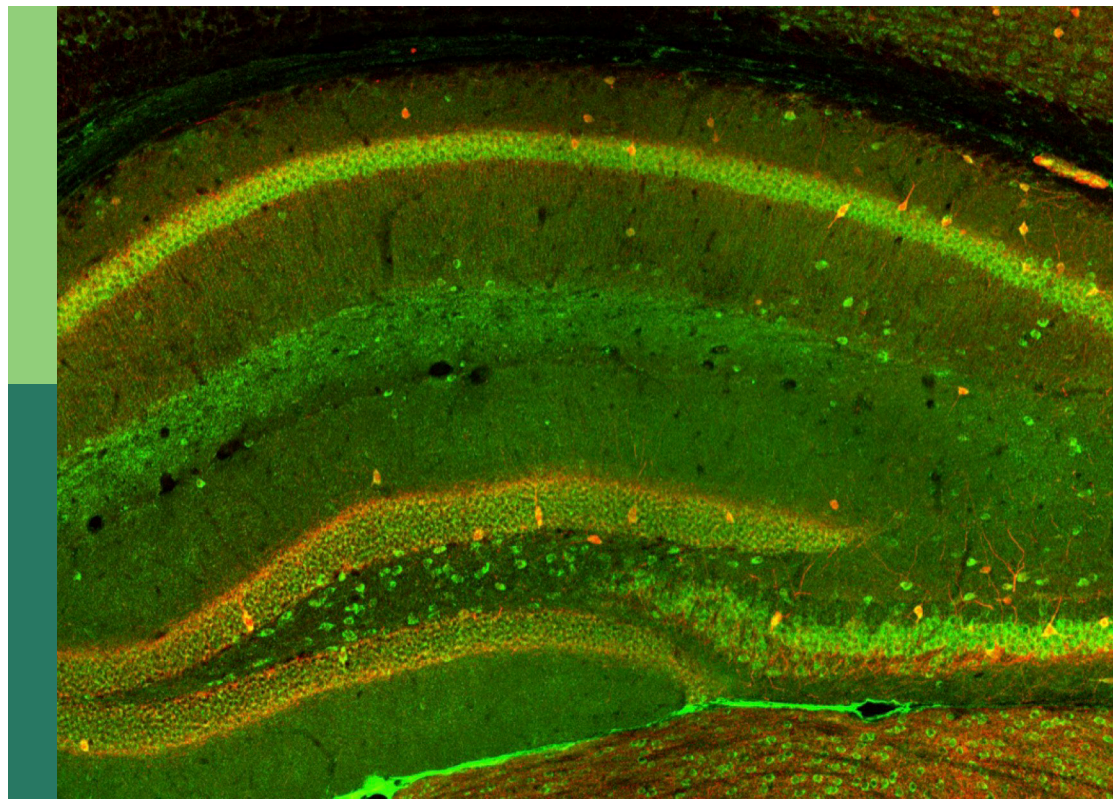
Restoring functional behaviors after traumatic peripheral nerve injuries

Edited by

George Davis Bittner, Jared Bushman, Jaimie Shores,
Joseph Alderete and Dale Sengelaub

Published in

Frontiers in Cellular Neuroscience
Frontiers in Neurology



FRONTIERS EBOOK COPYRIGHT STATEMENT

The copyright in the text of individual articles in this ebook is the property of their respective authors or their respective institutions or funders. The copyright in graphics and images within each article may be subject to copyright of other parties. In both cases this is subject to a license granted to Frontiers.

The compilation of articles constituting this ebook is the property of Frontiers.

Each article within this ebook, and the ebook itself, are published under the most recent version of the Creative Commons CC-BY licence. The version current at the date of publication of this ebook is CC-BY 4.0. If the CC-BY licence is updated, the licence granted by Frontiers is automatically updated to the new version.

When exercising any right under the CC-BY licence, Frontiers must be attributed as the original publisher of the article or ebook, as applicable.

Authors have the responsibility of ensuring that any graphics or other materials which are the property of others may be included in the CC-BY licence, but this should be checked before relying on the CC-BY licence to reproduce those materials. Any copyright notices relating to those materials must be complied with.

Copyright and source acknowledgement notices may not be removed and must be displayed in any copy, derivative work or partial copy which includes the elements in question.

All copyright, and all rights therein, are protected by national and international copyright laws. The above represents a summary only. For further information please read Frontiers' Conditions for Website Use and Copyright Statement, and the applicable CC-BY licence.

ISSN 1664-8714
ISBN 978-2-8325-4478-5
DOI 10.3389/978-2-8325-4478-5

About Frontiers

Frontiers is more than just an open access publisher of scholarly articles: it is a pioneering approach to the world of academia, radically improving the way scholarly research is managed. The grand vision of Frontiers is a world where all people have an equal opportunity to seek, share and generate knowledge. Frontiers provides immediate and permanent online open access to all its publications, but this alone is not enough to realize our grand goals.

Frontiers journal series

The Frontiers journal series is a multi-tier and interdisciplinary set of open-access, online journals, promising a paradigm shift from the current review, selection and dissemination processes in academic publishing. All Frontiers journals are driven by researchers for researchers; therefore, they constitute a service to the scholarly community. At the same time, the *Frontiers journal series* operates on a revolutionary invention, the tiered publishing system, initially addressing specific communities of scholars, and gradually climbing up to broader public understanding, thus serving the interests of the lay society, too.

Dedication to quality

Each Frontiers article is a landmark of the highest quality, thanks to genuinely collaborative interactions between authors and review editors, who include some of the world's best academicians. Research must be certified by peers before entering a stream of knowledge that may eventually reach the public - and shape society; therefore, Frontiers only applies the most rigorous and unbiased reviews. Frontiers revolutionizes research publishing by freely delivering the most outstanding research, evaluated with no bias from both the academic and social point of view. By applying the most advanced information technologies, Frontiers is catapulting scholarly publishing into a new generation.

What are Frontiers Research Topics?

Frontiers Research Topics are very popular trademarks of the *Frontiers journals series*: they are collections of at least ten articles, all centered on a particular subject. With their unique mix of varied contributions from Original Research to Review Articles, Frontiers Research Topics unify the most influential researchers, the latest key findings and historical advances in a hot research area.

Find out more on how to host your own Frontiers Research Topic or contribute to one as an author by contacting the Frontiers editorial office: frontiersin.org/about/contact

Restoring functional behaviors after traumatic peripheral nerve injuries

Topic editors

George Davis Bittner – The University of Texas at Austin, United States

Jared Bushman – University of Wyoming, United States

Jaimie Shores – Johns Hopkins University, United States

Joseph Alderete – San Antonio Military Medical Center, United States

Dale Sengelaub – Indiana University Bloomington, United States

Citation

Bittner, G. D., Bushman, J., Shores, J., Alderete, J., Sengelaub, D., eds. (2024).

Restoring functional behaviors after traumatic peripheral nerve injuries.

Lausanne: Frontiers Media SA. doi: 10.3389/978-2-8325-4478-5

Table of contents

- 04 **Muscle-Nerve-Nerve Grafting Improves Facial Reanimation in Rats Following Facial Nerve Injury**
Steven J. Charous, Michael J. Hutz, Samantha E. Bialek, Jane K. Schumacher and Eileen M. Foecking
- 11 **The Role of c-Jun and Autocrine Signaling Loops in the Control of Repair Schwann Cells and Regeneration**
Kristjan R. Jessen and Rhona Mirsky
- 28 **Compound Motor Action Potentials During a Modest Nerve Crush**
Mohammed Nazmy Hamad, Nickolas Boroda, Diego Barragan Echenique, Raymond A. Dieter, Farid M. L. Amirouche, Mark H. Gonzalez and James M. Kerns
- 43 **Intraneural Topography of Rat Sciatic Axons: Implications for Polyethylene Glycol Fusion Peripheral Nerve Repair**
Emily A. Hibbard and Dale R. Sengelaub
- 50 **Oral Treatments With the TrkB Ligand Prodrug, R13, Promote Enhanced Axon Regeneration Following Peripheral Nerve Injury**
Arthur W. English, Dario Carrasco, Dustin Hoffman, Robin Isaacson, Seong Su Kang, Samia Khan, Xia Liu and Keqiang Ye
- 60 **Brain-Derived Neurotrophic Factor Is an Important Therapeutic Factor in Mesenchymal Stem Cell Secretions for Treatment of Traumatic Peripheral Pelvic Injuries**
Xiaoyi Yuan, Brian M. Balog, Dan Li Lin, Brett Hanzlicek, Mei Kuang, Hao Yan, Steve J. A. Majerus and Margot S. Damaser
- 72 **The effects of graft source and orientation on outcomes after ablation of a branched peripheral nerve**
JuliAnne E. Allgood, Kelly C. Santos Roballo, Bridger B. Sparks and Jared S. Bushman
- 91 **Review: Myelin clearance is critical for regeneration after peripheral nerve injury**
YiMing Yuan, Yan Wang, ShanHong Wu and Ming Yue Zhao
- 112 **Treadmill training of rats after sciatic nerve graft does not alter accuracy of muscle reinnervation**
Mohammed Barham, Jonas Andermahr, Henryk Majczyński, Urszula Stawińska, Johannes Vogt and Wolfram F. Neiss
- 123 **Rapid and effective fusion repair of severed digital nerves using neurorrhaphy and bioengineered solutions including polyethylene glycol: A case report**
Stephen Lopez, George D. Bittner and Richard C. Treviño
- 130 **Experimental study on the repair of peripheral nerve injuries via simultaneously coapting the proximal and distal ends of peripheral nerves to the side of nearby intact nerves**
Dongdong Li, Qi Yang, Xin Liu, Jing Jia, Guangbo Liu, Kewen Bai, Shicheng Jia, Jun Peng and Fei Yu



Muscle-Nerve-Nerve Grafting Improves Facial Reanimation in Rats Following Facial Nerve Injury

Steven J. Charous¹, Michael J. Hutz¹, Samantha E. Bialek², Jane K. Schumacher³ and Eileen M. Foecking^{1,2*}

¹ Department of Otolaryngology–Head and Neck Surgery, Loyola University of Chicago, Maywood, IL, United States,

² Research Service, Edward Hines Jr. VA Hospital, Hines, IL, United States, ³ Stitch School of Medicine, Loyola University, Maywood, IL, United States

OPEN ACCESS

Edited by:

Jaimie Shores,
Johns Hopkins University,
United States

Reviewed by:

Branko Bojovic,
Massachusetts General Hospital and
Harvard Medical School,
United States
Diego Marre,
Pontificia Universidad Católica de
Chile, Chile

*Correspondence:

Eileen M. Foecking
efoecking@luc.edu

Specialty section:

This article was submitted to
Neurotrauma,
a section of the journal
Frontiers in Neurology

Received: 22 June 2021

Accepted: 05 November 2021

Published: 08 December 2021

Citation:

Charous SJ, Hutz MJ, Bialek SE,
Schumacher JK and Foecking EM
(2021) Muscle-Nerve-Nerve Grafting
Improves Facial Reanimation in Rats
Following Facial Nerve Injury.
Front. Neurol. 12:723024.
doi: 10.3389/fneur.2021.723024

Nerve injury resulting in muscle paralysis from trauma or surgery is a major medical problem. Repair of such injuries with existing nerve grafting and reconstructive techniques often results in less than optimal outcomes. After previously demonstrating significant return of function using muscle-nerve-muscle (MNM) grafting in a rat facial nerve model, this study compares a variant of the technique, muscle-nerve-nerve (MNN) neurotization to MNM and interposition (IP) nerve grafting. Thirty male rats were randomized into four groups (1) control with no intervention, (2) repair with IP grafts, (3) MNM grafts and (4) MNN grafts. All groups had the buccal and marginal mandibular branches of the right facial nerve resected. Return of vibrissae movement, orientation, and snout symmetry was measured over 16 weeks. Functional recovery and muscle atrophy were assessed and quantified. All interventions resulted in significant improvement in vibrissae movement and orientation as compared to the control group ($p < 0.05$). The MNM and MNN groups had significantly less time to forward vibrissae movement as compared to controls ($p < 0.05$), and a large number of animals in the MNN group had coordinated vibrissae movement at 16 weeks. MNN and IP grafts retained significantly more muscle mass as compared to control ($p < 0.05$). Thus, MNN grafting is a promising adjuvant or alternative technique for reanimation for patients with unilateral peripheral nerve injury who are not candidates for primary neurotization.

Keywords: interpositional grafting, muscle-nerve-muscle neurotization, facial nerve injury, muscle-nerve-nerve neurotization, functional recovery

INTRODUCTION

Nerve injuries resulting in muscle paralysis are usually a result of trauma or surgery and represent a major medical problem. Existing nerve grafting and reconstructive techniques for the repair of such injuries can result in less than ideal functional outcomes with synkinesis and unpaired movement. Immediate coaptation of the severed nerve is the optimal solution, but when this is not feasible, other strategies are necessary to induce restoration of muscle function. Such techniques include, nerve grafts, splitting nerves longitudinally to share fascicles with the denervated muscle, end-to-side grafting, nerve-muscle pedicles, and direct muscular neurotization by implanting the distal end of a nerve into denervated muscle (1–5).

Muscle-nerve-muscle (MNM) grafting uses an autogenous nerve graft that serves as a conduit pairing an innervated, normally functioning muscle with a denervated muscle. After interposing the harvested graft between the muscles, axonal sprouting is induced in the normal muscle and traverses the graft to innervate the denervated muscle. Thus, when the normal muscle is stimulated, simultaneous contraction of the paired, denervated muscle is observed. MNM grafting has the advantages of being relatively simple technically and having minimal associated risk or morbidity. This technique has been described to be effective in rat facial nerve and somatic nerve models, a dog laryngeal nerve model, and in a limited number of human facial nerve patients (5–8). We previously demonstrated the feasibility and comparable results of this grafting technique to other nerve grafting techniques, and the potential of using multiple grafts in order to try to “amplify” the nerve signal and improve results further (5, 9).

This paper is the first to describe a variant of the MNM model in which one end of the nerve conduit is embedded into the normal muscle and the other end is anastomosed to the severed distal nerve that supplied the denervated muscle. We hypothesized that this new MNN group would have improved functional movement, decreased muscle atrophy, and histologic evidence of increased reinnervation compared to controls and MNM grafted groups. Further, the MNN group would have improved innervation by utilizing the original intact nerve-muscle junctions of the denervated muscle and would be more effective than the MNM technique of embedding the nerve into the affected muscle and awaiting new nerve-muscle junctions to form. We also compared to the MNN to the “gold” standard of direct nerve coaptation. The potential applications of such a technique in treating facial nerve paralysis, paralysis of the larynx, and other unexplored areas are great.

MATERIALS AND METHODS

Animals

Thirty male Sprague-Dawley rats (200 g) from Envigo (Indianapolis, Indiana, USA) were housed under a 12-h light/dark cycle and received a standard rodent diet and water ad libitum. All surgical procedures were completed in accordance with the National Institutes of Health guidelines on care and use of laboratory animals for research purposes and approved by the institutional animal care and use committee at Edward Hines Jr. VA Hospital.

Animals were randomly assigned to one of four groups: no graft (CTL) (negative control), interposition (IP) graft, MNM graft, and MNN graft. All animals then underwent a right transfacial approach with concurrent parotidectomy. The buccal and marginal mandibular branches were immediately identified deep to the subcutaneous tissues. Retrograde dissection of these branches allowed for identification of the main trunk of the facial nerve. The buccal and marginal mandibular facial nerve branches were harvested from their initial ramification to their distal insertion into the muscles of the vibrissae, yielding ~2.0 cm segments, and were subsequently used as the nerve grafts. The

incision was extended across the snout to expose the contralateral vibrissae muscle pad in all groups.

The procedures are schematically depicted in **Figure 1**. Dashed lines represent nerves that were removed and the black “X” demonstrates where the nerve graft was sutured (adapted with permission from Braintree Scientific, Inc.) (10). The buccal (orange) and mandibular (red) branches were removed from the control animals with no further intervention as previously depicted (9).

Interposition (IP) Graft Repair

The buccal and marginal mandibular facial nerve branches were dissected and harvested as previously described (5). The buccal nerve graft served as the graft for the mandibular branch and was sutured to the nerve stumps of the mandibular branch. The mandibular nerve graft served as the graft for the buccal branch and was sutured to the nerve stumps of the buccal branch with 9-0 nylon sutures through the epineurium as previously depicted (9).

Muscle-Nerve-Muscle Grafting Repair

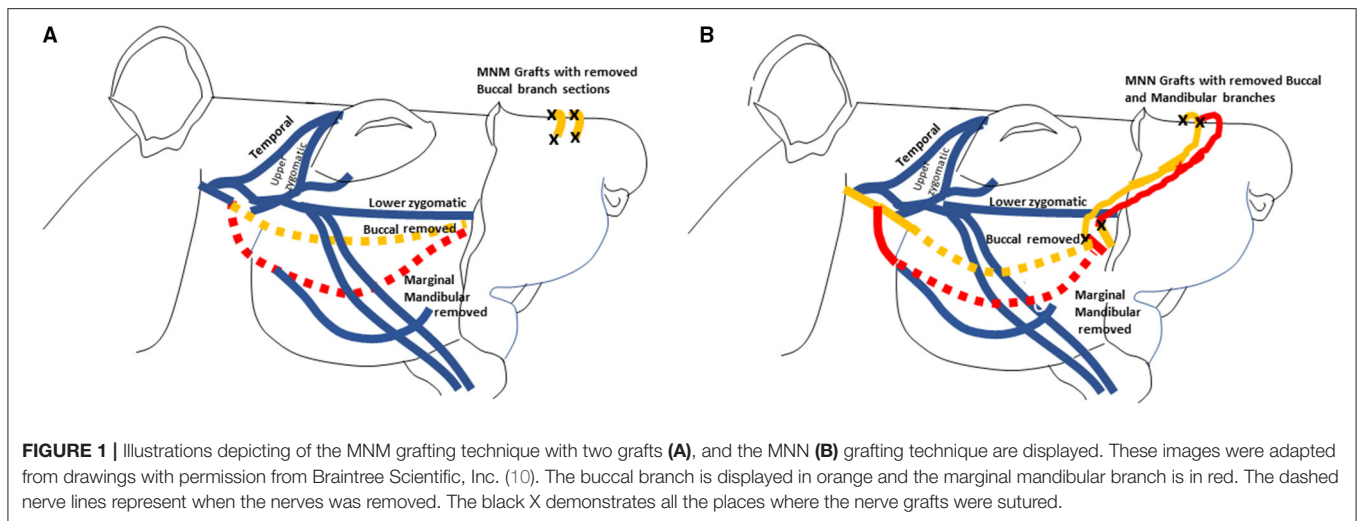
In the group that had the MNM repair technique, the buccal and mandibular nerve branches were harvested and sewn from the denervated right levator labii superioris muscle pad into the innervated left levator labii superioris muscle pad as previously described (5). The two nerve grafts were tunneled ~1–2 mm into superior portion of the right levator labii superioris muscle parallel to the muscle fibers, and secured with 9-0 nylon sutures through the epineurium (**Figure 1A**). An incision was then made in the innervated left levator labii superioris muscle bed where the graft was embedded to introduce trauma to the axons in the muscle pad to induce axonal sprouting into and across the grafts.

Muscle-Nerve-Nerve Grafting Repair

In the group undergoing MNN repair, the buccal, and mandibular nerve branches were harvested and the distal ends of the two nerve grafts were implanted into the superior portion of the left unaffected levator labii superioris muscle, parallel to the muscle fibers. The proximal end of the buccal branch were sutured to the nerve stump of the mandibular branch, and the proximal end of the mandibular branch was sutured to the nerve stump of the buccal branch (**Figure 1B**).

Functional Assessments

Animals were observed weekly for 16 weeks to assess functional recovery of vibrissae movement and orientation and snout symmetry. This time frame was chosen based on our previous study that demonstrated a large proportion of animals experienced some intervention dependent functional recovery by 16 weeks (5, 9). Recovery of facial nerve function on the right denervated side was compared to the innervated left side. All functions were assessed by two laboratory technicians in a blinded manner. Vibrissae movement was assessed utilizing a 6-point scale as previously described (9). Briefly, 1 represented no movement, 2 represents vibration, 3 represented the onset of whisking movement, 4 represented forward



but delayed whisking, 5 represented forward coordinated movement with the innervated side of unequal intensity, and 6 represented a forward coordinated movement with equal intensity to the innervated side. Vibrissae orientation was assessed on a 3-point scale, where 1 represented vibrissae on the denervated side flattened against the face, 2 represented vibrissae that are less flattened and oriented more forward, but not matching the innervated side, and 3 represented vibrissae on the denervated side indistinguishable from the innervated side. Symmetry of the snout from the midline was quantified on a 4-point scale, where 1 represented minimal symmetry (~45-degree deflection from midline), 2 represented mild symmetry (30 degrees from midline), 3 represented moderate symmetry (15 degrees from midline), and 4 represented complete symmetry.

Muscle Weights

At the end of the 16-week experiment, animals were euthanized by isoflurane overdose. The denervated and innervated mystacial vibrissae muscle pads, containing the levator labii superioris, dilator naris, nasolabialis profundus, and the maxiolabialis, were dissected out from the nasal bone through the premaxillary bone and weighed [anatomy described by Haidarliu et al. (11)]. Muscle atrophy was calculated as a standardized percentage of the denervated vibrissae muscle pad weight to the innervated vibrissae muscle pad weight.

Statistical Analysis

Significant changes in vibrissae movement, orientation, and nose symmetry were determined using a two-way analysis of variance [ANOVA; factors = time (days post-operative) and treatment], followed by a Newman Keuls' multiple comparison *post-hoc* test. Significant changes in muscle weights amongst the groups were determined using one-way ANOVA followed by Tukey's multiple comparison test (GraphPad Prism). All data is represented as Mean \pm SEM. An a priori repeated measures ANOVA (within-between interaction) power analysis was run (effect size $f = 0.24$,

$\alpha = 0.05$, power = 0.95) using G*Power 3.1 determined the total sample size for the 4 groups was 28.

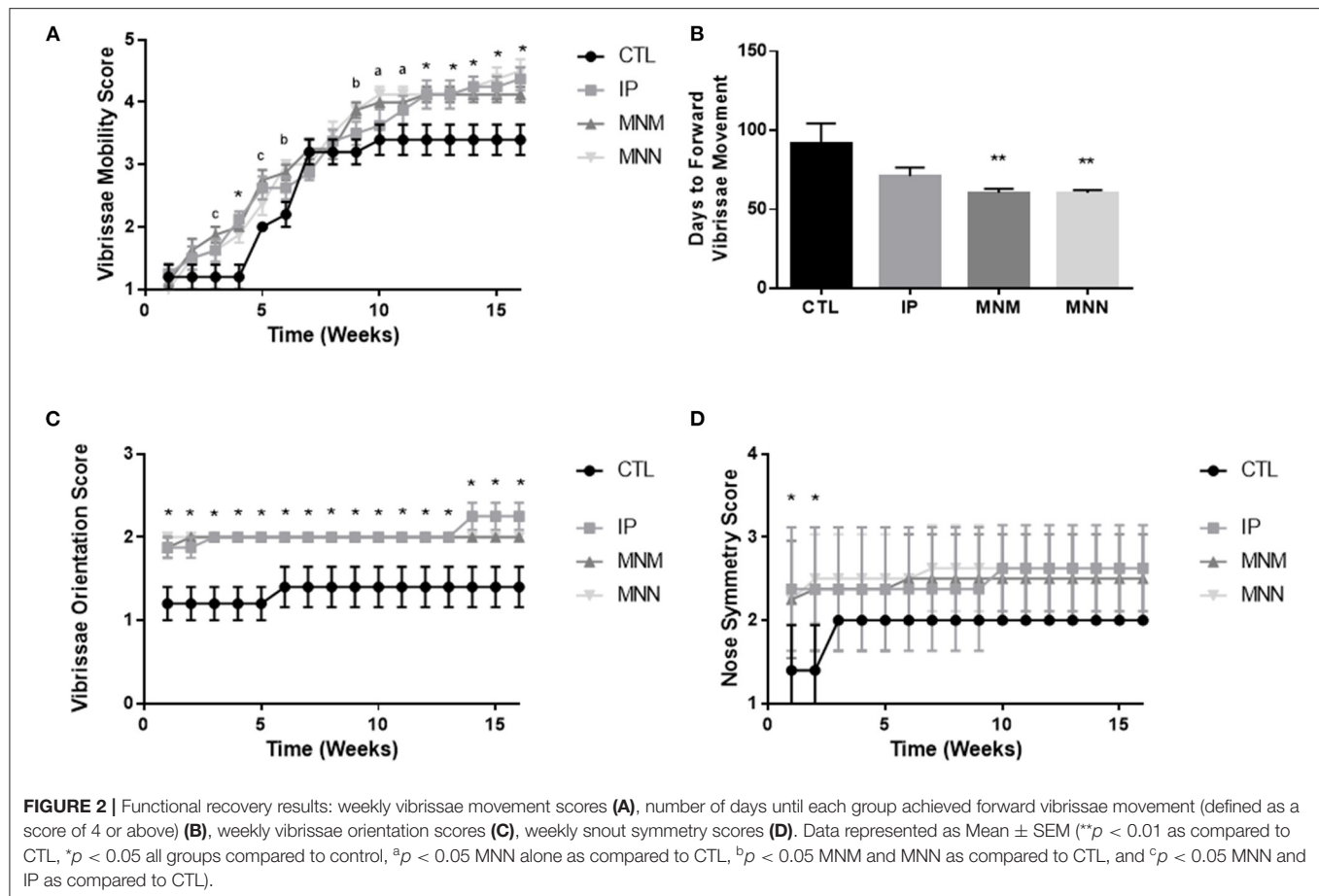
RESULTS

Functional Recovery

The effects of the grafting techniques on recovery of facial function was followed for 16 weeks following the surgical intervention. **Figure 2A** displays the significant improvement in vibrissae movement among all three intervention groups as compared to the CTL group. Significance in both grafting technique and time was shown by the two-way ANOVA. The multiple comparisons test revealed statistical significance amongst the three grafting techniques as compared to the CTL group ($**p < 0.01$ and $*p < 0.05$ all groups compared to control, $^ap < 0.05$ MNM alone as compared to CTL, $^bp < 0.05$ MNN and MNM as compared to CTL, and $^cp < 0.05$ MNN and IP as compared to CTL). The MNN and MNM grafting groups had a significantly faster return of forward vibrissae movement (defined as a score of 4 or greater) when compared to the CTL group ($**p < 0.01$), with an average return of movement at 60.38 ± 1.84 and 60.38 ± 2.63 days as compared to 91.00 ± 13.28 days, respectively (**Figure 2B**). At the end of the 16 experiment, 50% of MNN animals, 38% of IP, and 13% of MNM, achieved coordinated vibrissae movement (defined as a score of 5 or greater) (**Table 1**). However, none of the CTL animals achieved coordinated vibrissae movement. All interventions significantly improved vibrissae orientation compared to the CTL ($*p < 0.05$) (**Figure 2C**). In terms of snout symmetry (assessed on a 4-point scale), all three intervention groups reached a mean score of ~2.5 while the control group reached a score of 2. Although not statistically significant at 16 weeks, all three intervention groups reached their final symmetry scores sooner than the control group ($*p < 0.05$) (**Figure 2D**).

Muscle Atrophy

To determine the effect of the grafting techniques on muscle atrophy, the muscle pads were dissected and weighed. The muscle



pads of the CTL group, with no attempt at reinnervation, weighed 252.6 ± 28.5 milligrams (mg) or $55.86 \pm 0.63\%$ the size of the uninjured muscle pad weight at 16 weeks. A significant effect of the grafting techniques was determined by the ANOVA [$F_{(3,28)} = 1.990$, $p = 0.0076$]. The multiple comparisons test revealed that the IP and MNN groups retained significantly more muscle pad weight at 346.8 ± 23.5 and 400.5 ± 14.4 mg or 72.69 ± 4.35 and $70.94 \pm 2.78\%$, respectively (* $p < 0.05$ as compared to CTL) (Figure 3). Although the weight of the muscle pads from the MNM group increased to 428.7 ± 43.2 mg or $69.54 \pm 3.49\%$ of the uninjured muscle pad, this change was not significant.

DISCUSSION

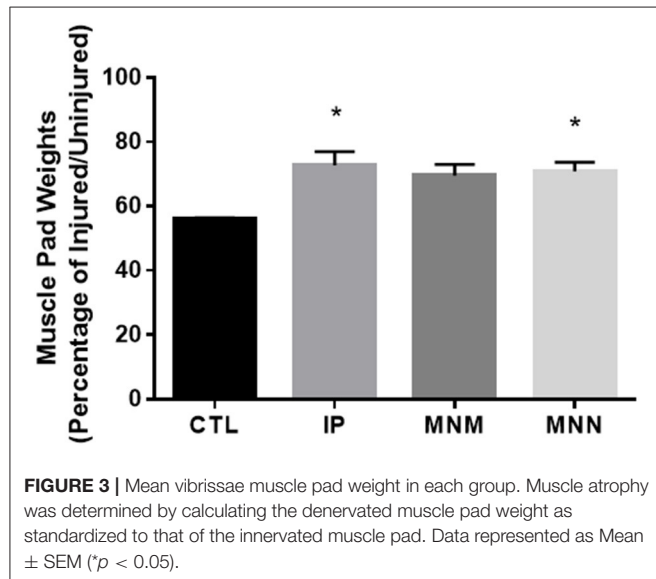
Neurotization, the implantation of a nerve directly into a denervated muscle, was first described in the early 1900's by Hacker. Direct neurotization was initially explored for use of denervated muscles in poliomyelitis (12). This technique has proven successful in multiple animal studies, but its clinical use has only sporadically been described in the literature (12). Clinically, more conventional methods for reconstruction, including nerve grafting and nerve transfer techniques, have been employed. These conventional methods require either the

presence of both ends of a severed nerve, or they utilize unrelated motor nerves that potentially provide muscle tone or learned muscle contractions.

In previous papers, we explored the method of direct neurotization using a muscle-nerve-muscle graft (5, 9). We demonstrated that an innervated muscle will sprout axons that enter and transverse the graft, and innervate a denervated muscle. In the current study, we describe the MNN grafting technique which is a variant to the MNM model in which one end of the nerve conduit is embedded into the normal muscle and the other end is anastomosed to the severed distal nerve that supplied the denervated muscle. Although IP grafting is typically the ideal surgical strategy, MNM and MNN grafting techniques have multiple advantages. IP grafting often times results in synkinesis and unpaired movements. In paired, symmetrically functioning muscles such as in the face and larynx, the potential of symmetrical movement can be realized with the MNM and MNN grafting techniques. It can be highly advantageous to capitalize on the property of symmetric movements with unilateral deficits and use the uninjured side to supply the injured side with innervation or some form of signaling (13). Although independent, unilateral functioning would not occur with neural pairing of these symmetrical muscles, for most purposes, the motor deficit would be minimized.

TABLE 1 | Percentage of animals per group achieving coordinated forward vibrissae movement (defined as a score of 5 or above) at 16 weeks.

Control	Interposition graft	MNM graft	MNN graft
0% (0/5)	37.5% (3/8)	12.5% (1/8)	50% (4/8)



Poor axonal regeneration across the injury site had been well-established in multiple peripheral nerve injury models and many studies have explored therapeutic agents, including the use of electrical stimulation, to improve the efficacy of axonal regeneration across the injury site (5, 14–18). The IP grafting technique requires two sutured sites to be traversed by the sprouting axons. Although the MNM and MNN grafting techniques does not eliminate the need for a harvest nerve graft, they do reduce the need for surgical neuroorrhaphy. The MNM grafting technique eliminates all surgical neuroorrhaphy while MNN grafting technique reduces the number of suture sites for the regenerating axon to transverse to only one. However, one limitation of the MNN and MNN techniques is that their success depends on sprouting axons from the donor muscle to enter the graft.

This paper is the first to demonstrate the use of muscle-nerve-nerve grafting as an alternative option to interpositional grafting. In this study, animals that had the MNN grafting repair recovered facial behavioral function similar to the animals that had the IP and MNM grafting repair techniques. The behavioral results from the IP and MNM grafting groups in this study were consistent with our previous findings (5, 9). These data suggest that in surgical situations when IP grafting may be challenging including trauma or tumor removal, the MNN grafting repair may be a promising alternative surgical option to gain symmetric axonal regeneration.

In our previous study, the lower zygomatic branch of the facial nerve was identified and noted to contribute to whisking outcomes (9). When the lower zygomatic branch was transected,

animals did not achieve any recovery of facial function. In the current study, we did not transect this branch in an attempt to have earlier and greater recovery in the intervention groups. Allowing the lower zygomatic branch to remain intact lead to some recovery in the control group, most likely as a result of axonal compensation. However, the improvement in movement in the MNN or MNM groups compared to the control group in this paper is considered the contribution of the nerve graft(s). Since it was hypothesized that earlier and potentially greater recovery would be observed because the lower zygomatic branch remained intact in these animals, the 16-week experimental time course remained consistent with our prior studies (9). However, this study could have benefited from a longer experimental time course which to capture the overall potential of the grafting techniques.

Muscle atrophy was significantly decreased, and vibrissae movement was significantly improved in the IP and MNN grafting groups compared to the control group. However, most promising was the finding that the MNN grafting technique was comparable to the clinically widely accepted IP grafting technique in both attaining vibrissae movement as well as minimizing muscle atrophy. No difference was observed between the MNM and MNN grafting. We hypothesize that since the IP and MNN grafting techniques utilize the distal nerve as part of the nerve conduit, the original neuromuscular junctions have the potential to provide enhanced muscle reinnervation. Future studies will examine the histological differences in neuromuscular junction occupancy in all groups.

In some regard, the MNM and MNN techniques are new paradigms for reinnervation. These are the only models in which neural input for a denervated muscle is not coming directly from the nervous system. All other techniques utilize damaged, altered, or misfit inputs directly from the peripheral nervous system (PNS). Common otolaryngologic examples include the XII-VII grafting for facial nerve paralysis and the ansa hypoglossi-recurrent laryngeal nerve anastomosis for vocal cord paralysis (19–23). These nerve grafts normally innervate multiple, independently functioning muscles and thus bring misfit signals from the PNS to muscles whose function is completely different from the nerves' intended purpose. To the contrary, the MNM and MNN grafts bring signals directly from muscles, not from the PNS. Also, the signals they carry are simplified, only transmitting neural input from a single source that induces muscle contraction from a similar, single functioning muscle (the dilator naris muscle). Although this technique can lead to damage to the healthy, contralateral muscle pad, trauma to this area is minimal and no significant detrimental effects were noted in the contralateral whisking and snout function.

It may be reasoned that innervating a paralyzed muscle with the nerves from an intact muscle is essentially creating one functioning muscle from two. By doing so, contraction of the denervated muscle has the potential to be more specific, more natural, and stronger. Stimulation of the intact muscle would result in near simultaneous contraction of both muscles. Note that this idea is only an extension of what actually occurs when reinnervation of the distal denervated portion of

a lacerated muscle transpires by ingrowth of nerves from the muscle's proximal intact nerve (18). Thus, the MNM and MNN techniques may also be considered when repairing lacerated muscles or when attaching muscle flaps to partially resected muscles. It is important to recognize that these techniques are unique in that they can be utilized in scenarios as described above in which a proximal nerve stump is not present. The MNM or MNN technique could create a muscle flap that potentially becomes a functional extension of the muscle from which it receives its graft.

Many questions remain regarding the efficacy and potential applications of MNM and MNN grafts. Future studies are needed to determine how long after muscle denervation the grafts will be effective and whether there is the limiting length of the graft. We will also explore possible neurotherapeutic strategies to enhance axonal sprouting from the innervated muscle as well as enhance axonal regeneration across the sutured site. Lastly, we will explore whether artificial grafts will function as well as autogenous ones.

CONCLUSION

This is the first study to evaluate the efficacy of MNN neurotization for facial nerve injury. Our results suggest MNN grafting is a viable technique for repair of unilateral peripheral nerve paralysis. For patients with unilateral peripheral nerve injury, particularly those who are not candidates for primary neurotization, this study provides a promising adjuvant or alternative technique for reanimation and reinnervation. Future studies may explore MNN grafting in the larynx, smaller facial nerve branches, extremities, and other areas of denervation.

REFERENCES

- Albert E. *Einige Operationen an Nerven*. Wien Med Presse. (1885). p. 1285–88.
- Viterbo F, Trindade JC, Hoshino K, Mazzoni Neto A. Latero-terminal neurotization without removal of the epineural sheath. experimental study in rats. *Rev Paul Med*. (1992) 110:267–75.
- Farber SJ, Glaus SW, Moore AM, Hunter DA, Mackinnon SE, Johnson PJ. Supercharge nerve transfer to enhance motor recovery: a laboratory study. *J Hand Surg Am*. (2013) 38:466–77. doi: 10.1016/j.jhsa.2012.12.020
- Tucker HM. Human laryngeal reinnervation. *Laryngoscope*. (1976) 86:769–79. doi: 10.1288/00005537-197606000-00004
- Charous SJ, Hotaling JM, Burgess BD, Sappington JM, Park J, Turek G, et al. Muscle-nerve-muscle grafting for facial reanimation in rats. *Ann Otol Rhinol Laryngol*. (2017) 126:261–7. doi: 10.1177/0003489416686587
- Kerner C, Milesi W, Paternostro T, Nuhr M. Muscle-nerve-muscle neurotization of the orbicularis oris muscle. *J Craniomaxillofac Surg*. (2001) 29:302–6. doi: 10.1054/jcms.2001.0233
- El-Kashlan HK, Carroll WR, Hogikyan ND, Chepeha DB, Kileny PR, Esclamado RM. Selective cricothyroid muscle reinnervation by muscle-nerve-muscle neurotization. *Arch Otolaryngol Head Neck Surg*. (2001) 127:1211–5. doi: 10.1001/archotol.127.10.1211
- Hogikyan ND, Johns MM, Kileny PR, Urbanchek M, Carroll WR, Kuzon WM. Motion-specific laryngeal reinnervation using muscle-nerve-muscle neurotization. *Ann Otol Rhinol Laryngol*. (2001) 110:801–10. doi: 10.1177/000348940111000901
- Foecking E, Burgess B, Fridirici Z, Bialek S, Low C, Charous S. Effects of the number of muscle-nerve-muscle grafts on rat facial nerve function recovery. *Ann Otol Rhinol Laryngol*. (2018) 127:791–7. doi: 10.1177/0003489418795980
- Greene E. Nervous system. In: *Anatomy of the Rat*. Braintree, MA: Braintree Scientific, Inc. (1935) 143 p.
- Haidarliu S, Simony E, Golomb D, Ahissar E. Muscle architecture in the mystacial pad of the rat. *Anat Rec*. (2010) 293:1192–206. doi: 10.1002/ar.21156
- Konofaos P, Wallace RD. Basic science of muscle neurotization: a review. *J Reconstr Microsurg*. (2015) 31:481–6. doi: 10.1055/s-0035-1554937
- Jacob DK, Stefkó ST, Hackworth SA, Lovell MR, Mickle MH. Communication between functional and denervated muscles using radiofrequency. *Otolaryngol Head Neck Surg*. (2006) 134:862–7. doi: 10.1016/j.otohns.2005.09.034
- Al-Majed AA, Neumann CM, Brushart TM, Gordon T. Brief electrical stimulation promotes the speed and accuracy of motor axonal regeneration. *J Neurosci*. (2000) 20:2602–8. doi: 10.1523/JNEUROSCI.20-07-02602.2000
- Brushart TM, Hoffman PN, Royall RM, Murinson BB, Witzel C, Gordon T. Electrical stimulation promotes motoneuron regeneration without increasing its speed or conditioning the neuron. *J Neurosci*. (2002) 22:6631–38. doi: 10.1523/JNEUROSCI.22-15-06631.2002
- Hetzler LE, Sharma N, Tanzer L, Wurster RD, Leonetti J, Marzo SJ, et al. Accelerating functional recovery after rat facial nerve injury: effects of gonadal steroids and electrical stimulation. *Otolaryngol Head Neck Surg*. (2008) 139:62–7. doi: 10.1016/j.otohns.2008.02.006

DATA AVAILABILITY STATEMENT

The raw data supporting the conclusions of this article will be made available by the authors, without undue reservation.

ETHICS STATEMENT

The animal use protocol was approved by the Institutional Animal Care and Use Committee (IACUC) of Edward Hines Jr. VA Hospital.

AUTHOR CONTRIBUTIONS

SC, MH, and EF contributed to conception and design of the study. MH, SB, and JS performed the technical work and gather the data. EF performed the statistical analysis. SC wrote the first draft of the manuscript. MH, EF, and SC wrote sections of the manuscript. All authors contributed to manuscript revision, read, and approved the submitted version.

FUNDING

Funding support from the Department of Otolaryngology—Head and Neck Surgery at Loyola Medical Center, Maywood, Illinois.

ACKNOWLEDGMENTS

The authors would like to thank the Department of Otolaryngology—Head and Neck Surgery for funding this research project.

17. Sharma N, Coughlin L, Porter RG, Tanzer L, Wurster RD, Marzo SJ, et al. Effects of electrical stimulation and gonadal steroids on rat facial nerve regenerative properties. *Restor Neurol Neurosci.* (2009) 27:633–44. doi: 10.3233/RNN-2009-0489
18. Gordon T. Electrical stimulation to enhance axon regeneration after peripheral nerve injuries in animal models and humans. *Neurotherapeutics.* (2016) 13:295–310. doi: 10.1007/s13311-015-0415-1
19. May M, Sobol SM, Mester SJ. Hypoglossal-facial nerve interpositional-jump graft for facial reanimation without tongue atrophy. *Otolaryngol Head Neck Surg.* (1991) 104:818–25. doi: 10.1177/019459989110400609
20. Smith ME, Roy N, Stoddard K. Ansa-RLN reinnervation for unilateral vocal fold paralysis in adolescents and young adults. *Int J Pediatr Otorhinolaryngol.* (2008) 72:1311–6. doi: 10.1016/j.ijporl.2008.05.004
21. Crumley RL. Update: Ansa cervicalis to recurrent laryngeal nerve anastomosis for unilateral laryngeal paralysis. *Laryngoscope.* (1991) 101:384–7; discussion 8. doi: 10.1002/lary.1991.101.4.384
22. Aynehchi BB, McCoul ED, Sundaram K. Systematic review of laryngeal reinnervation techniques. *Otolaryngol Head Neck Surg.* (2010) 143:749–59. doi: 10.1016/j.otohns.2010.09.031
23. Lim AY, Lahiri A, Pereira BP, Tan JA, Sebastin SJ, Tan BL, et al. The role of intramuscular nerve repair in the recovery of lacerated skeletal muscles. *Muscle Nerve.* (2006) 33:377–83. doi: 10.1002/mus.20468

Conflict of Interest: The authors declare that the research was conducted in the absence of any commercial or financial relationships that could be construed as a potential conflict of interest.

Publisher's Note: All claims expressed in this article are solely those of the authors and do not necessarily represent those of their affiliated organizations, or those of the publisher, the editors and the reviewers. Any product that may be evaluated in this article, or claim that may be made by its manufacturer, is not guaranteed or endorsed by the publisher.

Copyright © 2021 Charous, Hutz, Bialek, Schumacher and Foecking. This is an open-access article distributed under the terms of the Creative Commons Attribution License (CC BY). The use, distribution or reproduction in other forums is permitted, provided the original author(s) and the copyright owner(s) are credited and that the original publication in this journal is cited, in accordance with accepted academic practice. No use, distribution or reproduction is permitted which does not comply with these terms.



The Role of c-Jun and Autocrine Signaling Loops in the Control of Repair Schwann Cells and Regeneration

Kristjan R. Jessen* and Rhona Mirsky

Department of Cell and Developmental Biology, University College London, London, United Kingdom

OPEN ACCESS

Edited by:

Jared Bushman,
University of Wyoming,
United States

Reviewed by:

Yannick Pottelton,
Albany Medical College,
United States
Janos Groh,
University Hospital Würzburg,
Germany

*Correspondence:

Kristjan R. Jessen
k.jessen@ucl.ac.uk

Specialty section:

This article was submitted to
Cellular Neuropathology,
a section of the journal
Frontiers in Cellular Neuroscience

Received: 22 November 2021

Accepted: 30 December 2021

Published: 09 February 2022

Citation:

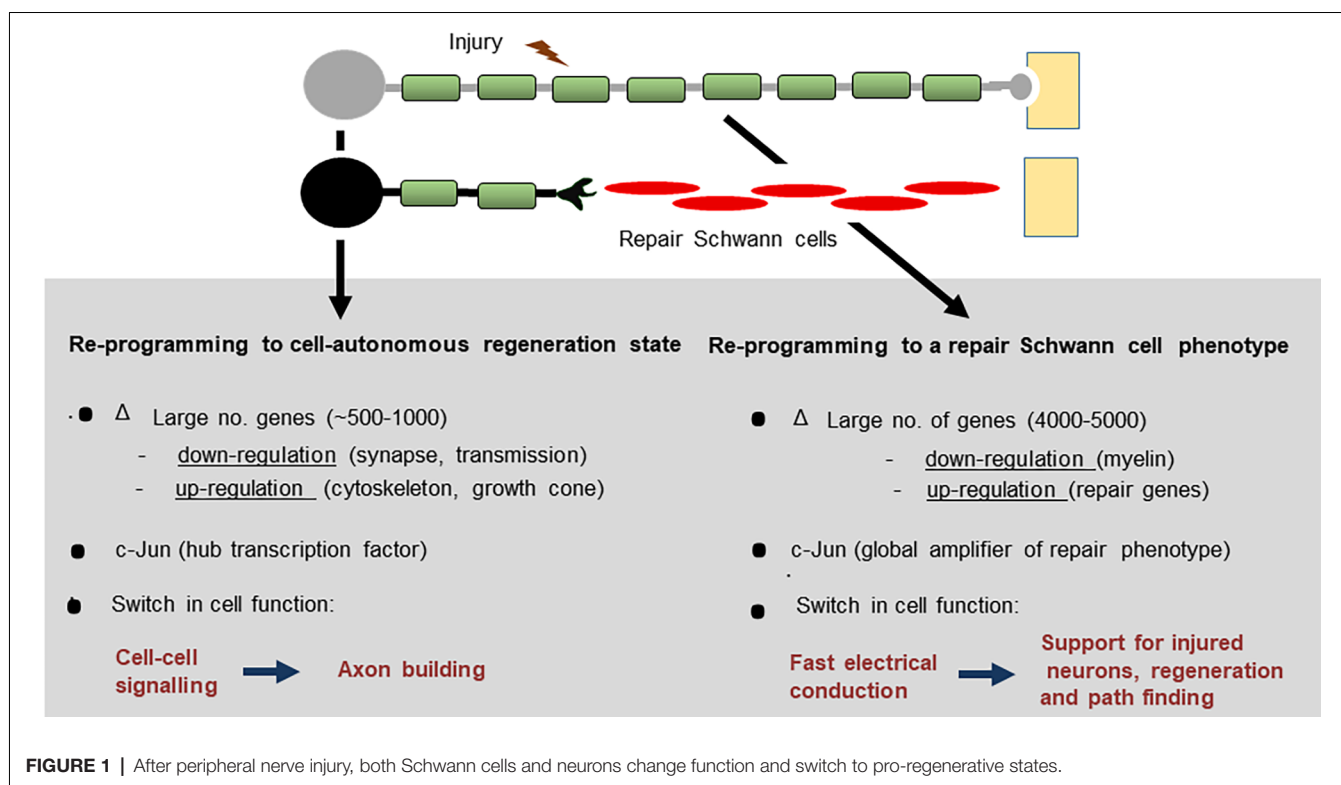
Jessen KR and Mirsky R (2022) The
Role of c-Jun and Autocrine Signaling
Loops in the Control of Repair
Schwann Cells and Regeneration.
Front. Cell. Neurosci. 15:820216.
doi: 10.3389/fncel.2021.820216

After nerve injury, both Schwann cells and neurons switch to pro-regenerative states. For Schwann cells, this involves reprogramming of myelin and Remak cells to repair Schwann cells that provide the signals and mechanisms needed for the survival of injured neurons, myelin clearance, axonal regeneration and target reinnervation. Because functional repair cells are essential for regeneration, it is unfortunate that their phenotype is not robust. Repair cell activation falters as animals get older and the repair phenotype fades during chronic denervation. These malfunctions are important reasons for the poor outcomes after nerve damage in humans. This review will discuss injury-induced Schwann cell reprogramming and the concept of the repair Schwann cell, and consider the molecular control of these cells with emphasis on c-Jun. This transcription factor is required for the generation of functional repair cells, and failure of c-Jun expression is implicated in repair cell failures in older animals and during chronic denervation. Elevating c-Jun expression in repair cells promotes regeneration, showing in principle that targeting repair cells is an effective way of improving nerve repair. In this context, we will outline the emerging evidence that repair cells are sustained by autocrine signaling loops, attractive targets for interventions aimed at promoting regeneration.

Keywords: PNS, repair Schwann cell, c-Jun, regeneration, nerve injury, Schwann cell

INTRODUCTION

After nerve injury, both neurons and Schwann cells undergo radical change as they adopt phenotypes dedicated to support repair (**Figure 1**). The neurons reprogramme to cell-autonomous regenerative units, a process that entails a substantial change in gene expression and a switch of function from that of cell-cell signaling to that of axon building. The injury response of Schwann cells is equally impressive, involving the reprogramming of myelin and Remak cells to repair Schwann cells, a Schwann cell phenotype specialized for promoting axonal regeneration. As a result, the PNS has a striking regenerative potential (Boyd and Gordon, 2003; Jessen and Mirsky, 2005; Allodi et al., 2012; Scheib and Höke, 2013; Doron-Mandel et al., 2015; Jessen et al., 2015; Fawcett and Verhaagen, 2018; Jessen and Arthur-Farraj, 2019; Jessen and Mirsky, 2019b; Stierli et al., 2019; Nocera and Jacob, 2020; Min et al., 2021). Despite this, nerve injuries remain an important clinical problem. Workers in the field of nerve repair will be familiar with two central issues: First, that the regenerative capacity of nerves declines dramatically with age and, second, that after injury, the chronically denervated distal nerve stump gradually loses the ability to support axonal



regeneration, an important reason for poor outcomes after all but the most distal nerve injuries (reviewed in Vaughan, 1992; Verdú et al., 2000; Höke, 2006; Sulaiman and Gordon, 2009; Painter, 2017).

What would cause the inherent regenerative capacity of the PNS to be compromised in this way? Are these two phenomena mechanistically unrelated, or perhaps linked? Might it even be possible to find common molecular mechanisms that connect these two apparently dissimilar situations in which regeneration falters?

The answers can be traced back to the identification of the transcription factor c-Jun in Schwann cells in the 1990s and to the seminal work of J. Z. Young and his colleagues half a century earlier. Not only were they the first to experimentally compare regeneration in young and aging animals (Gutmann et al., 1942), but they also provided the first evidence that axons regenerated poorly through chronically denervated distal nerve stumps (Holmes and Young, 1942). A striking elevation of c-Jun in Schwann cells after nerve injury was first reported by De Felipe and Hunt (1994), Stewart (1995), and Shy et al. (1996). The key function of this protein in Schwann cells was unknown until it was found that nerve regeneration was severely compromised in mice in which c-Jun had been selectively inactivated in Schwann cells (Arthur-Farraj et al., 2012; Fontana et al., 2012). High c-Jun levels were shown to be required for successful Schwann cell reprogramming to repair cells after injury, and for the maintenance of the repair phenotype (reviewed in Jessen and Mirsky, 2016, 2019b; Jessen and Arthur-Farraj, 2019). Most recently, defective c-Jun expression has been linked to the twin

problems outlined above, namely the adverse effects of advancing age and chronic denervation on nerve regeneration (Wagstaff et al., 2021). As a necessary amplifier of the repair Schwann cell phenotype, c-Jun is therefore central both to the success and failure of nerve repair.

This review will discuss injury-induced Schwann cell reprogramming and the concept of the repair Schwann cell. We will consider the molecular control of these cells with emphasis on the transcription factor c-Jun and examine the important role of c-Jun in the regeneration deficits imposed by age and chronic denervation. Lastly, we will outline the emerging evidence that repair cells are sustained by a set of autocrine signaling loops, attractive targets for interventions aimed at promoting regeneration.

NERVE INJURY TRIGGERS SCHWANN CELL c-Jun EXPRESSION

The first report of *in vivo* accumulation of c-Jun protein in Schwann cell nuclei after nerve transection in the adult was made by De Felipe and Hunt (1994), although c-Jun expression had previously been shown in cultures of perinatal Schwann cells (Monuki et al., 1989). The observation of De Felipe and Hunt was confirmed by Stewart (1995) and Shy et al. (1996) who also showed elevation of c-Jun mRNA after injury. If regeneration is prevented after nerve transection, c-Jun protein levels in the distal stump continue to rise for 1–2 weeks, to reach 80–100-fold those seen in intact nerves (Fazal et al., 2017; Wagstaff et al., 2021). In humans also, c-Jun in Schwann cells is elevated both

after acute nerve injury, and in various pathological conditions (Hutton et al., 2011; Wilcox et al., 2020, 2021).

In uninjured adult nerves, c-Jun protein and mRNA are detectable, although the levels are very low compared to the injured state. Using sensitive immunohistochemistry, nuclear c-Jun can be shown in 20–30% of myelin Schwann cells of uninjured nerves, while these low basal c-Jun levels are even more easily detectable in Remak cells (Hantke et al., 2014; Klein et al., 2014).

In two situations, repair cells fail to achieve or maintain high c-Jun levels after injury, namely, as animals get older and in chronically denervated distal stumps.

Aging results in altered expression of a significant number of genes, both in uninjured and injured nerves (Painter et al., 2014; Wagstaff et al., 2021). c-Jun is among these age-sensitive genes, and c-Jun mRNA levels are significantly lower in injured nerves of aging compared to young mice. In agreement, four days after transection, c-Jun protein levels in the distal nerve stump of middle-aged mice (8–10 months) are ~50% lower than in young (1–2 months) mice (Wagstaff et al., 2021).

In small animals like rodents, nerves regenerate within weeks after an injury such as nerve crush, and c-Jun is gradually down-regulated as axons direct repair cells back to myelin and Remak cells. In the much larger human nerves, however, it is notable that repair cells distal to regenerating axons may be without axonal contact for months, as axons make their way along the nerve more proximally. This long-term, or chronic, denervation can be modeled in experimental animals by preventing regeneration of axons into the distal stump following nerve transection. Measurements of c-Jun in such chronically denervated mouse distal stumps show that denervated Schwann cells fail to maintain the high c-Jun levels they achieved 1–2 weeks after injury. Instead, c-Jun levels gradually decline, so that eight to 10 weeks after injury, c-Jun is only present at 40–50% of peak levels (Fazal et al., 2017; Wilcox et al., 2020; Wagstaff et al., 2021).

Because high c-Jun levels are instrumental in the reprogramming of myelin and Remak cells to the repair phenotype, the reduced c-Jun expression in repair cells of older animals and in chronically denervated repair cells has important implications for regeneration capacity. These issues are discussed further in subsequent sections.

While high c-Jun levels, such as those seen after injury, are associated with Schwann cell reprogramming, myelin and Remak cells tolerate a lower but significant c-Jun elevation without significant change in their phenotypes. The evidence comes from studies on c-Jun mutants and mouse models of demyelinating disease as discussed in a subsequent section (Hantke et al., 2014; Klein et al., 2014; Fazal et al., 2017).

During development, c-Jun is clearly detectable in the immature Schwann cells of perinatal nerves but decreases to low adult levels during the first 1–2 weeks after birth (Parkinson et al., 2008). It is interesting that this perinatal c-Jun expression appears not to be of great functional significance, because in mice with conditional c-Jun inactivation in Schwann cells (c-Jun cKO mice), nerve development remains essentially normal (Arthur-Farraj et al., 2012). This contrasts with the fundamental

importance of c-Jun expression in Schwann cells of injured nerves.

Early observations on the mechanisms that regulate c-Jun levels showed that c-Jun is suppressed by cAMP (Monuki et al., 1989; De Felipe and Hunt, 1994), a signal that drives myelin differentiation *in vitro* and *in vivo* (Morgan et al., 1991; Bacallao and Monje, 2015; reviewed in Monk et al., 2015). On the other hand, c-Jun is elevated by Ca⁺⁺, a signal implicated in activation of the Schwann cell injury response (Smith et al., 1985; De Felipe and Hunt, 1994). In recent work, several other pathways have been implicated in the regulation of Schwann cell c-Jun (reviewed in Boerboom et al., 2017; Jessen and Arthur-Farraj, 2019). More remains to be learned about how Schwann cells first detect axonal injury, what triggers increased c-Jun expression, and how Schwann cell c-Jun levels are regulated subsequently.

WHEN REGENERATION FAILS: AGING AND CHRONIC DENERVATION

Numerous groups have followed up the pilot observations of Gutmann et al. (1942) and studied what happens to nerve regeneration during aging (reviewed in Vaughan, 1992; Verdú et al., 2000; Painter, 2017). This has established unambiguously that aging results in a substantial reduction in regenerative capacity, and that many of the adverse effects of aging are already seen in middle-age. Age-dependent decline in repair affects humans as well as experimental animals. Aging is accompanied by slower and less extensive axonal regrowth, delayed target innervation, and slow breakdown of myelin and axonal debris. There are significant changes in gene expression in peripheral nerves between young and aging animals, both before and after injury, including reduced expression of certain trophic factors such as GDNF and betacellulin (Painter et al., 2014; Wagstaff et al., 2021). Notably, age-dependent failures of regeneration are mainly caused by deterioration of repair Schwann cells rather than neurons (Painter et al., 2014).

While the adverse consequences of chronic denervation are particularly significant in larger animals such as humans, much has been learned about the underlying mechanisms from animal models. An early study (Holmes and Young, 1942) used rabbits to show that nerve stumps denervated for 3 months had reduced capacity to support axonal regeneration. Several groups confirmed these experiments using rats, although the time course of decline differs somewhat between reports. While regeneration support is little changed by 1 month of denervation, some studies already report deterioration by 2 months. Further reduction in regeneration is seen after 3 and 6 months of denervation (Fu and Gordon, 1995; Vuorinen et al., 1995; Sulaiman and Gordon, 2000; Jonsson et al., 2013; Ronchi et al., 2017; reviewed in Vaughan, 1992; Verdú et al., 2000). Our studies on mice show that by 2- and a-half month, the ability of chronically denervated distal stumps to support axon growth is reduced by about 50% (Wagstaff et al., 2021).

Holmes and Young (1942) concluded that “some factor is operating in these degenerated stumps to reduce the rate of advance of regenerating fibers”. It turns out the “factor” is more likely to be the absence of factors since during chronic

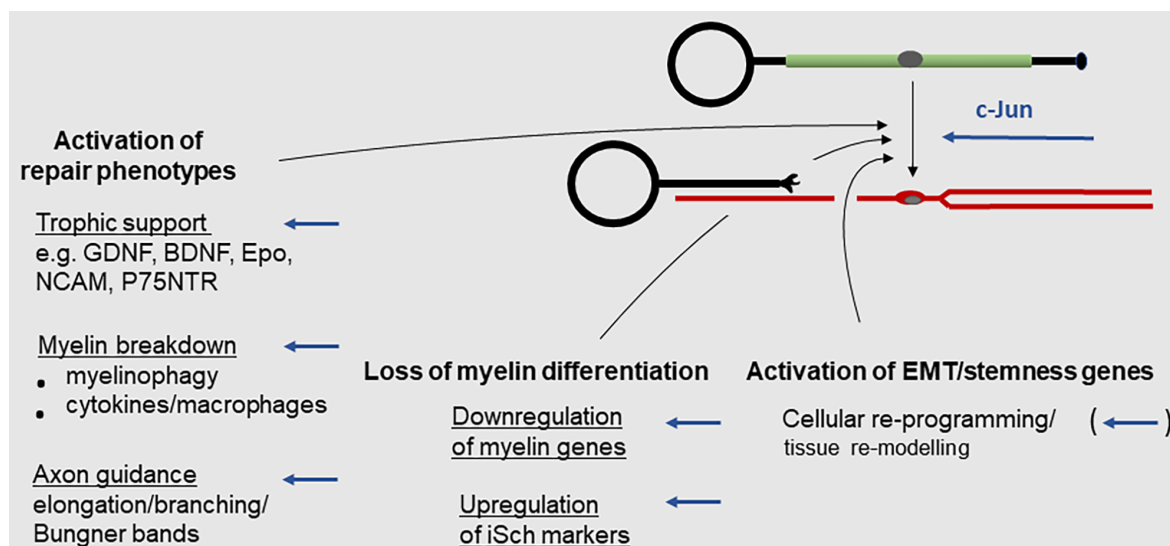


FIGURE 2 | The Schwann cell injury response. Key events during the reprogramming of myelin cells to repair Schwann cells. Arrows indicate events subject to c-Jun regulation (for references see text).

denervation repair Schwann cells gradually decrease expression of several genes implicated in the support of injured neurons and axon growth. This includes GDNF, BDNF, NT3, and NGF (Eggers et al., 2010; reviewed in Boyd and Gordon, 2003; Höke and Brushart, 2010). Thus, the repair phenotype represents a transient differentiation state that fades with time. In larger nerves, such as those in humans, this becomes a significant obstacle to effective repair. Eventually, Schwann cell numbers also decline during chronic denervation, although this has not been extensively quantified. For several reasons, this is unlikely to explain the decline in regeneration support provided by distal stumps after 2 to 3 months of denervation (for discussion see Jessen and Mirsky, 2019b) although it will become important at later times. Thus, repair cell deterioration during chronic denervation likely proceeds in two steps: First, the dedifferentiation of repair cells, namely the gradual loss of the repair-supportive features that characterize these cells soon after injury. Second, the eventual death of dedifferentiated repair cells.

As described in a previous section, c-Jun is among the repair genes that show decreased activation after injury in middle-aged animals compared to young ones, and both in rodents and humans c-Jun fails to be maintained at high levels during chronic denervation (Wilcox et al., 2020, 2021; Wagstaff et al., 2021). To appreciate the significance of reduced c-Jun in these situations, it is helpful to analyze the Schwann cell injury response and outline the function of c-Jun in repair Schwann cells.

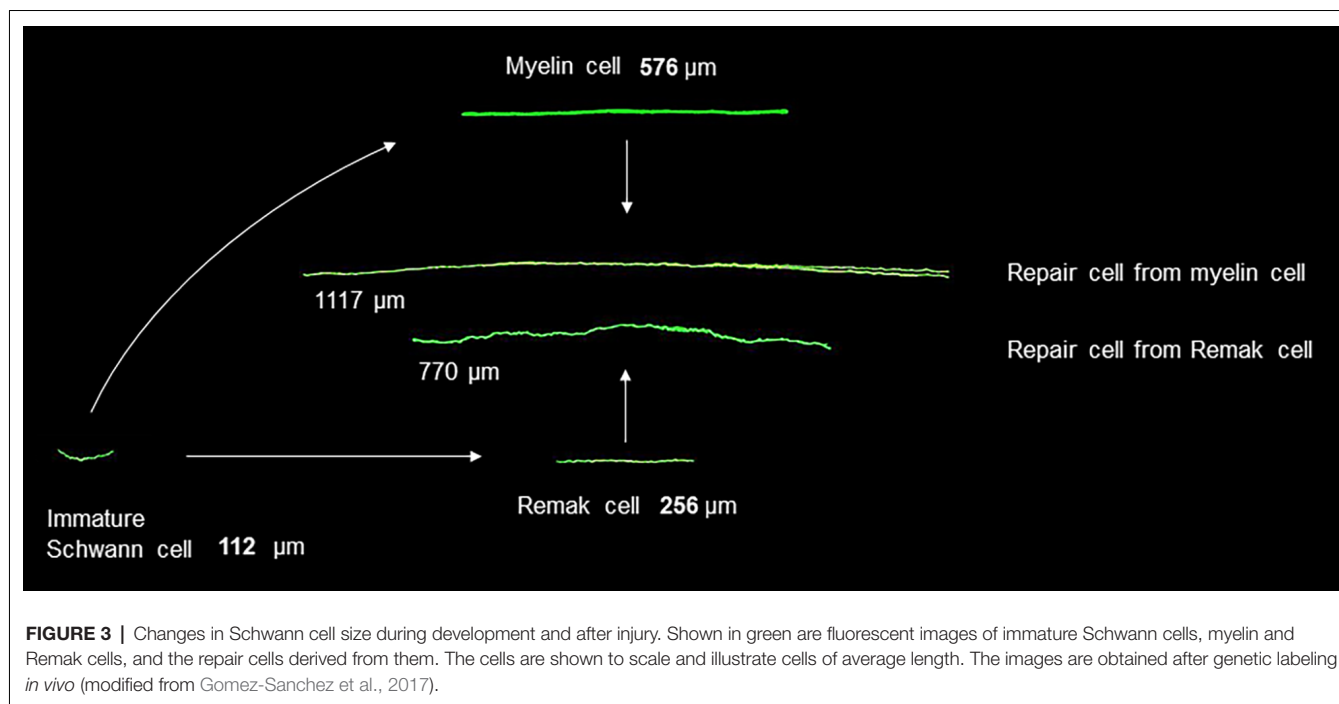
c-Jun IS A GLOBAL AMPLIFIER OF THE SCHWANN CELL INJURY RESPONSE

The Schwann cell injury response is more radical and better characterized in myelin cells than in Remak cells (Figures 2–4; reviewed in Chen et al., 2007; Glenn and Talbot, 2013; Jessen

et al., 2015; Jessen and Mirsky, 2016, 2019b; Jessen and Arthur-Farraj, 2019; Zigmond and Echevarria, 2019; Kolter et al., 2020; Nocera and Jacob, 2020; Arthur-Farraj and Coleman, 2021; Min et al., 2021). This reprogramming event involves three types of change: (i) Up-regulation of repair phenotypes. This includes activation of trophic support for neurons and of the innate-immune response and recruitment of macrophages, up-regulation of myelinophagy for myelin clearance, and cellular elongation and branching leading to the formation of regeneration tracks (Bungner bands). (ii) Down-regulation of myelin genes; (iii) Activation of EMT/stemness genes.

As with injured neurons, the injury-induced reprogramming of myelin to repair cells is accompanied by a change in function, in this case from that of promoting fast axonal conduction to that of supporting injured neurons. And, interestingly, not only in Schwann cells but also in neurons, c-Jun is necessary for the regenerative response to injury but unimportant for development. Thus, in mice without c-Jun in neurons, axonal growth and the general development of the nervous system is essentially normal although the intrinsic ability of adult neurons in these mice to regenerate axons after an injury is compromised (Raivich et al., 2004; Zhou et al., 2004).

Among the first reported functions of c-Jun in Schwann cells was the suppression of myelination and myelin genes, rather than the promotion of nerve repair (Parkinson et al., 2004). c-Jun showed a cross-inhibitory relationship with the pro-myelin transcription factor Krox20/Egr2 and suppressed the ability of Krox20/Egr2 to activate myelin genes (Parkinson et al., 2004, 2008). Several other factors expressed in perinatal nerves share this ability to suppress myelin genes and myelination. These negative regulators of myelination include, in addition to c-Jun, Notch, Sox2, and Id2 (Parkinson et al., 2008; Woodhoo et al., 2009; Roberts et al., 2017; Florio et al., 2018; reviewed



in Jessen and Mirsky, 2008). During development, negative regulation of myelination is not an important function of c-Jun, since developing and adult nerves are essentially normal in c-Jun cKO mice. During the Schwann cell injury response, however, c-Jun-mediated suppression of myelin genes has a significant role as outlined below.

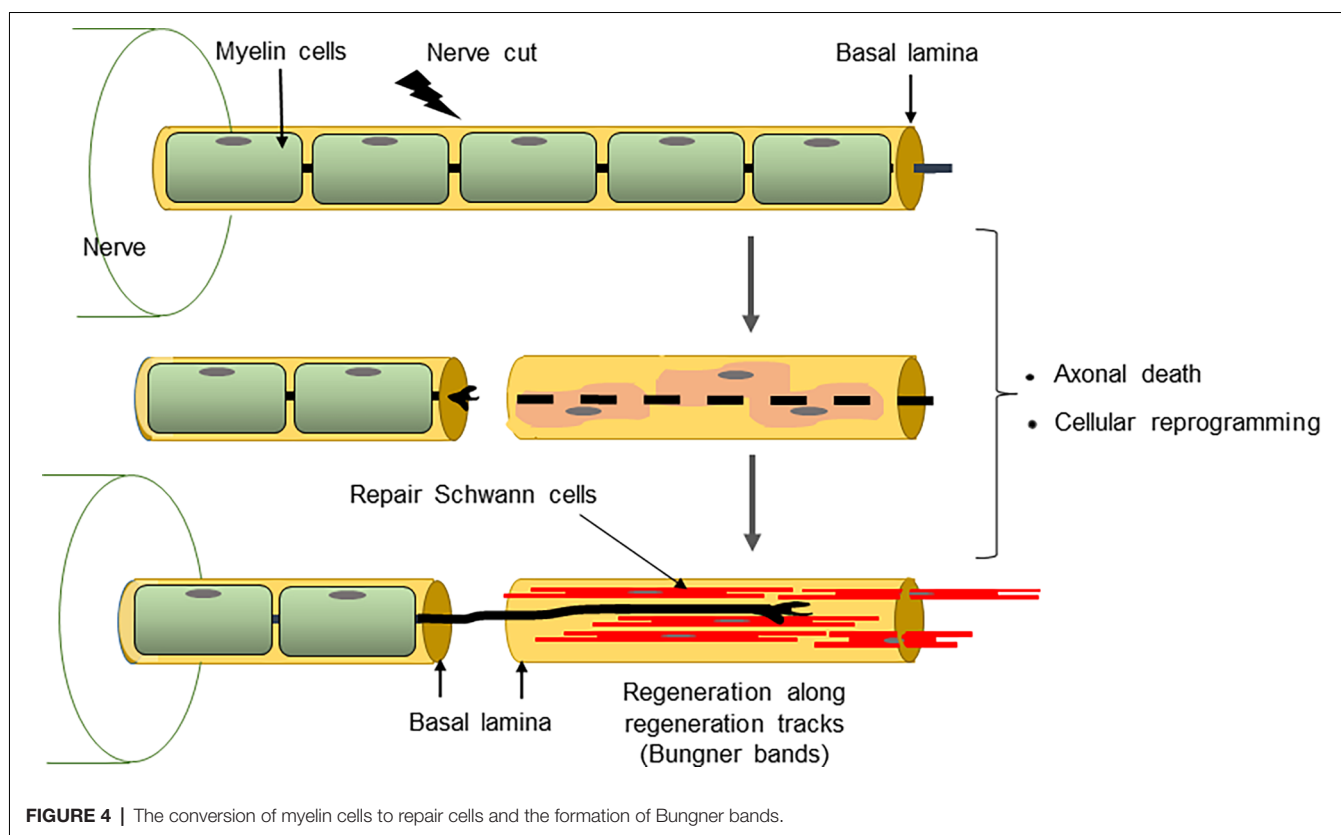
The importance of c-Jun for the Schwann cell injury response first became clear when it was found that in mice lacking c-Jun specifically in Schwann cells (c-Jun cKO mice), sciatic or facial nerve injury results in a broad spectrum of regenerative abnormalities (Figures 5–7; Arthur-Farraj et al., 2012; Fontana et al., 2012; reviewed in Jessen and Mirsky, 2016, 2019b). In these mice, axonal injury causes excessive death of sensory and motor neurons (Figure 5). Axonal regeneration *in vivo* is strongly compromised, and in line with this cell culture studies show directly that c-Jun levels in Schwann cells control the elongation rate of the axons associated with them (Arthur-Farraj et al., 2012; Huang et al., 2019). In the c-Jun cKO mice, down-regulation of myelin genes after an injury is delayed and incomplete, activation of myelinophagy is suppressed (Gomez-Sanchez et al., 2015) and myelin clearance is compromised (Figure 6). *In vitro*, c-Jun knockout Schwann cells adopt a flattened morphology rather than the typical bi- or tri-polar shape of cultured Schwann cells, and in line with this, the regeneration tracks (Bungner bands) in the cut nerves of c-Jun cKO mice are disorganized (Figure 7). In the distal stump of cut c-Jun cKO nerves, 173 genes are differentially expressed compared to cut wild type nerves and six miRNAs are also dis-regulated. At the protein level, NCAM and p75NTR are over-expressed while NCAD is under-expressed (Arthur-Farraj et al., 2012, 2017). It is striking that this c-Jun regulated program represents a relatively small fraction of the molecular changes induced by injury which extends to some

4,000–5,000 genes. This is in line with the notion that c-Jun has an important but restricted function in injured nerves, specifically regulating the collection of events involved in the reprogramming of Schwann cells to generate repair cells. Thus c-Jun functions as an essential global amplifier of the repair cell phenotype.

MAINTAINING SCHWANN CELL c-Jun PREVENTS REGENERATION FAILURE DUE TO AGE AND CHRONIC DENERVATION

The twin observations that c-Jun boosts repair cell function and that c-Jun levels are reduced as the cells lose the capacity to support regeneration in older animals and during chronic denervation, suggest a causal link. Namely that the failure of repair cells in these two situations is a consequence of reduced c-Jun. If this were the case, preventing the loss of c-Jun should also prevent the decline in regeneration. This question was addressed in a recent publication (Wagstaff et al., 2021). To prevent the reduction in c-Jun in older or chronically denervated Schwann cells, the authors generated a mouse in which Schwann cells alone expressed a c-Jun transgene in addition to endogenous c-Jun (c-Jun OE/+ mice). In these mice, c-Jun levels in uninjured nerves were still low, although about seven-fold higher than the very low levels in wild type control mice, and the nerves were normal except for a slight reduction in myelin thickness (Fazal et al., 2017).

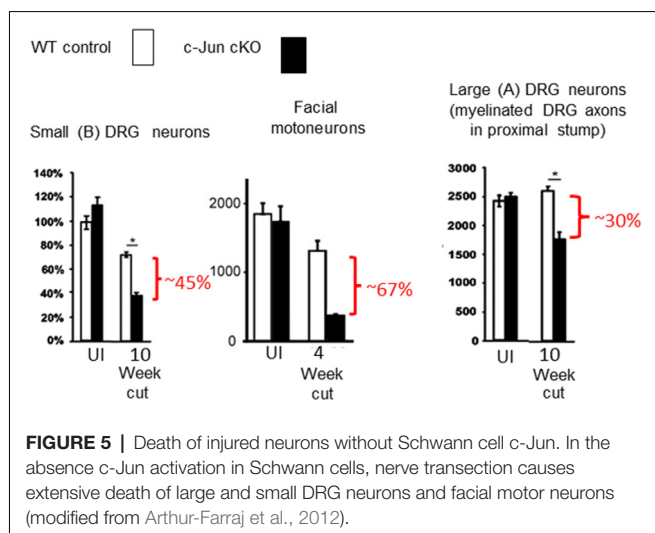
Studying the effects of age, Wagstaff et al. (2021) found that while the c-Jun response to acute nerve injury (3-day cut) in middle-aged wild type mice reached only ~50% of that in young ones, this drop was not seen in middle-aged c-Jun OE/+ mice,

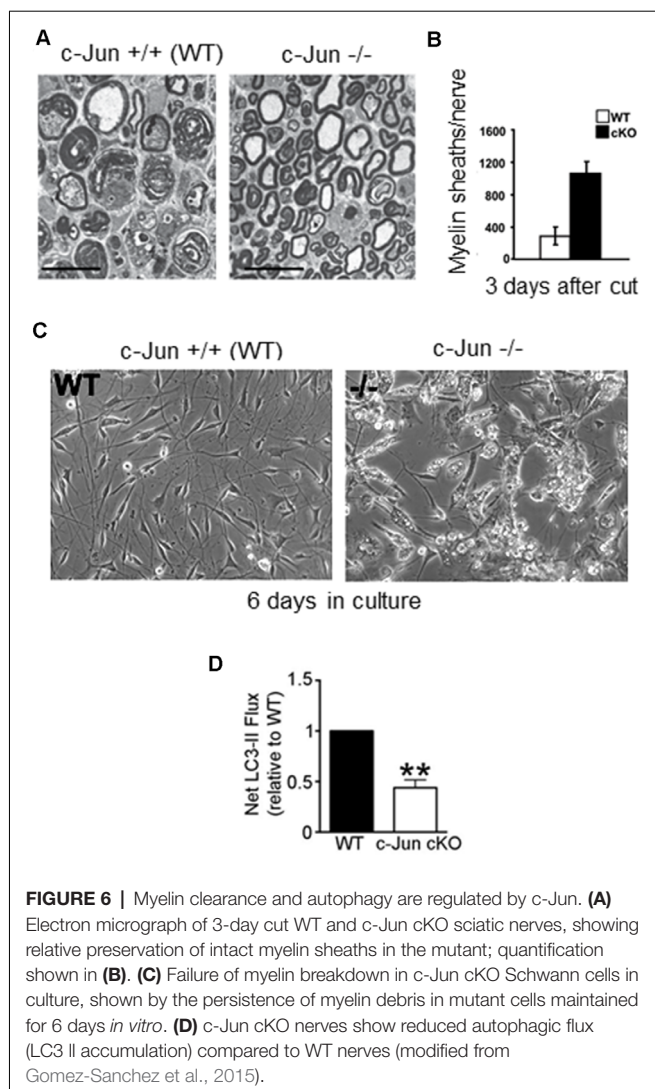


where c-Jun levels after injury remained similar to those in young ones. Measurements of regeneration after nerve crush using neuron backfilling showed that in wild type mice, age reduced regeneration by about 50%, as expected. This was not the case in c-Jun OE/+ mice, however, where regeneration capacity was undiminished by age, similar numbers of motor and DRG neurons regenerated in the nerves of young and middle-aged mice (Wagstaff et al., 2021).

Analyzing chronic denervation, it was found that one week after injury, c-Jun elevation was similar in wild type and c-Jun OE/+ mice. But in c-Jun OE/+ mice, c-Jun levels stayed constant during a subsequent 10 week period of chronic denervation, while they dropped by about 60% in wild type nerves (Wagstaff et al., 2021). Comparing regeneration through 1-week and 10-week denervated distal stumps of the c-Jun OE/+ and wild type mice showed, first, that regeneration through short-term (1-week) denervated stumps was similar in the two mouse strains, where c-Jun levels were similar; second, that in wild type mice regeneration through chronically (10-week) denervated stumps was substantially reduced, as expected, and third, that in c-Jun OE/+ mice, regeneration through 10-week denervated stumps, where c-Jun levels are maintained, did not decline but remained similar to that seen with 1-week stumps. These results were obtained both with spinal cord motor neurons and DRG sensory neurons. In these experiments, therefore, preventing the decline in Schwann cell c-Jun levels during chronic denervation prevented the decline in axonal regeneration (Wagstaff et al., 2021).

These experiments suggest that defective c-Jun expression in repair cells is an important factor in the regeneration failures, particularly those associated with both older age and chronic denervation (Figure 8). They show also that correcting defective c-Jun levels corrects regeneration deficits, pointing to the c-Jun regulated





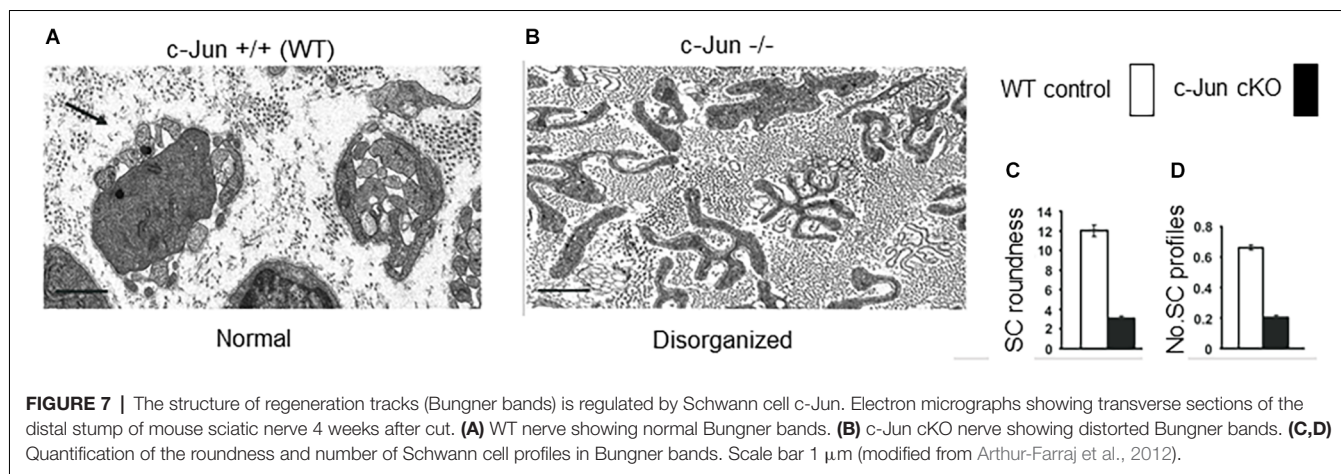
program as a target for treatments aimed at improving nerve regeneration.

THE c-Jun REGULATED SCHWANN CELL RESPONSE TO NEUROLOGICAL DISEASE

Schwann cell c-Jun is elevated in several human neuropathological conditions, although these disease states do not involve mechanical injury to axons, i.e., transection or crush, as mentioned above (Hutton et al., 2011; Wilcox et al., 2020, 2021). Increased c-Jun levels in uninjured nerves have also been studied in mice, both in disease models and c-Jun over-expressing mutants. This work has given rise to the idea that, in addition to the function of high Schwann cell c-Jun after injury, a more modest c-Jun elevation in uninjured nerves, even in Schwann cells that still retain myelin and Remak phenotypes, also activates a neuron-supportive Schwann cell program that protects against neurological damage.

This is based on studies on the dose-dependence of c-Jun function using heterozygous (c-Jun OE/+) and homozygous (c-Jun OE/OE) c-Jun over-expressing mice, and on examining mouse models of Charcot-Marie-Tooth (CMT)1A and CMT1X disease (Hantke et al., 2014; Klein et al., 2014; Fazal et al., 2017). In c-Jun homozygous over-expressing mice (c-Jun OE/OE mice; Fazal et al., 2017), a 28-fold elevation of c-Jun in Schwann cells causes hypomyelination pathology, implicating c-Jun as a candidate gene in demyelinating neuropathies. On the other hand, and as mentioned before, nerves in c-Jun heterozygous over-expressing mice (c-Jun OE/+ mice) where c-Jun is about 6-fold higher than WT are essentially normal (Fazal et al., 2017). Substantially normal myelin and Remak phenotypes despite significant elevation of c-Jun protein are also seen in mouse models of CMT1A and CMT1X (Hantke et al., 2014; Klein et al., 2014). Importantly, these CMT1 models reveal that already at low or moderate c-Jun levels compatible with myelination, c-Jun promotes neuron-supportive signaling from Schwann cells to neurons. Thus, in the C3 mouse model of CMT1A, Schwann cell c-Jun is elevated, but not sufficiently to disrupt myelination. Nevertheless, this results in a marked increase in axonal survival and sensory-motor performance in this disease model (Hantke et al., 2014). In Cx32def mice that mimic CMT1X Schwann cell c-Jun is also elevated. This does not disrupt myelin but is accompanied by increased GDNF expression in myelin Schwann cells (Klein et al., 2014). This suggests that the c-Jun elevation seen in pathological human nerves may indicate an adaptive neuron-supportive Schwann cell response to disease (Hutton et al., 2011; Wilcox et al., 2020, 2021).

While therapeutic boosting of the c-Jun pathway in diseases such as CMT1A might reduce axonal loss, it would need careful adjustment due to the potentially demyelinating effect of high c-Jun levels. Concerning the targeting of the Schwann cell c-Jun pathway for promoting regeneration after an injury it is important to note, first, that there is no evidence that elevation of c-Jun, such as that in the c-Jun overexpressing mice discussed above, is tumorigenic. Theoretically, this is, in any case, unlikely since after injury, wild type Schwann cells re-enter the cell cycle, alter their differentiation state and express very high levels of c-Jun, yet do not develop tumors. As expected, therefore, no tumors were found in 10-month-old homozygous c-Jun overexpressing mice (c-Jun OE/OE mice; Fazal et al., 2017). Second, the elevation of c-Jun that effectively promotes regeneration is compatible with myelination and functional recovery after injury. Thus, in c-Jun OE/+ mice, c-Jun overexpression is sufficient to fully correct regeneration deficits due to advancing age and chronic denervation, as discussed above (Wagstaff et al., 2021). Nevertheless, after nerve crush, sciatic nerves in these mice regenerate to achieve full functional recovery and myelination, although both proceed with a delay and myelin is somewhat thinner than WT, as seen also before injury (Fazal et al., 2017). As discussed further below, time limited and reversible elevation of c-Jun, for instance by hijacking the autocrine signaling loops of repair cells, would likely be an effective therapy for promoting nerve regeneration.

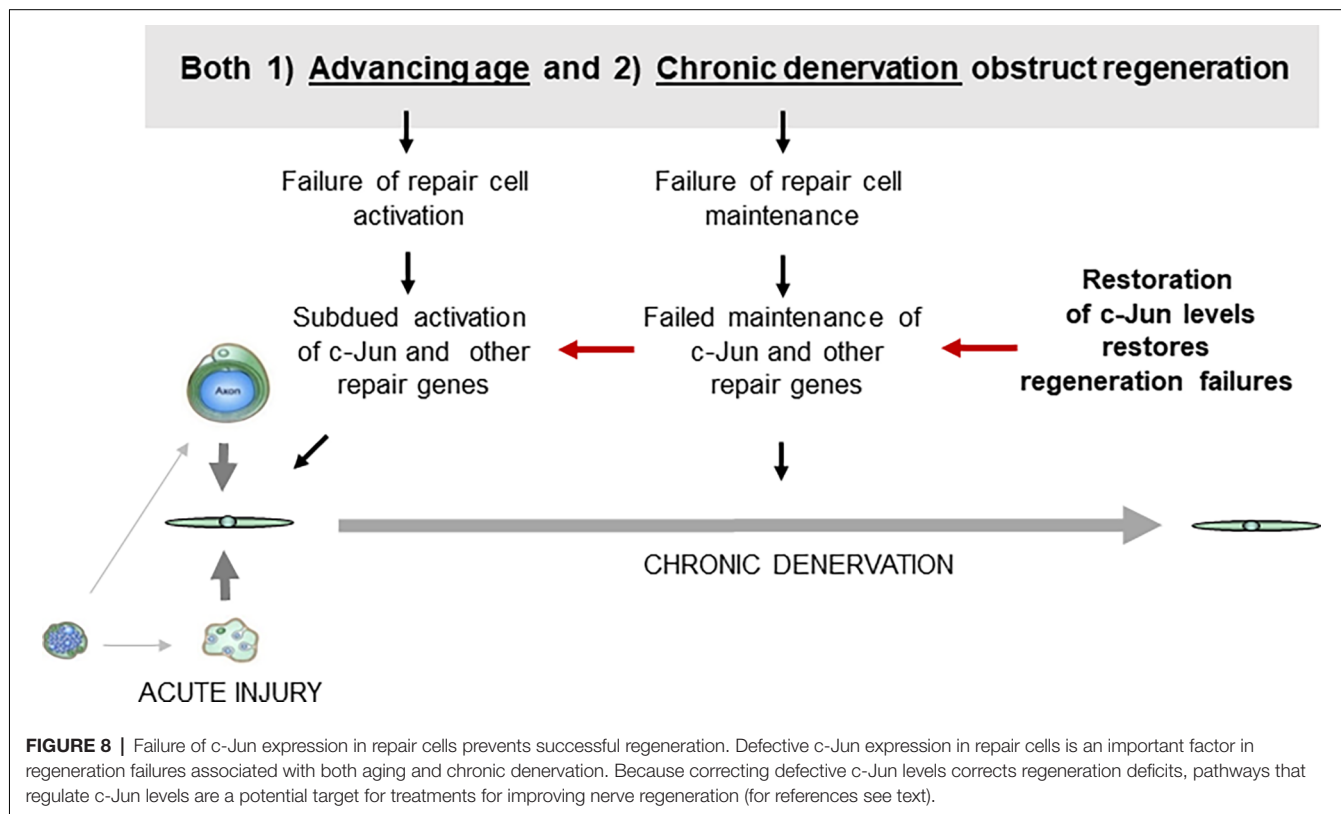


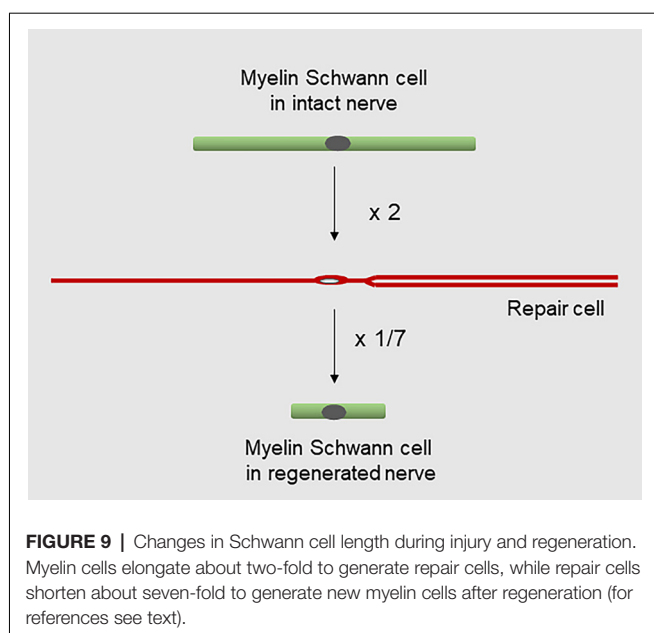
A COMPARISON BETWEEN REPAIR CELLS AND IMMATURE SCHWANN CELLS

Because repair Schwann cells in the adult, and immature Schwann cells in developing nerves, carry out quite different functions, it is not surprising that these cells also diverge in many other ways. This includes a strikingly dissimilar structure, distinct molecular expression and lineage relationships and numerous differences in the molecular machinery that regulates them.

The structure of repair cells is adapted to form the compact cellular columns (Bungner bands) that function as essential

regeneration tracks for regrowing axons (**Figures 4, 7**). As myelin and Remak cells transform to repair cells they undergo a surprising elongation that, together with two-three fold increase in Schwann cell number, will maximize cellular overlap within Bungner bands, and therefore the formation of uninterrupted tracks. Thus, repair cells are about two and three-fold longer than myelin and Remak cells, respectively and seven- to 10-fold longer than immature Schwann cells (**Figures 3, 9**). Repair cells also adopt a spiraling, corkscrew-like structure and frequently branch forming long parallel processes, both of which are likely to contribute to the generation of tight cellular columns (Gomez-Sanchez et al., 2017). While immature Schwann cells





derive from Schwann cell precursors in embryonic nerves (Jessen and Mirsky, 2019a), these and other lineage tracing studies also show conclusively that repair cells in injured nerves derive from adult myelin and Remak cells and revert to those phenotypes after regeneration (Gomez-Sanchez et al., 2017; Stierli et al., 2018).

It is well established that the myelin cells that form in nerves after regeneration are short, measuring only 25–30% of the length of myelin cells before injury (Jacobs and Cavanagh, 1969; Gomez-Sanchez et al., 2017). Remarkably, this means that repair cells undergo a radical shortening to only ~13% of their length to form the short internodes of regenerated nerves (**Figure 9**). The cytoskeletal mechanisms that control the striking elongation and shortening of Schwann cells during injury and regeneration remain to be elucidated.

The distinct structure of repair cells is in part controlled by c-Jun. The regeneration tracks that form in c-Jun cKO mice are conspicuously abnormal, loosely composed of irregular and flattened cells (**Figure 7**; Arthur-Farraj et al., 2012). Even in cell culture, Schwann cells from c-Jun cKO mice show increased flattening and roundness and lack of processes, instead of the characteristic bi- or tri-polar *in vitro* morphology of wild type Schwann cells, that reflects their structure *in vivo*. c-Jun is therefore an intrinsic regulator of the structure of denervated Schwann cells (Arthur-Farraj et al., 2012).

Probably the clearest example of a difference in molecular regulation between developing and repair Schwann cells is provided by c-Jun because this factor is unimportant in immature cells but is a key regulator of adult repair cells. Other examples include the tumor suppressor protein merlin, which is essential for the Schwann cell response to injury and nerve regeneration, although myelination is only slightly and transiently affected in mice with inactivation of merlin in Schwann cells (Mindos et al., 2017). Similarly, chromatin modifications, involving H3K27 demethylations and

acetylation and H3K4 methylation promote up-regulation of injury genes and down-regulation of myelin genes in repair cells, although these events are not involved in controlling developmental myelination (Hung et al., 2015; Ma et al., 2016; reviewed in Ma and Svaren, 2018). The transcription factor STAT3 is also unimportant for Schwann cell development but important for long-term repair cell maintenance (Benito et al., 2017).

Several other differences in the molecular regulation between repair cells and developing Schwann cells have also been identified. Autocrine neuregulin signals promote re-myelination by repair cells but not myelination by developing Schwann cells, and axon-associated neuregulin is necessary for developmental myelination but acts only as a timer for re-myelination by repair cells (Fricker et al., 2013; Stassart et al., 2013). Further, ERK1/2 promotes myelin thickness in developing cells but not during re-myelination in the adult, and injury-induced proliferation associated with repair cell generation is controlled by cyclin D1, while this protein does not control the proliferation of developing cells (Kim et al., 2000).

Together these findings demonstrate that the generation of repair cells, and the regulation of their function, depends on mechanisms, including c-Jun, that have minor or no roles during development.

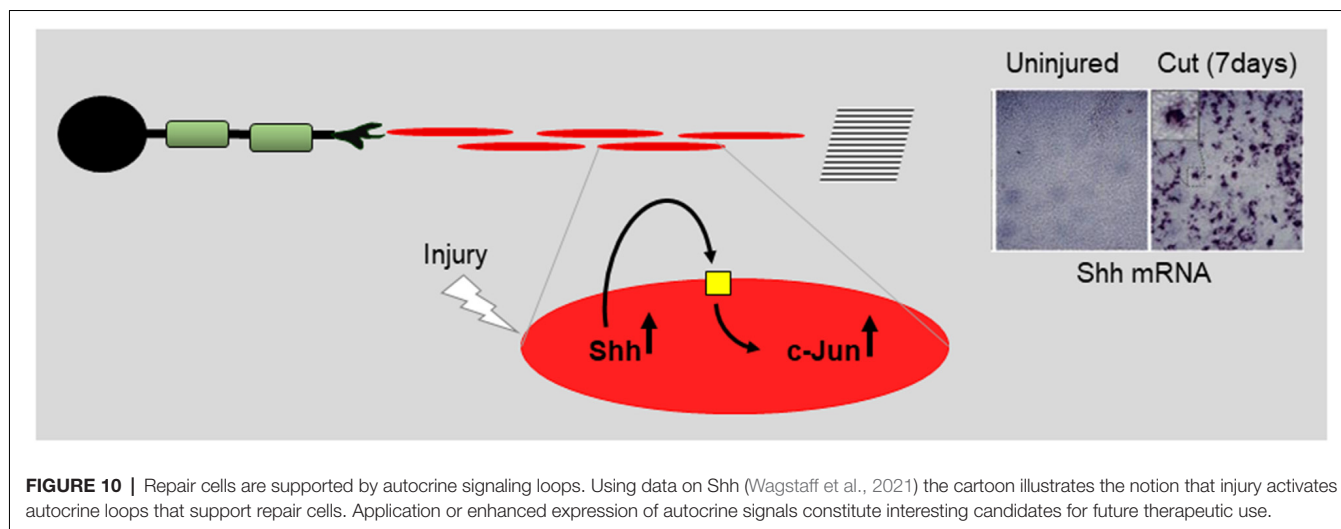
THE PHARMACOLOGY OF REGENERATION: HIJACKING THE AUTOCRINE LOOPS THAT SUPPORT REPAIR CELLS

There is still no generally recognized pharmacological treatment for the promotion of nerve repair. Schwann cells have multiple roles in regeneration, and repair cell malfunction underlies important regeneration failures. It is therefore an attractive option to develop treatments that promote the capacity of repair cells to support regeneration. In support of this, the work on Schwann cell c-Jun outlined above serves as a proof of principle. Namely, that manipulating signaling in repair Schwann cells can be an effective way to promote axonal regeneration.

Therefore, it is interesting that a group of Schwann cell derived signals, exemplified by Shh, neuregulin, TGFβ, GDNF, and IGF1, appear to work as endogenous boosters of repair cells. These factors are up-regulated in repair cells, act through autocrine loops to promote repair cell function, and promote regeneration when applied to damaged nerves *in vivo* (**Figure 10**). Targeting these pathways is a promising approach for the development of tools for therapeutic use. The data implicating these factors in autocrine repair cell support is outlined below.

Sonic Hedgehog

The most recently identified protein that appears to function in this way is Sonic hedgehog (Shh) (reviewed in Moreau and Boucher, 2020). Shh and Gli1, one of the downstream effectors of Shh signaling, are up-regulated in repair cells after injury, while Shh is also expressed in DRG neurons (Hashimoto et al., 2008; Arthur-Farraj et al., 2012;



Martinez et al., 2015; Yamada et al., 2018). During chronic denervation, Schwann cell Shh levels gradually fall, like those of c-Jun. In cultured Schwann cells, Shh agonists up-regulate c-Jun protein and c-Jun phosphorylation and promote the expression of two c-Jun targets, GDNF and BDNF (Hashimoto et al., 2008; Wagstaff et al., 2021). Further, *in vivo*, genetic inactivation of Shh selectively in Schwann cells results in reduced c-Jun expression and phosphorylation after injury and reduced levels of the c-Jun target p75NTR in repair cells. Additional support for a role for endogenous Shh in nerve repair comes from the observation that administration of cyclopamine, a specific blocker of Shh signaling, to injured nerves suppressed the normal injury-induced expression of BDNF and increased the injury-induced death of motoneurons (Hashimoto et al., 2008). Conversely, after nerve injury *in vivo*, exposure to Shh or Shh agonists promotes nerve regeneration in several experimental paradigms (Pepinsky et al., 2002; Bond et al., 2013; Martinez et al., 2015; Yamada et al., 2018). Since Schwann cells are the major source of Shh in injured nerves, all of this is consistent with autocrine Shh signaling in Schwann cells after injury. This suggestion is supported by the observation that the addition of cyclopamine alone to purified Schwann cell cultures suppresses c-Jun and c-Jun phosphorylation (Wagstaff et al., 2021).

Taken together, these experiments suggest that injury-activated Shh from repair cells promotes regeneration directly by acting on neurons (Martinez et al., 2015) and indirectly by acting back on repair cells to promote the expression of c-Jun and the repair cell phenotype (Figure 10).

Neuregulin

While axon-associated neuregulin 1 type III is an obligatory survival signal for Schwann cell precursors (Jessen et al., 1994; Dong et al., 1995) and drives developmental myelination (Taveggia et al., 2005), soluble neuregulin 1 type I is expressed by adult Schwann cells and has a role in repair. Nerve injury triggers a strong elevation of neuregulin 1 type I in the Schwann cells of the distal stump that peaks a few days

after injury but is significantly reduced after 10–14 days as axons regenerate and re-myelination takes place (Stassart et al., 2013). In chronically denervated Schwann cells, neuregulin 1 expression also declines, albeit much more slowly (Ronchi et al., 2017). Neuregulin 1 applied to regenerating nerves promotes repair in a variety of settings (Mancuso et al., 2016; Yasui et al., 2016; reviewed in Gambarotta et al., 2014; El Soury and Gambarotta, 2019). The mechanism by which this works is likely to be *via* direct effects on repair cells and perhaps macrophages. Neuregulin 1 activates multiple signaling pathways in Schwann cells including the PI3K–Akt pathway, ERK1/2–MAPK, and calcineurin–NFAT pathways among others (reviewed in Fricker and Bennett, 2011) and can promote Schwann cell proliferation and migration (Chang et al., 2013). Increased neuregulin signaling to repair cells *in vivo*, by overexpression of ErbB2 receptors strongly elevates c-Jun expression and promotes axonal regeneration (Han et al., 2017). In agreement, soluble neuregulin 1 type I applied at relatively high concentrations *in vitro*, activates c-Jun and other genes associated with the injury response and suppresses myelin genes (Syed et al., 2010; El Soury et al., 2018). These effects are concentration-dependent, since at lower concentrations, soluble neuregulin 1 promotes myelination (Syed et al., 2010). The effects of neuregulin 1 are also context-dependent and regulated by the cAMP pathway, an important driver of myelination (Monk et al., 2015). When cAMP activation is weak, a high concentration of soluble neuregulin 1 drives Schwann-cell proliferation (Arthur-Farraj et al., 2011), and under these conditions neuregulin 1 induces Schwann cells to secrete factors that promote sympathetic neuron survival and axon outgrowth (Mahanthappa et al., 1996), features characteristic of the repair cell phenotype. However, when cAMP activation is strong, neuregulin 1 triggers the appearance of non-dividing cells that express myelin genes (Arthur-Farraj et al., 2011).

These data are consistent with the view that Schwann cell neuregulin 1 activation functions in an autocrine manner to support nerve repair. Early after injury,

high levels of Schwann cell derived neuregulin suppress myelin genes, activate c-Jun and promote Schwann cell reprogramming to repair cells resulting, indirectly, in the stimulation of axonal regeneration (Mahanthappa et al., 1996; Gambarotta et al., 2014). At later times, when myelination starts, neuregulin 1 levels are lower and cAMP signaling stronger, and neuregulin 1 promotes myelination (Syed et al., 2010; Stassart et al., 2013).

Glial Derived Neurotrophic Factor (GDNF)

GDNF is expressed in Schwann cells and up-regulated at the mRNA and protein level after injury, while during chronic denervation, GDNF levels, like those of Shh and c-Jun, gradually decline (Trupp et al., 1995; Naveilhan et al., 1997; Höke et al., 2000, 2002; Barras et al., 2002; Eggers et al., 2010; Fontana et al., 2012; Xu et al., 2013). GDNF is a survival factor for spinal cord motor neurons and a subpopulation of DRG neurons, and application of GDNF to injured adult peripheral nerves protects the spinal cord and facial motor neurons and promotes axonal regeneration (Li et al., 1995; Yan et al., 1995; Naveilhan et al., 1997; Bennett et al., 1998; Chen et al., 2001; Piquilloud et al., 2007; Eggers et al., 2008). GDNF acts on Schwann cells through GFR α 1/NCAM signaling to affect multiple intracellular pathways, including ERK1/2, CREB, PKA, and PKC (Iwase et al., 2005). Notably, enhanced expression of GDNF in Schwann cells promotes the repair Schwann cell state and inhibits the switch to myelination (Eggers et al., 2013). GDNF is therefore likely to promote regeneration directly and indirectly through action on repair cells and neurons.

Transforming Growth Factor β (TGF β)

TGF β is expressed and secreted from Schwann cells and up-regulated after nerve injury (Unsicker et al., 1991; Scherer et al., 1993; Einheber et al., 1995; Stewart et al., 1995; Li et al., 2015). TGF β has multiple effects on Schwann cells. TGF β induces Schwann cell migration (Clements et al., 2017), and promotes either proliferation or apoptosis depending on the status of several other parameters. These include c-Jun levels, cell differentiation state, cell density, and the presence of other signals such as neuregulin 1 or activation of cAMP pathways (D'Antonio et al., 2006; Li et al., 2015 and references therein). TGF β inhibits cAMP-dependent myelin protein expression in Schwann cell cultures and myelination in neuron-Schwann cell cocultures (Morgan et al., 1994; Einheber et al., 1995; Stewart et al., 1995). TGF β applied to cultured Schwann cells also activates c-Jun (Parkinson et al., 2001), and up-regulates the adhesion molecules NCAM and L1 that are expressed by repair cells, but not myelin cells. All of this, suggests that the autocrine effect of TGF β after nerve injury is to promote Schwann cell reprogramming and the expression and function of the repair cell phenotype. Importantly, there is also evidence that TGF β is required for the neurotrophic effect of GDNF, a factor that, in turn, is thought to be central for nerve repair (see above; reviewed in Kriegelstein et al., 2002). Potentially, TGF β also suppresses the function of macrophages in injured nerves, a function that

has been suggested to promote nerve regeneration (Vidal et al., 2013).

Application of TGF β to injured peripheral nerves is reported to promote regeneration although this field has not yet been studied extensively (Sulaiman and Dreesen, 2014; Wang et al., 2016; reviewed in Sulaiman and Nguyen, 2016; Li et al., 2017). The underlying mechanisms are unclear. In view of the multiple functions of TGF β , they are likely to be complex and include the promotion of Schwann cell reprogramming and expression of repair supportive features by these cells, promotion of GDNF signaling to neurons, as well as immunosuppression, in addition to direct effects on regenerating axons.

Insulin-Like Growth Factor 1 (IGF-1)

IGF1, IGF binding proteins, and the type 1 IGF receptor are up-regulated in Schwann cells of injured nerves (Pu et al., 1995; Cheng et al., 1996; Hammarberg et al., 1998; reviewed in Sullivan et al., 2008). IGF-1 regulates several functions in Schwann cells that are relevant to the essential activity of repair cells after injury. This includes the promotion of cell motility, process extension, survival, and proliferation (Stewart et al., 1996; Syroid et al., 1999; Cheng et al., 2000; Delaney et al., 2001). Potentially, IGF-1 also promotes myelination, since in a defined culture medium in the presence of low cAMP pathway activation, IGF-1 induces the expression of the myelin lipid galactocerebroside and the major myelin protein P0 (MPZ; Stewart et al., 1996). IGF-1 also acts directly on neurons to support neurite outgrowth *in vitro*, and *in vivo* application of IGF-1 to injured nerves promotes regeneration in several different settings (Nachemson et al., 1990; Fansa et al., 2002; Apel et al., 2010; Bayrak et al., 2017; reviewed in Sullivan et al., 2008; Slavin et al., 2021). This is likely due to the combination of autocrine IGF-1 action to promote repair cell function and direct effects on neurons.

In addition to the molecules reviewed above, other factors, including neurotrophins, FGF2, PDGF, and VEGF may also function to support repair cells, in addition to their other effects in injured nerves, although the evidence, outlined below, is less complete.

Neurotrophins

These factors have been extensively studied in the context of Schwann cell development and myelination, but the role of neurotrophins in these processes is still unclear (reviewed in Xiao et al., 2009). Although Schwann cells express the neurotrophin receptors p75NTR, TrkC, and truncated TrkB, and Schwann cell levels of NGF, NT4, and BDNF increase after injury, it is unclear to what extent this represents autocrine signaling loops. The expression of Trk receptors on neurons is widespread and the application of neurotrophins to injured nerves increases axon sprouts. After chronic denervation when BDNF levels in repair cells have declined, application of BDNF increases the number of regenerating neurons, but in most other experimental situations it remains to be resolved whether application of neurotrophins to injured nerves promotes significant axonal regeneration, or is

mostly restricted to inducing axonal sprouting (reviewed in Gordon, 2009).

Fibroblast Growth Factor 2 (FGF2)

FGF2 and FGF receptors (FGFR) are up-regulated in Schwann cells and neurons after nerve injury. Yet, much remains to be learned about the role of this system in nerve repair, since the effects of FGF2 appear to be subtle and complex and depend on the neuron type, FGF2 isoform, and FGFR type involved (reviewed in Grothe and Nikkhah, 2001; Grothe et al., 2006). *In vitro*, FGF2 stimulates Schwann cell proliferation and inhibits myelin gene expression (Davis and Stroobant, 1990; Morgan et al., 1994), and studies on mice in which FGF2 is deleted or over-expressed suggest that these effects can also be seen near the site of nerve crush *in vivo* (Haastert et al., 2006; reviewed in Grothe et al., 2006). DRG neurons also up-regulate FGF2 and FGFRs after injury and FGF2 appears to act directly on neurons to stimulate neurite outgrowth (Unsicker et al., 1987 and references therein; Fujimoto et al., 1997). There is evidence that applied FGF2 promotes axonal regeneration across regeneration inserts and accelerates the functional recovery of sensory fibers (Aebischer et al., 1989; Haastert et al., 2006), but it is unclear to what extent these or other effects of FGF2 *in vivo* are due to direct effects on Schwann cells. Further, after nerve injury, up-regulation of FGF2 and FGFR is restricted to the site of damage (Grothe et al., 2001), suggesting a limited role for this system in the repair cells of the distal stump.

Platelet-Derived Growth Factor (PDGF)

PDGF and PDGF receptors are up-regulated in Schwann cells after nerve injury (Oya et al., 2002; Yamazaki et al., 2009), and cultured Schwann cells secrete PDGF that promotes both Schwann cell proliferation and survival (Davis and Stroobant, 1990; Eccleston et al., 1990; Hardy et al., 1992; Watabe et al., 1994; Meier et al., 1999; Lobsiger et al., 2000). Neurons also express PDGF receptors and it is likely that PDGF acts directly on neurons to promote neurite extension (Smits et al., 1991; Eccleston et al., 1993; Nakao et al., 1995). There is evidence that applied PDGF promotes nerve regeneration *in vivo*, although this appears not to have been studied extensively (Golzadeh and Mohammadi, 2016; Hong et al., 2018; see however Welch et al., 1997). These data suggest that in injured nerves, PDGF works through an autocrine PDGF loop to support survival and proliferation of repair Schwann cells, in addition to PDGF acting directly on regenerating axons.

Vascular Endothelial Growth Factor (VEGF)

VEGF is expressed by Schwann cells in uninjured nerves and in culture, but does not appear to be up-regulated by Schwann cells after nerve injury (Taiana et al., 2014; Muratori et al., 2018).

There is evidence that VEGF promotes Schwann cell migration (Sondell et al., 1999a; Muratori et al., 2018), but stimulation of proliferation is controversial (Sondell et al., 1999b; Muratori et al., 2018). Applied VEGF promotes regeneration after nerve injury (Pereira Lopes et al., 2011; Wu et al., 2021), which might be due to enhanced vascularization (Sondell et al., 1999a) or direct effects on neurons (reviewed in Rosenstein et al., 2010). It has also been proposed that Schwann cell derived VEGF acts through an autocrine loop to support Schwann cells (Rosenstein et al., 2010).

CONCLUSIONS

The presence of functional repair cells is indispensable for effective regeneration. It is therefore unfortunate that the expression of their phenotype is not robust: repair cell activation falters as animals get older and the repair phenotype fades during chronic denervation. These malfunctions are important reasons for the poor outcomes after nerve damage in humans. It is essential, therefore, to learn about the signals that control and maintain repair cells. In this context, the transcription factor c-Jun is important for several reasons: First, because it acts as an amplifier of the repair phenotype and is required for the generation of functional repair cells after injury. Second, failure of c-Jun expression is linked to failures of axonal regeneration in older animals and during chronic denervation. Third, manipulation of c-Jun signaling in repair cells has proved an effective way of promoting axonal regeneration. This demonstrates, in principle, that targeting repair cells to boost their function is an efficient way of improving nerve repair.

One way to amplify the function of repair cells would be to hijack endogenous autocrine support mechanisms since there is increasing evidence that repair cells are sustained by several autocrine signaling loops. The development of methods for the localized and timed delivery of such signals to injured nerves is an attractive option for the clinical improvement of nerve injuries.

AUTHOR CONTRIBUTIONS

Both authors contributed equally to the writing and editing of the manuscript. All authors contributed to the article and approved the submitted version.

FUNDING

The work from the author's laboratory discussed in this article was supported by the Wellcome Trust (Programme Grant 074665 to KJ and RM), the Medical Research Council (Project Grant G0600967 to KJ and RM), and the European Community (Grant HEALTH-F2-2008-201535 from FP7/2007-2013).

REFERENCES

- Aebischer, P., Salessiotis, A. N., and Winn, S. R. (1989). Basic fibroblast growth factor released from synthetic guidance channels facilitates peripheral nerve regeneration across long nerve gaps. *J. Neurosci. Res.* 23, 282–289. doi: 10.1002/jnr.490230306
- Allodi, I., Udina, E., and Navarro, X. (2012). Specificity of peripheral nerve regeneration: interactions at the axon level. *Prog. Neurobiol.* 98, 16–37. doi: 10.1016/j.pneurobio.2012.05.005
- Apel, P. J., Ma, J., Callahan, M., Northam, C. N., Alton, T. B., Sonntag, W., et al. (2010). Effect of locally delivered IGF-1 on nerve regeneration during aging: an experimental study in rats. *Muscle Nerve* 41, 335–341. doi: 10.1002/mus.21485

- Arthur-Farraj, P., and Coleman, M. P. (2021). Lessons from injury: how nerve injury studies reveal basic biological mechanisms and therapeutic opportunities for peripheral nerve diseases. *Neurotherapeutics* doi: 10.1007/s13311-021-01125-3. [Online ahead of print].
- Arthur-Farraj, P. J., Latouche, M., Wilton, D. K., Quintes, S., Chabrol, E., Banerjee, A., et al. (2012). c-Jun reprograms Schwann cells of injured nerves to generate a repair cell essential for regeneration. *Neuron* 75, 633–647. doi: 10.1016/j.neuron.2012.06.021
- Arthur-Farraj, P. J., Morgan, C. C., Adamowicz, M., Gomez-Sanchez, J. A., Fazal, S. V., Beucher, A., et al. (2017). Changes in the coding and non-coding transcriptome and dna methylome that define the schwann cell repair phenotype after nerve injury. *Cell Rep.* 20, 2719–2734. doi: 10.1016/j.celrep.2017.08.064
- Arthur-Farraj, P., Wanek, K., Hantke, J., Davis, C. M., Jayakar, A., Parkinson, D. B., et al. (2011). Mouse schwann cells need both NRG1 and cyclic AMP to myelinate. *Glia* 59, 720–733. doi: 10.1002/glia.21144
- Bacallao, K., and Monje, P. V. (2015). Requirement of cAMP signaling for schwann cell differentiation restricts the onset of myelination. *PLoS One* 10:e0116948. doi: 10.1371/journal.pone.0116948
- Barras, F. M., Pasche, P., Bouche, N., Aebischer, P., and Zurn, A. D. (2002). Glial cell line-derived neurotrophic factor released by synthetic guidance channels promotes facial nerve regeneration in the rat. *J. Neurosci. Res.* 70, 746–755. doi: 10.1002/jnr.10434
- Bayrak, A. F., Olgun, Y., Ozbakan, A., Aktas, S., Kulan, C. A., Kamaci, G., et al. (2017). The effect of insulin like growth factor-1 on recovery of facial nerve crush injury. *Clin. Exp. Otorhinolaryngol.* 10, 296–302. doi: 10.21053/ceo.2016.00997
- Benito, C., Davis, C. M., Gomez-Sanchez, J. A., Turmaine, M., Meijer, D., Poli, V., et al. (2017). STAT3 controls the long-term survival and phenotype of repair schwann cells during nerve regeneration. *J. Neurosci.* 37, 4255–4269. doi: 10.1523/JNEUROSCI.3481-16.2017
- Bennett, D. L., Michael, G. J., Ramachandran, N., Munson, J. B., Averill, S., Yan, Q., et al. (1998). A distinct subgroup of small drg cells express GDNF Receptor components and GDNF is protective for these neurons after nerve injury. *J. Neurosci.* 18, 3059–3072. doi: 10.1523/JNEUROSCI.18-08-03059.1998
- Boerboom, A., Dion, V., Chariot, A., and Franzen, R. (2017). Molecular mechanisms involved in Schwann cell plasticity. *Front. Mol. Neurosci.* 10:38. doi: 10.3389/fnmol.2017.00038
- Bond, C. W., Angeloni, N., Harrington, D., Stupp, S., and Podlasek, C. A. (2013). Sonic Hedgehog regulates brain-derived neurotrophic factor in normal and regenerating cavernous nerves. *J. Sex Med.* 10, 730–737. doi: 10.1111/jsm.12030
- Boyd, J. G., and Gordon, T. (2003). Neurotrophic factors and their receptors in axonal regeneration and functional recovery after peripheral nerve injury. *Mol. Neurobiol.* 27, 277–324. doi: 10.1385/MN:27:3:277
- Chang, H.-M., Shyu, M.-K., Tseng, G.-F., Liu, C.-H., Chang, H.-S., Lan, C.-T., et al. (2013). Neuregulin Facilitates Nerve Regeneration by Speeding Schwann Cell Migration via ErbB2/3-Dependent FAK Pathway. *PLoS One* 8:e53444. doi: 10.1371/journal.pone.0053444
- Chen, Z. Y., Chai, Y. F., Cao, L., Lu, C. L., and He, C. (2001). Glial cell line-derived neurotrophic factor enhances axonal regeneration following sciatic nerve transection in adult rats. *Brain Res.* 902, 272–276. doi: 10.1016/s0006-8993(01)02395-2
- Chen, Z. L., Yu, W. M., and Strickland, S. (2007). Peripheral regeneration. *Annu. Rev. Neurosci.* 30, 209–233. doi: 10.1146/annurev.neuro.30.051606.094337
- Cheng, H. L., Steinway, M. L., Russell, J. W., and Feldman, E. L. (2000). GTPases and phosphatidylinositol 3-kinase are critical for insulin-like growth factor-I-mediated Schwann cell motility. *J. Biol. Chem.* 275, 27197–27204. doi: 10.1074/jbc.M002534200
- Cheng, H.-L., Randolph, A., Yee, D., Delafontaine, P., Tennekoon, G., and Feldman, E. L. (1996). Characterization of insulin-like growth factor-I and its receptor and binding proteins in transected nerves and cultured schwann cells. *J. Neurochem.* 66, 525–536. doi: 10.1046/j.1471-4159.1996.66020525.x
- Clements, M. P., Byrne, E., Camarillo Guerrero, L. F., Cattin, A. L., Zakka, L., Ashraf, A., et al. (2017). The wound microenvironment reprograms Schwann cells to invasive mesenchymal-like cells to drive peripheral nerve regeneration. *Neuron* 96, 98–114.e7. doi: 10.1016/j.neuron.2017.09.008
- D'Antonio, M., Droggiti, M., Feltri, M. L., Roes, J., Wrabetz, L., Mirsky, R., et al. (2006). TGFbeta type II receptor signaling controls Schwann cell death and proliferation in developing nerves. *J. Neurosci.* 26, 8417–8427. doi: 10.1523/JNEUROSCI.1578-06.2006
- Davis, J. B., and Stroobant, P. (1990). Platelet-derived growth factors and fibroblast growth factors are mitogens for rat Schwann cells. *J. Cell Biol.* 110, 1353–1360. doi: 10.1083/jcb.110.4.1353
- De Felipe, C., and Hunt, S. P. (1994). The differential control of c-jun expression in regenerating sensory neurons and their associated glial cells. *J. Neurosci.* 14, 2911–2923. doi: 10.1523/JNEUROSCI.14-05-02911.1994
- Delaney, C. L., Russel, J. W., Cheng, H. L., and Feldman, E. L. (2001). Insulin-like growth factor-I and over-expression of bcl-xL prevent glucose-mediated apoptosis in Schwann cells. *J. Neuropathol. Exp. Neurol.* 60, 147–160. doi: 10.1093/jnen/60.2.147
- Dong, Z., Brennan, A., Liu, N., Yarden, Y., Lefkowitz, G., Mirsky, R., et al. (1995). Neu differentiation factor is a neuron-glia signal and regulates survival, proliferation and maturation of rat Schwann cell precursors. *Neuron* 15, 585–596. doi: 10.1016/0896-6273(95)90147-7
- Doron-Mandel, E., Fainzilber, M., and Terenzio, M. (2015). Growth control mechanisms in neuronal regeneration. *FEBS Lett.* 589, 1669–1677. doi: 10.1016/j.febslet.2015.04.046
- Eccleston, P. A., Collarini, E. J., Jessen, K. R., Mirsky, R., and Richardson, W. D. (1990). Schwann cells secrete a PDGF-like factor: evidence for an autocrine growth mechanism involving PDGF. *Eur. J. Neurosci.* 2, 985–992. doi: 10.1111/j.1460-9568.1990.tb00011.x
- Eccleston, P. A., Funa, K., and Heldin, C. H. (1993). Expression of platelet-derived growth factor (PDGF) and PDGF alpha- and beta-receptors in the peripheral nervous system: an analysis of sciatic nerve and dorsal root ganglia. *Dev. Biol.* 155, 459–470. doi: 10.1006/dbio.1993.1044
- Eggers, R., de Winter, F., Hoyng, S. A., Roet, K. C. D., Ehlert, E. M., Malessy, M. J. A., et al. (2013). Lentiviral vector-mediated gradients of GDNF in the injured peripheral nerve: effects on nerve coil formation, schwann cell maturation and myelination. *PLoS One* 8:e71076. doi: 10.1371/journal.pone.0071076
- Eggers, R., Hendriks, W. T. J., Tannemaat, M. R., van Heerikhuizen, J. J., Pool, C. W., Carlstedt, T. P., et al. (2008). Neuroregenerative effects of lentiviral vector-mediated GDNF expression in reimplanted ventral roots. *Mol. Cell. Neurosci.* 39, 105–117. doi: 10.1016/j.mcn.2008.05.018
- Eggers, R., Tannemaat, M. R., Ehlert, E. M., and Verhaagen, J. (2010). A spatio-temporal analysis of motoneuron survival, axonal regeneration and neurotrophic factor expression after lumbar ventral root avulsion and implantation. *Exp. Neurol.* 223, 207–220. doi: 10.1016/j.expneurol.2009.07.021
- Einheber, S., Hannocks, M. J., Metz, C. N., Rifkin, D. B., and Salzer, J. L. (1995). Transforming growth factor-beta 1 regulates axon/Schwann cell interactions. *J. Cell Biol.* 129, 443–458. doi: 10.1083/jcb.129.2.443
- El Soury, M., Fornasari, B. E., Morano, M., Grazio, E., Ronchi, G., Incarnato, D., et al. (2018). Soluble neuregulin1 down-regulates myelination genes in schwann cells. *Front. Mol. Neurosci.* 11:157. doi: 10.3389/fnmol.2018.00157
- El Soury, M., and Gambarotta, G. (2019). Soluble neuregulin-1 (NRG1): a factor promoting peripheral nerve regeneration by affecting Schwann cell activity immediately after injury. *Neural Regen. Res.* 14, 1374–1375. doi: 10.4103/1673-5374.253516
- Fansa, H., Schneider, W., Wolf, G., and Keilhoff, G. (2002). Influence of insulin-like growth factor-I (IGF-I) on nerve autografts and tissue-engineered nerve grafts. *Muscle Nerve* 26, 87–93. doi: 10.1002/mus.10165
- Fawcett, J. W., and Verhaagen, J. (2018). Intrinsic determinants of axon regeneration. *Dev. Neurobiol.* 78, 890–897. doi: 10.1002/dneu.22637
- Fazal, S. V., Gomez-Sanchez, J. A., Wagstaff, L. J., Musner, N., Otto, G., Janz, M., et al. (2017). Graded elevation of c-jun in Schwann Cells in vivo: gene dosage determines effects on development, remyelination, tumorigenesis and hypomyelination. *J. Neurosci.* 37, 12297–12313. doi: 10.1523/JNEUROSCI.0986-17.2017
- Florio, F., Ferri, C., Scapin, C., Feltri, M. L., Wrabetz, L., and D'Antonio, M. (2018). Sustained expression of negative regulators of myelination protects schwann cells from dysmyelination in a Charcot-Marie-Tooth 1B mouse model. *J. Neurosci.* 38, 4275–4287. doi: 10.1523/JNEUROSCI.0201-18.2018
- Fontana, X., Hristova, M., Da Costa, C., Patodia, S., Thei, L., Makwana, M., et al. (2012). c-Jun in Schwann cells promotes axonal regeneration and motoneuron survival via paracrine signaling. *J. Cell Biol.* 198, 127–141. doi: 10.1083/jcb.201205025

- Fricker, F. R., Antunes-Martins, A., Galino, J., Paramsothy, R., La Russa, F., Perkins, J., et al. (2013). Axonal neuregulin 1 is a rate limiting but not essential factor for nerve remyelination. *Brain* 136, 2279–2297. doi: 10.1093/brain/awt148
- Fricker, F. R., and Bennett, D. H. L. (2011). The role of neuregulin-1 in the response to nerve injury. *Future Neurol.* 6, 809–822. doi: 10.2217/fnl.11.45
- Fu, S. Y., and Gordon, T. (1995). Contributing factors to poor functional recovery after delayed nerve repair: prolonged denervation. *J. Neurosci.* 15, 3886–3895. doi: 10.1523/JNEUROSCI.15-05-03886.1995
- Fujimoto, E., Mizoguchi, A., Hanada, K., Yahima, M., and Ide, C. (1997). Basic fibroblast growth factor promotes extension of regenerating axons of peripheral nerve. *In vivo* experiments using a schwann cell basal lamina tube model. *J. Neurocytol.* 26, 511–528. doi: 10.1023/a:1015410023132
- Gambarotta, G., Ronchi, G., Geuna, S., and Perroteau, I. (2014). Neuregulin 1 isoforms could be an effective therapeutic candidate to promote peripheral nerve regeneration. *Neural Regen. Res.* 9, 1183–1185. doi: 10.4103/1673-5374.135324
- Glenn, T. D., and Talbot, W. S. (2013). Signals regulating myelination in peripheral nerves and the Schwann cell response to injury. *Curr. Opin. Neurobiol.* 23, 1041–1048. doi: 10.1016/j.conb.2013.06.010
- Golzadeh, A., and Mohammadi, R. (2016). Effect of local administration of platelet-derived growth factor B on functional recovery of peripheral nerve regeneration: a sciatic nerve transection model. *Dent. Res. J. (Isfahan)* 13, 225–232. doi: 10.4103/1735-3327.182181
- Gomez-Sanchez, J. A., Carty, L., Iruarizaga-Lejarreta, M., Palomo-Irigoyen, M., Varela-Rey, M., Griffith, M., et al. (2015). Schwann cell autophagy, myelinophagy, initiates myelin clearance from injured nerves. *J. Cell Biol.* 210, 153–168. doi: 10.1083/jcb.201503019
- Gomez-Sanchez, J. A., Pilch, K. S., van der Lans, M., Fazal, S. V., Benito, C., Wagstaff, L. J., et al. (2017). After nerve injury, lineage tracing shows that myelin and remak schwann cells elongate extensively and branch to form repair schwann cells, which shorten radically on remyelination. *J. Neurosci.* 37, 9086–9099. doi: 10.1523/JNEUROSCI.1453-17.2017
- Gordon, T. (2009). The role of neurotrophic factors in nerve regeneration. *Neurosurg. Focus* 26:E3. doi: 10.3171/FOC.2009.26.2.E3
- Grothe, C., Haastert, K., and Jungnickel, J. (2006). Physiological function and putative therapeutic impact of the FGF-2 system in peripheral nerve regeneration—lessons from *in vivo* studies in mice and rats. *Brain Res. Rev.* 51, 293–299. doi: 10.1016/j.brainresrev.2005.12.001
- Grothe, C., Meisinger, C., and Claus, P. (2001). *In vivo* expression and localization of the fibroblast growth factor system in the intact and lesioned rat peripheral nerve and spinal ganglia. *J. Comp. Neurol.* 434, 342–357. doi: 10.1002/cne.1181
- Grothe, C., and Nikkhah, G. (2001). The role of basic fibroblast growth factor in peripheral nerve regeneration. *Anat. Embryol. (Berl)* 204, 171–177. doi: 10.1007/s004290100205
- Gutmann, E., Guttmann, L., Medawar, P. B., and Young, J. Z. (1942). The rate of regeneration of nerve. *J. Exp. Biol.* 19, 14–44. doi: 10.1242/jeb.19.1.14
- Haastert, K., Lipokatic, E., Fischer, M., Timmer, M., and Grothe, C. (2006). Differentially promoted peripheral nerve regeneration by grafted Schwann cells over-expressing different FGF-2 isoforms. *Neurobiol. Dis.* 21, 138–153. doi: 10.1016/j.nbd.2005.06.020
- Hammarberg, H., Risling, M., Hökfelt, T., Cullheim, S., and Piehl, F. (1998). Expression of insulin-like growth factors and corresponding binding proteins (IGFBP 1–6) in rat spinal cord and peripheral nerve after axonal injuries. *J. Comp. Neurol.* 400, 57–72.
- Han, S. B., Kim, H., Lee, H., Grove, M., Smith, G. M., and Son, Y. J. (2017). Postinjury induction of activated ErbB2 selectively hyperactivates denervated schwann cells and promotes robust dorsal root axon regeneration. *J. Neurosci.* 37, 10955–10970. doi: 10.1523/JNEUROSCI.0903-17.2017
- Hantke, J., Carty, L., Wagstaff, L. J., Turmaine, M., Wilton, D. K., Quintes, S., et al. (2014). c-Jun activation in Schwann cells protects against loss of sensory axons in inherited neuropathy. *Brain* 137, 2922–2937. doi: 10.1093/brain/awu257
- Hardy, M., Reddy, U. R., and Pleasure, D. (1992). Platelet-derived growth factor and regulation of Schwann cell proliferation *in vivo*. *J. Neurosci. Res.* 31, 254–262. doi: 10.1002/jnr.490310206
- Hashimoto, M., Ishii, K., Nakamura, Y., Watabe, K., Kohsaka, S., and Akazawa, C. (2008). Neuroprotective effect of sonic hedgehog up-regulated in Schwann cells following sciatic nerve injury. *J. Neurochem.* 107, 918–927. doi: 10.1111/j.1471-4159.2008.05666.x
- Höke, A. (2006). Mechanisms of disease: what factors limit the success of peripheral nerve regeneration in humans? *Nat. Clin. Pract. Neurol.* 2, 448–454. doi: 10.1038/ncpneurol0262
- Höke, A., and Brushart, T. (2010). Introduction to special issue: challenges and opportunities for regeneration in the peripheral nervous system. *Exp. Neurol.* 223, 1–4. doi: 10.1016/j.expneurol.2009.12.001
- Höke, A., Cheng, C., and Zochodne, D. W. (2000). Expression of glial cell line-derived neurotrophic factor family of growth factors in peripheral nerve injury in rats. *Neuroreport* 11, 1651–1654. doi: 10.1097/00001756-200006050-00011
- Höke, A., Gordon, T., Zochodne, D. W., and Sulaiman, O. A. (2002). A decline in glial cell-line-derived neurotrophic factor expression is associated with impaired regeneration after long-term schwann cell denervation. *Exp. Neurol.* 173, 77–85. doi: 10.1002/ejhf.2419
- Holmes, W., and Young, J. Z. (1942). Nerve regeneration after immediate and delayed suture. *J. Anat.* 77, 63–96.10.
- Hong, M. H., Hong, H. J., Pang, H., Lee, H. J., Yi, S., and Koh, W. G. (2018). Controlled release of growth factors from multilayered fibrous scaffold for functional recoveries in crushed sciatic nerve. *ACS Biomater. Sci. Eng.* 4, 576–586. doi: 10.1021/acsbomaterials.7b00801
- Huang, L., Xia, B., Shi, X., Gao, J., Yang, Y., Xu, F., et al. (2019). Time-restricted release of multiple neurotrophic factors promotes axonal regeneration and functional recovery after peripheral nerve injury. *FASEB J.* 33, 8600–8613. doi: 10.1096/fj.201802065RR
- Hung, H. A., Sun, G., Keles, S., and Svaren, J. (2015). Dynamic regulation of Schwann cell enhancers after peripheral nerve injury. *J. Biol. Chem.* 290, 6937–6950. doi: 10.1074/jbc.M114.622878
- Hutton, E. J., Carty, L., Laurá, M., Houlden, H., Lunn, M. P., Brandner, S., et al. (2011). c-Jun expression in human neuropathies: a pilot study. *J. Peripher. Nerv. Syst.* 16, 295–303. doi: 10.1111/j.1529-8027.2011.00360.x
- Iwase, T., Jung, C. G., Bae, H., Zhang, M., and Soliven, B. (2005). Glial cell line-derived neurotrophic factor-induced signaling in Schwann cells. *J. Neurochem.* 94, 1488–1499. doi: 10.1111/j.1471-4159.2005.03290.x
- Jacobs, J. M., and Cavanagh, J. B. (1969). Species differences in internode formation following two types of peripheral nerve injury. *J. Anat.* 105, 295–306.
- Jessen, K. R., and Arthur-Farraj, P. (2019). Repair schwann cell update: adaptive reprogramming, EMT and stemness in regenerating nerves. *Glia* 67, 421–437. doi: 10.1002/glia.23532
- Jessen, K. R., and Mirsky, R. (2019a). Schwann cell precursors; multipotent glial cells in embryonic nerves. *Front. Mol. Neurosci.* 12:69. doi: 10.3389/fnmol.2019.00069
- Jessen, K. R., and Mirsky, R. (2019b). The success and failure of the Schwann cell response to nerve injury. *Front. Cell. Neurosci.* 13:33. doi: 10.3389/fncel.2019.00033
- Jessen, K. R., Brennan, A., Morgan, L., Mirsky, R., Kent, A., Hashimoto, Y., et al. (1994). The Schwann cell precursor and its fate: a study of cell death and differentiation during gliogenesis in rat embryonic nerves. *Neuron* 12, 509–527. doi: 10.1016/0896-6273(94)90209-7
- Jessen, K. R., and Mirsky, R. (2005). The origin and development of glial cells in peripheral nerves. *Nat. Rev. Neurosci.* 6, 671–682. doi: 10.1038/nrn1746
- Jessen, K. R., and Mirsky, R. (2016). The repair Schwann cell and its function in regenerating nerves. *J. Physiol.* 594, 3521–3531. doi: 10.1113/JP270874
- Jessen, K. R., and Mirsky, R. (2008). Negative regulation of myelination: relevance for development, injury and demyelinating disease. *Glia* 56, 1552–1565. doi: 10.1002/glia.20761
- Jessen, K. R., Mirsky, R., and Arthur-Farraj, P. (2015). The role of cell plasticity in tissue repair: adaptive cellular reprogramming. *Dev. Cell* 34, 613–620. doi: 10.1016/j.devcel.2015.09.005
- Jonsson, S., Wiberg, R., McGrath, A. M., Novikov, L. N., Wiberg, M., Novikova, L. N., et al. (2013). Effect of delayed peripheral nerve repair on nerve regeneration, schwann cell function and target muscle recovery. *PLoS One* 8:e56484. doi: 10.1371/journal.pone.0056484
- Kim, H. A., Pomeroy, S. L., Whoriskey, W., Pawlitzky, I., Benowitz, L. I., Sicinski, P., et al. (2000). A developmentally regulated switch directs regenerative growth of Schwann cells through cyclin D1. *Neuron* 26, 405–416. doi: 10.1016/s0896-6273(00)81173-3

- Klein, D., Groh, J., Wettmarshausen, J., and Martini, R. (2014). Nonuniform molecular features of myelinating Schwann cells in models for CMT1: distinct disease patterns are associated with NCAM and c-Jun upregulation. *Glia* 62, 736–750. doi: 10.1002/glia.22638
- Kolter, J., Kierdorf, K., and Henneke, P. (2020). Origin and differentiation of nerve-associated macrophages. *J. Immunol.* 204, 271–279. doi: 10.4049/jimmunol.1901077
- Kriegstein, K., Strelau, J., Schober, A., Sullivan, A., and Unsicker, K. (2002). TGF-beta and the regulation of neuron survival and death. *J. Physiol. Paris* 96, 25–30. doi: 10.1016/s0928-4257(01)00077-8
- Li, S., Gu, X., and Yi, S. (2017). The regulatory effects of transforming growth factor- β on nerve regeneration. *Cell Transplant.* 26, 381–394. doi: 10.3727/096368916X693824
- Li, L., Wu, W., Lin, L. F., Lei, M., Oppenheim, R. W., and Houenou, L. J. (1995). Rescue of adult mouse motoneurons from injury-induced cell death by glial cell line-derived neurotrophic factor. *Proc. Natl. Acad. Sci. U S A* 92, 9771–9775. doi: 10.1073/pnas.92.21.9771
- Li, M., Zhang, P., Li, H., Zhu, Y., Cui, S., and Yao, D. (2015). TGF- β 1 is critical for Wallerian degeneration after rat sciatic nerve injury. *Neuroscience* 284, 759–767. doi: 10.1016/j.neuroscience.2014.10.051
- Lobsiger, C. S., Schweitzer, B., Taylor, V., and Suter, U. (2000). Platelet-derived growth factor-BB supports the survival of cultured rat Schwann cell precursors in synergy with neurotrophin-3. *Glia* 30, 290–300. doi: 10.1002/(sici)1098-1136(200005)30:3<290::aid-glia8>3.0.co;2-6
- Ma, K. H., Hung, H. A., and Svaren, J. (2016). Epigenomic regulation of Schwann cell reprogramming in peripheral nerve injury. *J. Neurosci.* 36, 9135–9147. doi: 10.1523/JNEUROSCI.1370-16.2016
- Ma, K. H., and Svaren, J. (2018). Epigenetic control of schwann cells. *Neuroscientist* 24, 627–638. doi: 10.1177/1073858417751112
- Mahanthappa, N. K., Anton, E. S., and Matthew, W. D. (1996). Glial growth factor 2, a soluble neuregulin, directly increases Schwann cell motility and indirectly promotes neurite outgrowth. *J. Neurosci.* 16, 4673–4683. doi: 10.1523/JNEUROSCI.16-15-04673.1996
- Mancuso, R., Martínez-Muriana, A., Leiva, T., Gregorio, D., Ariza, L., Morell, M., et al. (2016). Neuregulin-1 promotes functional improvement by enhancing collateral sprouting in SOD1(G93A) ALS mice and after partial muscle denervation. *Neurobiol. Dis.* 95, 168–178. doi: 10.1016/j.nbd.2016.07.023
- Martinez, J. A., Kobayashi, M., Krishnan, A., Webber, C., Christie, K., Guo, G., et al. (2015). Intrinsic facilitation of adult peripheral nerve regeneration by the Sonic hedgehog morphogen. *Exp. Neurol.* 271, 493–505. doi: 10.1016/j.expneurol.2015.07.018
- Meier, C., Parmantier, E., Brennan, A., Mirsky, R., and Jessen, K. R. (1999). Developing Schwann cells acquire the ability to survive without axons by establishing an autocrine circuit involving insulin-like growth factor, neurotrophin-3 and platelet-derived growth factor-BB. *J. Neurosci.* 19, 3847–3859. doi: 10.1523/JNEUROSCI.19-10-03847.1999
- Min, Q., Parkinson, D. B., and Dun, X. P. (2021). Migrating Schwann cells direct axon regeneration within the peripheral nerve bridge. *Glia* 69, 235–254. doi: 10.1002/glia.23892
- Mindos, T., Dun, X. P., North, K., Doddrell, R. D., Schulz, A., Edwards, P., et al. (2017). Merlin controls the repair capacity of Schwann cells after injury by regulating Hippo/YAP activity. *J. Cell Biol.* 216, 495–510. doi: 10.1083/jcb.201606052
- Monk, K. R., Feltri, M. L., and Taveggia, C. (2015). New insights on Schwann cell development. *Glia* 63, 1376–1393. doi: 10.1002/glia.22852
- Monuki, E. S., Weinmaster, G., Kuhn, R., and Lemke, G. (1989). SCIP: a glial POU domain gene regulated by cyclic AMP. *Neuron* 3, 783–793. doi: 10.1016/0896-6273(89)90247-x
- Moreau, N., and Boucher, Y. (2020). Hedging against neuropathic pain: role of hedgehog signaling in pathological nerve healing. *Int. J. Mol. Sci.* 21:9115. doi: 10.3390/ijms21239115
- Morgan, L., Jessen, K. R., and Mirsky, R. (1994). Negative regulation of the Po gene in Schwann cells: suppression of Po mRNA and protein induction in cultured Schwann cells by FGF2 and TGF beta 1, TGF beta 2 and TGF beta 3. *Development* 120, 1399–1409.
- Morgan, L., Jessen, K. R., and Mirsky, R. (1991). The effects of cAMP on differentiation of cultured Schwann cells: progression from an early phenotype (04+) to a myelin phenotype (P0+, GFAP-, N-CAM-, NGF-receptor-) depends on growth inhibition. *J. Cell Biol.* 112, 457–467. doi: 10.1083/jcb.112.3.457
- Muratori, L., Gnani, S., Fregnan, F., Mancardi, A., Raimondo, S., Perroteau, I., et al. (2018). Evaluation of vascular endothelial growth factor (VEGF) and its family member expression after peripheral nerve regeneration and denervation. *Anat. Rec. (Hoboken)* 301, 1646–1656. doi: 10.1002/ar.23842
- Nachemson, A. K., Lundborg, G., and Hansson, H. A. (1990). Insulin-like growth factor I promotes nerve regeneration: an experimental study on rat sciatic nerve. *Growth Factors* 3, 309–314. doi: 10.3109/08977199009003673
- Nakao, N., Brundin, P., Funa, K., Lindvall, O., and Odin, P. (1995). Trophic and protective actions of brain-derived neurotrophic factor on striatal DARPP-32-containing neurons *in vitro*. *Brain Res. Dev. Brain Res.* 90, 92–101. doi: 10.1016/0165-3806(96)83489-4
- Naveilhan, P., ElShamy, W. M., and Ernfors, P. (1997). Differential regulation of mRNAs for GDNF and its receptors Ret and GDNFR alpha after sciatic nerve lesion in the mouse. *Eur. J. Neurosci.* 9, 1450–1460. doi: 10.1111/j.1460-9568.1997.tb01499.x
- Nocera, G., and Jacob, C. (2020). Mechanisms of Schwann cell plasticity involved in peripheral nerve repair after injury. *Cell. Mol. Life Sci.* 77, 3977–3989. doi: 10.1007/s00018-020-03516-9
- Oya, T., Zhao, Y.-L., Takagawa, K., Kawaguchi, M., Shirakawa, K., Yamauchi, T., et al. (2002). Platelet-derived growth factor-b expression induced after rat peripheral nerve injuries. *Glia* 38, 303–312. doi: 10.1002/glia.10074
- Painter, M. W. (2017). Aging Schwann cells: mechanisms, implications, future directions. *Curr. Opin. Neurobiol.* 47, 203–208. doi: 10.1016/j.conb.2017.10.022
- Parkinson, D. B., Bhaskaran, A., Arthur-Farraj, P., Noon, L. A., Woodhoo, A., Lloyd, A. C., et al. (2008). c-Jun is a negative regulator of myelination. *J. Cell Biol.* 181, 625–637. doi: 10.1083/jcb.200803013
- Parkinson, D. B., Bhaskaran, A., Droggiti, A., Dickinson, S., D'Antonio, M., Mirsky, R., et al. (2004). Krox-20 inhibits Jun-NH2-terminal kinase/c-Jun to control Schwann cell proliferation and death. *J. Cell Biol.* 164, 385–394. doi: 10.1083/jcb.200307132
- Painter, M. W., Brosius Lutz, A., Cheng, Y. C., Latremoliere, A., Duong, K., Miller, C. M., et al. (2014). Diminished Schwann cell repair responses underlie age-associated impaired axonal regeneration. *Neuron* 83, 331–343. doi: 10.1016/j.neuron.2014.06.016
- Parkinson, D. B., Dong, Z., Bunting, H., Whitfield, J., Meier, C., Marie, H., et al. (2001). Transforming growth factor beta (TGF β) mediates Schwann cell death *in vitro* and *in vivo*: examination of c-Jun activation, interactions with survival signals and the relationship of TGF-mediated death to Schwann cell differentiation. *J. Neurosci.* 21, 8572–8585. doi: 10.1523/JNEUROSCI.21-21-08572.2001
- Pepinsky, R. B., Shapiro, R. I., Wang, S., Chakraborty, A., Gill, A., Lepage, D. J., et al. (2002). Long-acting forms of sonic hedgehog with improved pharmacokinetic and pharmacodynamic properties are efficacious in a nerve injury model. *J. Pharm. Sci.* 91, 371–387. doi: 10.1002/jps.10052
- Pereira Lopes, F. R., Lisboa, B. C. G., Frattini, F., Almeida, F. M., Tomaz, M. A., Matsumoto, P. K., et al. (2011). Enhancement of sciatic nerve regeneration after vascular endothelial growth factor (VEGF) gene therapy. *Neuropathol. Appl. Neurobiol.* 37, 600–612. doi: 10.1111/j.1365-2990.2011.01159.x
- Piquilloud, G., Christen, T., Pfister, L. A., Gander, B., and Papaliozios, M. Y. (2007). Variations in glial cell line-derived neurotrophic factor release from biodegradable nerve conduits modify the rate of functional motor recovery after rat primary nerve repairs. *Eur. J. Neurosci.* 26, 1109–1117. doi: 10.1111/j.1460-9568.2007.05748.x
- Pu, S. F., Zhuang, H. X., and Ishii, D. N. (1995). Differential spatio-temporal expression of the insulin-like growth factor genes in regenerating sciatic nerve. *Brain Res. Mol. Brain Res.* 34, 18–28. doi: 10.1016/0169-328x(95)00116-a
- Raivich, G., Bohatschek, M., Da Costa, C., Iwata, O., Galiano, M., Hristova, M., et al. (2004). The AP-1 transcription factor c-Jun is required for efficient axonal regeneration. *Neuron* 43, 57–67. doi: 10.1016/j.neuron.2004.06.005
- Roberts, S. L., Dun, X. P., Doddrell, R. D. S., Mindos, T., Drake, L. K., Onaitis, M. W., et al. (2017). Sox2 expression in Schwann cells inhibits myelination *in vivo* and induces influx of macrophages to the nerve. *Development* 144, 3114–3125. doi: 10.1016/j.neuron.2004.06.005
- Ronchi, G., Cillino, M., Gambarotta, G., Fornasari, B. E., Raimondo, S., Pugliese, P., et al. (2017). Irreversible changes occurring in long-term

- denervated Schwann cells affect delayed nerve repair. *J. Neurosurg.* 127, 843–856. doi: 10.3171/2016.9.JNS16140
- Rosenstein, J. M., Krum, J. M., and Ruhrberg, C. (2010). VEGF in the nervous system. *Organogenesis* 6, 107–114. doi: 10.4161/org.6.2.11687
- Scheib, J., and Höke, A. (2013). Advances in peripheral nerve regeneration. *Nat. Rev. Neurol.* 9, 668–676. doi: 10.1038/nrneurol.2013.227
- Scherer, S. S., Kamholz, J., and Jakowlew, S. B. (1993). Axons modulate the expression of transforming growth factor-betas in Schwann cells. *Glia* 8, 265–276. doi: 10.1002/glia.440080407
- Shy, M. E., Shi, Y., Wrabetz, L., Kamholz, J., and Scherer, S. S. (1996). Axon-Schwann cell interactions regulate the expression of c-jun in Schwann cells. *J. Neurosci. Res.* 43, 511–525. doi: 10.1002/(SICI)1097-4547(19960301)43:5<511::AID-JNR1>3.0.CO;2-L
- Slavin, B. R., Sarhane, K. A., von Guionneau, N., Hanwright, P. J., Qiu, C., Mao, H.-Q., et al. (2021). Insulin-like growth factor-1: a promising therapeutic target for peripheral nerve injury. *Front. Bioeng. Biotechnol.* 9:695850. doi: 10.3389/fbioe.2021.695850
- Smith, K. J., Hall, S. M., and Schauf, C. L. (1985). Vesicular demyelination induced by raised intracellular calcium. *J. Neurol. Sci.* 71, 19–37. doi: 10.1016/0022-510x(85)90034-6
- Smits, A., Kato, M., Westermark, B., Nistér, M., Heldin, C. H., and Funa, K. (1991). Neurotrophic activity of platelet-derived growth factor (PDGF): Rat neuronal cells possess functional PDGF beta-type receptors and respond to PDGF. *Proc. Natl. Acad. Sci. U S A* 88, 8159–8163. doi: 10.1073/pnas.88.18.8159
- Sondell, M., Lundborg, G., and Kanje, M. (1999a). Vascular endothelial growth factor stimulates Schwann cell invasion and neovascularization of acellular nerve grafts. *Brain Res.* 846, 219–228. doi: 10.1016/s0006-8993(99)02056-9
- Sondell, M., Lundborg, G., and Kanje, M. (1999b). Vascular endothelial growth factor has neurotrophic activity and stimulates axonal outgrowth, enhancing cell survival and Schwann cell proliferation in the peripheral nervous system. *J. Neurosci.* 19, 5731–5740. doi: 10.1523/JNEUROSCI.19-14-05731.1999
- Stassart, R. M., Fledrich, R., Velanac, V., Brinkmann, B. G., Schwab, M. H., Meijer, D., et al. (2013). A role for Schwann cell-derived neuregulin-1 in remyelination. *Nat. Neurosci.* 16, 48–54. doi: 10.1038/nn.3281
- Stewart, H. J. (1995). Expression of c-Jun, Jun B, Jun D and cAMP response element binding protein by Schwann cells and their precursors *in vivo* and *in vitro*. *Eur. J. Neurosci.* 7, 1366–1375. doi: 10.1111/j.1460-9568.1995.tb01128.x
- Stewart, H. J., Bradke, F., Taberner, A., Morrell, D., Jessen, K. R., and Mirsky, R. (1996). Regulation of rat Schwann cell Po expression and DNA synthesis by insulin-like growth factors *in vitro*. *Eur. J. Neurosci.* 8, 553–564. doi: 10.1111/j.1460-9568.1996.tb01240.x
- Stewart, H. J., Rougon, G., Dong, Z., Dean, C., Jessen, K. R., and Mirsky, R. (1995). TGF-betas upregulate NCAM and L1 expression in cultured Schwann cells, suppress cyclic AMP-induced expression of O4 and galactocerebroside and are widely expressed in cells of the Schwann cell lineage *in vivo*. *Glia* 15, 419–436. doi: 10.1002/glia.440150406
- Stierli, S., Imperatore, V., and Lloyd, A. C. (2019). Schwann cell plasticity-roles in tissue homeostasis, regeneration and disease. *Glia* 67, 2203–2215. doi: 10.1002/glia.23643
- Stierli, S., Napoli, I., White, I. J., Cattin, A. L., Montez Cabrejos, A., Garcia Calavia, N., et al. (2018). The regulation of the homeostasis and regeneration of peripheral nerve is distinct from the CNS and independent of a stem cell population. *Development* 145:dev170316. doi: 10.1242/dev.170316
- Sulaiman, W., and Dreesen, T. D. (2014). Effect of local application of transforming growth factor-beta at the nerve repair site following chronic axotomy and denervation on the expression of regeneration-associated genes. Laboratory Investigation. *J. Neurosurg.* 121, 859–874. doi: 10.3171/2014.4.JNS131251
- Sulaiman, O. A., and Gordon, T. (2000). Effects of short- and long-term Schwann cell denervation on peripheral nerve regeneration, myelination and size. *Glia* 32, 234–246. doi: 10.1002/1098-1136(200012)32:3<234::aid-glia40>3.0.co;2-3
- Sulaiman, O. A., and Gordon, T. (2009). Role of chronic Schwann cell denervation in poor functional recovery after nerve injuries and experimental strategies to combat it. *Neurosurgery* 65, A105–A114. doi: 10.1227/01.NEU.0000358537.30354.63
- Sulaiman, W., and Nguyen, D. H. (2016). Transforming growth factor beta 1, a cytokine with regenerative functions. *Neural Regen. Res.* 11, 1549–1552. doi: 10.4103/1673-5374.193223
- Sullivan, K. A., Kim, B., and Feldman, E. L. (2008). Insulin-like growth factors in the peripheral nervous system. *Endocrinology* 149, 5963–5971. doi: 10.1210/en.2008-1020
- Syed, N., Reddy, K., Yang, D. P., Taveggia, C., Salzer, J. L., Maurel, P., et al. (2010). Soluble neuregulin-1 has bifunctional, concentration-dependent effects on Schwann cell myelination. *J. Neurosci.* 30, 6122–6131. doi: 10.1523/JNEUROSCI.1681-09.2010
- Syroid, D. E., Zorick, T. S., Arbet-Engels, C., Kilpatrick, T. J., Eckhart, W., and Lemke, G. (1999). A role for insulin-like growth factor I in the regulation of Schwann cell survival. *J. Neurosci.* 19, 2059–2068. doi: 10.1523/JNEUROSCI.19-06-02059.1999
- Taiana, M. M., Lombardi, R., Porretta-Serapiglia, C., Ciusani, E., Oggioni, N., Sassone, J., et al. (2014). Neutralization of schwann cell-secreted VEGF is protective to *in vitro* and *in vivo* experimental diabetic neuropathy. *PLoS One* 9:108403. doi: 10.1371/journal.pone.0108403
- Taveggia, C., Zanazzi, G., Petrylak, A., Yano, H., Rosenbluth, J., Einheber, S., et al. (2005). Neuregulin-1 type III determines the ensheathment fate of axons. *Neuron* 47, 681–694. doi: 10.1016/j.neuron.2005.08.017
- Trupp, M., Rydén, M., Jörnvall, H., Funakoshi, H., Timmusk, T., Arenas, E., et al. (1995). Peripheral expression and biological activities of GDNF, a new neurotrophic factor for avian and mammalian peripheral neurons. *J. Cell Biol.* 130, 137–148. doi: 10.1083/jcb.130.1.137
- Unsicker, K., Flanders, K. C., Cissel, D. S., Lafyatis, R., and Sporn, M. B. (1991). Transforming growth factor beta isoforms in the adult rat central and peripheral nervous system. *Neuroscience* 44, 613–625. doi: 10.1016/0306-4522(91)90082-y
- Unsicker, K., Reichert-Preibsch, H., Schmidt, R., Pettmann, B., Labourdette, G., and Sensenbrenner, M. (1987). Astroglial and fibroblast growth factors have neurotrophic functions for cultured peripheral and central nervous system neurons. *Proc. Natl. Acad. Sci. U S A* 84, 5459–5463. doi: 10.1073/pnas.84.15.5459
- Vaughan, D. W. (1992). Effects of advancing age on peripheral nerve regeneration. *J. Comp. Neurol.* 323, 219–237. doi: 10.1002/cne.903230207
- Verdú, E., Ceballos, D., Vilches, J. J., and Navarro, X. J. (2000). Influence of aging on peripheral nerve function and regeneration. *J. Peripher. Nerv. Syst.* 5, 191–208. doi: 10.1046/j.1529-8027.2000.00026.x
- Vidal, P. M., Lemmens, E., Dooley, D., and Hendrix, S. (2013). The role of “anti-inflammatory” cytokines in axon regeneration. *Cytokine Growth Factor Rev.* 24, 1–12. doi: 10.1016/j.cytogfr.2012.08.008
- Vuorinen, V., Siironen, J., and Røyttä, M. (1995). Axonal regeneration into chronically denervated distal stump. I. Electron microscope studies. *Acta Neuropathol.* 89, 209–218. doi: 10.1007/BF00309336
- Wagstaff, L. J., Gomez-Sanchez, J. A., Fazal, S. V., Otto, G. W., Kilpatrick, A. M., Michael, K., et al. (2021). Failures of nerve regeneration caused by aging or chronic denervation are rescued by restoring Schwann cell c-Jun. *eLife* 10:e62232. doi: 10.1007/BF00309336
- Wang, Y., Zhao, X., Huojia, M., Xu, H., and Zhuang, Y. (2016). Transforming growth factor-beta3 promotes facial nerve injury repair in rabbits. *Exp. Ther. Med.* 11, 703–708. doi: 10.3892/etm.2016.2972
- Watabe, K., Fukuda, T., Tanaka, J., Toyohara, K., and Sakai, O. (1994). Mitogenic effects of platelet-derived growth factor, fibroblast growth factor, transforming growth factor-beta and heparin-binding serum factor for adult mouse Schwann cells. *J. Neurosci. Res.* 39, 525–534. doi: 10.1002/jnr.490390504
- Welch, J. A., Kraus, K. H., Wells, M. R., Blunt, D. G., and Weremowitz, J. (1997). Effect of combined administration of insulin-like growth factor and platelet-derived growth factor on the regeneration of transected and anastomosed sciatic nerve in rats. *Am. J. Vet. Res.* 58, 1033–1037.
- Wilcox, M. B., Jessen, K. R., Quick, T. J., and Phillips, J. B. (2021). The molecular profile of nerve repair: humans mirror rodents. *Neural Regen. Res.* 16, 1440–1441. doi: 10.4103/1673-5374.301014
- Wilcox, M. B., Laranjeira, S. G., Eriksson, T. M., Jessen, K. R., Mirsky, R., Quick, T. J., et al. (2020). Characterising cellular and molecular features

- of human peripheral nerve degeneration. *Acta Neuropathol. Commun.* 8:51. doi: 10.1186/s40478-020-00921-w
- Woodhoo, A., Alonso, M. B., Droggiti, A., Turmaine, M., D'Antonio, M., Parkinson, D. B., et al. (2009). Notch controls embryonic Schwann cell differentiation, postnatal myelination and adult plasticity. *Nat. Neurosci.* 12, 839–847. doi: 10.1038/nn.2323
- Wu, P., Tong, Z., Luo, L., Zhao, Y., Chen, F., Li, Y., et al. (2021). Comprehensive strategy of conduit guidance combined with VEGF producing Schwann cells accelerates peripheral nerve repair. *Bioact. Mater.* 6, 3515–3527. doi: 10.1016/j.bioactmat.2021.03.020
- Xiao, J., Kilpatrick, T. J., and Murray, S. S. (2009). The role of neurotrophins in the regulation of myelin development. *Neurosignals* 17, 265–276. doi: 10.1159/000231893
- Xu, P., Rosen, K. M., Hedstrom, K., Rey, O., Guha, S., Hart, C., et al. (2013). Nerve injury induces glial cell line-derived neurotrophic factor (gdnf) expression in schwann cells through purinergic signaling and the pkc-pkd pathway. *Glia* 61, 1029–1040. doi: 10.1002/glia.22491
- Yamada, Y., Ohazama, A., Maeda, T., and Seo, K. (2018). The Sonic Hedgehog signaling pathway regulates inferior alveolar nerve regeneration. *Neurosci. Lett.* 671, 114–119. doi: 10.1016/j.neulet.2017.12.051
- Yamazaki, T., Sabit, H., Oya, T., Ishii, Y., Hamashima, T., Tokunaga, A., et al. (2009). Activation of MAP kinases, Akt and PDGF receptors in injured peripheral nerves. *J. Peripher. Nerv. Syst.* 14, 165–176. doi: 10.1111/j.1529-8027.2009.00228.x
- Yan, Q., Matheson, C., and Lopez, O. T. (1995). *in vivo* neurotrophic effects of GDNF on neonatal and adult facial motor neurons. *Nature* 373, 341–344. doi: 10.1038/373341a0
- Yasui, G., Yamamoto, Y., Shichinohe, R., Funayama, E., Oyama, A., Hayashi, T., et al. (2016). Neuregulin-1 released by biodegradable gelatin hydrogels can accelerate facial nerve regeneration and functional recovery of traumatic facial nerve palsy. *J. Plast. Reconstr. Aesthet. Surg.* 69, 328–334. doi: 10.1016/j.bjps.2015.10.037
- Zhou, F.-Q., Walzer, M. A., and Snider, W. D. (2004). Turning on the machine: genetic control of axon regeneration by c-Jun. *Neuron* 43, 1–2. doi: 10.1016/j.neuron.2004.06.020
- Zigmond, R. E., and Echevarria, F. D. (2019). Macrophage biology in the peripheral nervous system after injury. *Prog. Neurobiol.* 173, 102–121. doi: 10.1016/j.pneurobio.2018.12.001

Conflict of Interest: The authors declare that the research was conducted in the absence of any commercial or financial relationships that could be construed as a potential conflict of interest.

Publisher's Note: All claims expressed in this article are solely those of the authors and do not necessarily represent those of their affiliated organizations, or those of the publisher, the editors and the reviewers. Any product that may be evaluated in this article, or claim that may be made by its manufacturer, is not guaranteed or endorsed by the publisher.

Copyright © 2022 Jessen and Mirsky. This is an open-access article distributed under the terms of the Creative Commons Attribution License (CC BY). The use, distribution or reproduction in other forums is permitted, provided the original author(s) and the copyright owner(s) are credited and that the original publication in this journal is cited, in accordance with accepted academic practice. No use, distribution or reproduction is permitted which does not comply with these terms.



Compound Motor Action Potentials During a Modest Nerve Crush

Mohammed Nazmy Hamad¹, Nickolas Boroda¹, Diego Barragan Echenique¹, Raymond A. Dieter², Farid M. L. Amirouche¹, Mark H. Gonzalez¹ and James M. Kerns^{1*}

¹Department of Orthopedic Surgery, University of Illinois Chicago, Chicago, IL, United States, ²Hines Veterans Affairs Hospital Research Service, Hines, IL, United States

OPEN ACCESS

Edited by:

George Davis Bittner,
University of Texas at Austin,
United States

Reviewed by:

Yuanyuan Liu,
National Institute of Dental and
Craniofacial Research (NIH),
United States

Cameron Ghergherehchi,
Johns Hopkins Medicine,
United States

*Correspondence:

James M. Kerns
jkerns.kerns@gmail.com

Specialty section:

This article was submitted to
Cellular Neuropathology,
a section of the journal
Frontiers in Cellular Neuroscience

Received: 19 October 2021

Accepted: 03 March 2022

Published: 30 March 2022

Citation:

Hamad MN, Boroda N,
Echenique DB, Dieter RA,
Amirouche FML, Gonzalez MH and
Kerns JM (2022) Compound Motor
Action Potentials During a Modest
Nerve Crush.
Front. Cell. Neurosci. 16:798203.
doi: 10.3389/fncel.2022.798203

Nerve crush injury results in axonotmesis, characterized by disruption of axons and their myelin sheaths with relative sparing of the nerve's connective tissue. Despite the widespread use of crush injury models, no standardized method for producing these lesions has been established. We characterize a crush model in which a narrow forceps is used to induce a modest and controlled compressive injury. The instantaneous compound motor action potential (CMAP) is monitored *in situ* and in real-time, allowing the characterization of neuromuscular response during and after injury. The tibial nerves of 11 anesthetized rats were surgically isolated. After the placement of electrodes, CMAPs were elicited and registered using a modular-data-acquisition system. Dumont-#5 micro-forceps were instrumented with a force transducer allowing force measurement via a digital sensor. Baseline CMAPs were recorded prior to crush and continued for the duration of the experiment. Nerve crushing commenced by gradually increasing the force applied to the forceps. At a target decrease in CMAP amplitude of 70%–90%, crushing was halted. CMAPs were continually recorded for 5–20 min after the termination of the crushing event. Nerves were then fixed for histological assessment. The following post-crush mean values from 19 trials were reported: peak CMAP amplitude decreased by 81.6% from baseline, duration of crush was 17 sec, rate of applied force was 0.03 N/sec, and maximal applied force was 0.5 N. A variety of agonal phenomena were evident post-lesion. Following the initial decrease in CMAP, 8 of 19 trials demonstrated a partial and transient recovery, followed by a further decline. Thirteen trials exhibited a CMAP amplitude near zero at the end of the recording. Twelve trials demonstrated a superimposed EMG background response during and after the crush event, with disappearance occurring within 4–8 min. Qualitative histology assessment at the lesion site demonstrated a correspondence between CMAP response and partial sparing of nerve fibers. By using a targeted decline in CMAP amplitude as the endpoint, researchers may be able to produce controlled, brief, and reproducible crush injuries. This model can also be used to test interventions aimed at enhancing subsequent regeneration and behavioral recovery.

Keywords: nerve crush with feedback, instrumented forceps with force transducer, axonotmesis, controlled crush parameters, controlled compression parameters, force-impulse, rat sciatic tibial nerve crush injury, compound motor action potential (CMAP)

INTRODUCTION

Axonotmesis is a peripheral nerve lesion paradigm characterized by disruption of axons and their myelin sheath with relative sparing of the nerve's supporting connective tissues. Preservation of these supporting structures allows regenerating axonal growth cones to re-grow through their original paths and to re-innervate their distal targets after injury (Seddon, 1943; Sunderland, 1951; Campbell, 2008). This confers an excellent prognosis. Hence, following axonotmesis, nerves typically achieve complete or nearly complete restoration of motor and sensory function by 4–5 postoperative weeks (De Koning et al., 1986; Malushte et al., 2004). This feature of axonotmesis has made it invaluable in the study of nerve degeneration and regeneration (Chung et al., 2014; Dun and Parkinson, 2018).

Experimentally, axonotmesis is usually produced by maximally applying mechanical pressure to the nerve *via* micro-forceps (Kurtoglu et al., 2005; Fan et al., 2015; Ni et al., 2017; Suzuki et al., 2017), clamps (Zhang et al., 2013; Yuce et al., 2015; Korkmaz et al., 2016), tourniquets (Chen et al., 1992), or other instruments (Sarikcioglu et al., 2007; Feng and Yuan, 2015; Hei et al., 2016). Despite published attempts to produce more consistent lesions (Beer et al., 2001), no standardized method for inducing axonotmesis has been established (Varejao et al., 2004; Ronchi et al., 2009). Studies vary widely with regards to the instrument used, the duration of force applied, the lesion size, and the magnitude/reproducibility of the resulting lesion (Tos et al., 2009; Alvites et al., 2018). Consequently, the lack of a defined standard often makes comparisons between different experimental investigations difficult.

The parameters which characterize the severity of a crush lesion are described by the force-impulse (F-i), which is the product of the force and duration of the compressive pressure applied to the nerve (Liu et al., 2020). The extent of nerve regeneration has been shown to be dependent on the F-i of the trauma sustained to the nerve (Chen et al., 1992; Sarikcioglu et al., 2007). Compound motor action potentials (CMAPs) have been used to quantify neuromuscular function following induced nerve injury (Robinson, 2000; Sta et al., 2014; Vannucci et al., 2019). This electrophysiological measure reflects summations of the evoked action potentials generated by motor units as measured by electrodes inserted at the target muscles (Menorca et al., 2013; Bhatt et al., 2016).

In the present study, we investigate whether CMAP can be used as a reliable endpoint for conducting nerve crush injuries and whether this may offer a more standardized approach for cross-comparison of nerve injuries. To characterize all the parameters of the induced crush injury, we used instrumented micro-forceps to allow real-time monitoring and recording of the F-i applied while conducting the injury. The applied F-i is controlled by the investigator based on feedback from the instantaneous CMAP, which is used as a surrogate for functional decline of motoneuron-activity (Navarro and Udina, 2009; Navarro, 2016). We hypothesize that if nerves are crushed by a graded force to a targeted decline in CMAP amplitude, then the resulting lesions will exhibit similar degrees of injury, and the injury will be highly reproducible. Using our proposed

technique, we characterize the electrophysiological changes of neuromuscular response during and immediately following crush injury. Qualitative histology is also used to characterize and provide structural confirmation of the degree of nerve injury.

MATERIALS AND METHODS

Experimental Animals

Sprague Dawley female rats ($n = 11$) were used in this study. Two rats were housed per cage at the University of Illinois Biological Research Laboratory Vivarium under an *ad libitum* diet with a 12-h light/dark cycle. The rats were acquired at a weight between 175 and 200 g (Charles River Laboratory; Chicago, IL, United States) and allowed to acclimate until they reached a weight of approximately 250–275 g. Animals were numbered and weighed before undergoing surgery. All experimental procedures were in accordance with the National Institute of Health Guide for the Care and Use of Laboratory Animals and the University of Illinois at Chicago Institutional Care and Use Committee.

Anesthesia and Surgical Procedure

Prior to the procedure, the animals were anesthetized with an intraperitoneal injection (ketamine HCL 90 mg/kg and xylazine 10 mg/kg) and given a subcutaneous injection of buprenorphine SR Lab (1.0 mg/kg) for acute pain management. After shaving the operative area of the experimental limbs, rats were placed on a heating pad and a rectal probe was inserted to monitor body temperature for the duration of the procedure. A solution of 10% povidone iodine was applied in triplicate to the surgical area, followed by a 70% alcohol solution to sterilize the field. A sterile drape was applied over the area and a chevron incision was created directly caudal to the femur and the tibia of the rat. After retracting the skin overlying the incision, the exposed biceps femoris muscle was split using a lateral approach, exposing the sciatic nerve as well as both heads of the gastrocnemius muscle. Using micro-instruments, the sciatic nerve was isolated from the surrounding tissue. The tibial, peroneal, and sural fascicles were isolated. To avoid recording CMAPs from the peroneal and sural nerve fascicles, these branches were transected. The nerve crush was performed while monitoring and recording the CMAP. Following the procedure, the incision was closed with a running stitch using a 4.0 Nylon suture (Ethicon, Inc.; Raritan, NJ, United States). The procedure was repeated on the animal's contralateral side, allowing a total of 22 crush lesion trials. The animals were euthanized while fully anesthetized and unconscious following our institution's guidelines.

CMAP Recordings

Continuous two-channel CMAP recordings were obtained by placing wire-hook bipolar electrodes (EMG Hook Electrodes, Model EMT-2-30; Microprobes, Inc.; Gaithersburg, MD, United States) at four different locations (**Figure 1**). One recording electrode each was placed at the muscle belly of the lateral and medial heads of the gastrocnemius, and two corresponding electrodes were placed in the Achilles tendon. A ground electrode was placed under the skin of the back of the rat. A bipolar stimulating cuff electrode was placed around the sciatic nerve

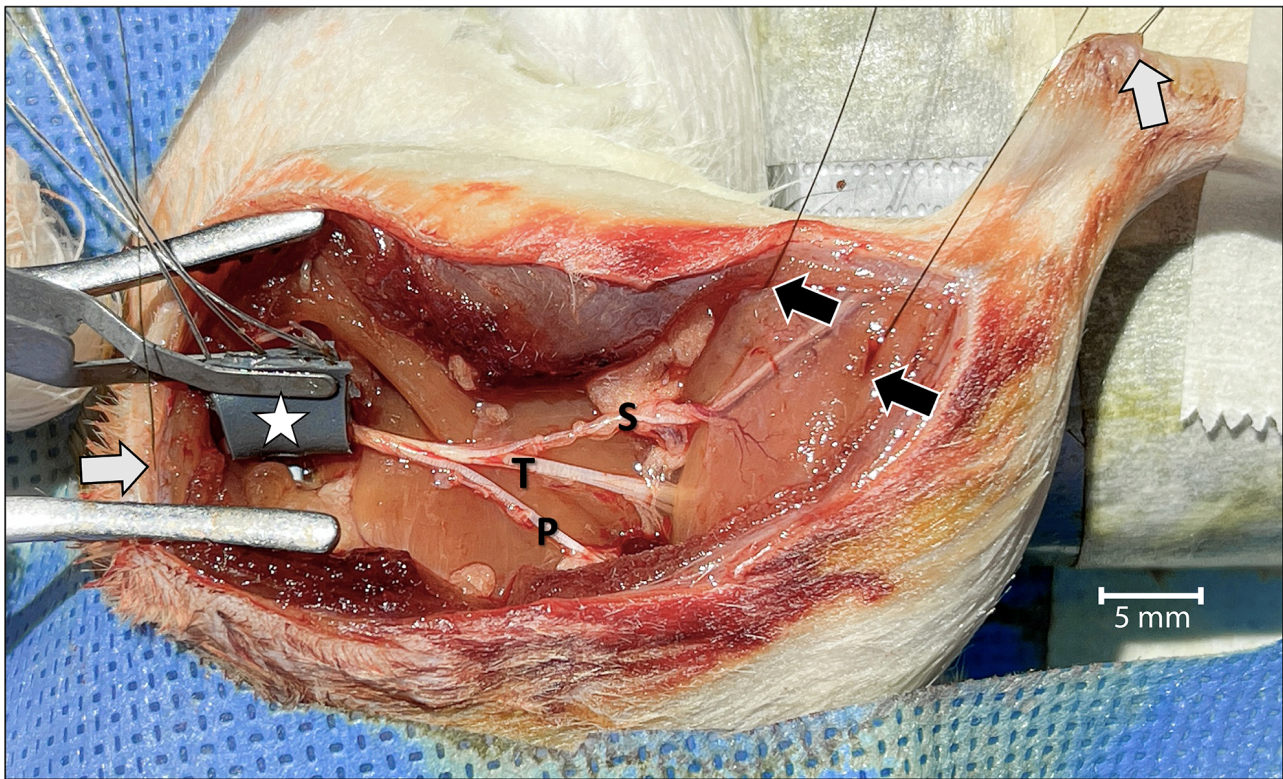


FIGURE 1 | Surgical view of the left leg showing the acute dissection and the methods used to establish two-channel CMAP recording and nerve stimulation. Wire-hook recording electrodes were inserted into the belly of the lateral and medial gastrocnemius muscles (black arrows) and Achilles tendon (white arrow in the upper right). A grounding electrode was placed under the skin of the back of the rat (white arrow on the left). The bipolar stimulating nerve cuff electrode with its connecting wires was wrapped around the proximal sciatic nerve at the level of the sciatic notch (star). To isolate motor unit activation corresponding only to the tibial (T) nerve, and to prevent signal interference, the sural (S) and peroneal (P) nerves were cut. The tibial nerve was crushed just distal to the point of sural nerve take-off. For orientation, the rostral direction is down to the left.

proximal to the level of the trifurcation in order to complete the circuit.

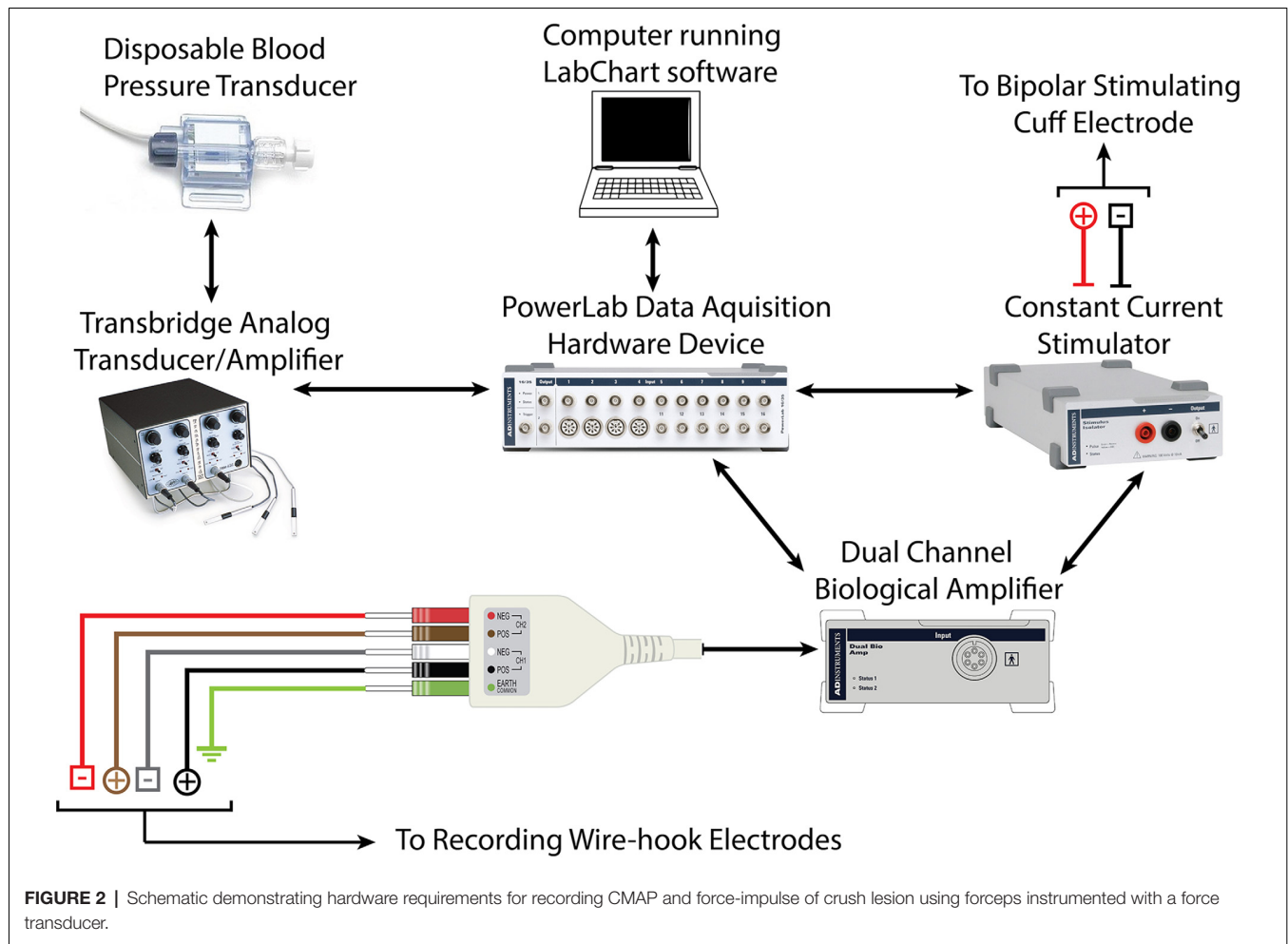
Recordings were obtained using a Power Lab Modular Data Acquisition System, LabChart recording software, and dual-channel EMG Bioamplifier (ADInstruments, Inc.; Dunedin, New Zealand). CMAP data were processed through a low pass filter at 1 KHz, and a high pass filter at 1 Hz. An active main filter was applied with a 3 sec delay to eliminate 60 Hz interference once recordings start (Figure 2).

Each motor unit has a different threshold stimulus intensity at which it can be activated. To ensure that all motor units of the target muscles were activated and accounted for in the CMAP data obtained, a current-response curve was generated prior to each experimental trial (Maathuis et al., 2011). The sciatic nerve was stimulated with electrical pulses of gradually increasing current intensities ranging from subthreshold to supramaximal. This was implemented using a constant-current stimulator (ADInstruments, Inc.; Dunedin, New Zealand) which induced stimulation pulses of 0.05 ms durations at increments of 0.1 mA. The current which corresponded to 150% of the maximal CMAP millivolt peak was used for nerve stimulation for the respective experiment (Figure 3).

CMAP recordings were initiated prior to inducing the nerve lesion in order to capture the baseline CMAP amplitudes before the trauma. Recordings were implemented continuously for the duration of the experiment and for 5–20 min after the termination of the crushing event. This allowed the CMAP response to be monitored in real-time *in situ*.

Nerve Crush Using Instrumented Micro-forceps

A precise and controlled compressive nerve lesion was delivered to the tibial nerve using a Dumont No. 5 micro-forceps (INOX 0508-L5-PO, Catalog No. 10-001-130, Hatfield, PA, United States: Electron Microscopy Sciences; Figure 4A). The absolute tip of the forceps had a contact-width of 0.1 mm, however, we conducted lesions at a point ~2 mm from the tip. This point had a contact width of ~0.3 mm, as measured using a digital caliper. Forceps were instrumented with a force transducer to allow real-time measurement of the applied compressive pressure. The force transducer consisted of a thin-walled water-filled balloon made of relatively inelastic low-density polyethylene attached to a disposable blood pressure transducer (Blood Pressure Transducer and Cable, Model BLPR2, Sarasota, FL, United



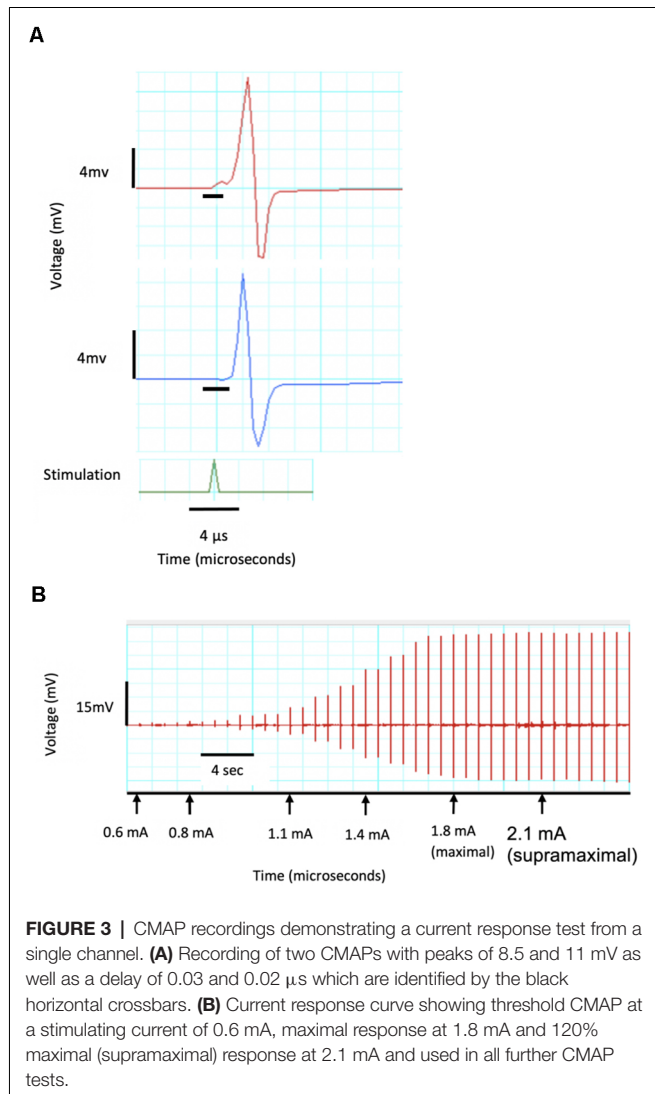
States: World Precision Instruments Inc.). The balloon was adopted from a modified commercially-available rectal catheter (Urodynamic Rectal Catheter, Model 023121, Orangeburg, NY, United States: Laborie Inc.) in which the distal end was filled with a silastic tube, sealed with silastic, and secured with 0-grade suture thread. The sealed balloon, its associated tubing, and the pressure transducer were filled with water *via* an attached three-way connector in order to improve the fidelity of the recordings. The assembled device was connected to a bridge-circuit transducer, quad-channel amplifier (4-Channel Transducer Amplifier, Model TBM4M, Sarasota, FL, United States: World Precision Instruments Inc.), and to the PowerLab Modular Data Acquisition System to allow monitoring and recording of applied force (**Figure 2**). The limited elasticity of the balloon resulted in an accurate recording of finger pressure applied and force transmitted to the micro-forceps.

The balloon of the force transducer was fixed to one side of the forceps such that a mark on the balloon was aligned over a mark on the forceps. This mark, located 0.63 the distance from the fulcrum of the forceps to the tip, provided a consistent location for the user to rest their thumb and to apply pressure when crushing. This distance, between the fulcrum and the point of

force application, was taken into account during the calculation of the crush force. In order to reflect only the force applied at the tip of the forceps, the recording software was adjusted to report a factor of 0.63 of the total detected applied force.

The force transducer was calibrated with standard weights before each use. A calibration device was constructed for this purpose. The instrumented forceps were placed in the center of the device such that a suspended weight could apply pressure to the balloon transducer and forceps in a manner similar to that of the thumb of the user during crushing. Using both 50- and 20-gram weights, the recording software was calibrated to detect 0.49 and 0.20 Newtons, respectively.

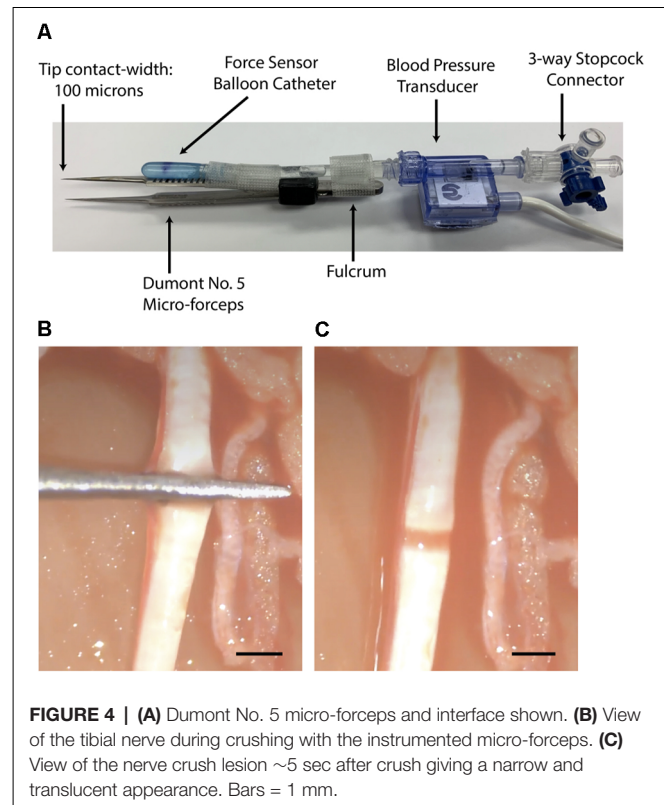
The baseline force involved in touching, but not crushing, the nerve with the forceps was recorded for 5 sec prior to crushing the nerve. While observing the nerve under direct light microscopy at 20× magnification, the primary investigator commenced crushing of the nerve by gradually increasing the force applied to the forceps at a rate of approximately 0.03 N/sec (**Figures 4B,C**). As the primary investigator was crushing, a second investigator monitored the CMAP response in real-time on-screen using the recording software. At a target decrease in CMAP amplitude of 70%–90% compared to baseline, the second investigator called



out STOP. At this point, the primary investigator immediately ceased crushing by releasing the forceps. The total crush time was then recorded, in addition to the maximally applied force, and the rate of force increased over time.

Statistical Analysis

CMAP amplitude data representing the duration before, during, and after each nerve crush trial was extracted from the LabChart recording software (ADInstruments LabChart for macOS, Version 8.1.17. Dunedin, New Zealand: ADInstruments Inc). Average CMAP amplitude values at each point of interest were determined as the average of five consecutive peaks. Maximal crush force was measured as the difference between the magnitude of touching the nerve and the maximal magnitude applied. Duration of crush was determined from the terminal time-point involved in touching the nerve to the moment of release of the forceps. The rate of graded increase in force application was determined by the slope of Δ Netwons/ Δ time during the crushing interval. Data analysis was performed using



SPSS (IBM SPSS Statistics for macOS, Version 24.0. Armonk, NY, United States: IBM Corp.) and Excel (Microsoft Excel for macOS, Version 16.47. Redmond, WA, United States: Microsoft Corporation).

Histology

After completion of the CMAP testing and while the rat was still anesthetized, Karnovsky's fixative (2.5% glutaraldehyde and 2.5% paraformaldehyde in 0.1 M phosphate buffer at 4°C) was applied to the tibial nerve at the lesion location. After 10 min, a 10 mm segment of the tibial nerve was removed and placed in fresh fixative in the refrigerator for at least 1 week. Selected nerve specimens were rinsed in saline, post-fixed in 1% OsO₄ (with 1% potassium ferrocyanide) for 60–90 min, dehydrated in serial alcohols, cleared in propylene oxide, and embedded in Epon. Semi-thin sections (1 micron) of the tibial nerve cut in either the longitudinal or transverse plane were stained with methylene blue for light microscopy. The control lesion specimen was a comparable segment from either the contralateral unoperated side or a location proximal to the lesion. Slides containing selected stained tibial nerve sections at the injury site were uploaded to AperioImageScope (Version 12.4; Leica Biosystems; Wetzlar, Germany) software. A qualitative assessment of the crush lesion was to confirm the extent of the crush lesion with respect to the appearance of any intact axons and the longitudinal extent of the crushed zone.

Selected tibial nerve specimens were stained en bloc with 1% uranyl acetate in 50% ethanol for 1 h followed by further ultrathin sectioning and staining with Reynold's lead citrate for 2 min for

transmission electron microscopy (TEM). TEM was performed on a JEOL (JEM 1220) electron microscope (Tokyo, Japan). Qualitative TEM was used to correlate, confirm, and clarify the findings seen on light microscopy.

RESULTS

Of the 22 crush lesion trials performed, 19 were included in our analysis. Three trials were excluded due to technical failures or animal death before the contralateral side could be operated on. The average weight of the rats used was 268.9 ± 37.5 g.

The average baseline CMAP amplitude before nerve injury was 25 ± 9.7 mV. This decreased to 4.1 ± 3.4 mV immediately after the controlled crush injury was induced (measured at the moment the crushing forceps were released). This corresponds to an average decrease in CMAP amplitude of $81.6 \pm 17.9\%$, as shown in **Figure 5**.

The average duration of crush was 17 ± 6.6 sec. The average maximal applied force for all trials was 0.5 ± 0.3 N. This force was achieved by gradually increasing applied pressure at an average rate of 0.03 ± 0.02 N/sec over the duration of the crushing interval. The Pearson correlation coefficient between the rate of force application and crush duration is -0.61 at a significance level <0.01 , indicating significance (**Figure 6A**). Thus, as the rate of applied force increased, overall crush duration was reduced. The correlation between applied F-i and the resulting percent decrease in CMAP amplitude was assessed for all trials (**Figure 6B**). The relationship between these crush parameters was found to be statistically insignificant: correlation of $r = 0.127$ ($p = 0.604$).

After crushing, CMAP was continually monitored for 5–20 min in 13 of 19 trials (68%), and for 5 min in 6 of 19 trials (32%). Following the initial injury-induced decrease in CMAP, eight of 19 trials (42%) demonstrated a partial and transient recovery of CMAP amplitude. The average maximal recovery in CMAP amplitude for these eight trials was 13.5 ± 10 mV, corresponding to an average recovery in CMAP amplitude of $45.7 \pm 30.7\%$. This recovery was followed by a further decline, occurring within 2–4 min, for all eight trials. CMAP amplitude became zero in 13 of 19 trials (68%) by the end of the recordings. The average baseline CMAP amplitude at the end of the recordings was 2.4 ± 3.9 mV for all six trials which did not reach zero.

Twelve of 19 trials (63%) demonstrated a superimposed electromyographic background response during and after the crush event, with disappearance occurring within 4–8 min. Four two-channel CMAP recordings, which are representative of the typical CMAPs observed, are shown in **Figures 7–10**.

Light photomicrographs examining the crush zones of the tibial nerves in transverse and longitudinal sections are shown in **Figures 11–13**. A qualitative evaluation demonstrates that the majority of myelinated axons were damaged by the crush. However, small-sized fibers located near the surface (periphery) were preferentially spared, compared to larger more centrally located fibers. The perineurium and blood vessels were also affected in some cases (**Figure 11A**). Follow-up TEM confirmed the preferential sparing among small fibers and

further demonstrated that the axoplasmic changes may occur prior to myelin sheath breakdown (**Figure 11B**). In addition, the small non-myelinated axons were also spared. It is unclear why the myelin is less sensitive to the crush forces compared to the axoplasm. Spared fibers were also seen crossing the lesion zone in the longitudinal sections (**Figure 12**). Measurement on these sections confirmed that the respective lesion width is ~ 250 μm , as suggested at the time of surgery (**Figure 4B**). Since the lesion is noticeably “crunched”, or contracted in on itself, the actual lesion width is likely larger than the measured distance.

When compared to their respective CMAPs, we notice that axonal sparing on histology is likely associated with the non-zero CMAP amplitude baseline seen several minutes post-crush. Hence, an incomplete crush of the tibial nerve may have been captured on the CMAP recordings as continued electrical signaling (non-zero baseline), post-crush.

DISCUSSION

In the present study, we demonstrate a technique by which real-time CMAP amplitude changes are used as an endpoint for conducting crush injuries to the rat tibial nerve. We also demonstrate how CMAPs can be used to characterize and quantify the loss of neuromuscular function sustained during and after controlled compressive injury. By instrumenting our crushing device with a force transducer, we were able to quantify the F-i of the induced lesion using data acquisition software. This allowed us to quantify all the parameters of the crush injury.

CMAPs are widely used for evaluating functional restitution after nerve injury in experimental animal models (Smith et al., 2000; Mikesch et al., 2018). In the study of axonotmesis, CMAPs are particularly useful for determining the course and extent of nerve regeneration and muscle reinnervation after injury (Navarro and Udina, 2009). To our knowledge, this is the first study to measure CMAP in real-time during actual induction of nerve injury, and to attempt use of the data gleaned as an objective endpoint, serving as a surrogate for crush effectiveness. By using CMAPs in this way, we have demonstrated a crushing technique that is controlled by a feedback loop, with the ultimate decision of whether to cease or continue applying pressure to the nerve being controlled by the human operator. The operator makes this decision based on the percent decrease in CMAP amplitude, which is displayed on screen in real-time and continually updated. As a proof of concept, we arbitrarily decided to continue crushing until observing a 70%–90% decline in CMAP amplitude from baseline. We continued recording CMAP amplitude changes even after the crushing event terminated in order to characterize and quantify the archetypal electrophysiological response of the tibial nerve immediately after sustaining crushing trauma. To our knowledge, this has not been described previously.

Appraisal of the crush parameters we used to induce nerve injury demonstrated that, for different crush trials, the F-i required to produce a $\sim 70\%$ – 90% decrease in CMAP amplitude varied significantly. Although most nerves required ~ 8 – 10 N·sec to reach this endpoint, some nerves required as little as ~ 4 N·sec or as much as ~ 17 N·sec. Thus, the F-i required to produce a

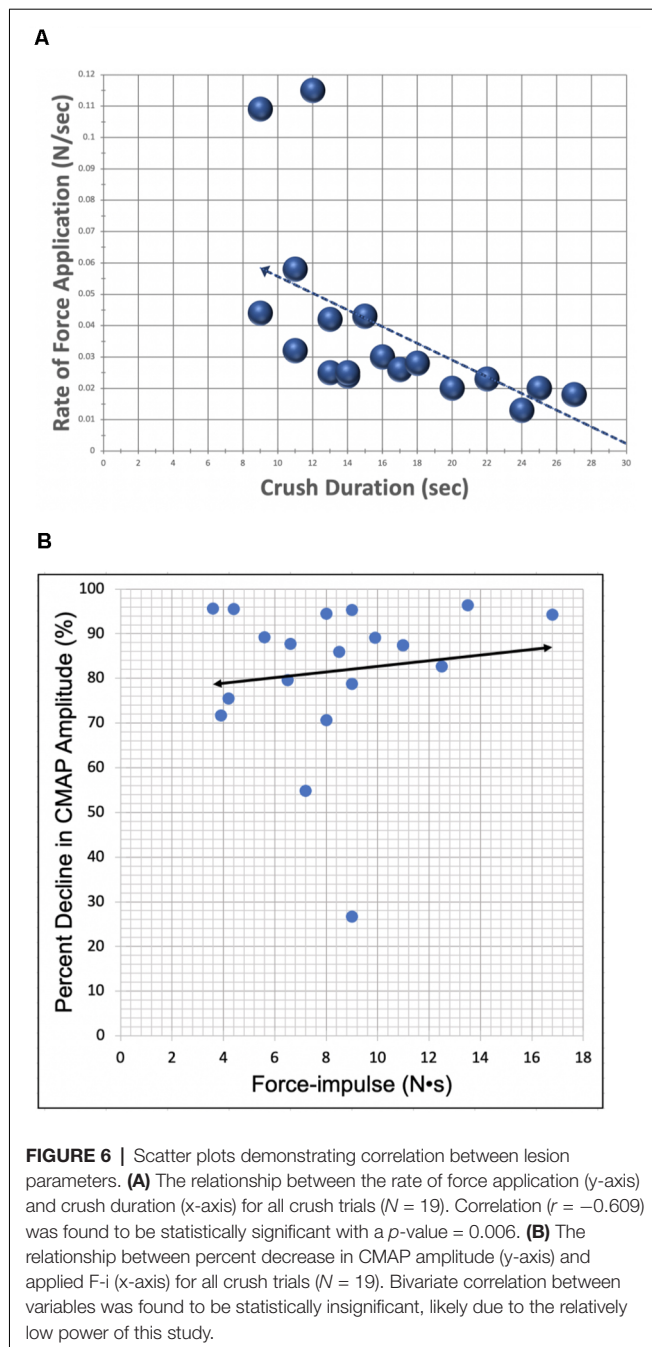
Animal Number	Operative Side	Crush Trial	Baseline CMAP Before Injury (mV)	Peak CMAP After Injury (mV)	CMAP Reduction (%)	Maximal Applied Force (N)	Crush Duration (sec)	Rate of Force Application (N/sec)	Applied Force-Impulse (N•sec)
1	Left	1	23.0	1.3	94.3	1.4	12.0	0.12	16.8
1	Right	2	19.3	1.1	94.5	0.5	16.0	0.03	8.0
2	Left	3	13.5	10.0	26.7	0.6	15.0	0.04	9.0
2	Right	4	12.0	3.0	75.5	0.3	14.0	0.02	4.2
3	Left	5	33.5	4.0	87.7	0.6	11.0	0.06	6.6
3	Right	6	29.5	6.0	79.6	0.5	13.0	0.04	6.5
4	Left	7	34.5	1.6	95.4	1.0	9.0	0.11	9.0
4	Right	8	28.5	1.1	96.4	0.5	27.0	0.02	13.5
5	Left	9	24.5	1.1	95.5	0.4	11.0	0.03	4.4
6	Left	10	14.0	0.6	95.7	0.4	9.0	0.04	3.6
7	Left	11	45.5	12.5	71.7	0.3	13.0	0.03	3.9
7	Right	12	17.5	7.5	54.9	0.3	24.0	0.01	7.2
8	Left	13	26.0	2.5	89.1	0.3	33.0	0.01	9.9
8	Right	14	28.3	3.0	89.3	0.4	14.0	0.03	5.6
9	Right	15	21.3	6.3	70.6	0.4	20.0	0.02	8.0
10	Left	16	29.5	4.0	86.0	0.5	17.0	0.03	8.5
10	Right	17	32.0	6.5	78.8	0.5	18.0	0.03	9.0
11	Left	18	27.5	4.5	82.7	0.5	25.0	0.02	12.5
11	Right	19	15.0	2.0	87.4	0.5	22.0	0.02	11.0
Mean			25.0	4.1	81.6	0.5	17.0	0.03	8.3
Standard Deviation			9.7	3.4	17.9	0.3	6.6	0.02	3.5

FIGURE 5 | CMAP amplitude responses induced by our controlled compressive nerve lesions are shown. For each trial, CMAPs displayed represent values averaged from dual channel recordings, representing motor unit activity in both the lateral and medial gastrocnemius muscles. Peak CMAP values after injury represent the peaks immediately after the crushing forceps were released and extricated from the nerve. Crush duration represents only the time in which the graded force was applied. Rate of force application represents the slope of the graded force applied over the crushing interval.

given electromyographic response is not fixed and seems to vary widely, even within the same animal species and when applied to the same nerve, as was the case in this study. Given that CMAP is itself a quantitative characterization of neuromuscular function, we can extrapolate that this variable response threshold to sustained trauma may also translate to corporeal variability, as observable behavioral motor deficits. In the context of producing axonotmesis, our results highlight the importance of not being too minimalist with regard to applied crush force and duration. Applying too small a force-impulse when conducting the nerve lesion may produce lesions with variable extents of injury.

Assessment of the electrophysiologic response patterns which occurred immediately after cessation of crushing revealed that, even when subjected to injuries of similar parameters, nerve CMAPs varied significantly in the temporal arrangement, propagation, and magnitude of electrical potential. While some crush trials displayed a transient recovery of CMAP amplitude immediately after cessation of injury conduction, others did not. Of those which displayed a transient recovery, some did so with relatively high electrical potentials, while others yielded only a few millivolts. Quantitatively, 42% of all analyzed crush trials demonstrated this temporary “rebound” in CMAP

amplitude. The magnitude of recovery in CMAP amplitude ranged from 15% to 75% relative to each trial’s respective baseline. Interestingly, this recovery of electrical potential disappeared in all cases within 4 min after crush, and was then often followed by a further decline. A few minutes post-crush, some trials resulted in the complete abolishment of CMAP signal (at or near zero millivolts) while others retained residual signal propagation and reestablished a baseline at lower amplitudes. We believe that these residual electrical potentials may be related to extent of sparing within the lesion. Spared motor nerve fibers would theoretically continue propagating electrical potentials to their respectively innervated motor units. Given that CMAPs inherently reflect summations of all the evoked potentials produced by the motor units in the captured region (i.e., gastrocnemius), those axons which are disrupted by the crush would cease their contribution of electric potential. As a consequence, recorded CMAP amplitude would diminish in magnitude. However, it would not reach 0 mV if some spared nerve fibers maintained neuromuscular innervation. Given the complexity of the physiology involved, this relationship between acute residual electromyographic signaling and the extent of axonal sparing after crush injury requires further study.



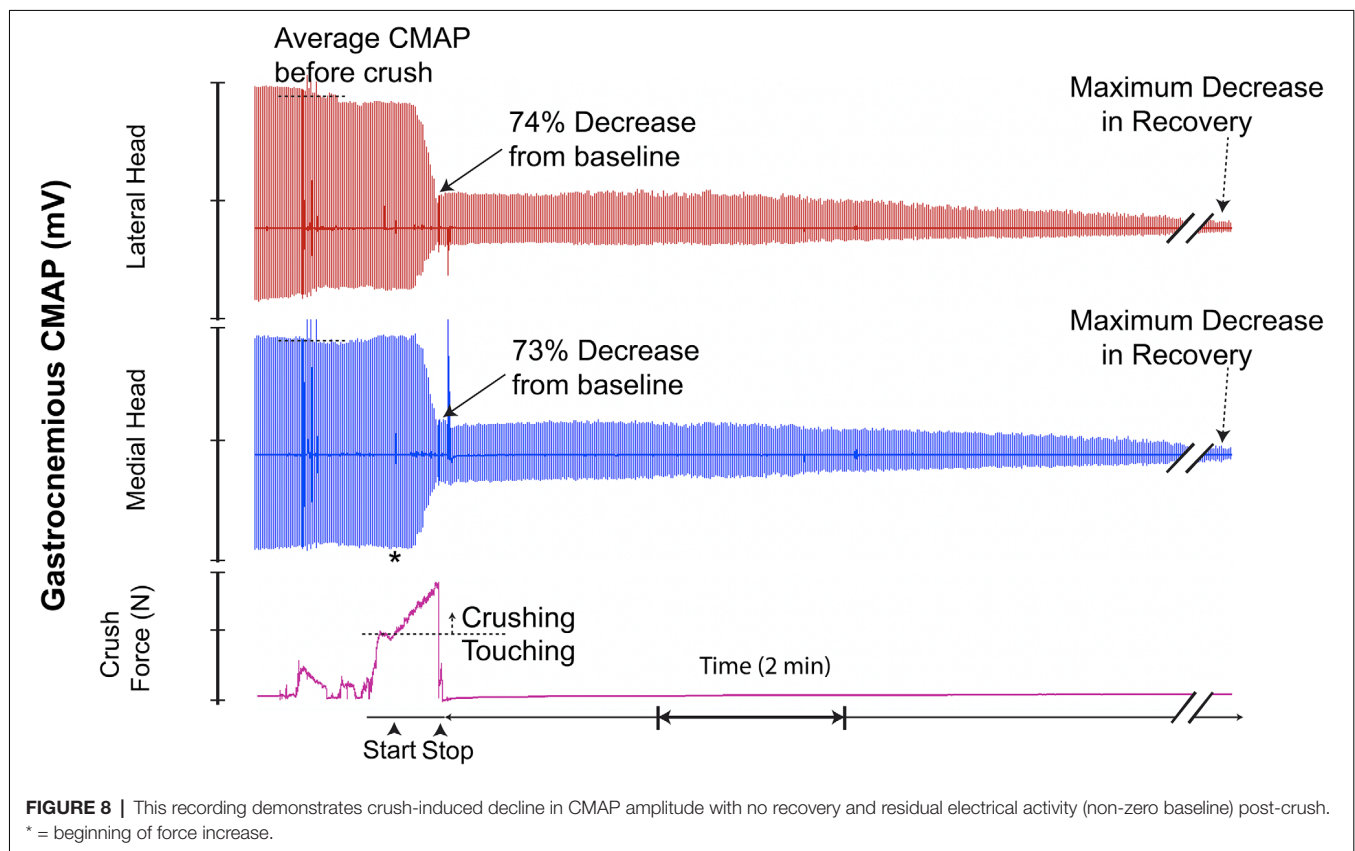
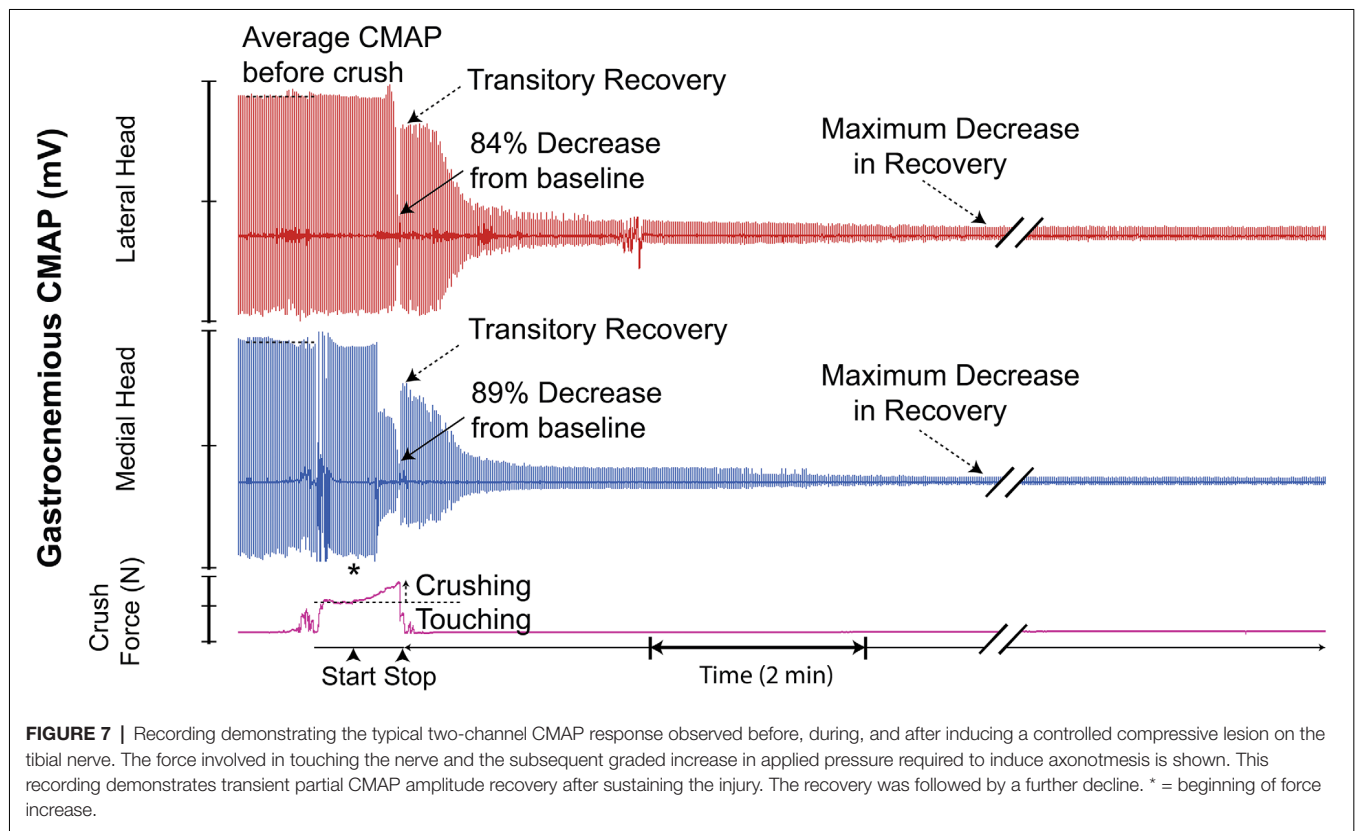
As our resulting CMAP data suggests, the relationship between crush parameters, severity, and uniformity of nerve lesions, and captured electromyographic signal is further complicated by another observed phenomenon. Upon initiation of crushing, 63% of our crush trials demonstrated an emergence of erratic electrical signaling, akin to the appearance of electromyographic “noise”. Given that our CMAP recordings were obtained *via* an open and relatively invasive surgery, we were able to exclude potential sources of electrical interference (i.e., technical malfunctions, improper placement of electrodes, and animal death) quite easily. Moreover, this phenomenon,

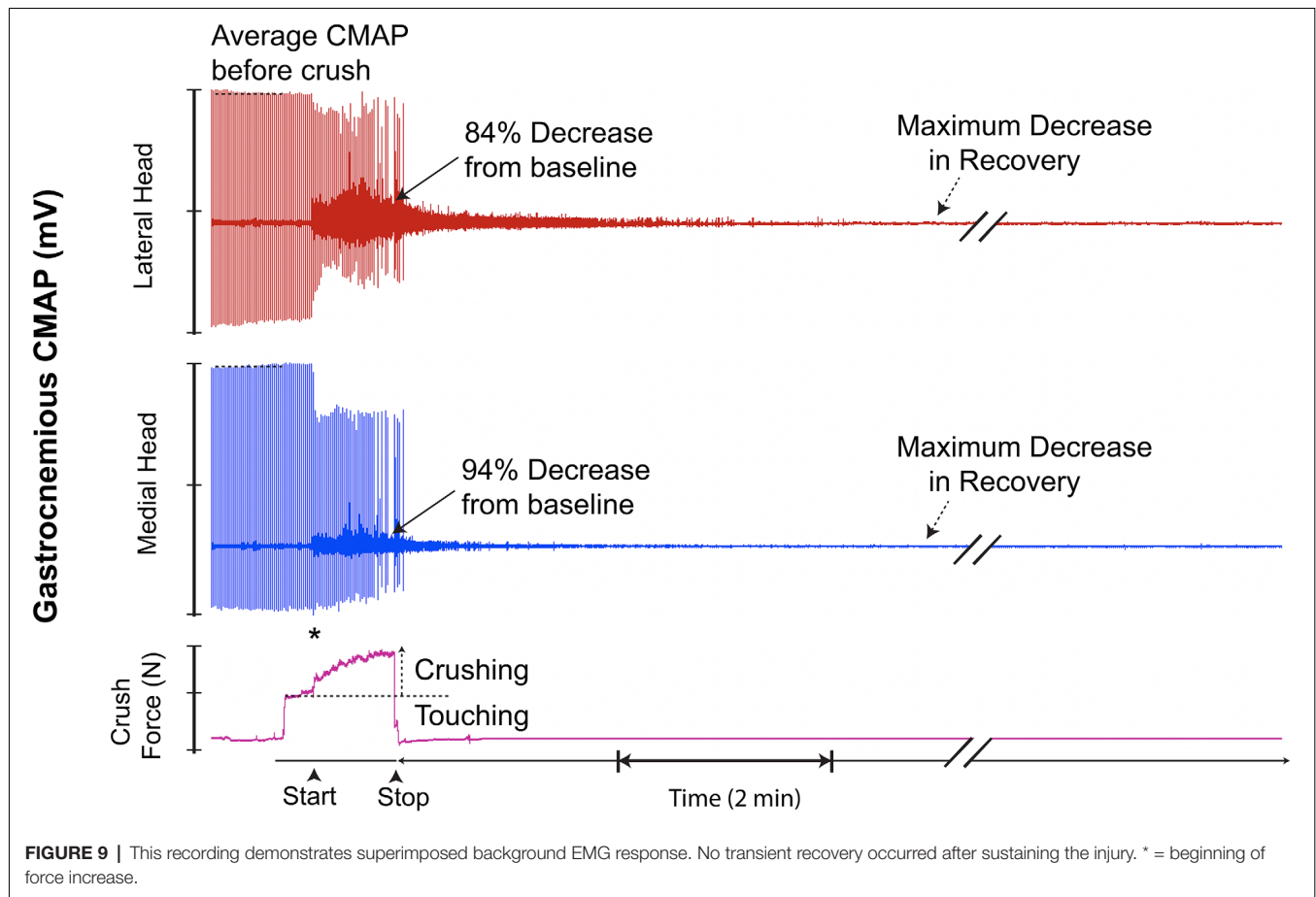
which can further be described as a brief, temporally dynamic CMAP amplitude change, with high frequency widely fluctuating electrical potentials, consistently appeared at the moment of crush initiation. This “noise” also consistently dissipated during or briefly after cessation of crushing.

Among the histological preparations assessed in the present study, we were surprised to see the consistent extent of axon sparing, especially among the small myelinated fibers. Compared to our previous study, the sequential breakdown of the axoplasm prior to myelin sheath was very similar to the Wallerian degeneration observed 5 days post-crush in the rat tibial nerve (Kerns et al., 2020). In the present study, the sequence of the observed changes was a result of injury itself, rather than Wallerian degeneration. In regards to the sparing observed, even a small proportion of fibers involved could have significance for subsequent regeneration and recovery. It has been shown that spinal cord injury (contusion) can have ~10% sparing, which translates to significant motor recovery (Kloos et al., 2005). This concept was first attributed to Andrew Blight in 1986 and deserves some reservations (personal communication). It remains to be shown that such possibilities also apply to the peripheral nervous system. The precise mechanism by which smaller axons are spared also needs to be determined. We propose that endoneurial tissue along with the large nerve fibers may play a protective role in producing this phenomenon, by cushioning. This is consistent in part, with the patterns of susceptibility given by Lundborg (2004) (pp. 49 and 58); motor > sensory, superficial > central, large > small. This observed sparing may involve sensory and non-myelinated axons as well as motor axons.

The importance of producing compressive lesions with quantitatively consistent parameters is highlighted by previous studies. In the context of axonotmesis, it has been reported that the extent of nerve recovery is dependent on the magnitude and duration of force applied during injury (Chen et al., 1992, 1993; Sarikcioglu and Ozkan, 2003). Despite this, no perfect standardized crushing method has been established. Moreover, no particular crushing device has become the mainstay for conducting crush lesions (Alvites et al., 2018).

Historically, various tools and methods have been used to induce compressive injury to peripheral nerves, each having advantages and disadvantages. The most elemental crush technique involves the use of simple or hemostatic forceps without modifications or instrumentation. Using these devices, a crush is produced by applying maximal compressive pressure to the nerve for 30–60 sec, or longer. Although this is a commonly used technique, its use experimentally is limited as it does not allow precise quantification of applied force. The use of tourniquets, applied around the limbs of an animal for minutes or hours, has been used to produce non-invasive compressive nerve injuries. However, owing to the difficulty in controlling the precise location and pressure applied to the nerve, the use of tourniquets has been deemed quantitative but indirect (Chen et al., 1992). The use of various commercially-available clamps has also been proposed. While these devices allow control of crush duration, they are limited by their inability to control applied force in a continuous manner



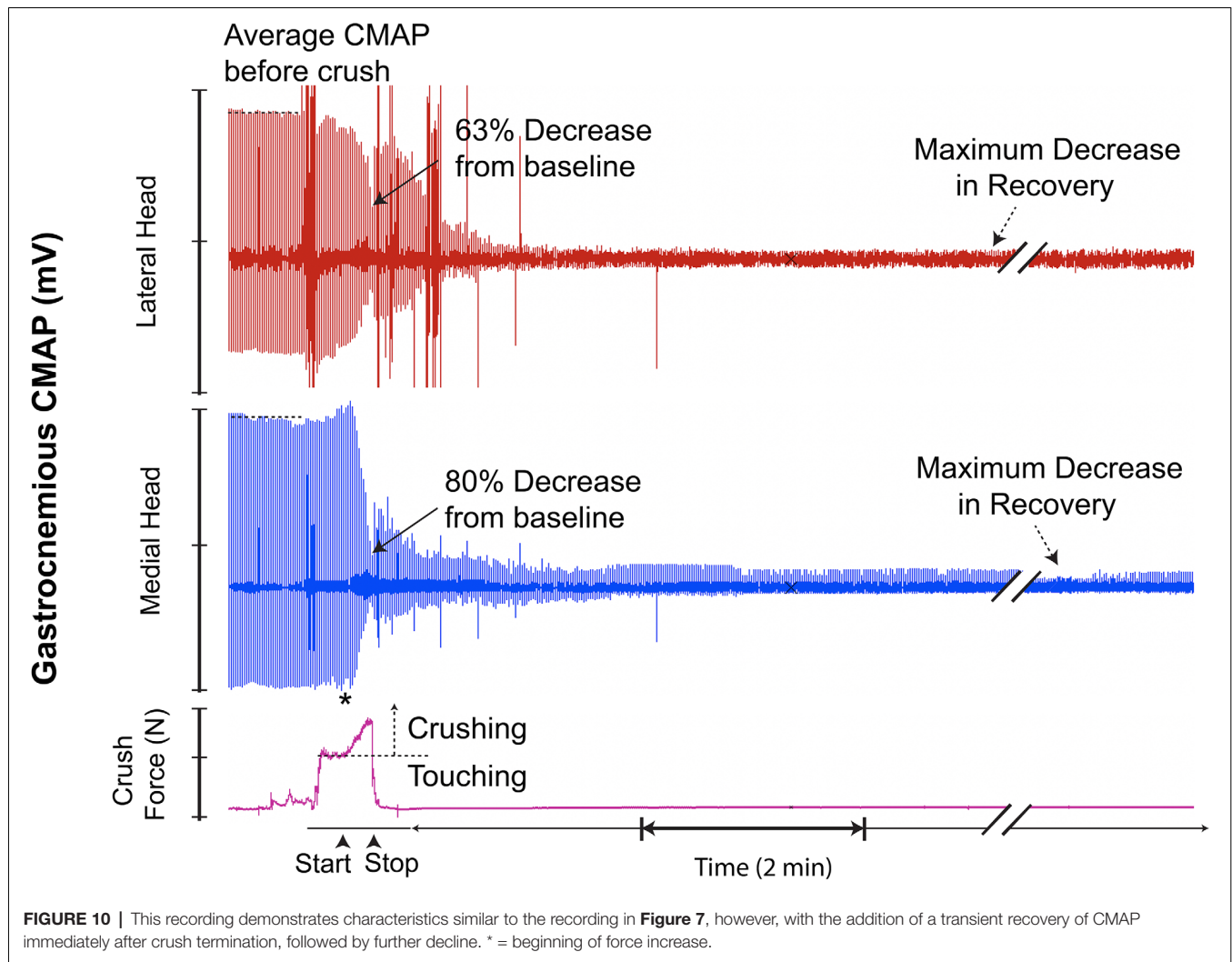


and by the fact that it is not possible to obtain a graded compression through their use (Beer et al., 2001). Other innovative devices designed to experimentally compress nerves, such as compression boxes/chambers have also been proposed. While these devices allow induction of quantitatively controlled lesions, they must be specifically designed to suit the size of the animal model used as well as the nerve location (Rydevik and Lundborg, 1977; Chen et al., 1993). Despite the wide range of crushing devices available, the Dumont No. 5 micro-forceps seems to be the instrument of choice for conducting axonotmesis (Alvites et al., 2018).

In an attempt to address the heterogeneity of crushing instruments, previous studies have used various techniques to measure and report the approximate pressure applied by the crushing device onto the nerve (Alvites et al., 2018). However, only a few have sensorized their crushing device to allow real-time *in situ* measurement of applied force. Liu et al. (2020) used a miniature foil strain gauge sensor to achieve this, while Wandling et al. (2021) used a force-sensitive resistor (FSR). The former is known to be highly sensitive, accurate, and reliable for measuring applied force (Tamura et al., 2021). On the other hand, FSRs, which are composed of a piezoresistive material whose resistance decreases as applied mechanical pressure increases, are known to be limited by their relatively low accuracy

(Schofield et al., 2016). Independent testing of the Flexiforce sensor used by Wandling et al. found that for forces up to 110 N, the sensors had an accuracy within ± 0.5 N (Sadun et al., 2016; Parmar et al., 2017). The results of this study demonstrate that the average applied force necessary to produce axonotmesis is ~ 0.5 N, therefore, this margin of error may not be acceptable for this application. The method we used to quantify applied force utilized a medical-grade disposable blood pressure (BP) transducer. In accordance with the standards of the American National Standards Institute (ANSI), disposable BP transducers designed for clinical use, such as the one used in this study, must be accurate within a range of $\pm 3\%$. A study by Gardner in which several commercially-available BP transducers were tested found that even the worst device was twice as accurate as required by the ANSI (Gardner, 1996). Having taken these factors into consideration, while also preferring an easily accessible, standardized, off-the-shelf product, we have successfully demonstrated the use of BP transducers for measurement of applied force in the context of nerve crush injury.

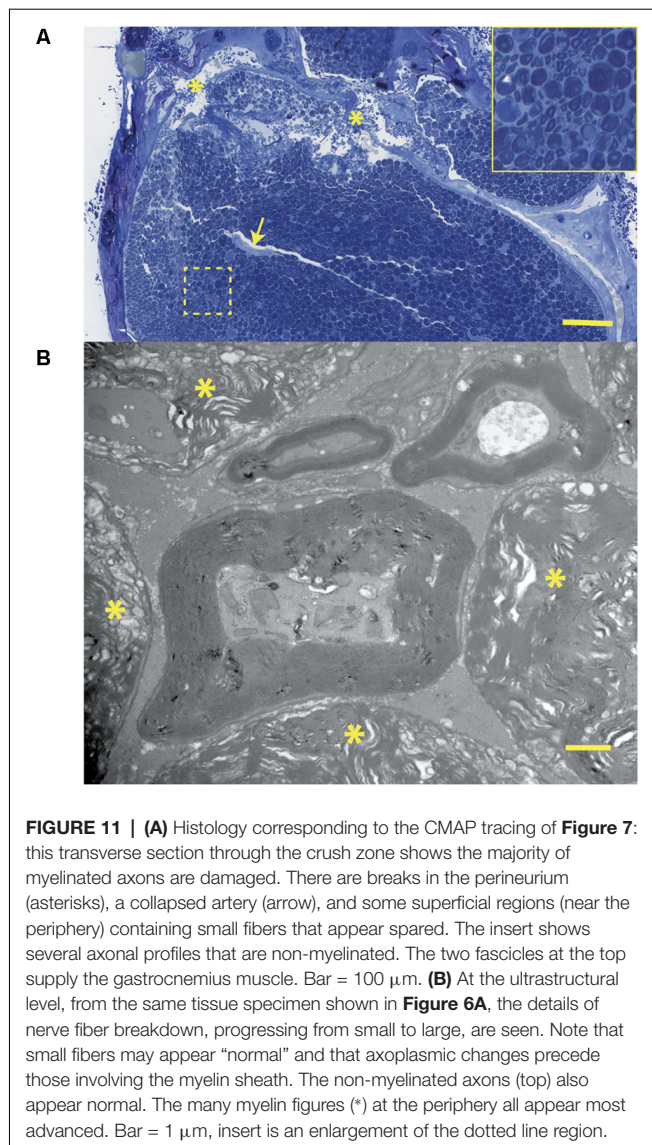
This study, and our proposed crush model, has a few notable limitations. Firstly, the power of our study was limited, involving only 11 animals and 19 crush trials ($N = 19$). Although a correlation between applied F-i during crush and



a corresponding decrease in CMAP amplitude was detected, it was found to be statistically insignificant. This may be related to the limited sample size of our data. Secondly, we conducted all crush lesions manually—by hand. This intrinsically introduces an element of human error which is difficult to quantify, but which can be observed in our results. For instance, in several trials, we unintentionally under-shot or over-shot our target 70%–90% decrease in CMAP amplitude while conducting the crush. This is most likely attributable to delays in conveying and acting upon the real-time CMAP changes. Human error was also evident in producing the graded increase in applied pressure on the nerve, as the rate of force increase often varied from trial to trial. Despite this, we have shown an overall statistical correlation between the rate of increase in applied force and crush duration for all trials (**Figure 6A**). Potential future research could perhaps address the issue of human error by applying actuators to the crushing process. For example, using readily-available programmable microcontrollers and servos, a small, portable, highly accurate device can be developed to automate the crushing process

through a closed-loop feedback system. This automated system would not only remove the error associated with a human operator but also make factors such as instrument positioning, response-time, and rate of force application more controllable and precise.

Thirdly, although our study provides preliminary data identifying the minimal threshold parameters of a crush lesion required to induce complete axonotmesis, with respect to force, duration, and extent—the precise parameters were not determined. This is a limitation of our experimental design as a more extensive histological study (e.g., quantitative and ultrastructural) would be required to determine the definitive threshold parameters in the rat tibial nerve, as well as the relationship between these parameters. Nonetheless, the primary reason we included histology in the present study was to determine the extent of the nerve lesion and the preliminary correlation with CMAPs. Moreover, although we could have easily applied our crush model to determine these lesion-specific threshold parameters, we chose not to ascertain them due to certain fundamental impediments



which diminish the clinical relevancy and application of the results. For instance, determination of these parameters using a rat model alone is in itself a fundamental limitation because the extent of protection afforded by the nerve epineurium varies according to species being investigated and is greater in humans than in rats (Kerns, 2008; Alvites et al., 2018; Kerns et al., 2019). Threshold parameters also vary based on the specific nerve being investigated and on its anatomical location, with crushing parameters likely being greater at or near joints (Alvites et al., 2018). For these reasons, we considered the determination and characterization of threshold parameters to be outside the scope of our study.

Lastly, this study was also limited by the crushing device used—a Dumont No. 5 micro-forceps. Although the contact-width at the absolute tip was 100 microns, we conducted lesions ~ 2 mm down from the tip, where the contact width was ~ 300 microns. This was done with the idea of making

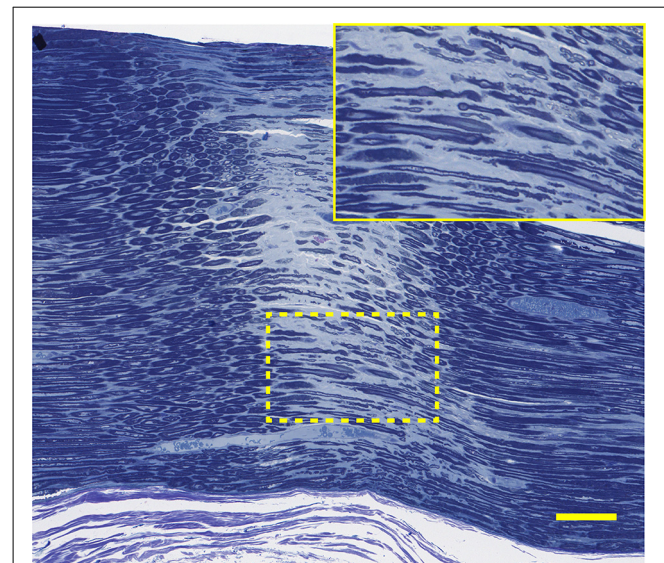


FIGURE 12 | Histology corresponding to the CMAP tracing of 5D: this longitudinal section through the narrow nerve crush zone with distinct borders shows sparing of some small nerve fibers in the gap. Lesion width is ~ 300 μm . Bar = 100 μm , insert is an enlargement of the dotted line region.

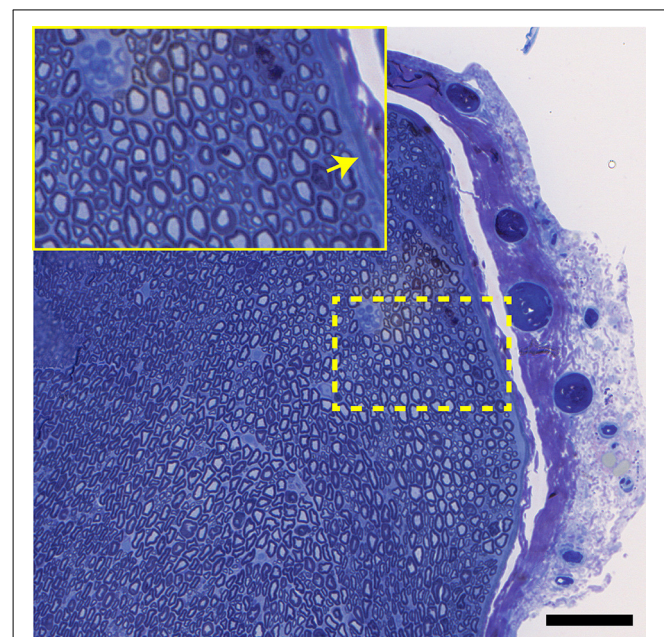


FIGURE 13 | A transverse view of the normal tibial nerve. Note the normal appearance of the perineurium (arrow), as well as the large and small myelinated axons. Bar = 100 μm , insert is an enlargement of the dotted line region.

the nerve easier to hold in between the clasps of the forceps during crushing. However, this was subject to slippage and may have resulted in variation in lesion width between trials. This highlights a disadvantage of using standard surgical forceps—the contact-width is not uniform and widens as one moves down from the tip. Therefore, if an investigator was attempting to

produce a narrow lesion (≤ 100), and could not risk allowing slippage which would change the resulting lesion's width, the use of surgical forceps would not be recommended.

Although the variability demonstrated by our results indicates that the use of CMAP amplitude decline may not be a reliable and objective endpoint for producing axonotmesis, we have shown that monitoring and recording CMAP data while concurrently inducing injury allows for the study and characterization of acute nerve responses and subsequent recovery. As previously alluded to, the modest crush parameters used in our study were found to inconsistently produce complete and uniform axonotmesis. Taken together with the variable electrophysiological responses observed during and after relatively equivalent injuries, we suggest that investigators maximize crush force and duration when producing axonotmesis. This may reduce the potential for partial sparing, the degree of which would be difficult to replicate.

Since nerve crush injury is recognized to be a clinically relevant entity, it can potentially benefit from a variety of interventions aimed at accelerating recovery or preventing functional declination. Interventions worthy of exploration could be aimed at reversing associated edema, regulating endoneurial pressure and blood flow, and especially, protecting nerves from the reactive oxygen species associated with reperfusion injury (Alvites et al., 2018). Experimentally conducting nerve injuries with concurrent monitoring of CMAP activity would allow characterization of the effects of a wide range of neurotrophic factors, growth factors, antioxidants, alkaloids, and pharmacological agents. For instance, real-time assessment of acute electrophysiological response post-injury would be particularly well-suited for exploration of the dramatic and early effects of fusogens, such as polyethylene glycol (PEG; Riley et al., 2015; Ghergherehchi et al., 2019). The study of the effects of PEG on nerve regeneration is of particular interest to researchers and has received significant coverage and discussion in recent literature (Riley et al., 2015; Bittner et al., 2016b; Ghergherehchi et al., 2019). Given PEG's time-sensitive efficacy, elucidation of its acute effects on the restitution of nerve electrical conductivity and neuromuscular response may have considerable clinical implications (Bittner et al., 2016a). Moreover, with relatively few adaptations, CMAP data could be obtained *via* minimally-invasive (Nijhuis et al., 2011) or non-invasive techniques (Kerns et al., 1987; Wang et al., 2015) thus allowing collection of interval data, hours, days, or even weeks after the injury, without the risks associated with surgery. This paradigm can be applied to the study of all forms of nerve injury, including less severe lesions such as neuropraxia, more severe lesions such as neurotmesis, and to both complete or partial axonotmesis.

CONCLUSION

Due to differences in tools and methods used, it's often difficult to compare results obtained from different experimental investigations studying nerve axonotmesis. These differences are a manifestation of variations in crush parameters, including force exerted, crush duration, and contact-width. We have demonstrated a technique which overcomes some of these

problems by using specially instrumented micro-forceps. Compared to other tools, the use of our crushing device allows quantification of all the parameters of the lesion. Moreover, we have shown that recording of CMAP during and after conduction of nerve lesions allows characterization of the acute nerve electrophysiological responses to trauma. Nerves have been shown to respond to acute trauma in a variety of ways, but with consistent patterns. Although too variable to be used as an objective endpoint for crushing, real-time *in situ* CMAP recordings may still offer some insight into the partiality of damage sustained and the sparing of axonal fibers post-traumatic injury. This model can also be used to test interventions aimed at enhancing subsequent regeneration and behavioral recovery.

DATA AVAILABILITY STATEMENT

The original contributions presented in the study are included in the article, further inquiries can be directed to the corresponding author.

ETHICS STATEMENT

The animal study was reviewed and approved by the University of Illinois at Chicago Institutional Animal Care and Use Committee.

AUTHOR CONTRIBUTIONS

The authors confirm contribution to the article as follows: JK, MG, FA, and RD: study conception and design. MH, NB, DE, MG, FA, and JK: data collection. MH, NB, DE, and JK: analysis and interpretation of results. MH, NB, DE, RD, FA, MG, and JK: draft manuscript preparation. All authors reviewed the results and approved the final version of the manuscript. All authors contributed to the article and approved the submitted version.

FUNDING

This research was supported in part by Departmental Funds. The authors received no extra-mural financial support for the research, authorship, and/or publication of this article.

ACKNOWLEDGMENTS

We thank Dr. James S. Walter (Hines Veterans Affairs Hospital Research Service, Hines, IL) for supporting us in developing the interface used in this study and for his guidance in overcoming the technical challenges we encountered. This work would not have been possible without his support. We thank Figen A. Seiler (Research Resources Center, University of Illinois Chicago, Chicago, IL) for her service and support in generating the histology used in this study. We thank Dr. Sanjay Singh (Hines Veterans Affairs Hospital Research Service, Hines, IL) for his thoughtful contributions to our discussion.

REFERENCES

- Alvites, R., Rita Caseiro, A., Santos Pedrosa, S., Vieira Branquinho, M., Ronchi, G., Geuna, S., et al. (2018). Peripheral nerve injury and axonotmesis: state of the art and recent advances. *Cog. Med.* 5:1466404. doi: 10.1080/2331205X.2018.1466404
- Beer, G. M., Steurer, J., and Meyer, V. E. (2001). Standardizing nerve crushes with a non-serrated clamp. *J. Reconstr. Microsurg.* 17, 531–534. doi: 10.1055/s-2001-17755
- Bhatt, N. K., Park, A. M., Al-Lozi, M., and Paniello, R. C. (2016). Compound motor action potential quantifies recurrent laryngeal nerve innervation in a canine model. *Ann. Otol. Rhinol. Laryngol.* 125, 584–590. doi: 10.1177/0003489416637386
- Bittner, G. D., Mikes, M., and Ghergherechi, C. L. (2016a). Polyethylene glycol-fusion retards Wallerian degeneration and rapidly restores behaviors lost after nerve severance. *Neural. Regen. Res.* 11, 217–219. doi: 10.4103/1673-5374.177716
- Bittner, G. D., Sengelaub, D. R., Trevino, R. C., Peduzzi, J. D., Mikes, M., Ghergherechi, C. L., et al. (2016b). The curious ability of polyethylene glycol fusion technologies to restore lost behaviors after nerve severance. *J. Neurosci. Res.* 94, 207–230. doi: 10.1002/jnr.23685
- Campbell, W. W. (2008). Evaluation and management of peripheral nerve injury. *Clin. Neurophysiol.* 119, 1951–1965. doi: 10.1016/j.clinph.2008.03.018
- Chen, L. E., Seaber, A. V., and Urbaniak, J. R. (1993). The influence of magnitude and duration of crush load on functional recovery of the peripheral nerve. *J. Reconstr. Microsurg.* 9, 299–306. doi: 10.1055/s-2007-1006671
- Chen, L. E., Seaber, A. V., Glisson, R. R., Davies, H., Murrell, G. A., Anthony, D. C., et al. (1992). The functional recovery of peripheral nerves following defined acute crush injuries. *J. Orthop. Res.* 10, 657–664. doi: 10.1002/jor.1100100508
- Chung, T., Prasad, K., and Lloyd, T. E. (2014). Peripheral neuropathy: clinical and electrophysiological considerations. *Neuroimaging Clin. N Am.* 24, 49–65. doi: 10.1016/j.nic.2013.03.023
- De Koning, P., Brakkee, J. H., and Gispens, W. H. (1986). Methods for producing a reproducible crush in the sciatic and tibial nerve of the rat and rapid and precise testing of return of sensory function. beneficial effects of melanocortins. *J. Neurol. Sci.* 74, 237–246. doi: 10.1016/0022-510x(86)90109-7
- Dun, X. P., and Parkinson, D. B. (2018). Transection and crush models of nerve injury to measure repair and remyelination in peripheral nerve. *Methods Mol. Biol.* 1791, 251–262. doi: 10.1007/978-1-4939-7862-5_20
- Fan, L. Y., Wang, Z. C., Wang, P., Lan, Y. Y., and Tu, L. (2015). Exogenous nerve growth factor protects the hypoglossal nerve against crush injury. *Neural Regen. Res.* 10, 1982–1988. doi: 10.4103/1673-5374.172316
- Feng, X., and Yuan, W. (2015). Dexamethasone enhanced functional recovery after sciatic nerve crush injury in rats. *Biomed. Res. Int.* 2015:627923. doi: 10.1155/2015/627923
- Gardner, R. M. (1996). Accuracy and reliability of disposable pressure transducers coupled with modern pressure monitors. *Crit. Care Med.* 24, 879–882. doi: 10.1097/00003246-199605000-00025
- Ghergherechi, C. L., Mikes, M., Sengelaub, D. R., Jackson, D. M., Smith, T., Nguyen, J., et al. (2019). Polyethylene glycol (PEG) and other bioactive solutions with neurorrhaphy for rapid and dramatic repair of peripheral nerve lesions by PEG-fusion. *J. Neurosci. Methods* 314, 1–12. doi: 10.1016/j.jneumeth.2018.12.015
- Hei, W. H., Byun, S. H., Kim, J. S., Kim, S., Seo, Y. K., Park, J. C., et al. (2016). Effects of electromagnetic field (PEMF) exposure at different frequency and duration on the peripheral nerve regeneration: *in vitro* and *in vivo* study. *Int. J. Neurosci.* 126, 739–748. doi: 10.3109/00207454.2015.1054032
- Kerns, J. M., Fakhouri, A. J., and Pavkovic, I. M. (1987). A twitch tension method to assess motor nerve function in rat. *J. Neurosci. Methods* 19, 259–266. doi: 10.1016/0165-0270(87)90069-0
- Kerns, J. (2008). The microstructure of peripheral nerves. *Tech. Reg. Anesth. Pain Manag.* 12, 127–133.
- Kerns, J., Piponov, H., Helder, C., Amirouche, F., Solitro, G., and Gonzalez, M. (2019). Mechanical properties of the human tibial and peroneal nerves following stretch with histological correlations. *Anat. Rec. (Hoboken)* 302, 2030–2039.
- Kerns, J. M., Walter, J. S., Patetta, M. J., Sood, A., Hussain, A. K., Chung, J. J., et al. (2020). Histological assessment of Wallerian degeneration of the rat tibial nerve following crush and transection injuries. *J. Reconstr. Microsurg.* 37, 1–14. doi: 10.1055/s-0040-1716870
- Kloos, A. D., Fisher, L. C., Detloff, M. R., Hassenzahl, D. L., and Basso, D. M. (2005). Stepwise motor and all-or-none sensory recovery is associated with non-linear sparing after incremental spinal cord injury in rats. *Exp. Neurol.* 191, 251–265. doi: 10.1016/j.expneurol.2004.09.016
- Korkmaz, M. F., Parlakpinar, H., Ceylan, M. F., Ediz, L., Samdanci, E., Kekilli, E., et al. (2016). The effect of sildenafil on recuperation from sciatic nerve injury in rats. *Balkan Med. J.* 33, 204–211. doi: 10.5152/balkanmedj.2016.14701
- Kurtoglu, Z., Ozturk, A. H., Bagdatoglu, C., Polat, G., Aktekin, M., Uzansel, D., et al. (2005). Effects of trapidil after crush injury in peripheral nerve. *Acta Med. Okayama.* 59, 37–44. doi: 10.18926/AMO/31967
- Liu, X., Feng, L., Shinde, I., Cole, J. D., Troy, J. B., and Saggere, L. (2020). Correlation between retinal ganglion cell loss and nerve crush force-impulse established with instrumented tweezers in mice. *Neural. Res.* 42, 379–386. doi: 10.1080/01616412.2020.1733322
- Lundborg, G. (2004). *Nerve Injury and Repair: Regeneration, Reconstruction and Cortical Remodeling*. Philadelphia, PA: Elsevier/Churchill Livingstone.
- Maathuis, E. M., Drenthen, J., Visser, G. H., and Blok, J. H. (2011). Reproducibility of the CMAP scan. *J. Electromyogr. Kinesiol.* 21, 433–437. doi: 10.1016/j.jelekin.2010.11.007
- Malushte, T. S., Kerns, J. M., Huang, C. C., Shott, S., Safanda, J., and Gonzalez, M. (2004). Assessment of recovery following a novel partial nerve lesion in a rat model. *Muscle Nerve* 30, 609–617. doi: 10.1002/mus.20152
- Menorca, R. M., Fussell, T. S., and Elfar, J. C. (2013). Nerve physiology: mechanisms of injury and recovery. *Hand. Clin.* 29, 317–330. doi: 10.1016/j.hcl.2013.04.002
- Mikes, M., Ghergherechi, C. L., Hastings, R. L., Ali, A., Rahesh, S., Jagannath, K., et al. (2018). Polyethylene glycol solutions rapidly restore and maintain axonal continuity, neuromuscular structures and behaviors lost after sciatic nerve transections in female rats. *J. Neurosci. Res.* 96, 1223–1242. doi: 10.1002/jnr.24225
- Navarro, X. (2016). Functional evaluation of peripheral nerve regeneration and target reinnervation in animal models: a critical overview. *Eur. J. Neurosci.* 43, 271–286. doi: 10.1111/ejn.13033
- Navarro, X., and Udina, E. (2009). Chapter 6: methods and protocols in peripheral nerve regeneration experimental research: part III-electrophysiological evaluation. *Int. Rev. Neurobiol.* 87, 105–126. doi: 10.1016/S0074-7742(09)87006-2
- Ni, X. J., Wang, X. D., Zhao, Y. H., Sun, H. L., Hu, Y. M., Yao, J., et al. (2017). The effect of low-intensity ultrasound on brain-derived neurotrophic factor expression in a rat sciatic nerve crushed injury model. *Ultrasound Med. Biol.* 43, 461–468. doi: 10.1016/j.ultrasmedbio.2016.09.017
- Nijhuis, T. H., Smits, E. S., Van Neck, J. W., Visser, G. H., Walbeehm, E. T., Blok, J. H., et al. (2011). Ultrasound-guided needle positioning near the sciatic nerve to elicit compound muscle action potentials from the gastrocnemius muscle of the rat. *J. Neurosci. Methods* 194, 283–286. doi: 10.1016/j.jneumeth.2010.10.026
- Parmar, S., Khodasevych, I., and Troynikov, O. (2017). Evaluation of flexible force sensors for pressure monitoring in treatment of chronic venous disorders. *Sensors* 17:1923. doi: 10.3390/s17081923
- Riley, D. C., Bittner, G. D., Mikes, M., Cardwell, N. L., Pollins, A. C., Ghergherechi, C. L., et al. (2015). Polyethylene glycol-fused allografts produce rapid behavioral recovery after ablation of sciatic nerve segments. *J. Neurosci. Res.* 93, 572–583. doi: 10.1002/jnr.23514
- Robinson, L. R. (2000). Traumatic injury to peripheral nerves. *Muscle Nerve* 23, 863–873. doi: 10.1002/(sici)1097-4598(200006)23:6<863::aid-mus4>3.0.co;2-0
- Ronchi, G., Nicolino, S., Raimondo, S., Tos, P., Battiston, B., Papalia, I., et al. (2009). Functional and morphological assessment of a standardized crush injury of the rat median nerve. *J. Neurosci. Methods* 179, 51–57. doi: 10.1016/j.jneumeth.2009.01.011
- Rydevik, B., and Lundborg, G. (1977). Permeability of intraneural microvessels and perineurium following acute, graded experimental nerve compression. *Scand. J. Plast. Reconstr. Surg.* 11, 179–187. doi: 10.3109/02844317709025516
- Sadun, A., Jalani, J., and Sukor, J. A. (2016). Force Sensing Resistor (FSR): a brief overview and the low-cost sensor for active compliance control. *SPIE* 10011, 12–18. doi: 10.1117/12.2242950

- Sarikcioglu, L., and Ozkan, O. (2003). Yasargil-Phynox aneurysm clip: a simple and reliable device for making a peripheral nerve injury. *Int. J. Neurosci.* 113, 455–464. doi: 10.1080/00207450390162218
- Sarikcioglu, L., Yaba, A., Tanriover, G., Demirtop, A., Demir, N., and Ozkan, O. (2007). Effect of severe crush injury on axonal regeneration: a functional and ultrastructural study. *J. Reconstr. Microsurg.* 23, 143–149. doi: 10.1055/s-2007-974649
- Schofield, J. S., Evans, K. R., Hebert, J. S., Marasco, P. D., and Carey, J. P. (2016). The effect of biomechanical variables on force sensitive resistor error: Implications for calibration and improved accuracy. *J. Biomech.* 49, 786–792. doi: 10.1016/j.jbiomech.2016.01.022
- Seddon, H. J. (1943). Peripheral nerve injuries. *Glasgow. Med. J.* 139, 61–75.
- Smith, K. J., Felts, P. A., and John, G. R. (2000). Effects of 4-aminopyridine on demyelinated axons, synapses and muscle tension. *Brain* 123, 171–184. doi: 10.1093/brain/123.1.171
- Sta, M., Cappaert, N. L., Ramekers, D., Baas, F., and Wadman, W. J. (2014). The functional and morphological characteristics of sciatic nerve degeneration and regeneration after crush injury in rats. *J. Neurosci. Methods* 222, 189–198. doi: 10.1016/j.jneumeth.2013.11.012
- Sunderland, S. (1951). A classification of peripheral nerve injuries producing loss of function. *Brain* 74, 491–516. doi: 10.1093/brain/74.4.491
- Suzuki, K., Tanaka, H., Ebara, M., Uto, K., Matsuoka, H., Nishimoto, S., et al. (2017). Electrospun nanofiber sheets incorporating methylcobalamin promote nerve regeneration and functional recovery in a rat sciatic nerve crush injury model. *Acta Biomater.* 53, 250–259. doi: 10.1016/j.actbio.2017.02.004
- Tamura, R., Sakaino, S., and Tsuji, T. (2021). High dynamic range uniaxial force/torque sensor using metal foil and semiconductor strain gauge. *IEEE J. Industry Appl.* 10, 506–511. doi: 10.1541/ieejia.20007411
- Tos, P., Ronchi, G., Papalia, I., Sallen, V., Legagneux, J., Geuna, S., et al. (2009). Chapter 4: Methods and protocols in peripheral nerve regeneration experimental research: part I-experimental models. *Int. Rev. Neurobiol.* 87, 47–79. doi: 10.1016/S0074-7742(09)87004-9
- Vannucci, B., Santosa, K. B., Keane, A. M., Jablonka-Shariff, A., Lu, C. Y., Yan, Y., et al. (2019). What is normal? neuromuscular junction reinnervation after nerve injury. *Muscle Nerve* 60, 604–612. doi: 10.1002/mus.26654
- Varejao, A. S., Cabrita, A. M., Meek, M. F., Bulas-Cruz, J., Melo-Pinto, P., Raimondo, S., et al. (2004). Functional and morphological assessment of a standardized rat sciatic nerve crush injury with a non-serrated clamp. *J. Neurotrauma* 21, 1652–1670. doi: 10.1089/neu.2004.21.1652
- Wandling, G. D., Lee, J. I., Talukder, M. A. H., Govindappa, P. K., and Elfar, J. C. (2021). Novel real-time digital pressure sensor reveals wide variations in current nerve crush injury models. *Mil. Med.* 186, 473–478. doi: 10.1093/milmed/usaa346
- Wang, Y., Wang, H., Mi, D., Gu, X., and Hu, W. (2015). Periodical assessment of electrophysiological recovery following sciatic nerve crush via surface stimulation in rats. *Neurol. Sci.* 36, 449–456. doi: 10.1007/s10072-014-2005-0
- Yuce, S., Cemal Gokce, E., Iskdemir, A., Koc, E. R., Cemil, D. B., Gokce, A., et al. (2015). An experimental comparison of the effects of propolis, curcumin and methylprednisolone on crush injuries of the sciatic nerve. *Ann. Plast. Surg.* 74, 684–692. doi: 10.1097/SAP.0000000000000026
- Zhang, X., Xin, N., Tong, L., and Tong, X. J. (2013). Electrical stimulation enhances peripheral nerve regeneration after crush injury in rats. *Mol. Med. Rep.* 7, 1523–1527. doi: 10.3892/mmr.2013.1395

Conflict of Interest: The authors declare that the research was conducted in the absence of any commercial or financial relationships that could be construed as a potential conflict of interest.

Publisher's Note: All claims expressed in this article are solely those of the authors and do not necessarily represent those of their affiliated organizations, or those of the publisher, the editors and the reviewers. Any product that may be evaluated in this article, or claim that may be made by its manufacturer, is not guaranteed or endorsed by the publisher.

Copyright © 2022 Hamad, Boroda, Echenique, Dieter, Amirouche, Gonzalez and Kerns. This is an open-access article distributed under the terms of the Creative Commons Attribution License (CC BY). The use, distribution or reproduction in other forums is permitted, provided the original author(s) and the copyright owner(s) are credited and that the original publication in this journal is cited, in accordance with accepted academic practice. No use, distribution or reproduction is permitted which does not comply with these terms.



Intraneural Topography of Rat Sciatic Axons: Implications for Polyethylene Glycol Fusion Peripheral Nerve Repair

Emily A. Hibbard and Dale R. Sengelaub*

Department of Psychological and Brain Sciences, Indiana University, Bloomington, IN, United States

OPEN ACCESS

Edited by:

Giovanna Gambarotta,
University of Turin, Italy

Reviewed by:

André Luis Bombeiro,
Universidade de Lisboa, Portugal
Kirsten Haastert-Talini,
Hannover Medical School, Germany
Arthur W. English,
Emory University, United States

*Correspondence:

Dale R. Sengelaub
sengelaub@indiana.edu

Specialty section:

This article was submitted to
Cellular Neuropathology,
a section of the journal
Frontiers in Cellular Neuroscience

Received: 11 January 2022

Accepted: 11 February 2022

Published: 30 March 2022

Citation:

Hibbard EA and Sengelaub DR
(2022) Intraneural Topography of Rat
Sciatic Axons: Implications
for Polyethylene Glycol Fusion
Peripheral Nerve Repair.
Front. Cell. Neurosci. 16:852933.
doi: 10.3389/fncel.2022.852933

Peripheral nerve injuries are the most common type of nerve trauma. We have been working with a novel repair technique using a plasmalemmal fusogen, polyethylene glycol (PEG), to re-fuse the membranes of severed axons. PEG-fusion repair allows for immediate re-innervation of distal targets, prevents axonal degeneration, and improves behavioral recovery. PEG-fusion of severed axons is non-specific, and we have previously reported that following injury and PEG-fusion misconnections between spinal motoneurons and their distal targets were present. Surprisingly, appropriately paired proximal and distal motor axons were observed in all PEG-fused animals. We hypothesized that a topographic organization of axons contributing to the sciatic nerve could explain the incidence of appropriate connections. We traced the course of specific axon populations contributing to the sciatic nerve in young adult male and female rats. Following intraneural injection of Fast Blue into the tibial branch, labeled axons were confined to a discrete location throughout the course of the nerve. Following intramuscular injection of cholera toxin-conjugated horseradish peroxidase into the anterior tibialis, labeled axons were confined to a smaller but still discrete location throughout the nerve. In both cases, the relative locations of labeled axons were consistent bilaterally within animals, as well as across animals and sexes. Thus, the relatively consistent location of specific axon populations could allow for realignment of appropriate populations of axons, and enhanced behavioral recovery seen in PEG-fused animals. Knowing the organization of axons within the sciatic nerve promotes accurate territory realignment during repair, therefore aiding in recovery outcomes.

Keywords: sciatic nerve, topography, rat, retrograde labeling, morphology

INTRODUCTION

Peripheral nerve injuries (PNIs) that disrupt axonal continuity, therefore denervating distal musculature and tissue, have serious consequences on both the peripheral and central nervous systems. The peripheral consequences include the immediate loss of both motor and sensory function distal to the injury, rapid and irreversible degeneration of the distal nerve segment (Wallerian degeneration), as well as neuromuscular junction loss and muscle atrophy over time (Brushart, 2011). Centrally, PNIs lead to motoneuron somal atrophy (Ma et al., 2002;

Wiberg et al., 2017), retraction of synaptic inputs from somata and dendrites (Alvarez et al., 2011; Rotterman et al., 2014; Wiberg et al., 2017), and dendritic atrophy (Rotterman et al., 2014; Wiberg et al., 2017). Reinnervation of distal targets depends upon the slow outgrowth of axons from the proximal nerve stump which may take several weeks to reestablish any connectivity (Wolfe et al., 2010). The current standard of treatment for PNIs is neurorrhaphy which involves microsuturing the epineuria of the proximal and distal severed nerve stumps (Brushart, 2011). Unfortunately, this leaves internal axons in their severed state, does not prevent Wallerian degeneration, and only marginally improves recovery (Allen, 2000; Bertelli and Ghizoni, 2009, 2011). Overall, behavioral recovery, with and without standard treatment, is very poor, which reinforces the need for a new treatment protocol for PNIs.

A novel repair technique for PNIs called polyethylene glycol (PEG) fusion repair has shown tremendous therapeutic potential. PEG-fusion uses a plasmalemmal fusogen, PEG, to fuse severed axonal membranes after injury thus immediately restoring axonal continuity and distal innervation. PEG-fusion repair improves behavioral recovery remarkably, and has been shown to prevent both the peripheral and central consequences of PNI including Wallerian degeneration (Britt et al., 2010; Riley et al., 2015; Ghergherehchi et al., 2016; Mikesch et al., 2018a,b) and somal/dendritic atrophy (Ghergherehchi et al., 2019). Fusion of severed axonal membranes by PEG-fusion is non-specific; therefore, PEG-fusion indiscriminately fuses axonal membranes that are in close approximation without regard for their modality or original connectivity. We have previously reported that this non-specificity leads to misconnections between motoneurons and their distal targets (Ghergherehchi et al., 2019). After sciatic nerve injury and PEG-fusion, we performed an intramuscular injection of retrograde tracer into the anterior tibialis (TA) muscle in order to label innervating motoneurons, and found labeled motoneurons in inappropriate spinal segments, indicating misconnections (Ghergherehchi et al., 2019). Surprisingly, labeled motoneurons were also found in the appropriate spinal segment in every PEG-fused animal, regardless of repair type, either single-cut or allograft (Ghergherehchi et al., 2019). Despite PEG-fusion non-specifically fusing severed axons, proximal TA motor axons were reliably fused to distal axons that projected to TA.

We hypothesized that the consistent pattern of correctly connected TA axons after PEG-fusion repair was due to a topographic organization of axons within the sciatic nerve. It has been previously reported in a variety of species that axons which serve specific distal branches of peripheral nerves travel in organized bundles along the course of the nerve (Sunderland, 1978; Brushart, 1991; Hallin et al., 1991). The sciatic nerve of rats has been shown to exhibit a similar organization of its major branches (Suaïd et al., 2016; Ravagli et al., 2020) as well as its more distal branches (Badia et al., 2010). We investigated the topographic organization of axons within the rat sciatic nerve at the level of an individual muscle (TA), and looked for consistencies in this topography bilaterally within animals as well as across animals and sexes.

MATERIALS AND METHODS

All procedures were performed in accordance with the Indiana University Animal Care and Use Guidelines (Protocol #20-038). A total of 14 adult Sprague-Dawley rats (approximately 70 days old; Envigo, Indianapolis) were used (male, $n = 8$; female, $n = 6$). Rats were maintained on a 12:12-hr light/dark cycle with unlimited access to food and water.

Tracer Injections

Intraneural labeling: The location of an axon population of a specific branch of the sciatic nerve was examined in a total of 12 nerves in adult male ($n = 4$) and female ($n = 3$) rats. Rats were anesthetized with isoflurane, and the sciatic nerve trifurcation was exposed along the dorsolateral aspect of the hindlimb. Just distal to the trifurcation, the tibial branch was isolated and crushed for ten seconds using atraumatic forceps in order to encourage uptake of the tracer. Using a Hamilton syringe connected to a 31G needle, 2 μ L of Fast Blue (2.5%; Polysciences, Inc., Warrington, PA, United States) was injected into the tibial branch just proximal to the crush injury. Fast Blue is a fluorescent tracer that is retrogradely transported by motor and sensory axons (Kuyper and Huisman, 1984). Dissected muscles were sutured, and the skin incision was closed with wound clips. The same procedure was performed on the opposite hindlimb, and the animal was allowed to recover for six days, a period that ensures optimal transport (Steward, 1981).

Intramuscular labeling: The location of an axon population innervating a specific muscle was examined in a total of 14 sciatic nerves in adult male ($n = 4$) and female ($n = 3$) rats. Rats were anesthetized as above, and the anterior tibialis muscle was exposed and injected with horseradish peroxidase conjugated to the beta subunit of the cholera toxin molecule (BHRP; 2 μ L, 0.2%; Invitrogen, Carlsbad, CA, United States). At this volume and concentration, BHRP is specifically taken up by motor axons and does not label dorsal root ganglion cells that lack GM1 ganglioside required to actively transmembrane transport BHRP (Alisky et al., 2002; Lappi et al., 2014). The skin incision was closed as above, and the animals were allowed to recover for two days, a period that ensures optimal transport (Kurz et al., 1986, 1991; Goldstein et al., 1990).

Anatomical Dissection

All animals for both injection groups followed the same dissection methodology. After the appropriate transport period, animals were weighed, given an overdose of urethane (approximately 0.5g/100g body weight), and perfused intracardially with saline followed by cold fixative (4% paraformaldehyde). The entirety of the sciatic nerve was exposed along the dorsolateral aspect of the hindlimb by blunt dissection of the muscles from the sciatic notch to the distal trifurcation. Two 10 mm sciatic nerve segments were removed, a proximal segment starting at the sciatic notch and a distal segment terminating at the trifurcation. Heat lesions were placed on the lateral aspect of each segment to serve as fiduciary marks to maintain orientation of nerve segments throughout processing. The same dissection process was performed on the

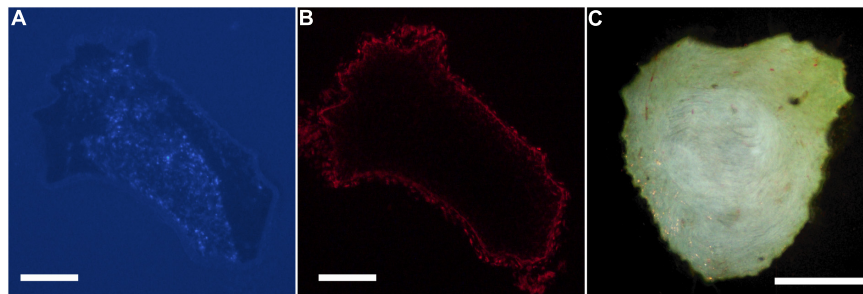


FIGURE 1 | Digital micrographs of a transverse section of a proximal segment of a sciatic nerve visualizing. **(A)** Fast Blue-labeled axons contributing to the tibial branch (DAPI filter), and **(B)** the same section visualizing propidium iodide staining for total nerve area (Texas Red filter). **(C)** Darkfield digital micrograph of a transverse section of a proximal segment of a sciatic nerve showing BHRP-labeled TA motoneurons. Scale bars = 250 μm .

opposite hindlimb. The nerve segments were post-fixed in the same fixative for two hours, then transferred to 30% sucrose phosphate buffer overnight for cryoprotection.

Histological Processing and Visualization

Nerve segments were embedded in a known orientation in M-1 Embedding Matrix (Shandon, Thermo Fisher Scientific Waltham, MA, United States) and sectioned transversely (50 μm , sampled at 500 μm intervals) on a cryostat at -15°C , thaw-mounted onto glass slides, and allowed to dry for 24 h.

For visualization of Fast Blue-labeled axons, sections were coverslipped with Vectashield antifade mounting medium with propidium iodide (Vector Laboratories, Inc., Burlingame, CA, United States). Sections spanning the length of the nerve segments (an average of 19.4 ± 1.4 sections per nerve segment) were observed under epifluorescence using a DAPI filter for visualization of Fast Blue and a Texas Red filter for visualization of propidium iodide. Digital micrographs of each section were taken at a final magnification of 166X using an NIS-Elements Imaging system (Nikon Instruments, Melville, NY, United States). Using the digital micrographs of propidium iodide-stained sections, the total nerve area was measured using a computer-based morphometry system (Stereo Investigator, MBF Bioscience, Williston, VT, United States). Using the matching digital micrographs of Fast Blue labeling, the area occupied and the distribution of labeled axons was mapped using the same computer-based morphometry system.

For visualization of BHRP-labeled axons, nerve sections were reacted using a modified tetramethyl benzidine protocol (Mesulam, 1982). Sections were counterstained with thionin and coverslipped with Permount (Fisher Scientific, Pittsburgh, PA, United States). Sections spanning the length of the nerve segments (an average of 19.2 ± 2.7 sections per nerve segment) were observed under darkfield illumination at a final magnification of 250X. The area and distribution of labeled axons within each section was reconstructed in three dimensions using a computer-based morphometry system (NeuroLucida, MBF Bioscience). Digital light micrographs were obtained using an MDS 290 digital camera system (Eastman Kodak Company, Rochester, NY, United States). An analysis of variance with

repeated measures was used to analyze the size of axon territories within the nerve.

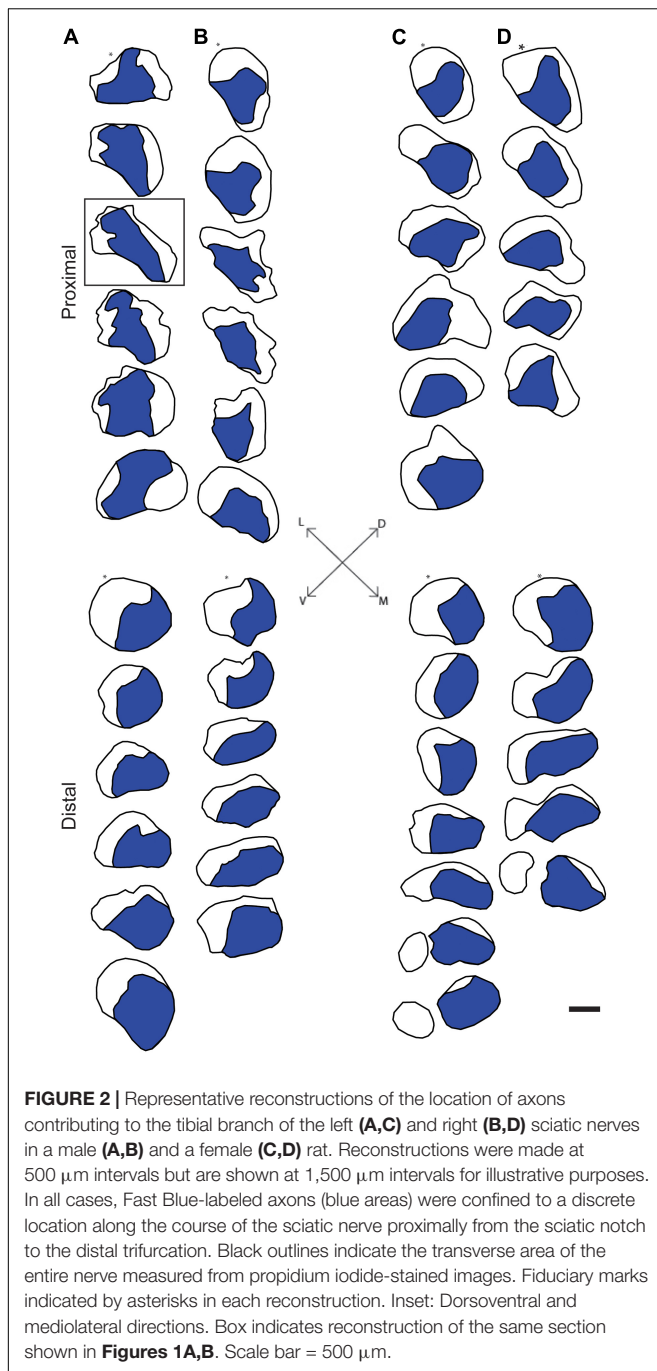
RESULTS

Fast Blue Labeling

Digital micrographs of transverse sciatic nerve sections visualizing Fast Blue-labeled axons (**Figure 1A**) and propidium iodide staining (**Figure 1B**) showed a discrete localization of labeled axons. Reconstructions of Fast Blue-labeled axons within the sciatic nerve revealed a clearly defined and reproducible topographic organization (**Figure 2**). Labeled axons were found in a discrete location within the nerve from the sciatic notch to the distal trifurcation, rather than widely distributed across the entire transverse area. The tibial branch was also determined to occupy a relatively large transverse area of the sciatic nerve at an average of $53.40 \pm 3.79\%$. We also examined the proximal, middle, and distal portions of the entire nerve for evidence of consistency in the size of the area occupied by Fast Blue-labeled axons. The area occupied by Fast Blue-labeled axons in the proximal portion of the nerve was $0.276 \pm 0.034 \text{ mm}^2$ (mean \pm SEM). This area did not differ along the proximo-distal course of the nerve (middle portion, $0.302 \pm 0.034 \text{ mm}^2$; distal portion, $0.281 \pm 0.029 \text{ mm}^2$) [$F(2,20) = 2.95$, *ns*]. The size and position of the tibial branch territory was consistent bilaterally within animals, as well as across animals and sexes.

BHRP Labeling

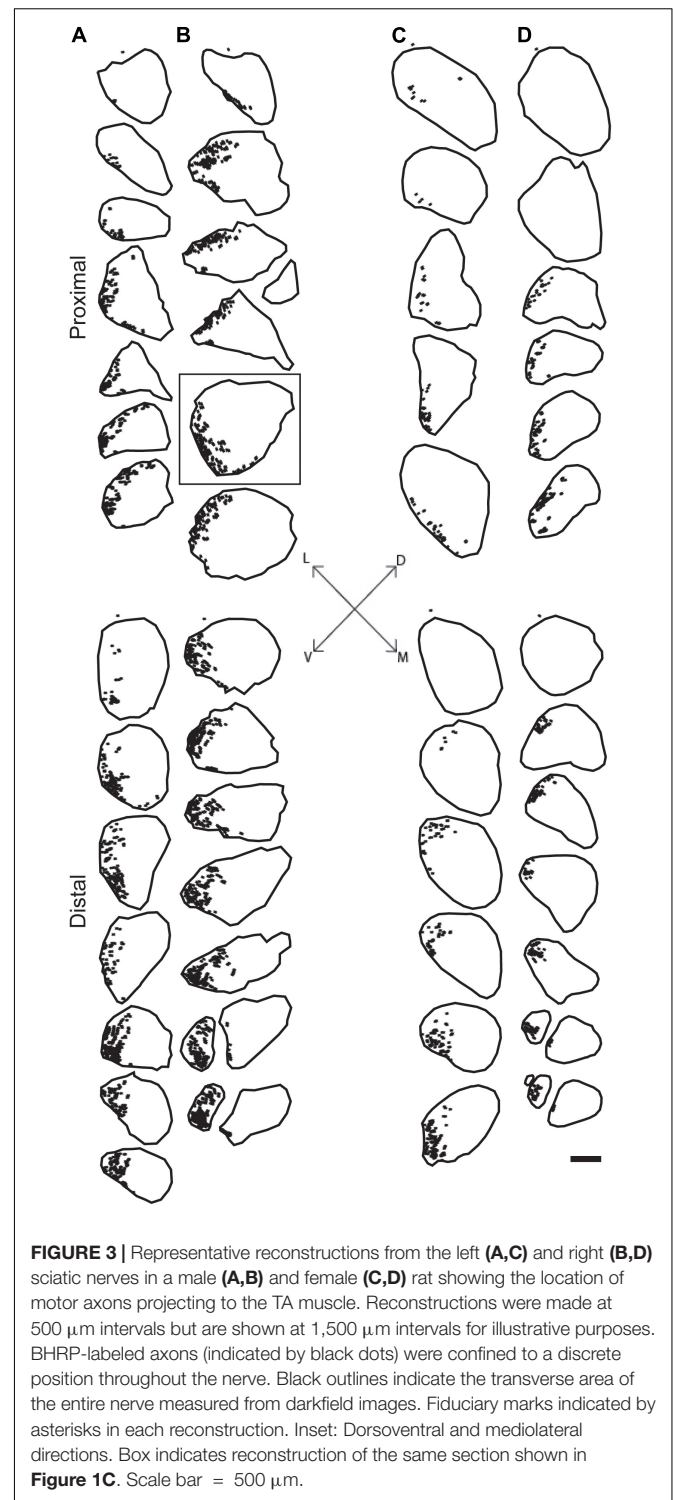
Digital micrographs of BHRP-labeled axons (**Figure 1C**) showed a discrete localization of labeled axons. Reconstructions of BHRP-labeled axons within the sciatic nerve (**Figure 3**) revealed a clearly defined and reproducible topographic organization (one nerve was excluded from further analysis due to compromised histology). Labeled axons were found in a discrete location throughout the entire nerve, rather than widely distributed across the entire transverse area. This territory was also relatively large, occupying $12.02 \pm 1.01\%$ of the total transverse area. The area occupied by BHRP-labeled axons in the proximal portion of the nerve was $0.035 \pm 0.005 \text{ mm}^2$. This area increased linearly along the proximo-distal course of the nerve to $0.047 \pm 0.007 \text{ mm}^2$.



distally, an increase of 54.29% [$F(2,22) = 17.92, p < 0.0001$]. The size and position of the anterior tibialis territory was consistent bilaterally within animals, as well as across animals and sexes.

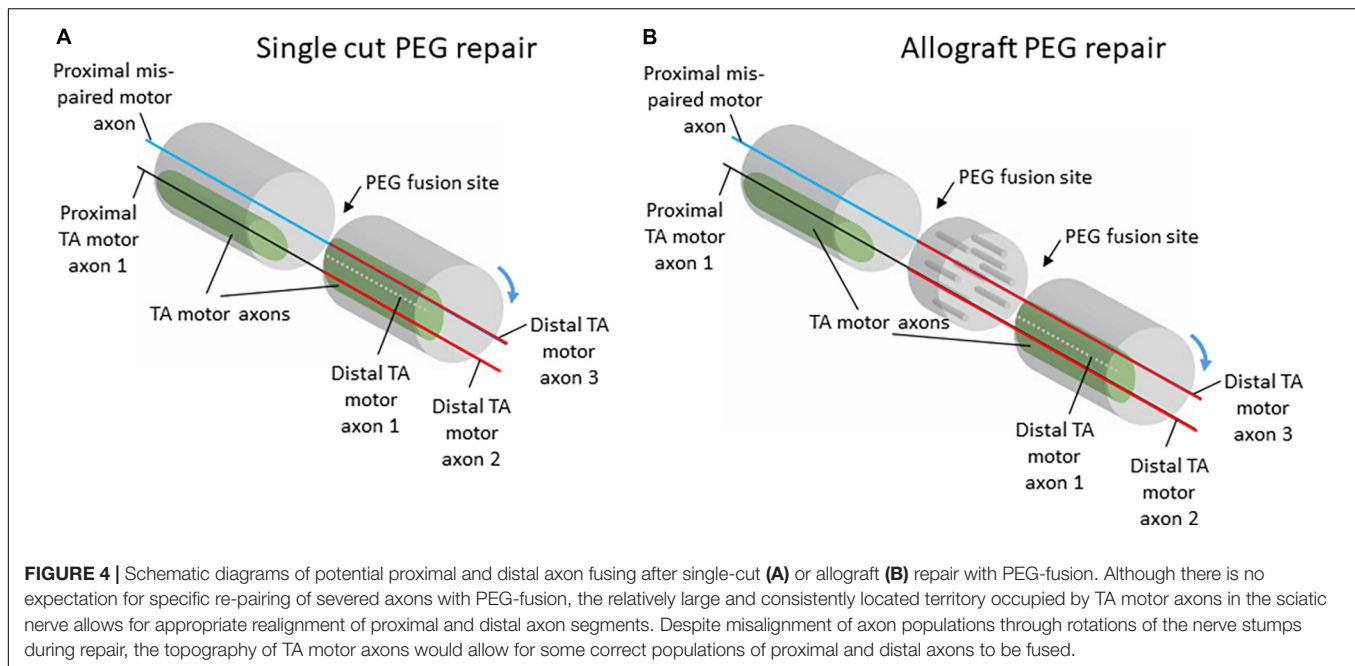
DISCUSSION

We assessed the distribution of axons contributing to either the tibial branch or the anterior tibialis muscle within the sciatic nerve. We found that both populations of axons occupy



consistent and discrete territories within the nerve proximally from the sciatic notch to the distal trifurcation. The location and size of these territories was consistent bilaterally within animals as well as across animals and sexes.

Previous work has shown that specific populations of axons serving particular branches of a peripheral nerve run together



along the course of the nerve. This theme has been replicated in a variety of species (humans, monkeys, rats), peripheral nerves (median, ulnar, radial, sciatic), and using a variety of techniques including anatomical dissection, retrograde labeling, microCT, and intrafascicular microstimulation. Sunderland's work in human peripheral nerves demonstrated a somatotopic fascicular organization of axons within the distal portion of the nerve; however, this organization is lost in more proximal segments (Sunderland, 1978). Brushart's work demonstrated the same distal organization in median nerves of monkeys, and confirmed its consistency more proximally using retrograde labeling techniques. Importantly, the position of these bundles of axons remained consistent throughout the nerve until the brachial plexus, and was consistent bilaterally within and across animals (Brushart, 1991). Previous work by Hallin et al. (1991) also confirmed intrafascicular organization of human peripheral nerves by showing sensory axons within the median nerve are segregated by sensory modality along the entirety of the nerve. More specifically, the human sciatic nerve also exhibits a somatotopic organization of intraneural fascicles as evidenced by magnetic resonance neurography of patients with spinal nerve root lesions (Bäumer et al., 2015).

The rat sciatic nerve exhibits a similar organization of specific axon populations. For instance, Suaïd et al., 2016; Ravagli et al., 2020 both demonstrated that the axons contributing to the main branches of the sciatic (peroneal, tibial, and sural) stay discretely organized and do not intermingle for a significant distance proximal to the trifurcation. The same organization was found in the tibial branch of the sciatic nerve after retrogradely labeling individual distal branches contributing to small populations of muscles and tissue in the rat hindlimb (Badia et al., 2010). Our results are consistent with these previous findings: Tibial axons consistently occupied a discrete territory within the sciatic

nerve proximally from the sciatic notch to the distal trifurcation. Importantly, these findings were consistent bilaterally within animals, as well as across animals and sexes.

The consistent organization of axons within the sciatic nerve could potentially explain the consistent pattern of anterior tibialis (TA) motoneuron labeling seen after PEG-fusion repair. The population of axons serving the TA muscle was reliably located in a consistent, discrete location along the length of the sciatic nerve. In addition to the consistency in location, the territory occupied by TA axons was also relatively large. These two features of the organization of TA axons within the sciatic nerve would allow for close approximation of severed proximal and distal TA axons during PEG-fusion repair (Figure 4). Therefore, proximal TA axons are extremely likely to be fused to distal axons projecting to TA, leading to the consistent pattern of appropriate connections induced after PEG-fusion repair seen in Ghergherehchi et al., 2019. Although these fusions are appropriate (i.e., proximal motor axons projecting to the TA are often fused to distal TA motor axons), there is no expectation that these fusions are rematches to the original axon segments.

In our previous work, the consistent pattern of appropriate connections to TA was present regardless of repair type, either single-cut or allograft repair (Ghergherehchi et al., 2019). For single-cut repairs, the organization of axons on the proximal stump will mirror the organization on the distal stump; therefore, territories should experience significant realignment even with the minimal, unavoidable rotations of the nerve stumps during repair (Figure 4). For allograft repairs, the same issue is relevant. Minimal rotations of the host nerve stumps should still leave large, consistent axon territories, like TA, mostly aligned. The allograft itself can be assumed to work similarly to a nerve conduit based on our results that show consistency in territory location along the course of the nerve (Figures 2, 3). Therefore, the

allograft still allows for realignment of territories to be attained. Although appropriately fused TA axons were present regardless of repair type, the frequency of distal TA axons being fused to proximal axons from other populations of motoneurons was higher after allograft repairs (Ghergherehchi et al., 2019). This higher frequency of mispairing is likely due to there being two sites of PEG-fusion repair (one at each end of the donor graft) compared to the one site of PEG-fusion in single-cut repairs.

Reducing the frequency of mispairing through realignment of axon territories during repair may promote better behavioral recovery. Like rats, human peripheral nerves display a topographical organization (Sunderland, 1978; Bäumer et al., 2015), and thus realignment of axon territories within nerves should translate to humans. Successful PEG-fusion repair in human digital nerves has been reported. PEG-fusion repair of human digital nerves showed quick reestablishment of sensation as assessed by static two-point discrimination (Bamba et al., 2016). Clinical case studies of PEG-fusion repair of larger mixed nerves, like the sciatic, have yet to be reported; however, given the topographic organization in human peripheral nerves, it is likely that PEG-fusion repair of these nerves would show similar enhanced recovery as seen in rats (Ghergherehchi et al., 2019).

In conclusion, the presence of appropriately fused TA motor axons after PEG-fusion repair we previously reported (Ghergherehchi et al., 2019) is likely due to the topographic organization of TA axons within the sciatic nerve. This realignment of appropriate populations of axons could have contributed to the enhanced behavioral recovery seen in PEG-fused animals compared to those who received nerve injury without PEG-fusion repair. Based on our results, future work using PEG-fusion repair should prioritize realignment of territories in order to promote better behavioral recovery.

REFERENCES

- Alisky, J. M., van de Weyerling, C. I., and Davidson, B. L. (2002). Widespread dispersal of cholera toxin subunit B to brain and spinal cord neurons following systemic delivery. *Exp. Neurol.* 178, 139–146. doi: 10.1006/exnr.2002.8031
- Allen, C. H. (2000). Functional results of primary nerve repair. *Hand Clin.* 16, 67–72.
- Alvarez, F. J., Titus-Mitchell, H. E., Bullinger, K. L., Kraszpulski, M., Nardelli, P., and Cope, T. C. (2011). Permanent central synaptic disconnection of proprioceptors after nerve injury and regeneration. I. Loss of VGLUT1/IA synapses on motoneurons. *J. Neurophysiol.* 106, 2450–2470. doi: 10.1152/jn.01095.2010
- Badia, J., Pascual-Font, A., Vivó, M., Udina, E., and Navarro, X. (2010). Topographical distribution of motor fascicles in the sciatic-tibial nerve of the rat. *Muscle Nerve* 42, 192–201. doi: 10.1002/mus.21652
- Bamba, R., Waitayawinyu, T., Nookala, R., Riley, D. C., Boyer, R. B., Sexton, K. W., et al. (2016). A novel therapy to promote axonal fusion in digital nerves. *J. Trauma Acute Care Surg.* 81, S177–S183. doi: 10.1097/TA.0000000000001203
- Bäumer, P., Weiler, M., Bendszus, M., and Pham, M. (2015). Somatotopic fascicular organization of the human sciatic nerve demonstrated by MR neurography. *Neurology* 84, 1782–1787. doi: 10.1212/WNL.0000000000001526
- Bertelli, J. A., and Ghizoni, M. F. (2009). Results of c5 root grafting to the musculocutaneous nerve using pedicled, vascularized ulnar nerve grafts. *J. Hand Surg. Am.* 34, 1821–1826. doi: 10.1016/j.jhsa.2009.08.004
- Bertelli, J. A., and Ghizoni, M. F. (2011). Very distal sensory nerve transfers in high median nerve lesions. *J. Hand Surg. Am.* 36, 387–393. doi: 10.1016/j.jhsa.2010.11.049
- Britt, J. M., Kane, J. R., Spaeth, C. S., Zuzek, A., Robinson, G. L., Gbanaglo, M. Y., et al. (2010). Polyethylene glycol rapidly restores axonal integrity and improves the rate of motor behavior recovery after sciatic nerve crush injury. *J. Neurophysiol.* 104, 695–703. doi: 10.1152/jn.01051.2009
- Brushart, T. M. (1991). Central course of digital axons within the median nerve of *Macaca Mulatta*. *J. Comp. Neurol.* 311, 197–209. doi: 10.1002/cne.903110203
- Brushart, T. M. (2011). *Nerve Repair*. New York, NY: Oxford University Press.
- Ghergherehchi, C. L., Bittner, G. D., Hastings, R. L., Mikes, M., Riley, D. C., Trevino, R. C., et al. (2016). Effects of extracellular calcium and surgical techniques on restoration of axonal continuity by polyethylene glycol fusion following complete cut or crush severance of rat sciatic nerves. *J. Neurosci. Res.* 94, 231–245. doi: 10.1002/jnr.23704
- Ghergherehchi, C. L., Hibbard, E. A., Mikes, M., Bittner, G. D., and Sengelaub, D. R. (2019). Behavioral recovery and spinal motoneuron remodeling after polyethylene glycol fusion repair of singly cut and ablated sciatic nerves. *PLoS One* 14:e0223443. doi: 10.1371/journal.pone.0223443
- Goldstein, L. A., Kurz, E. M., and Sengelaub, D. R. (1990). Androgen regulation of dendritic growth and retraction in the development of a sexually dimorphic spinal nucleus. *J. Neurosci.* 10, 935–946. doi: 10.1523/JNEUROSCI.10-03-00935.1990
- Hallin, R. G., Ekedahl, R., and Frank, O. (1991). Segregation by modality of myelinated and unmyelinated fibers in human sensory nerve fascicles. *Muscle Nerve* 14, 157–165. doi: 10.1002/mus.880140211
- Kurz, E. M., Brewer, R. G., and Sengelaub, D. R. (1991). hormonally mediated plasticity of motoneuron morphology in the adult rat spinal cord: a cholera toxin-HRP study. *J. Neurobiol.* 22, 976–988. doi: 10.1002/neu.480220909

DATA AVAILABILITY STATEMENT

The original contributions presented in the study are included in the article; further inquiries can be directed to the corresponding author.

ETHICS STATEMENT

The animal study was reviewed and approved by Bloomington Institutional Animal Care and Use Committee.

AUTHOR CONTRIBUTIONS

EH: study concept, experiments, data analysis, and first draft of manuscript. DS: experiments and manuscript. Both authors contributed to the article and approved the submitted version.

FUNDING

This work was supported by intramural support from the Department of Psychological and Brain Sciences, Indiana University.

ACKNOWLEDGMENTS

We thank George Bittner for his useful comments on data presentation.

- Kurz, E. M., Sengelaub, D. R., and Arnold, A. P. (1986). Androgens regulate the dendritic length of mammalian motoneurons in adulthood. *Science* 232, 395–398. doi: 10.1126/science.3961488
- Kuyppers, H. G. J. M., and Huisman, A. M. (1984). Fluorescent neuronal tracers. *Adv. Cell. Neurobiol.* 5, 307–340.
- Lappi, D., Feldman, J., Sengelaub, D. R., and McGaughy, J. (2014). “Nervous system research with RIP conjugates: from determination of function to therapy,” in *Ribosome-Inactivating Proteins: Ricin and Related Proteins*, eds F. Stirpe and D. Lappi (New York, NY: Wiley-Blackwell), 253–269. doi: 10.2174/138920310790274662
- Ma, J., Novikov, L. N., Wiberg, M., and Kellerth, J. O. (2002). delayed loss of spinal motoneurons after peripheral nerve injury in adult rats: a quantitative morphological study. *Exp. Brain. Res.* 139, 216–223. doi: 10.1007/s002210100769
- Mesulam, M. M. (1982). *Tracing Neural Connections with Horseradish Peroxidase*. Chichester: Wiley.
- Mikesh, M., Ghergherehchi, C. L., Hastings, R. L., Ali, A., Rahesh, S., Jagannath, K., et al. (2018a). Polyethylene glycol solutions rapidly restore and maintain axonal continuity, neuromuscular structures and behaviors lost after sciatic nerve transections in female rats. *J. Neurosci. Res.* 96, 1223–1242.
- Mikesh, M., Ghergherehchi, C. L., Rahesh, S., Jagannath, K., Ali, A., Sengelaub, D. R., et al. (2018b). Polyethylene glycol treated allografts not tissue matched nor immunosuppressed rapidly repair sciatic nerve gaps, maintain neuromuscular functions, and restore voluntary behaviors in female rats. *J. Neurosci. Res.* 96, 1243–1264.
- Ravagli, E., Mastitskaya, S., Thompson, N., Iacoviello, F., Shearing, P. R., Perkins, J., et al. (2020). Imaging fascicular organization of rat sciatic nerves with fast neural electrical impedance tomography. *Nat. Commun.* 11:6241. doi: 10.1038/s41467-020-20127-x
- Riley, D. C., Bittner, G. D., Mikesh, M., Cardwell, N. L., Polloms, A. C., Ghergherehchi, C. L., et al. (2015). Polyethylene glycol-fused allografts produce rapid behavioral recovery after ablation of sciatic nerve segments. *J. Neurosci. Res.* 93, 572–583. doi: 10.1002/jnr.23514
- Rotterman, T. M., Nardelli, P., Cope, T. C., and Alvarez, F. J. (2014). Normal distribution of VGLUT1 synapses on spinal motoneuron dendrites and their reorganization after nerve injury. *J. Neurosci.* 34, 3475–3492. doi: 10.1523/JNEUROSCI.4768-13.2014
- Steward, O. (1981). “Horseradish peroxidase and fluorescent substances and their combination with other techniques,” in *Neuroanatomical Tract-Tracing Methods*, eds L. Heimer and M. J. Robards (New York, NY: Plenum Press), 270–310.
- Suaib, C. A., Santos, A. P., Yamane, F. O., Fazan, V. P. S., and Barreira, A. A. (2016). Aspects of the macro and microscopic anatomy of the sciatic nerve in wistar rats. *Int. J. Morphol.* 34, 877–884.
- Sunderland, S. (1978). *Nerves and Nerve Injuries*. Edinburgh: Churchill Livingstone.
- Wiberg, R., Kingham, P. J., and Novikova, L. N. (2017). a morphological and molecular characterization of the spinal cord after central root avulsion or distal peripheral nerve axotomy injuries in adult rats. *J. Neurotrauma* 34, 652–660.
- Wolfe, S. W., Hotchkiss, R. N., Pederson, W. C., and Kozin, S. H. (2010). *Green's Operative Hand Surgery*, 6th Edn. New York, NY: Churchill Livingstone.

Conflict of Interest: The authors declare that the research was conducted in the absence of any commercial or financial relationships that could be construed as a potential conflict of interest.

Publisher's Note: All claims expressed in this article are solely those of the authors and do not necessarily represent those of their affiliated organizations, or those of the publisher, the editors and the reviewers. Any product that may be evaluated in this article, or claim that may be made by its manufacturer, is not guaranteed or endorsed by the publisher.

Copyright © 2022 Hibbard and Sengelaub. This is an open-access article distributed under the terms of the Creative Commons Attribution License (CC BY). The use, distribution or reproduction in other forums is permitted, provided the original author(s) and the copyright owner(s) are credited and that the original publication in this journal is cited, in accordance with accepted academic practice. No use, distribution or reproduction is permitted which does not comply with these terms.



Oral Treatments With the TrkB Ligand Prodrug, R13, Promote Enhanced Axon Regeneration Following Peripheral Nerve Injury

Arthur W. English^{1,2*}, Dario Carrasco¹, Dustin Hoffman¹, Robin Isaacson¹, Seong Su Kang³, Samia Khan¹, Xia Liu³ and Keqiang Ye^{3,4}

¹ Department of Cell Biology, Emory University School of Medicine, Atlanta, GA, United States, ² Rehabilitation Medicine, Emory University School of Medicine, Atlanta, GA, United States, ³ Pathology and Laboratory Medicine, Emory University School of Medicine, Atlanta, GA, United States, ⁴ Faculty of Life and Health Sciences, Brain Cognition and Brain Disease Institute, Shenzhen Institute of Advanced Technology, Chinese Academy of Sciences, Shenzhen, China

OPEN ACCESS

Edited by:

Fengquan Zhou,
Johns Hopkins Medicine,
United States

Reviewed by:

Sara Morcuende,
University of Seville, Spain
Petr Dubový,
Masaryk University, Czechia

*Correspondence:

Arthur W. English
medae@emory.edu

Specialty section:

This article was submitted to
Cellular Neuropathology,
a section of the journal
Frontiers in Cellular Neuroscience

Received: 18 January 2022

Accepted: 24 March 2022

Published: 15 April 2022

Citation:

English AW, Carrasco D,
Hoffman D, Isaacson R, Kang SS,
Khan S, Liu X and Ye K (2022) Oral
Treatments With the TrkB Ligand
Prodrug, R13, Promote Enhanced
Axon Regeneration Following
Peripheral Nerve Injury.
Front. Cell. Neurosci. 16:857664.
doi: 10.3389/fncel.2022.857664

Axon regeneration after peripheral nerve injury is slow and inefficient, leading to generally poor functional recovery. Activity-dependent experimental therapies that increase expression of brain-derived neurotrophic factor (BDNF) and its TrkB receptors enhance regeneration, suggesting that treatments with BDNF might also be effective. However, recombinant human BDNF (rhBDNF), as well as 7,8-dihydroxyflavone (7,8-DHF), a small molecular BDNF mimetic, may have limited treatment applications because of their modest oral bioavailability and pharmacokinetic profile. R13 is a 7,8-DHF prodrug. Upon oral administration, it is converted in the liver to 7,8-DHF. In immunoblots from tissues at the site of nerve injury, a single oral treatment with R13 to mice following sciatic nerve transection and repair produced a rapid and prolonged increase in immunoreactivity to phosphorylated TrkB, prolonged phosphorylation of mitogen activated protein kinase (MAPK/Erk1/2), and a rapid but transient increase in phosphorylated AKT (protein kinase B). Intramuscular injections of fluorescent retrograde tracers into the gastrocnemius and tibialis anterior muscles 4 weeks after nerve injury resulted in significantly greater numbers of labeled motoneurons and dorsal root ganglion neurons in R13-treated mice than in vehicle-treated controls. Direct electromyographic (EMG) responses (M waves) were significantly larger in R13-treated mice 4 weeks after injury than vehicle-treated controls or mice treated with oral 7,8-DHF. Oral treatments with the prodrug, R13, are a potent therapy for stimulating axon regeneration and functional recovery after peripheral nerve injury.

Keywords: BDNF (brain derived neurotrophic factor), nerve injuries, retrograde tracer, M response, small molecule

INTRODUCTION

Poor recovery from peripheral nerve injuries (PNIs) is a significant public health problem. These injuries are common and even though it is widely held that axons in injured nerves have greater regenerative potential than injured central nervous system axons, the process is slow and inefficient. The result is that only a very small proportion of individuals with injuries to peripheral nerves

ever recover significant function (Portincasa et al., 2007; Scholz et al., 2009). Novel approaches to stimulating the regeneration of injured peripheral axons are needed to improve these poor outcomes and reduce the burden on affected individuals.

Among the most successful experimental therapies for PNI evaluated in preclinical models are application of low frequency (20 Hz) electrical stimulation (ES) and moderate treadmill exercise. Both have resulted in increased elongation of regenerating axons and reinnervation of their targets in the periphery (English et al., 2011; Gordon and English, 2016) and both have resulted in an increase in the number of neurons whose axons have regenerated successfully (Al-Majed et al., 2000; English et al., 2009). Both ES and exercise rely on an increase in the signaling between brain derived neurotrophic factor (BDNF) and its TrkB receptor in the regenerating axons (Gordon and English, 2016). Indeed, application of recombinant human BDNF (rhBDNF) to the repair site of a cut nerve in mice resulted in a marked enhancement of axon regeneration (Sabatier and English, 2015).

However, we sought alternate TrkB ligands because rhBDNF has a very short half-life in tissues. We identified two such small molecules, 7,8-dihydroxyflavone (7,8-DHF) (Jang et al., 2010b) and deoxygedunin (Jang et al., 2010a), and showed that their treatment, delivered either by local application to the injured nerve or by systemic injection, markedly enhanced axon regeneration in mouse models (English et al., 2013). Treatments with these small molecules did not simply promote the release of endogenous BDNF, as they enhanced regeneration in BDNF knockout mice. They did not promote axon regeneration in TrkB knockout mice, indicating that their success required intact TrkB receptors (English et al., 2013).

Despite the successful use of these small molecular TrkB ligands in enhancing axon regeneration, their translational potential has limitations. Local treatments with them are usually limited to singular surgical interventions. Stimulation of axon regeneration over longer distances, as is commonly necessary in human patients and which might require more than one application, would therefore be unlikely. In addition, the biological half-life of systemically applied 7,8-DHF is only slightly longer than that of rhBDNF (Chen et al., 2018), meaning that injections would have to be repeated often to be effective. For these reasons, we have examined the use of a prodrug, R13, that after oral administration is converted into 7,8-DHF by the liver (Chen et al., 2018). This approach significantly extends the duration of TrkB signaling and offers the advantage of oral dosing. The goal of this study was to evaluate the effectiveness of oral treatments with R13 on axon regeneration following peripheral nerve injury in a commonly used mouse model system.

MATERIALS AND METHODS

All experimental methods were approved by the Institutional Animal Care and Use Committee of Emory University (Protocol #PROTO201800101) and were consistent with the guidelines for Animal Research of the Society for Neuroscience. All animals

used were C57B6 strain wild type (WT) mice. R13 was obtained from Sundia MediTech, Shanghai, China (Lot No: A0257-10014-16). It was dissolved in a 5% DMSO/0.5% methylcellulose vehicle solution.

Site of Action Experiments

To evaluate whether oral R13 treatments resulted in TrkB activation at the nerve repair site, we used immunoblotting to evaluate the expression of phosphorylated TrkB (pTrkB Y705) and its effect on phosphorylation of the downstream effector molecules, AKT and MAPK/Erk1/2.

Animal treatment and sample preparation: In isoflurane-anesthetized 3-month-old WT mice of both sexes, we exposed the sciatic nerve in the mid-thigh and cut and repaired it by end-to-end anastomosis, as described in more detail below. Three days later, the mice were orally administered R13 (43.6 mg/Kg). This dose is equivalent to 30 mg/Kg of 7,8-DHF, and was chosen because it was the intermediate of three concentrations used to study the pharmacokinetics of R13 in brain and plasma (Chen et al., 2018). Other mice were given a similar volume of vehicle (5% DMSO/0.5% methylcellulose). Prior to (0 min) and at 15, 30, 60, 120, 240, and 480 min after R13/vehicle administration, mice were euthanized with Euthasol® solution (sodium pentobarbital, 390 mg/mL) and the cut and repaired nerves were harvested, including 1 mm proximal and distal to the injury site.

Western blot analysis: The frozen nerves were lysed in Laemmli buffer (62.5 mM Tris-HCL, pH 6.8, 10% glycerol, 2% SDS, 5% 2-mercaptoethanol, 0.005% bromophenol blue) and followed by homogenization with sonication. After heating at 98°C for 5 min, similar amounts of tissue lysate from different nerves were separated by SDS-PAGE, transferred to nitrocellulose membranes, and probed with the antibodies listed in **Table 1**. Antibody binding was detected using appropriate peroxidase conjugated secondary antibodies and visualized using enhanced chemiluminescence.

Quantification of intensity of immunoreactivity was performed using ImageJ. Values from blots probed for phosphorylated TrkB, AKT, and MAPK/Erk1/2 were compared

TABLE 1 | Antibodies used in immunoblots.

Antibody	Source	Dilution
pTrkB Y705	Cat# ab52191, Abcam	1:500
TrkB	Cat# 4603S, Cell Signaling	1:500
pAKT	Cat# 9271S, Cell Signaling	1:1,000
AKT	Cat# 4691s, Cell Signaling	1:2,000
pMAPK/ERK1/2	Cat# 9106S, Cell Signaling	1:1,000
MAPK/ERK1/2	Cat# 9102S, Cell Signaling	1:2,000
β-Actin	Cat# A1978, Sigma	1:10,000
Goat-anti-rabbit IgG HRP	Cat# 20-304, Genesee	1:2,000
Goat-anti-rabbit IgG HRP	Cat# 20-303, Genesee	1:2,000

For processing of immunoblots

Product name	Source
Immobilon Forte western HRP substrate (ECL)	Cat# WBLUF050, Millipore

to values of blots loaded with identical amounts of the same samples and probed for total TrkB, AKT, and MAP kinase. Ratios of phosphorylated to total protein in samples of nerves at different times after administration of R13 or vehicle were compared to the corresponding ratios obtained from mice prior to any administration of R13 or vehicle. Significance of differences in these ratios at different times after R13 administration, to that obtained prior to administration, was evaluated using unpaired *t*-tests.

Electromyographic Studies

In young adult (6–8-week-old) mice anesthetized with isoflurane, the sciatic nerve was exposed in the mid-thigh and cut and repaired. The protocol for repair is similar to that described in more detail elsewhere (Akhter et al., 2019). Briefly, a small (1 × 2 mm) rectangle of medical grade silastic film was placed beneath the nerve and secured to it with one microliter of fibrin glue, a mixture of fibrinogen and thrombin. Once the glue had set, the nerve was cut near the center of the silastic mat and a second application of fibrin glue was applied to secure the anastomosed segments in place. Wounds were then closed in layers. Daily oral treatments with R13 (21.8 mg/Kg) (four male and four female mice), vehicle (four male and four female mice), or 7,8-DHF (15 mg/Kg) (four male and four female mice) were conducted 5 days per week for 2 weeks, beginning on the third day after injury. The timing of this treatment was designed to be similar to that used to treat animals with exercise (English et al., 2011). The dose of R13 used was the lowest effective dose reported by others. Based on their molecular weights, this dose of R13 is similar to a dose of 15 mg/Kg of 7,8-DHF (Chen et al., 2018).

To evaluate the extent of reinnervation of skeletal muscles by motor axons, direct muscle electromyographic (EMG) responses (M responses) were evoked in the gastrocnemius (GAST) and tibialis anterior (TA) muscles 4 weeks after injury, 2 weeks after the end of treatments with R13, 7,8-DHF, or vehicle. In isoflurane-anesthetized animals, the sciatic nerve was exposed as it exited the pelvis via short skin incision and two monopolar needle electrodes (Ambu #74325-36/40, Columbia, MD, United States) were placed next to it and used to deliver electrical stimulus pulses to the nerve. Bipolar fine wire EMG electrodes (Basmajian and Stecko, 1963) were placed transcutaneously into the GAST and TA muscles using a 25G hypodermic needle. Once in place the wires were connected to differential amplifiers. Ongoing background EMG activity was sampled by a laboratory computer system running custom Labview® software, and when activity fell within a user-defined resting level, the computer delivered a 0.3 ms duration constant voltage stimulus pulse to the needle electrodes. Evoked EMG activity, sampled at 10 KHz, was recorded, beginning from 20 ms prior to the stimulus and lasting until 50 ms after the stimulus. Stimulus intensity was increased gradually until a maximum amplitude M response (Mmax) was obtained. Stimuli were delivered no more frequently than once every 3 s to avoid fatigue.

Amplitudes of Mmax were measured off-line as the average full wave rectified voltage within the boundaries of the triphasic responses observed. In all the mice, these amplitudes were scaled to Mmax amplitudes recorded 4 weeks after sciatic nerve

transection and repair in untreated animals, reported previously (Park et al., 2019). Scaled Mmax values were compared between the three treatment groups in the two muscles studied. The significance of differences in scaled M response amplitudes between groups was evaluated using ANOVA.

Retrograde Labeling

Four R13-treated (two male and two female) and four vehicle-treated (two male and two female) 6–8-week-old mice were studied. Four weeks after bilateral sciatic nerve transection and repair and 2 weeks of daily oral administration of R13 or vehicle, as described above, retrograde fluorescent tracers were injected into the GAST and TA muscles. These would mark the cell bodies of motor and sensory neurons whose axons had regenerated and successfully reinnervated those muscle targets. In isoflurane-anesthetized mice, one microliter of a 1% solution of wheat germ agglutinin (WGA), conjugated either to Alexafluor 488 or Alexafluor 555, was injected into each of the medial and lateral heads of the GAST and into the TA muscle on both sides of the animals using a 35G needle attached to a 1 µl Hamilton syringe. The injections were made at two locations in each muscle/head and the needle was left in place for 5 min between injections to avoid leakage of the solutions. After the injections were completed the surgical field was flushed three times with sterile saline solution before the surgical wounds were closed and the mice were returned to their cages.

Three days after tracer injection, mice were euthanized with Euthasol® solution and perfused transcardially with 4% paraformaldehyde solution, pH 6.9. Lumbar spinal cords and L4 dorsal root ganglia (DRGs) were harvested, post-fixed for 1 h, and cryoprotected overnight in 20% sucrose solution. Cryostat sections of spinal cords, at 40 µm thickness, were mounted onto charged slides and cover slipped using Vectashield®. Images of these sections at 20X magnification, using a Leica DM6000 upright fluorescence microscope and Hamamatsu low-light camera, were made using HCLImage software. Labeled motoneurons were identified if the retrograde fluorescence filled the soma and extended into the proximal dendrites and if a clear area of the cell corresponding to the nucleus could be visualized, as we have described previously (English, 2005). Labeled profiles that did not meet these criteria were not counted. Counts of labeled motoneurons were made separately on the two sides of each spinal cord. Data from R13-treated mice were compared to those found in vehicle-treated animals.

Fourth lumbar (L4) dorsal root ganglia were sectioned on a cryostat at 40 µm thickness, mounted onto charged slides and cover slipped using Vectashield®. Imaging of these sections was identical to that used for spinal cords, above. A DRG neuron was considered labeled if the fluorescent marker filled the entire soma and a nuclear region could be identified. The soma cross sectional area of each labeled DRG neuron was measured using FIJI software. The relative numbers of small (<300 µm²), medium sized (300–700 µm²), and large (> 700 µm²) DRG neurons (Ruscheweyh et al., 2007) in the L4 DRGs of R13-treated and vehicle-treated were compared.

Statistical Analyses

All statistical comparisons were performed using GraphPad Prism software. Alpha for significance of differences was set at $p < 0.05$ throughout.

RESULTS

Oral R13 Treatment Induces TrkB Activation and Phosphorylation of Downstream Effectors at the Nerve Injury Site

We have shown previously that oral treatment with R13 resulted in a prolonged metabolic production of 7,8-DHF and TrkB receptor activation (Chen et al., 2018). In the present experiments, we chose to investigate whether a similar treatment following peripheral nerve transection and repair would produce such effects *at the injury site*. We harvested cut and repaired sciatic nerves at different times after a single oral administration of R13 or vehicle, and analyzed the tissue for the presence of TrkB activation. In immunoblots we found a rapid increase in immunoreactivity, relative to pre-treatment levels (unpaired t -test, $t_6 = 4.937$, $p = 0.0013$) to phosphorylation of TrkB at tyrosine residue 705 (pTrkB Y705), a marker of TrkB activation, within the first 15 min following oral administration of R13. This significant increase over pre-treatment immunoreactivity ($p < 0.002$) remained for the entire 8-h duration of the experiment (Figure 1A). In contrast, using similar analyses, immunoreactivity to phosphorylated AKT (protein kinase B), a downstream effector of the activated phosphoinositide 3-kinase (PI3K) signaling pathway, was only transiently increased in R13-treated mice (Figure 1B). A statistically significant increase relative to pre-treatment immunoreactivity ($t_6 = 2.670$, $p = 0.037$) was found only at the earliest post-application time (15 min), but not at later times. A single oral treatment with R13 resulted in a slightly slower (after 30 min) increase ($t_6 = 2.712$, $p = 0.035$) in phosphorylation of mitogen-activated protein kinase (MAPK/Erk1/2) (Figure 1C). This significant ($p < 0.05$) increase persisted for the 8-h duration of the experiment. No visible change in relative immunoreactivity to pTrkB Y705, pAKT, or pMAPK/Erk1/2 was found in nerves from mice treated orally with vehicle under similar conditions (Supplementary Figure 1).

Oral R13 Treatments Promote Successful Regeneration of Axons of More Motoneurons

Motoneurons whose axons had regenerated and successfully reinnervated the two heads of GAST and the TA muscle were marked using retrograde fluorescent tracers. Examples of labeled TA (green) and GAST (red) motoneurons, and motoneurons labeled with both tracers (yellow, arrows), are shown in Figure 2A. Counts (mean \pm SEM) of labeled motoneurons reinnervating these two muscles in vehicle-treated and R13-treated mice are shown in Figure 2B.

Using a two-way (sex vs. treatment) ANOVA to evaluate the neuron counts from the two muscles, we found a significant difference due to treatment [$F_{(1, 28)} = 4.662$, $p = 0.040$] but not sex [$F_{(1, 28)} = 0.006$, $p = 0.938$] or interaction [$F_{(1, 28)} = 0.215$, $p = 0.647$]. Counts from males and females were then combined and data from the different treatments compared using a one-way ANOVA. Significant differences were found [$F_{(5, 42)} = 79.15$, $p < 0.0001$], and using *post hoc* (Tukey) paired testing, significantly more retrogradely labeled motoneurons were found in the R13-treated mice than in the vehicle-treated controls for both TA ($p < 0.003$) and GAST ($p < 0.0001$). For both treatment groups studied a small number of motoneurons contained both retrograde tracers, suggesting that their regenerating axons had branched and reinnervated both the GAST and TA muscles. Differences in the numbers of these doubly labeled cells between the two groups was not significant ($p = 0.620$). R13 treatments thus resulted in successful regeneration of axons of more motoneurons than vehicle-treated controls.

Oral R13 Treatments Promote Successful Regeneration of Axons of More Sensory Neurons

We counted retrogradely labeled neurons in histological sections of the L4 DRGs (Figure 3A) 4 weeks after sciatic nerve transection and repair. Using a two-way (sex vs. treatment) ANOVA to evaluate the data from counts of sensory neurons retrogradely labeled from the two muscles together, we found a significant difference due to treatment [$F_{(1, 23)} = 21.37$, $p < 0.0001$] but not sex [$F_{(1, 23)} = 0.037$, $p = 0.845$] or interaction [$F_{(1, 23)} = 0.894$, $p = 0.354$]. Counts from males and females were then combined and those from vehicle-treated (Figure 3B: light bars) and R13-treated (Figure 3B: dark bars) mice were compared using a one-way ANOVA. Significant differences were found [$F_{(5, 32)} = 15.56$, $p < 0.0001$], and using *post hoc* paired testing, significant differences were found between R13-treated and vehicle-treated groups for both TA ($p < 0.0001$) and GAST ($p < 0.023$). No significant differences were found between these two groups for the small number of DRG neurons that were doubly labeled from tracer injections in both TA and GAST. Thus, R13 treatments resulted in the successful regeneration of more muscle sensory axons than controls.

We next evaluated the proportion of labeled DRG cells in three different size groupings (Ruscheweyh et al., 2007). We approached this size-based separation as a convenient way to compare the extent of success of axon regeneration among different groups of DRG neurons, not to distinguish between neurons of different functional classes. We expressed the number of small ($< 300 \mu\text{m}^2$), medium-sized ($300\text{--}700 \mu\text{m}^2$), and large ($> 700 \mu\text{m}^2$) neurons as a function of the total number of labeled neurons in the two treatment groups. Mean proportions of all DRG neurons labeled from GAST and TA in these size classes are shown in Figure 3C. We compared these proportions using a one-way ANOVA [$F_{(5, 24)} = 8.402$, $p = 0.0001$]. Significantly ($p < 0.001$) more medium-sized labeled neurons were found in both

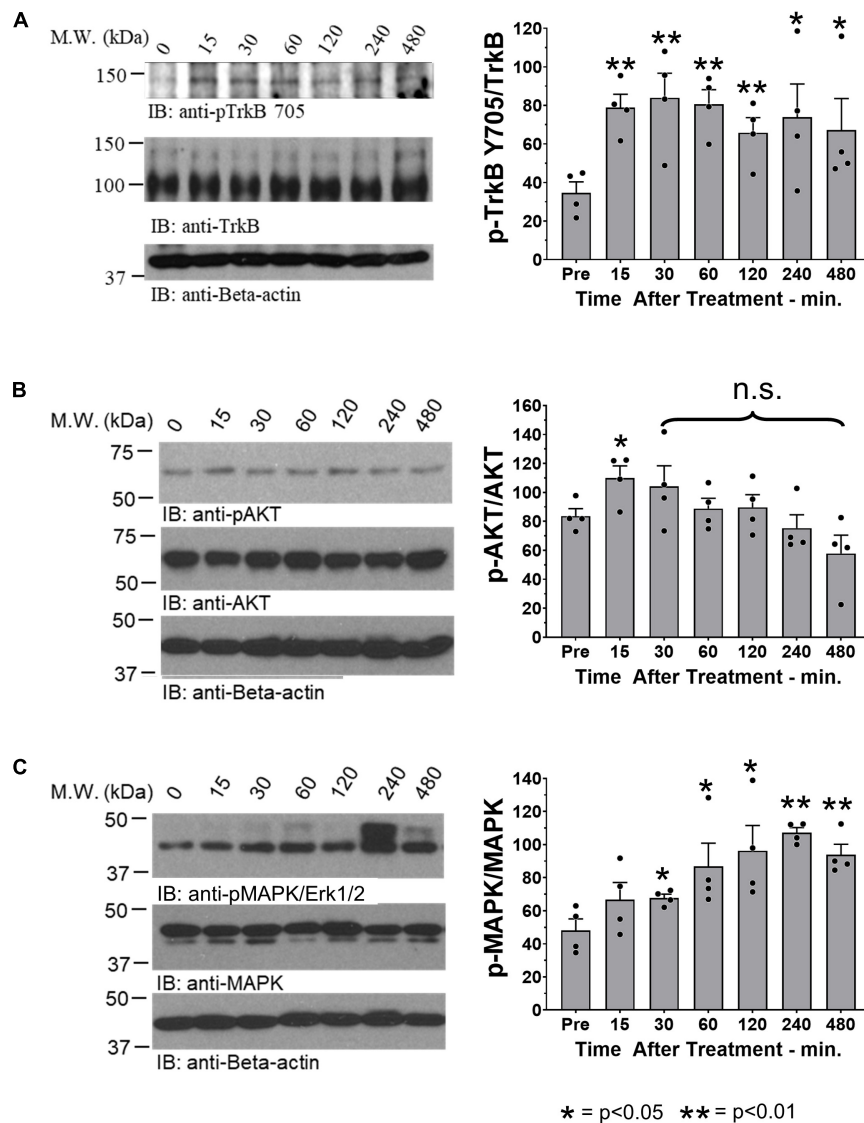


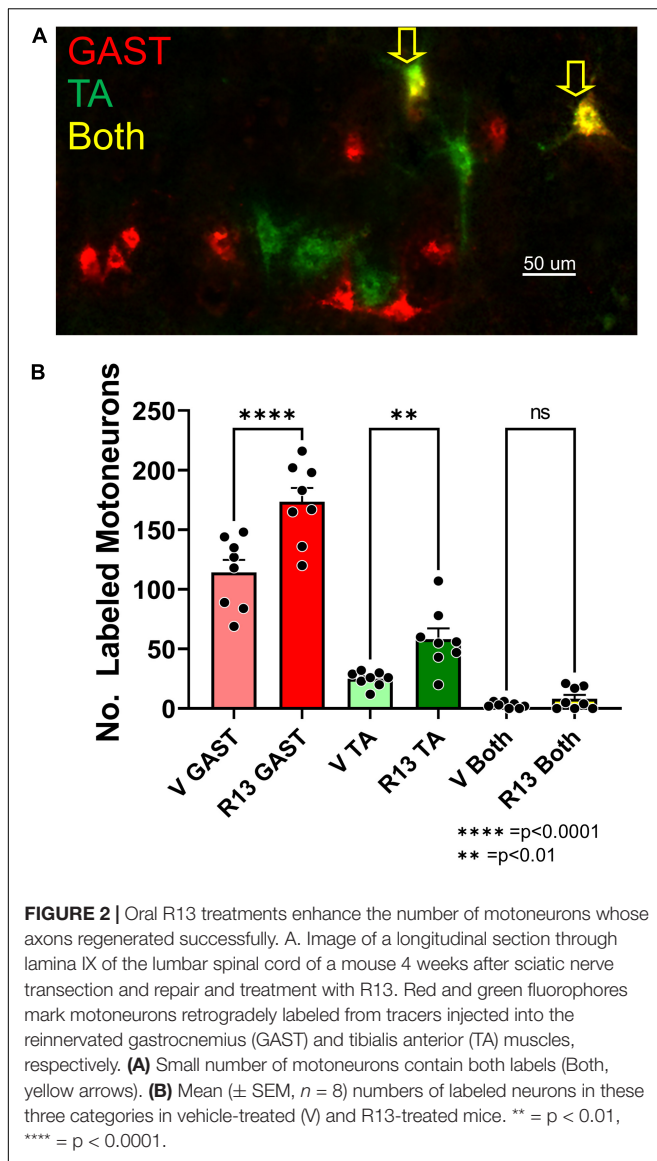
FIGURE 1 | Oral R13 treatment stimulates TrkB phosphorylation and a downstream effector at the site of nerve injury. On the left side of each panel, examples of blots of sciatic nerves at the site of injury prior to (0 min) and at 15, 30, 60, 120, 240, and 480 min after oral administration of R13 are shown. On the right are quantitative results from blots from four nerves ($n = 4$). Bands of specific protein were densitometrically analyzed and normalized to the signal intensity of beta-actin. For each of the three proteins studied, the ratio of the expression of their activated (phosphorylated) form relative to total protein expression was calculated. Significance of differences at different times after administration from that prior to R13 administration was evaluated using an unpaired t -test: * $p < 0.05$ ** $p < 0.01$, $n = 4$. **(A)** Immunoblots for anti- phosphorylated TrkB (pTrkB Y705), TrkB, and beta-actin. **(B)** Immunoblots for anti- phosphorylated AKT (pAKT), AKT, and beta-actin. **(C)** Immunoblots for anti- phosphorylated MAP kinase (pMAPK/Erk1/2), MAPK/Erk1/2, and beta-actin.

treatment groups from both muscles than either small or large neurons. However, no significant differences were found in the proportions of these sensory neurons in each of the size classes between R13-treated and vehicle-treated mice for both TA and GAST.

Oral R13 Treatments Result in Greater Muscle Reinnervation Than Controls

To evaluate the effects of R13 treatments on functional motor recovery after sciatic nerve transection and repair, we evoked

direct muscle EMG responses (M responses) to sciatic nerve stimulation in GAST and TA muscles 4 weeks after injury. Examples of M responses recorded at that time from an R13-treated mouse, a vehicle-treated mouse, and a mouse treated with oral 7,8 DHF are shown in **Figure 4A**. The amplitudes of full wave rectified Mmax responses in the R13-treated, vehicle-treated, and oral 7,8-DHF-treated mice were scaled to the mean Mmax amplitude recorded from a series of untreated mice 4 weeks after sciatic nerve transection and repair (Park et al., 2019). Differences in these scaled Mmax amplitudes were first compared between male and female mice



treated either with R13 or vehicle or 7,8-DHF ($N = 4$ of each sex in each group) using a two-way (sex and treatment) ANOVA. A significant effect of treatment [$F_{(1, 12)} = 6.775$, $p = 0.023$ for GAST, $F_{(1, 12)} = 4.973$, $p = 0.04$ for TA] was found, but not for sex or for interaction, so that data from the sexes were combined. Significance of differences between treatment groups was determined using a one-way ANOVA. Significant differences were found for both GAST [$F_{(2, 19)} = 12.01$, $p = 0.0004$] and TA [$F_{(2, 19)} = 8.892$, $p = 0.019$]. Using *post hoc* paired testing, scaled Mmax amplitudes from both muscles were found to be significantly greater in the R13-treated mice than in either the vehicle-treated mice ($p < 0.002$ for GAST, $p < 0.010$ for TA) or the mice treated with oral 7,8-DHF ($p < 0.001$ for GAST, $p < 0.002$ for TA) (Figure 4B). The scaled Mmax responses in vehicle-treated mice and mice treated with oral 7,8-DHF were not significantly different from each other, and their

mean scaled Mmax amplitudes were not significantly different from unity (mean + 95% confidence interval > 1.0), indicating that among these treatments, only oral administration of R13 produced a significant enhancing effect on functional muscle reinnervation.

DISCUSSION

Poor functional recovery from peripheral nerve injuries is a significant clinical problem. Even though axons in peripheral nerves are capable of regenerating after injury, very few nerve injury patients experience significant functional recovery (Portincasa et al., 2007; Scholz et al., 2009). The most common reason given for these poor outcomes is the slow and inefficient process of axon regeneration. Novel treatments are required if this situation is to be improved. The present study reports the initial results of examination of one such novel experimental approach, oral administration of the prodrug R13 following sciatic nerve transection and repair.

We and others have argued that successful axon regeneration following PNI could be improved by increasing the activation of the TrkB receptor by BDNF, by either direct application of recombinant human BDNF (rhBDNF), or by activity-dependent treatments such as brief 20 Hz electrical stimulation or treadmill exercise (Gordon and English, 2016). Systemic injections of the small molecule TrkB ligands deoxydunin or 7,8-DHF also proved effective (English et al., 2013). However, the bioavailability of rhBDNF and even 7,8-DHF is limited (Chen et al., 2018) so that successful enhancement of axon regeneration over distances like those often encountered in human patients could require multiple daily injections or/and high doses that could contribute to unwanted side effects or even toxicity. The development of the R13 prodrug sought to circumvent these limitations. It is metabolized in the liver, releasing 7,8-DHF into the systemic circulation gradually, thereby prolonging the bioavailability of that BDNF mimetic (Chen et al., 2018).

We show here that oral administration of R13 following sciatic nerve transection and repair results in a rapid and prolonged increase of TrkB phosphorylation at the site of the nerve injury. Phosphorylation of TrkB at tyrosine residue 705 is considered a critical step in TrkB receptor activation, which further regulates the phosphorylation of other TrkB positions leading to activation of downstream signaling pathways (Huang and Reichardt, 2003; Huang and McNamara, 2010). Increased BDNF and TrkB expression at the site of nerve injury has been reported (Funakoshi, 1993) and it might be presumed, therefore, that some activation of TrkB might be found. Indeed, we did find modest immunoreactivity to pTrkB Y705, relative to full length TrkB, in cut nerves prior to administration of either R13 or vehicle. However, an increase in relative pTrkB Y705 immunoreactivity was noted later only after R13 administration. We also found that R13, but not vehicle administration produced prolonged activation of pMAPK/Erk1/2, a notable downstream effector of TrkB activation. We found modest immunoreactivity for pMAPK/Erk1/2 in cut nerves prior to either R13 or vehicle

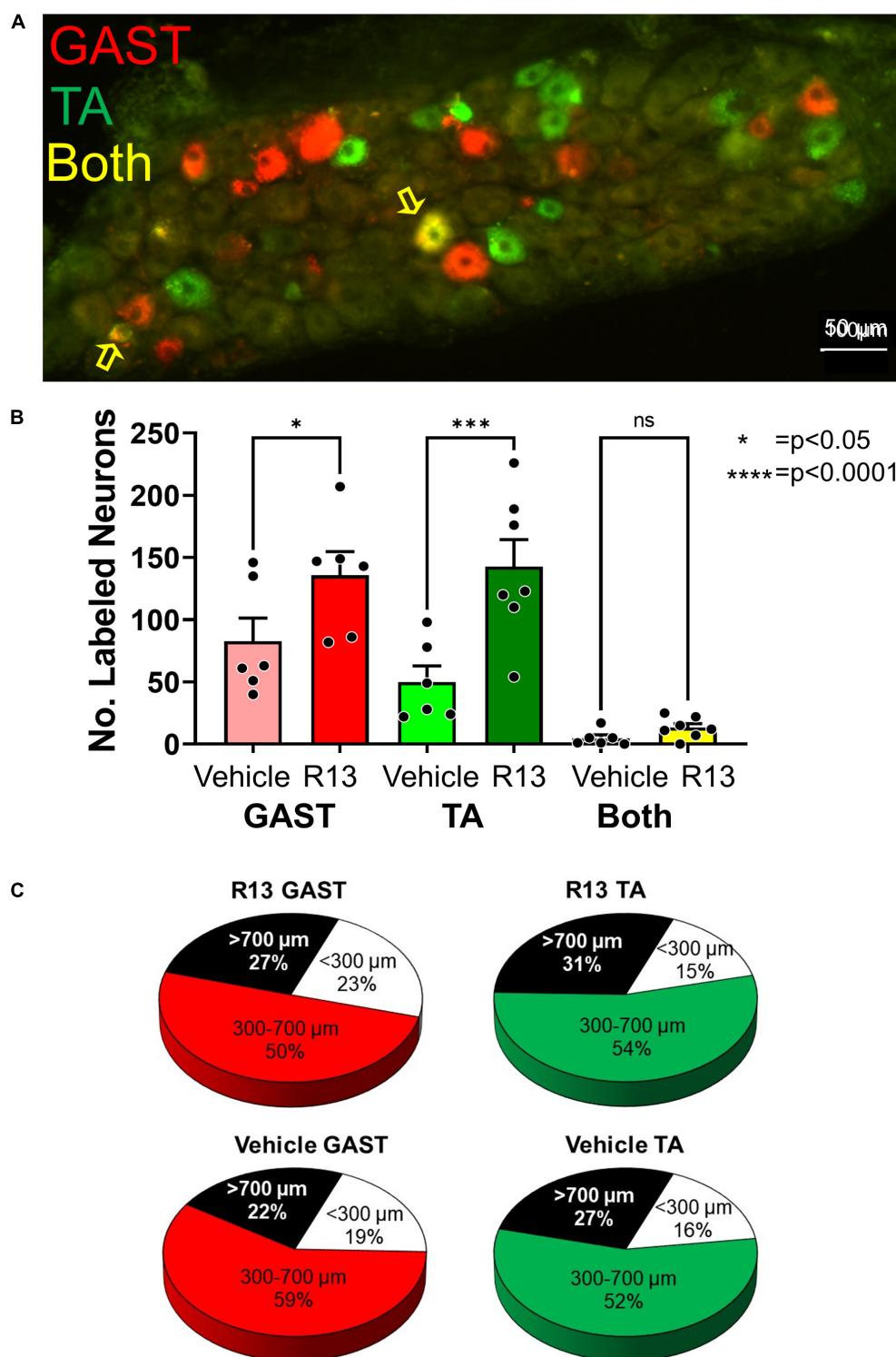


FIGURE 3 | Oral R13 treatments promote regeneration of muscle afferent neurons. **(A)** Histological section through an L4 dorsal root ganglion (DRG) from a mouse treated with R13. Cell bodies of primary afferent neurons successfully reinnervating the gastrocnemius (GAST, red) or tibialis anterior (TA, green) muscles 4 weeks after sciatic nerve transection and repair are shown. Sensory neurons labeled by both tracers (yellow) are indicated by the yellow arrows. **(B)** Counts of labeled neurons (mean \pm SEM, $n = 6$) in the L4 dorsal root ganglia of vehicle-treated and R13-treated mice. **(C)** Mean proportions of labeled DRG neurons in different size classes in the two different treatment groups. No significant differences were found between R13-treated and vehicle-treated mice. * = $p < 0.05$, **** = $p < 0.0001$.

administration. This observation is consistent with the findings of others in the proximal and distal segments of cut nerves (Sheu et al., 2000), where it has been implicated in the formation of repair Schwann cells (Harrisingh et al., 2004). Because Schwann cells express only the truncated form of TrkB (Funakoshi, 1993), we suggest that our finding of increased pTrkB Y705 and pMAPK/Erk1/2 activity after R13 treatments are related to signaling in other cell types, including neurons.

Consistent with its effects on TrkB signaling, oral treatment with R13 enhanced axon regeneration. The number of both motoneurons and muscle sensory neurons whose axons had regenerated and successfully reinnervated two target muscles was increased with R13 treatments. In addition, after oral treatment with R13, the mean number of motoneurons labeled by retrograde tracers injected into these muscles was within the confidence limits of those reported for intact mice (Xu et al., 2021), suggesting that oral R13 treatments produced a near complete regeneration of motor axons in as little as 4 weeks. Similarly, the restoration of muscle innervation was enhanced by R13 treatments. Amplitudes of M responses in R13-treated mice were increased 2–3-fold in R13-treated animals over both vehicle-treated controls and mice treated with oral dosing of 7,8-DHF.

The number of muscle sensory neurons labeled after tracer injections into the GAST and TA muscles also increased after R13 treatments. Similar increases in small, medium, and large neurons were noted, suggesting that the improved axon regeneration provided by increased availability of the TrkB ligand in R13-treated mice was not restricted to a particular size class. It is known that after PNI, the expression of TrkB in DRG neurons is expanded to include neurons of all size classes if those neurons are activated by electrical stimulation (English et al., 2007; Geremia et al., 2007), a treatment known to increase BDNF release (Gordon and English, 2016). We speculate that our R13 treatments improved regeneration of these different sizes of muscle sensory axons via a similar expansion of TrkB expression. Whether R13 treatments also promote the accurate reinnervation of muscle proprioceptive end organs like muscle spindles, as well as improved reinnervation of non-muscle sensory targets such as skin, awaits further investigation.

We treated mice with R13 multiple times after the nerve injury to be comparable to the application of moderate daily exercise that we have used successfully in previous studies (English et al., 2011; Sabatier and English, 2015; Gordon and English, 2016) and that also relies on increased BDNF-TrkB signaling for its effectiveness (Wilhelm et al., 2012). Our findings at 4 weeks after injury are that the numbers of successfully regenerating motor axons and the amplitudes of M responses are similar to what we have reported in mice treated with exercise. We believe that the effectiveness of our experimental R13 therapy is the result of the gradual release of the BDNF mimetic 7,8-DHF over the 2-week treatment period. However, unlike BDNF, 7,8-DHF does not bind to and signal through the common neurotrophin receptor, p75^{NTR} (Wurzelmann et al., 2017). It is thus possible that our R13 treatments were so effective also because they avoided any anti-growth effects on regenerating axons resulting

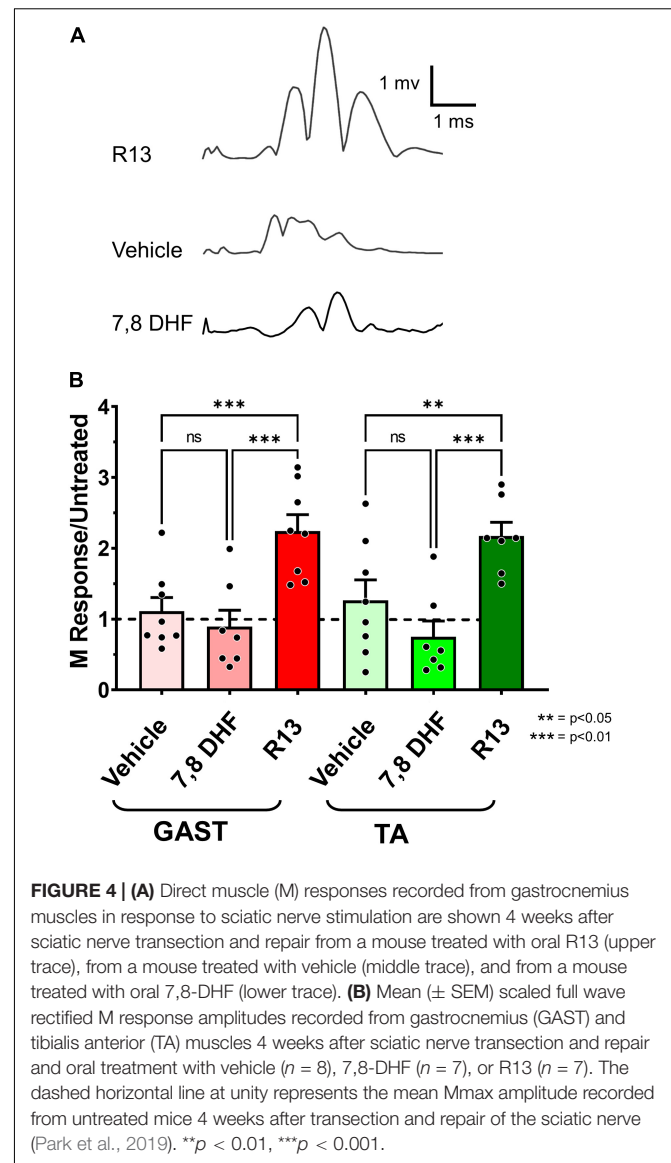


FIGURE 4 | (A) Direct muscle (M) responses recorded from gastrocnemius muscles in response to sciatic nerve stimulation are shown 4 weeks after sciatic nerve transection and repair from a mouse treated with oral R13 (upper trace), from a mouse treated with vehicle (middle trace), and from a mouse treated with oral 7,8-DHF (lower trace). **(B)** Mean (\pm SEM) scaled full wave rectified M response amplitudes recorded from gastrocnemius (GAST) and tibialis anterior (TA) muscles 4 weeks after sciatic nerve transection and repair and oral treatment with vehicle ($n = 8$), 7,8-DHF ($n = 7$), or R13 ($n = 7$). The dashed horizontal line at unity represents the mean Mmax amplitude recorded from untreated mice 4 weeks after transection and repair of the sciatic nerve (Park et al., 2019). ** $p < 0.01$, *** $p < 0.001$.

from p75^{NTR} binding (Boyd and Gordon, 2001; McGregor et al., 2021).

CONCLUSION

In conclusion, R13 treatments show considerable promise as a novel approach to enhancing functional recovery following PNI. The convenience of its oral administration, its prolonged biological activity at the site of injury, and its stimulation of both sensory and motor axon regeneration make it an experimental therapy worthy of further consideration.

DATA AVAILABILITY STATEMENT

The raw data supporting the conclusions of this article will be made available by the authors, without undue reservation.

ETHICS STATEMENT

The animal study was reviewed and approved by the Institutional Animal Care and Use Committee of Emory University.

AUTHOR CONTRIBUTIONS

AE conceived the study, supervised the experiments, analyzed the data, and wrote the manuscript. DC, RI, and SSK performed the experiments, analyzed the data, and commented on the manuscript. DH assisted in the experiments, analyzed EMG data, and commented on the manuscript. SK assisted in the experiments, analyzed neuroanatomical data, and commented on the manuscript. XL performed immunoblot experiments, analyzed the data, and commented on the manuscript. KY conceived study, provided R13 reagents, and commented on the manuscript. All authors contributed to the article and approved the submitted version.

REFERENCES

- Akhter, E. T., Rotterman, T. M., English, A. W., and Alvarez, F. J. (2019). Sciatic nerve cut and repair using fibrin glue in adult mice. *Bio. Protoc.* 9:e3363. doi: 10.21769/BioProtoc.3363
- Al-Majed, A. A., Neumann, C. M., Brushart, T. M., and Gordon, T. (2000). Brief electrical stimulation promotes the speed and accuracy of motor axonal regeneration. *J. Neurosci.* 20, 2602–2608. doi: 10.1523/jneurosci.20-07-02602.2000
- Basmajian, J. V., and Stecko, G. (1963). The role of muscles in arch support of the foot. *J. Bone Joint Surg. Am.* 45, 1184–1190. doi: 10.2106/00004623-196345060-00006
- Boyd, J. G., and Gordon, T. (2001). The neurotrophin receptors, trkB and p75, differentially regulate motor axonal regeneration. *J. Neurobiol.* 49, 314–325. doi: 10.1002/neu.10013
- Chen, C., Wang, Z., Zhang, Z., Liu, X., Kang, S. S., Zhang, Y., et al. (2018). The prodrug of 7,8-dihydroxyflavone development and therapeutic efficacy for treating Alzheimer's disease. *Proc. Natl. Acad. Sci. U.S.A.* 115, 578–583. doi: 10.1073/pnas.1718683115
- English, A. W. (2005). Enhancing axon regeneration in peripheral nerves also increases functionally inappropriate reinnervation of targets. *J. Comp. Neurol.* 490, 427–441. doi: 10.1002/cne.20678
- English, A. W., Liu, K., Nicolini, J. M., Mulligan, A. M., and Ye, K. (2013). Small-molecule trkB agonists promote axon regeneration in cut peripheral nerves. *Proc. Natl. Acad. Sci. U.S.A.* 110, 16217–16222. doi: 10.1073/pnas.1303646110
- English, A. W., Mulligan, A., Cucoranu, D., and Sabatier, M. J. (2009). Treadmill training enhances axon regeneration in cut peripheral nerves without effecting topographic specificity of reinnervating motoneurons. *J. Comp. Neurol.* 517, 245–255. doi: 10.1002/cne.22149
- English, A. W., Schwartz, G., Meador, W., Sabatier, M. J., and Mulligan, A. (2007). Electrical stimulation promotes peripheral axon regeneration by enhanced neuronal neurotrophin signaling. *Dev. Neurobiol.* 67, 158–172. doi: 10.1002/dneu.20339
- English, A. W., Wilhelm, J. C., and Sabatier, M. J. (2011). Enhancing recovery from peripheral nerve injury using treadmill training. *Ann. Anat.* 193, 354–361. doi: 10.1016/j.aanat.2011.02.013
- Funakoshi, H. (1993). Differential expression of mRNAs for neurotrophins and their receptors after axotomy of the sciatic nerve. *J. Cell Biol.* 123, 455–465. doi: 10.1083/jcb.123.2.455
- Geremia, N. M., Gordon, T., Brushart, T. M., Al-Majed, A. A., and Verge, V. M. (2007). Electrical stimulation promotes sensory neuron regeneration and growth-associated gene expression. *Exp. Neurol.* 205, 347–359. doi: 10.1016/j.expneurol.2007.01.040
- Gordon, T., and English, A. W. (2016). Strategies to promote peripheral nerve regeneration: electrical stimulation and/or exercise. *Eur. J. Neurosci.* 43, 336–350. doi: 10.1111/ejn.13005
- Harrisingh, M. C., Perez-Nadales, E., Parkinson, D. B., Malcolm, D. S., Mudge, A. W., and Lloyd, A. C. (2004). The Ras/Raf/ERK signalling pathway drives Schwann cell dedifferentiation. *EMBO J.* 23, 3061–3071. doi: 10.1038/sj.emboj.7600309
- Huang, E. J., and Reichardt, L. F. (2003). Trk receptors: roles in neuronal signal transduction. *Ann. Rev. Biochem.* 72, 609–642. doi: 10.1146/annurev.biochem.72.121801.161629
- Huang, Y. Z., and McNamara, J. O. (2010). Mutual regulation of Src family kinases and the neurotrophin receptor TrkB. *J. Biol. Chem.* 285, 8207–8217. doi: 10.1074/jbc.m109.091041
- Jang, S. W., Liu, X., Yepes, M., Shepherd, K. R., Miller, G. W., Liu, Y., et al. (2010b). A selective TrkB agonist with potent neurotrophic activities by 7,8-dihydroxyflavone. *Proc. Natl. Acad. Sci. U.S.A.* 107, 2687–2692. doi: 10.1073/pnas.0913572107
- Jang, S. W., Liu, X., Chan, C. B., France, S. A., Sayeed, I., Tang, W., et al. (2010a). Deoxydunin, a natural product with potent neurotrophic activity in mice. *PLoS One* 5:e11528. doi: 10.1371/journal.pone.0011528
- McGregor, C., Sabatier, M., and English, A. (2021). Early regeneration of axons following peripheral nerve injury is enhanced if p75(NTR) is eliminated from the surrounding pathway. *Eur. J. Neurosci.* 53, 663–672. doi: 10.1111/ejn.14943
- Park, S., Liu, C. Y., Ward, P. J., Jaiswal, P. B., and English, A. W. (2019). Effects of repeated 20-Hz electrical stimulation on functional recovery following peripheral nerve injury. *Neurorehabil. Neural Repair* 33, 775–784.
- Portincasa, A., Gozzo, G., Parisi, D., Annacontini, L., Campanale, A., Basso, G., et al. (2007). Microsurgical treatment of injury to peripheral nerves in upper and lower limbs: a critical review of the last 8 years. *Microsurgery* 27, 455–462. doi: 10.1002/micr.20382
- Ruscheweyh, R., Forsthuber, L., Schoffnegger, D., and Sandkuhler, J. (2007). Modification of classical neurochemical markers in identified primary afferent neurons with Abeta-, Delta-, and C-fibers after chronic constriction injury in mice. *J. Comp. Neurol.* 502, 325–336. doi: 10.1002/cne.21311
- Sabatier, M. J., and English, A. W. (2015). Pathways mediating activity-induced enhancement of recovery from peripheral nerve injury. *Exerc. Sport Sci. Rev.* 43, 163–171. doi: 10.1249/JES.0000000000000047
- Scholz, T., Krichevsky, A., Sumarto, A., Jaffurs, D., Wirth, G. A., Paydar, K., et al. (2009). Peripheral nerve injuries: an international survey of current treatments and future perspectives. *J. Reconstr. Microsurg.* 25, 339–344. doi: 10.1055/s-0029-1215529

FUNDING

This study was conducted with support from NIH grant NS105982 from the USPHS.

SUPPLEMENTARY MATERIAL

The Supplementary Material for this article can be found online at: <https://www.frontiersin.org/articles/10.3389/fncel.2022.857664/full#supplementary-material>

Supplementary Figure 1 | Immunoblots of extracts of cut and repaired sciatic nerves from mice that had been administered the R13 vehicle (5% DMSO/0.5% methylcellulose) orally. The different lanes are from nerves collected at different times (minutes) after administration. Administration of the vehicle produced no notable change in TrkB activation (pTrkB Y705) or in either of the downstream effectors, AKT or MAPK/Erk1/2.

- Sheu, J. Y., Kulhanek, D. J., and Eckenstein, F. P. (2000). Differential patterns of ERK and STAT3 phosphorylation after sciatic nerve transection in the rat. *Exp. Neurol.* 166, 392–402. doi: 10.1006/exnr.2000.7508
- Wilhelm, J. C., Cucoranu, D., Xu, M., Chmielewski, S., Holmes, T., Lau, K. S., et al. (2012). Cooperative roles of BDNF expression in neurons and Schwann cells are modulated by exercise to facilitate nerve regeneration. *J. Neurosci.* 32, 5002–5009. doi: 10.1523/JNEUROSCI.1411-11.2012
- Wurzelmann, M., Romeika, J., and Sun, D. (2017). Therapeutic potential of brain-derived neurotrophic factor (BDNF) and a small molecular mimics of BDNF for traumatic brain injury. *Neural Regen. Res.* 12, 7–12. doi: 10.4103/1673-5374.198964
- Xu, J., Xuan, A., Liu, Z., Li, Y., Zhu, J., Yao, Y., et al. (2021). An approach to maximize retrograde transport based on the spatial distribution of motor endplates in mouse hindlimb muscles. *Front. Cell. Neurosci.* 15:707982. doi: 10.3389/fncel.2021.707982

Conflict of Interest: The authors declare that the research was conducted in the absence of any commercial or financial relationships that could be construed as a potential conflict of interest.

Publisher's Note: All claims expressed in this article are solely those of the authors and do not necessarily represent those of their affiliated organizations, or those of the publisher, the editors and the reviewers. Any product that may be evaluated in this article, or claim that may be made by its manufacturer, is not guaranteed or endorsed by the publisher.

Copyright © 2022 English, Carrasco, Hoffman, Isaacson, Kang, Khan, Liu and Ye. This is an open-access article distributed under the terms of the Creative Commons Attribution License (CC BY). The use, distribution or reproduction in other forums is permitted, provided the original author(s) and the copyright owner(s) are credited and that the original publication in this journal is cited, in accordance with accepted academic practice. No use, distribution or reproduction is permitted which does not comply with these terms.



Brain-Derived Neurotrophic Factor Is an Important Therapeutic Factor in Mesenchymal Stem Cell Secretions for Treatment of Traumatic Peripheral Pelvic Injuries

Xiaoyi Yuan^{1,2,3†}, Brian M. Balog^{1,2,4†}, Dan Li Lin^{1,2}, Brett Hanzlicek^{1,2}, Mei Kuang¹, Hao Yan^{1,5}, Steve J. A. Majerus² and Margot S. Damaser^{1,2,6*}

¹Department of Biomedical Engineering, Lerner Research Institute, Cleveland Clinic, Cleveland, OH, United States,

²Advanced Platform Technology Center, Louis Stokes Cleveland Veterans Affairs Medical Center, Cleveland, OH, United States, ³Department of Urology, Tongji Hospital, Huazhong University of Science and Technology, Wuhan, China,

⁴Department of Biology, University of Akron, Akron, OH, United States, ⁵Department of Urology, Xuanwu Hospital, Capital Medical University, Beijing, China, ⁶Glickman Urological and Kidney Institute, Cleveland Clinic, Cleveland, OH, United States

OPEN ACCESS

Edited by:

Dale Sengelaub,
Indiana University Bloomington,
United States

Reviewed by:

Beatriz Benitez-Temino,
Sevilla University, Spain
Yongchao Mou,
University of Illinois at Rockford,
United States

*Correspondence:

Margot S. Damaser
damasem@ccf.org

[†]These authors have contributed
equally to this work

Specialty section:

This article was submitted to
Cellular Neuropathology,
a section of the journal
Frontiers in Cellular Neuroscience

Received: 30 January 2022

Accepted: 12 April 2022

Published: 18 May 2022

Citation:

Yuan X, Balog BM, Lin DL,
Hanzlicek B, Kuang M, Yan H,
Majerus SJA and Damaser MS
(2022) Brain-Derived Neurotrophic
Factor Is an Important Therapeutic
Factor in Mesenchymal Stem Cell
Secretions for Treatment of Traumatic
Peripheral Pelvic Injuries.
Front. Cell. Neurosci. 16:866094.
doi: 10.3389/fncel.2022.866094

Traumatic neuromuscular injury to the pudendal nerve and urethra during childbirth does not regenerate well and contributes to stress urinary incontinence in women. Mesenchymal stem cells (MSCs) can improve neuroregeneration via their secretions, or secretome, which includes brain-derived neurotrophic factor (BDNF). In this study, we investigated whether BDNF is a key factor in the secretome of MSCs for the facilitation of functional recovery following a dual simulated childbirth injury. BDNF knockdown (KD) MSCs were created using an anti-BDNF shRNA lentivirus vector. A scrambled sequence was used as a transduction control (scrambled). Cells were cultured for 24 h before media was concentrated 50x to create concentrated conditioned media (CCM) containing MSC secretome. CCM of unmanipulated MSCs was screened for high BDNF expression (high BDNF CCM). Concentrated control media (CM) was created by concentrating media not conditioned by cells. Female Sprague-Dawley rats underwent bilateral pudendal nerve crush and vaginal distension (Injury) or sham injury. One hour and 1 week after injury, sham injured rats received CM, and injured rats received CM, high BDNF CCM, KD CCM, or scrambled CCM (300 μ l intraperitoneally). Three weeks after injury, rats underwent leak point pressure (LPP) and pudendal nerve sensory branch potential (PNSBP) recordings. The urethra and pudendal nerve were harvested for anatomical assessment. ANOVA followed by the Student-Newman-Keuls test determined significant differences between groups ($p < 0.05$). BDNF KD CCM had significantly decreased BDNF concentration compared to scrambled CCM, while the concentration in high BDNF CCM was significantly increased. LPP was significantly decreased in CM and KD CCM treated animals compared to sham injury, but not with scrambled or high BDNF CCM. PNSBP firing rate showed a significant decrease with CM treatment compared to sham injury. Neuromuscular junctions in the urethral sphincter in KD CCM, scrambled CCM, and high BDNF CCM were healthier than CM treated rats.

While anatomical and nerve function tests demonstrate regeneration of the pudendal nerve with any CCM treatment, LPP results suggest it takes longer to recover continence with reduced BDNF in CCM. BDNF in MSC CCM is an important factor for the acceleration of recovery from a dual nerve and muscle injury.

Keywords: siRNA knockdown, leak point pressure, neuromuscular junctions, reinnervation, urethra, external urethral sphincter, neuroregeneration, pudendal nerve

INTRODUCTION

Traumatic injuries can be caused by automobile or industrial accidents, violence, and combat injuries; however, while not typically characterized as traumatic, childbirth also causes damage to nerves, muscles, and the supportive tissues of the pelvic floor (Noble et al., 1998; Gray, 2004; Taylor et al., 2008). Traumatic injuries lead to loss of motor and sensory function and potentially the development of neuropathic pain (Chan et al., 2014). Since few patients achieve full recovery, patients will live the rest of their lives with these symptoms, affecting many patients in the prime of their lives (Karsy et al., 2019).

While modern medicine has helped save maternal and newborn lives in childbirth, damage to the lower urinary tract and pelvic floor during delivery can lead to stress urinary incontinence (SUI), the unwanted leakage of urine from increased abdominal pressure (Meyer et al., 1993; Abrams et al., 2002; Gray, 2004; Salam et al., 2014; Ng et al., 2017; Daly et al., 2018). Women suffering from post-partum SUI are 2.5× more likely to develop it later in life, suggesting insufficient regeneration after childbirth as a contributor to SUI (Meyer et al., 1993; Eftekhar et al., 2006).

One of the critical components of urethral closure pressure and maintenance of continence is the external urethral sphincter (EUS; Delancey et al., 2008). The EUS is innervated by the pudendal nerve (PN) and both can be injured as the baby's head passes through the birth canal during delivery (Snooks et al., 1984, 1986; Meyer et al., 1993). It has been theorized that this combinational neuromuscular injury contributes to the pathophysiology of SUI (Swash, 1990).

Preclinical rodent studies of simulated childbirth injuries have shown that the combination of vaginal distension (VD), which injures the EUS, and a PN crush (PNC), significantly delays recovery of urinary continence (Jiang et al., 2009a,b). Additionally, while VD does not itself reduce PN function when VD is added to PNC, it significantly delays PN functional recovery (Jiang et al., 2009a,b). This delay in functional recovery is supported by inadequate expression of brain-derived neurotrophic factor (BDNF) by the EUS after dual injury (Pan et al., 2009). However, administration of BDNF or electrical stimulation of the PN in turn accelerates functional recovery after injury (Gill et al., 2013a; Jiang et al., 2013). The above facts suggest that BDNF may be a key factor for PN regeneration.

Mesenchymal stem cells (MSCs) have great regenerative potential, primarily *via* their secretions, which include growth factors, cytokines, and extracellular vehicles (Zhang et al., 2007; Barzilay et al., 2009; Mias et al., 2009; Penn, 2012; Peter et al., 2012; Tran and Damaser, 2015). We have previously

demonstrated that MSCs or their secretions, termed the secretome, accelerate functional recovery after a dual simulated childbirth injury consisting of PNC and VD (Deng et al., 2015; Janssen et al., 2019). The aim of this study was to investigate whether BDNF is a critical factor in the secretome of MSCs for the facilitation of functional recovery following a dual neuromuscular simulated childbirth injury. We hypothesized that BDNF is necessary to facilitate functional regeneration *via* the secretome of MSCs.

MATERIAL AND METHODS

Study Design

This research was approved by the Institutional Animal Care and Use Committee of the Cleveland Louis Stokes Veterans Affairs Medical Center. Sixty-six female, adult, age-matched virgin Sprague-Dawley rats (Envigo, Indianapolis, IN, USA, 226–283 g) were randomly divided into five groups (**Figure 1A**). The first group underwent sham injury and received concentrated control media (CM; Sham Injury + CM; $n = 17$). The remaining groups underwent dual injury to create SUI and received either one of four treatments: CM (Injury + CM; $n = 16$), concentrated conditioned media (CCM) from MSCs in which BDNF had been knocked down by small interfering RNA (siRNA) transduction (Injury + BDNF KD CCM; $n = 12$), CCM from MSC with scrambled siRNA transduction (Injury + scrambled CCM; $n = 11$), or CCM from unmanipulated MSCs selected for their high BDNF concentrations (Injury + high BDNF CCM; $n = 10$). Each animal received two 300 μ l treatments *via* intraperitoneal (i.p.) injections, 1 h after the injury, and 1 week later. All rats underwent functional testing 3 weeks after injury, including leak point pressure (LPP) with simultaneous EUS electromyography (EMG), as well as PN sensory branch potential (PNsBP) recording. Rats were then euthanized and the pudendal nerve and urethra were dissected for anatomical assessment of pudendal nerve regeneration *via* immunofluorescence.

Mesenchymal Stem Cells (MSCs)

Bone marrow was collected from femurs and tibias of Sprague Dawley female donor rats to obtain MSCs as described previously (Dissaranan et al., 2014). Cells were cultured in normoxic conditions with 5% CO₂ at 37°C in Dulbecco's modified Eagle's low glucose (DMEM) media supplemented with 10% and 12.5% fetal bovine serum (FBS). MSCs were selected by sorting the cells at passage 3 for intracellular adhesion molecule 1 (ICAM-1) *via* flow cytometry (**Figure 1B**). MSCs were transduced at passage 5 with either short hairpin BDNF RNA (shRNA; a form of siRNA), scrambled shRNA, or were not transduced and were

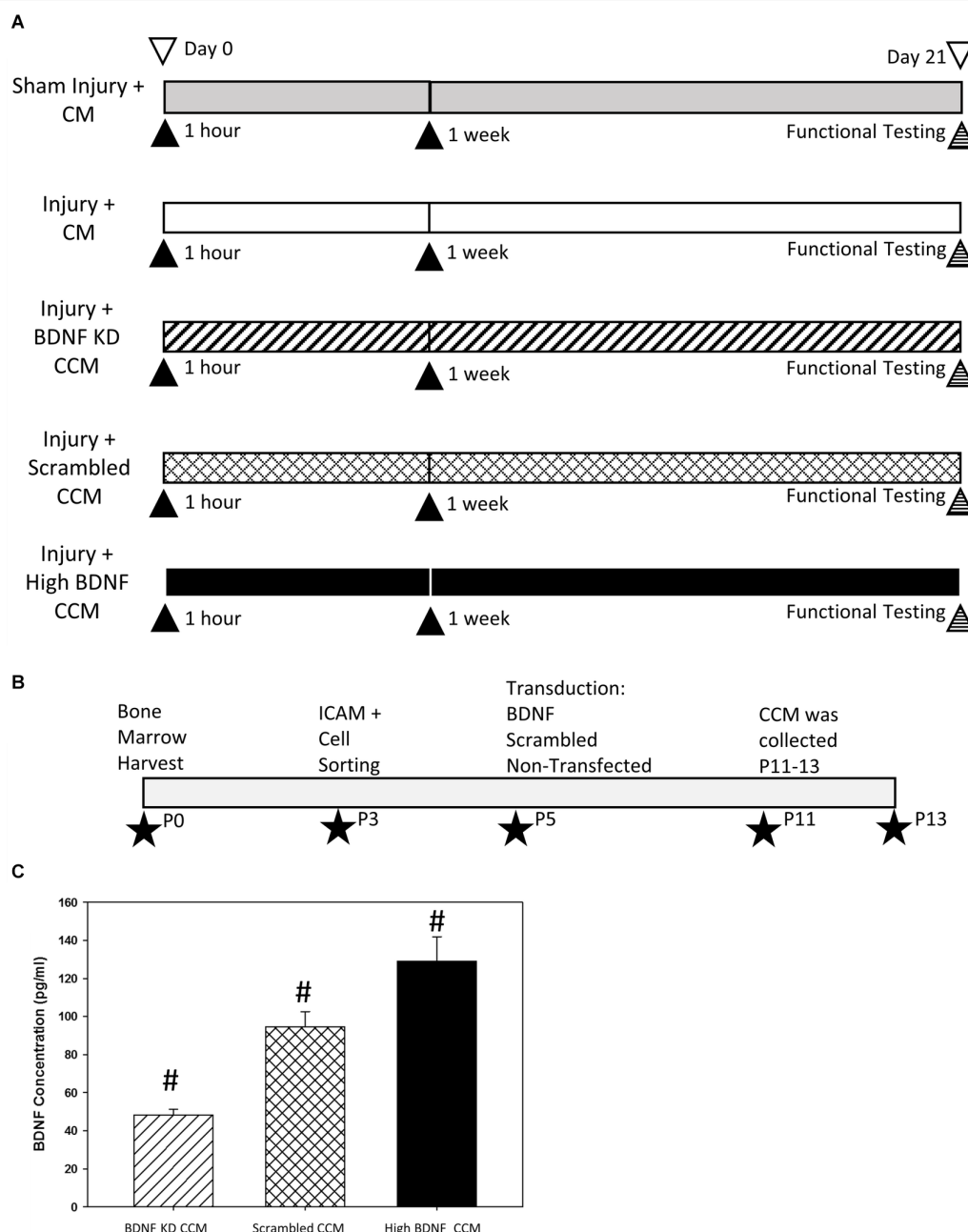


FIGURE 1 | Experimental design diagrams and BDNF knockdown validation. Experimental design **(A)** indicating the five experimental groups: Sham Injury + Control Media (CM), Injury (Pudendal Nerve Crush + Vaginal Distension) + CM, Injury + Brain-Derived Neurotrophic Factor Knockdown (BDNF KD) Concentrated Conditioned Media (CCM), Injury + Scrambled CCM, or Injury + High BDNF CCM. ▲ Indicates an intraperitoneal injection of treatment. Experimental timeline of mesenchymal stem cell (MSC) purification, transductions, and CCM production **(B)**. ★ Indicates the passage at which the procedure was performed. Validation of BDNF concentration **(C)**. CCM BDNF concentration. Bars are mean \pm standard error of the means from 3 to 5 samples per group. ANOVA followed by a Student-Newman-Keuls *post-hoc* test was used to indicate significant differences. #Indicates a significant difference compared to the other two groups.

cultured to passage 11–13 before being used to prepare CCM, containing the secretome of MSCs.

Transduction and Modulation of CCM

H9C2 (ATCC) cells were maintained in Dulbecco's modified Eagle's low glucose (DMEM) media supplemented with 10%

and 12.5% fetal bovine serum (FBS) respectively, and 1% anti-antimycotic (ThermoFisher/Gibco, Carlsbad, CA, USA, 15240-062). 293-FT (ATCC) cells were maintained in DMEM high glucose (ThermoFisher/Gibco, #11965-084) with 10% FBS, 1% MEM NEAA (ThermoFisher/Gibco, 11140-050), 1% L-Glutamine (media core 527-45) 1% anti-anti, 1%

100 mM Napyruvate Solution with or without 1% Geneticin (ThermoFisher/Gibco, #11811-023).

Six shRNA sequences were selected for initial testing to determine which would decrease BDNF expression. Six different lentiviruses were produced from co-transduced 293-FT cells with the vector pLKO.1 (Addgene, Watertown, MA, USA) with one of six shRNAs against BDNF mRNA with packaging plasmids (pMDL, pRev, and pVSVG, Invitrogen, Carlsbad, CA, USA) according to the manufacturer's instructions. Forty-eight hours after transduction, the medium from the 293FT cells was collected and concentrated by 20,000 rpm ultracentrifugation for 2 h. The concentrated supernatant was used to transduce H9C2 cells as a test case and 4 µg/ml of puromycin was added 48 h post-transduction. Cells resistant to puromycin were selected and knockdown purity was detected by ELISA. The sequence that produced the greatest decrease in BDNF expression (5'ccggGGCGGTTTCATAAGGATAGACActcagTGTCTATCCTTATGAACCGCCttttg3') was chosen for the experiment and a scramble of this sequence (5'ccggGACAGAATGCGATCGGAGTTActcagTAACTCCGATCGCATTCTGTCTttttg3') was chosen to serve as a transduction control.

Rat MSCs were transduced at Passage 5 with the BDNF KD or scrambled lentivirus (**Figure 1B**). Forty-eight hours after transduction, 4 µg/ml puromycin was added to the media to select transduced cells for the first 10 days. The concentration of puromycin was reduced to 2 µg/ml in the medium to maintain the selection. Transduced MSCs were expanded and CCM was collected at passages P11-P13 (**Figure 1B**). CCM BDNF levels were then detected using ELISA. CCM from naive MSCs with BDNF concentration greater than 110 pg/300 µl were selected for the High BDNF CCM group.

Characterization of CCM With Total Protein and Differentiation Assays

The concentration of total protein of each CCM batch was estimated using a PierceTM BCA Protein Assay Kit (Thermo Fisher Scientific, #23225) with bovine serum albumin (BSA, Life Technologies, Carlsbad, CA, USA, #15561020) as a standard. Adipogenesis, chondrogenesis, and osteogenesis differentiation assays (ThermoFisher/Gibco, #A10070-1, A10071-1, and A10072-1) were done according to the manufacturer's instructions to confirm that MSCs retained stem cell characteristics after shRNA transduction in all three MSC groups at P12-P13. After differentiation, adipocytes were stained with oil red O stain on day 14, chondrocytes were stained with toluidine blue stain on day 11, and osteocytes were stained with alizarin red S stain on day 21. Images were taken with an Olympus light microscope (Center Valley, PA, USA; model: BH2-HLSH).

Concentrated Conditioned Medium (CCM) and Concentrated Control Media (CM)

When BDNF KD, scrambled, or naive MSCs grew close to confluent (P11-P13), regular MSC culture media was replaced with antibiotic- and serum-free DMEM media for 24 h and were concentrated 50× by 4,000 rpm centrifugation for one and half hours at 4°C using Amicon ultra-15 Centrifugal Filters

(Millipore, Burlington, MA, USA, #UFC900324). By the same process, CM was produced by concentrating the serum-free DMEM media not exposed to the cells. Each dose of CCM consisted of 300 µl, which was the CCM from 1 T-75 flask of MSCs, or approximately 1.5×10^6 MSCs.

ELISA

BDNF in BDNF KD, scrambled, and high BDNF CCM was quantified using a BDNF ELISA kit (G7610, Promega Madison WI, USA) according to the manufacturer's protocol. In brief, 50 µl of CCM and 50 µl of blocker and sample buffer were added to each well. Based on duplicate assays, results were reported as total protein of BDNF pg/injection (300 µl of CCM).

Model Creation and Treatment With CCM or CM

All rats were anesthetized with 2% isoflurane and underwent 4 h VD after bilateral PNC to create the dual injury model of SUI, as described previously (Jiang et al., 2009b; Deng et al., 2015; Janssen et al., 2019). In brief, the pudendal nerve was isolated and crushed in the ischiorectal fossa with a Castroviejo needle holder twice, each for 30 s. The vagina was accommodated for VD with increasing sizes of bouge a boule urethral dilators (24–32 Fr). A modified 10 Fr catheter was then inserted into the vagina, and then the balloon was inflated with 3 ml water for 4 h.

Sham injured rats received incisions in the dorsal skin at the same position and length as injured rats, and the vagina was accommodated with the urethral dilators. The catheter was inserted into the vagina for 4 h, but the balloon was not inflated. All rats received two subcutaneous doses of Rimadyl: one dose immediately before surgery and the second 24 h later. All rats received two doses of CM or CCM (300 µl i.p.) 1 h and 1 week after injury or sham injury.

Functional Testing: Urinary Function and Pudendal Nerve Sensory Nerve Testing

In vivo functional tests, including LPP, EUS EMG, and PNSBP, were performed as described previously (Deng et al., 2019; Balog et al., 2021). Under 2% isoflurane anesthesia, a PE-50 polyethylene catheter was inserted into the rat bladder dome and a purse-string suture was used to fix the catheter before closing the abdominal wall. The catheter was then connected to a syringe pump (5 ml/h, model 200; KD Scientific, New Hope, PA) and a pressure transducer (model PT300; Natus Neurology, Providence, RI, USA). Straight parallel bipolar platinum-iridium electrodes, 1.0 mm apart (250 µm diameter; FHC, Inc., Bowdoin, ME, USA) were placed on the surface of the EUS, located at the mid-urethra, and were connected to an amplifier (band-pass frequencies: 3 Hz–3 KHz, model P511; AC Amplifier, Natus Neurology, Middleton, WI, USA) and electrophysiological recording system (10-kHz sampling rate, Power-Lab 8/35, AD Instruments, Colorado Springs, CO, USA). The pudendal nerve sensory branch was identified and isolated at the ventral side of the pudendal canal. It was suspended over a curved, parallel bipolar platinum-iridium recording electrode (250 µm diameter wire, 0.8 mm apart, 1.0 mm hook diameter; FHC, Inc., Bowdoin, ME, USA) connected to the amplifier and electrophysiological

recording system and was recorded after LPP and EUS EMG recording.

Before recording, the rats were anesthetized with urethane (1.2 g/kg i.p.) and the isoflurane anesthesia was disconnected to better preserve continence and voiding function (Cannon and Damaser, 2001). The bladder was slowly filled with room temperature saline (5 ml/h) via the syringe pump connected to the suprapubic bladder catheter, with rats in a supine position. For LPP with simultaneous EUS EMG recording, with the bladder approximately half full, the bladder was gently and slowly depressed while recording bladder pressure and EUS EMG. The external pressure was rapidly removed when saline leakage was visualized at the urethral meatus. LPP with simultaneous EUS EMG testing was repeated several times in each rat until at least three consistent results were obtained. After LPP and EUS EMG testing, the clitoris was brushed with gauze at a moderate speed while PNSBP was recorded. This procedure was repeated four times in each animal.

Histology

The urethra (harvested *en bloc* with the anterior vagina) and pudendal nerves were dissected, stored at -80°C , and sectioned transversely (14 μm). Transverse urethral sections underwent immunofluorescence to assess the innervation of neuromuscular junctions (NMJ) of the EUS after injury, with primary antibodies (anti-neurofilament 68, cat #N5137, and anti-neurofilament 200, cat #N0142, both 1:400 dilution, Sigma-Aldrich, St Louis, MO, USA) and secondary antibody (Alexa Fluor 488-conjugated donkey anti-mouse IgG, cat #A21202, 1:400 dilution, ThermoFisher) to identify axons, with 4 $\mu\text{g/ml}$ of tetramethylrhodamine-conjugated α bungarotoxin (Rh- α -BTX, cat #T1175; ThermoFisher) to identify acetylcholine receptors at the NMJs, and with Alexa 350-conjugated phalloidin (1:20 in PBS, cat #A22281 ThermoFisher) to identify striated muscles of the EUS. Transverse pudendal nerve sections also underwent immunofluorescence to identify axons using Neurofilament 68 and 200 as the primary antibodies as above.

Data Analysis

In vivo physiological data, including LPP, EUS EMG, and PNSBP, were analyzed as described previously (Deng et al., 2019). LPP was defined as baseline pressure just prior to LPP testing subtracted from peak pressure at leakage. The mean of LPP for each animal was calculated by selecting all LPPs (3–5) performed in a given animal and determining the mean LPP. Quantitative assessment of EUS EMG and PNSBP was performed by selecting a 1-s segment of baseline and a 1-s segment at peak activity to determine the mean amplitude and firing rate of muscle and nerve activity as done previously (Jiang et al., 2009b). In brief, electrophysiological analysis was performed with an automated methodology in Matlab software (R2012B, MathWorks Natick, MA, USA). EMG recordings were digitally filtered using a 60-Hz notch filter with 2-Hz bandwidth to remove powerline interference. Paired, one-second segments from EMG recordings were extracted for each LPP recording: just before the LPP manipulation (Baseline) and at peak LPP pressure (Peak). For each paired recording, a spike crossing

threshold was calculated based on the interquartile range (IQR). This statistically-calculated threshold was derived entirely from the data itself, and was used rather than a fixed threshold, to adapt for intra- and inter-animal recording differences commonly encountered in EMG analysis.

Each segment was centered on a mean value of 0, and scaled to the electrode-referred voltage by dividing by the instrumentation amplifier gain, such that segments represented the amplitude in μV as recorded at the nerve. Baseline and Peak segments were combined, and the interquartile range (IQR) of paired recordings was calculated. For spike counting, any spike in the EMG waveform with the peak magnitude exceeding the IQR was identified. Spike peak values and locations were selected where the maximum signal magnitude occurred between successive crossings of the IQR threshold. For each EMG segment pair, the mean spike amplitude for identified spikes was calculated based on magnitude (in μV), and the mean firing rate was calculated as the number of identified spikes divided by the EMG segment length (1 s). An increase in EUS EMG amplitude and firing rate at peak bladder pressure during LPP testing was calculated by subtracting values at baseline from values at peak bladder pressure for each LPP trial, as modified from our prior work (Jiang et al., 2009b; Deng et al., 2019).

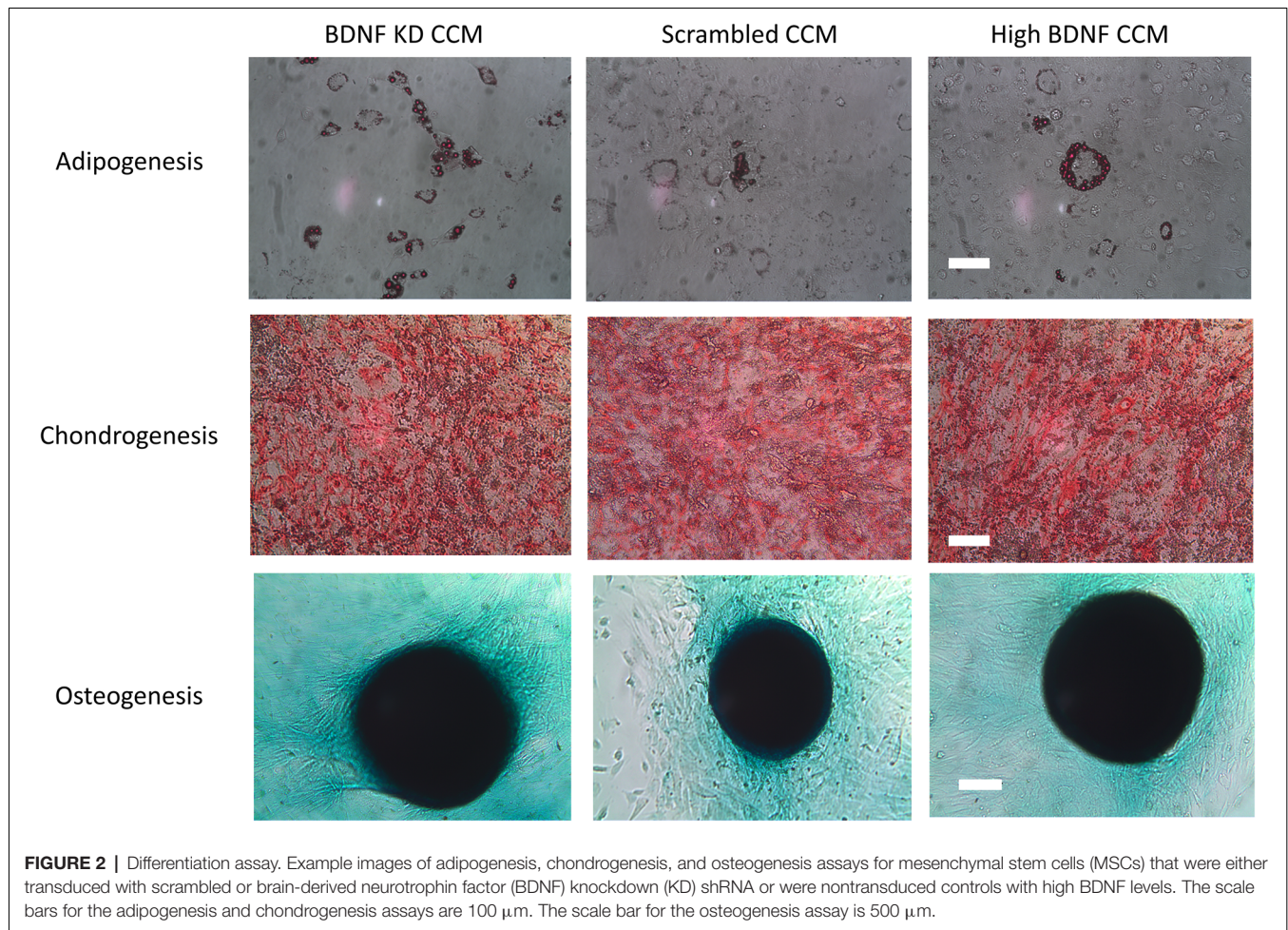
Mean values of each quantitative variable from each animal were determined and used to calculate a mean and standard error (SE) for each experimental group. One-way ANOVA followed by the Student-Newman-Keuls test was used to compare LPP, EUS EMG, and PNSBP results since these data were normally distributed. $P < 0.05$ indicated a statistically significant difference between groups for all statistical tests.

Immunofluorescence was evaluated qualitatively by a blinded observer. The thickness of innervating axons, the concentration of NMJs in the EUS, and integrity of the NMJs were used to evaluate the innervation of the EUS qualitatively. Nerve fascicle density and axon morphology/organization were used to assess pudendal nerve regeneration qualitatively.

RESULTS

BDNF concentration in CCM was significantly decreased in BDNF KD CCM (48.2 ± 3.1 pg/300 μl) compared to both scrambled CCM (94.6 ± 8.0 pg/300 μl) and high BDNF CCM (129.0 ± 13.0 pg/300 μl , **Figure 1C**). The concentration of BDNF in high BDNF CCM was also significantly increased compared to scrambled CCM (**Figure 1C**).

MSCs transduced with either BDNF KD or scrambled siRNA demonstrated the ability to differentiate into chondrocytes, osteocytes, and adipocytes (**Figure 2**), as we have shown previously for these rat bone marrow derived MSCs. This demonstrated that transduction did not alter their status as MSCs (Dissaranan et al., 2014). Images were collected at the end of the differentiation, as specified in the manufactures instructions: day 14 for adipocytes, day 11 for chondrocytes, and day 21 for osteocytes. Total protein assays of CCM demonstrated no significant differences between the three different CCM groups.



LPP examples 3 weeks after injury showed a visible decrease in LPP and EUS EMG in the injury + CM and injury + BDNF KD CCM groups compared to the sham injury + CM group (**Figure 3A**). When all groups were compared, LPP was significantly decreased in the injury + CM (28.3 ± 2.1 cm H₂O) and injury + BDNF KD CCM (31.1 ± 2.5 cm H₂O) groups compared to sham injured animals (40.9 ± 3.3 cm H₂O, **Figure 3B**). LPP in the injury + scrambled CCM group (36.0 ± 3.1 cm H₂O) was not significantly different from that of the sham injury + CM group (**Figure 3B**). LPP was significantly increased in the injury + high BDNF CCM group (51.1 ± 3.1 cm H₂O) compared to all the other groups (**Figure 3B**).

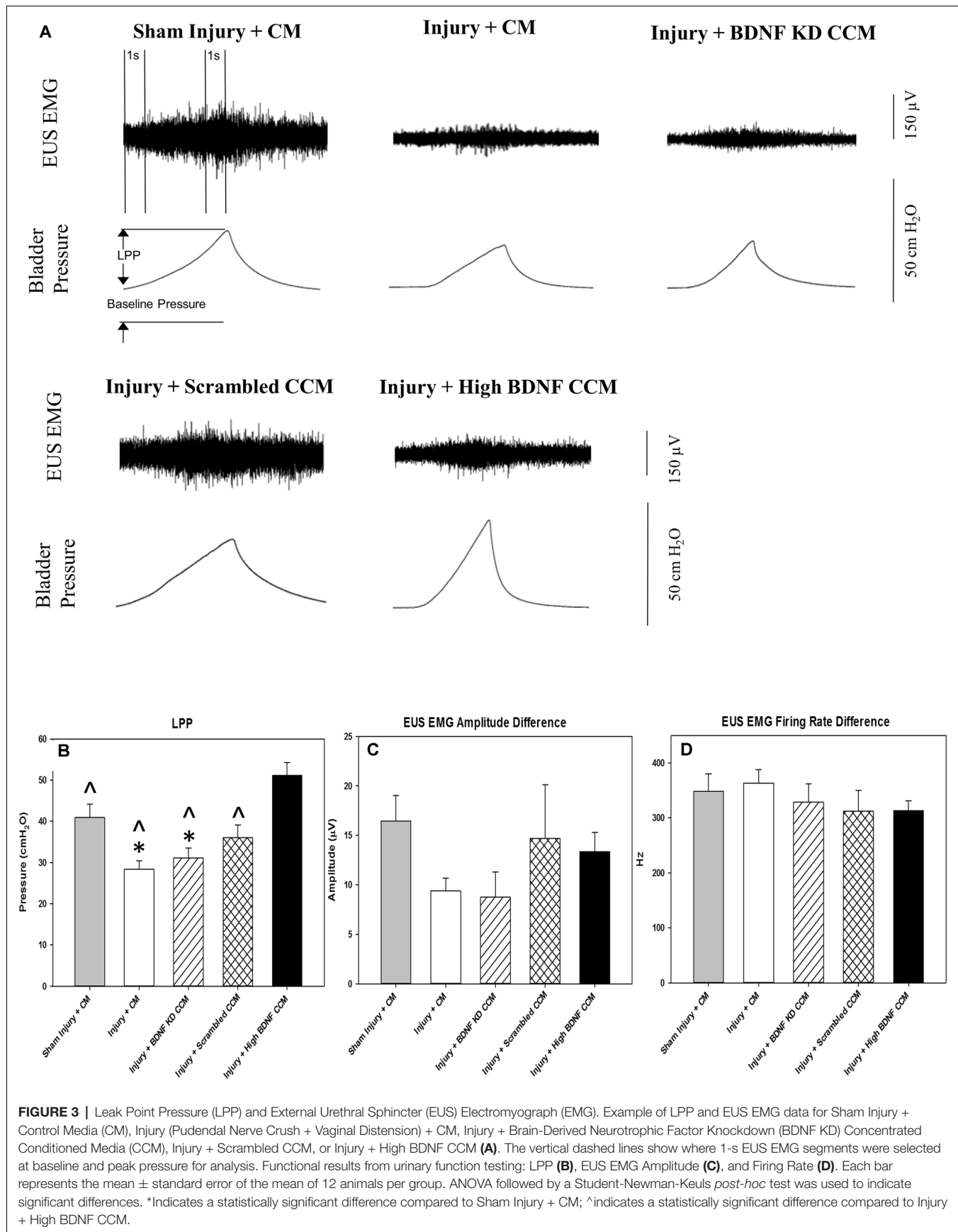
Although the EUS EMG amplitude increase with LPP was visibly decreased in the injury + CM and injury + BDNF KD CCM groups, there were no significant differences in EUS EMG amplitude and firing rate between any of the groups: sham injury + CM (16.4 ± 2.6 μ V; 348.2 ± 31.8 Hz.), injury + CM (9.4 ± 1.3 μ V; 363.3 ± 53.1 Hz), injury + BDNF KD CCM (8.7 ± 2.5 μ V; 328.1 ± 74.5 Hz), injury + scrambled CCM (14.7 ± 5.4 μ V; 312.3 ± 84.5 Hz.), or injury + high BDNF CCM (13.4 ± 1.9 μ V; 312.9 ± 42.9 Hz, **Figures 3C,D**).

Examples of pudendal sensory nerve functional testing showed visibly decreased activity in the injury + CM and injury

+ BDNF KD CCM groups compared to the sham injury + CM group (**Figure 4A**). Sensory nerve amplitude increased with clitoral brushing was significantly decreased in the injury + CM (0.3 ± 0.1 μ V), injury + BDNF KD CCM (0.6 ± 0.1 μ V), injury + scrambled (0.5 ± 0.1 μ V), and injury + high BDNF CCM groups (0.6 ± 0.1 μ V), compared to the sham injury + CM group (1.0 ± 0.1 μ V, **Figure 4B**). In contrast, the sensory nerve firing rate difference was only significantly decreased in the injury + CM group (399.4 ± 100.4 Hz.) compared to the sham injury + CM group (977.4 ± 92.5 Hz, **Figure 4C**).

Neuromuscular junction (NMJ) immunofluorescence from EUS specimens in the injury + CM group had fewer axons and non-compact NMJ than in the sham injury + CM group, which had compact NMJs with a single innervating axon (**Figure 5**). NMJs of the EUS in the injury + BDNF KD CCM group demonstrated more innervating axons than in the injury + CM group but nonetheless had non-compact NMJs. The Injury + scrambled CCM group had compact NMJs innervated by a single axon, and the injury + high BDNF CCM group showed compact NMJs innervated by a single axon with many branches (**Figure 5**).

Immunofluorescence of sensory axons of the pudendal nerve in the injury + CM group had decreased axon



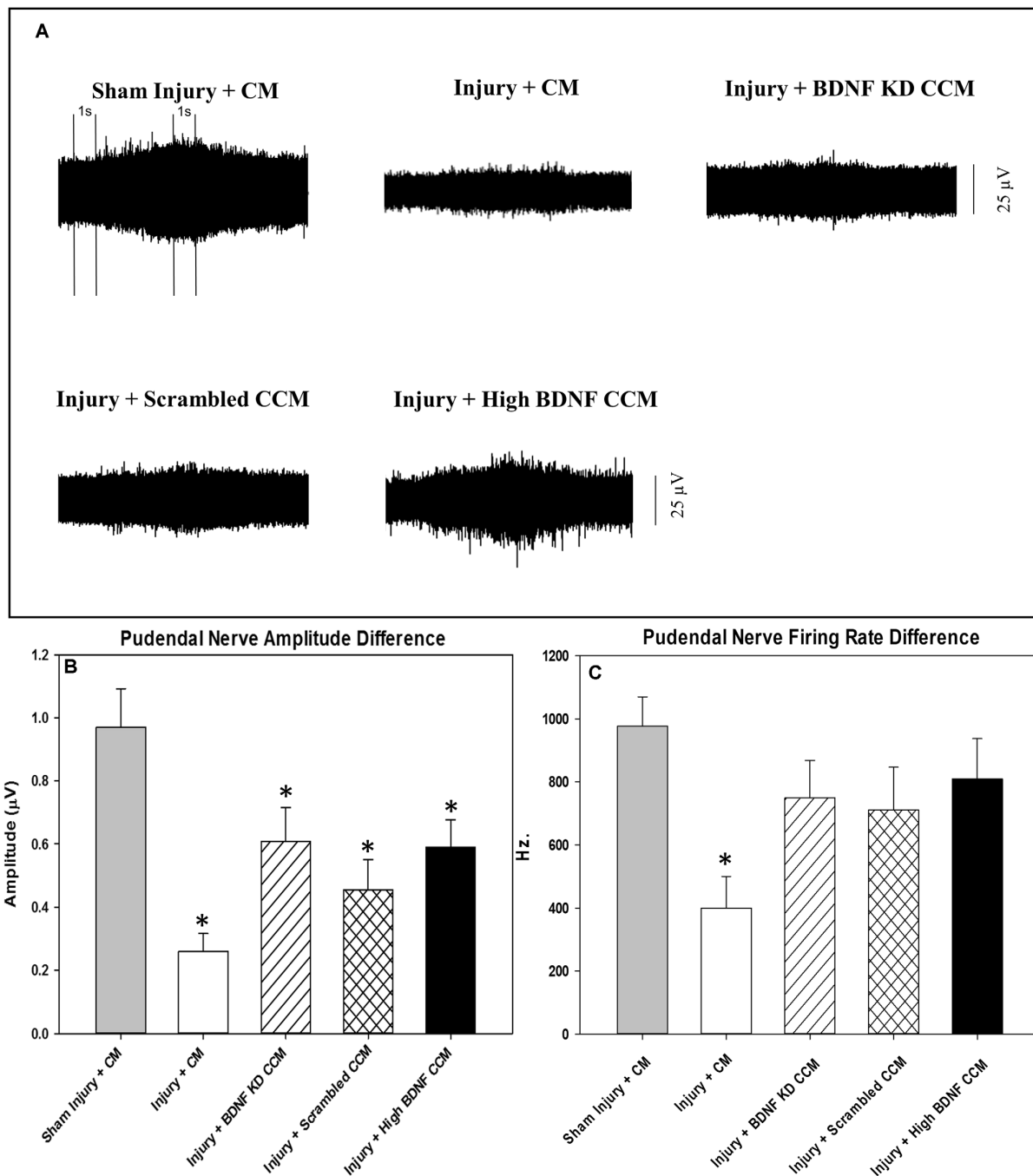


FIGURE 4 | Pudendal nerve sensory branch results. Examples of sensory nerve recording from each group: Sham Injury + Control Media (CM), Injury (Pudendal Nerve Crush + Vaginal Distension) + CM, Injury + Brain-Derived Neurotrophic Factor Knockdown (BDNF KD) Concentrated Conditioned Media (CCM), Injury + Scrambled CCM, or Injury + High BDNF CCM (**A**). The vertical dashed lines show where 1-s recording segments were selected at baseline and during brushing for analysis. Quantitative sensory nerve testing results of Amplitude (**B**) and Firing Rate (**C**). Each bar represents the mean \pm standard error of the mean of 12 animals per group. ANOVA followed by a Student-Newman-Keuls *post-hoc* test was used to indicate significant differences. *Indicates a statistically significant difference compared to Sham Injury + CM.

density and organization, while the injury + BDNF KD CCM group demonstrated decreased axon density compared to the sham injury + CM group (**Figure 6**). In contrast, the injury + scrambled CCM and injury +

high BDNF CCM groups had similar axon densities to the sham injury + CM group, demonstrating improved neuroregeneration compared to the other treated groups.

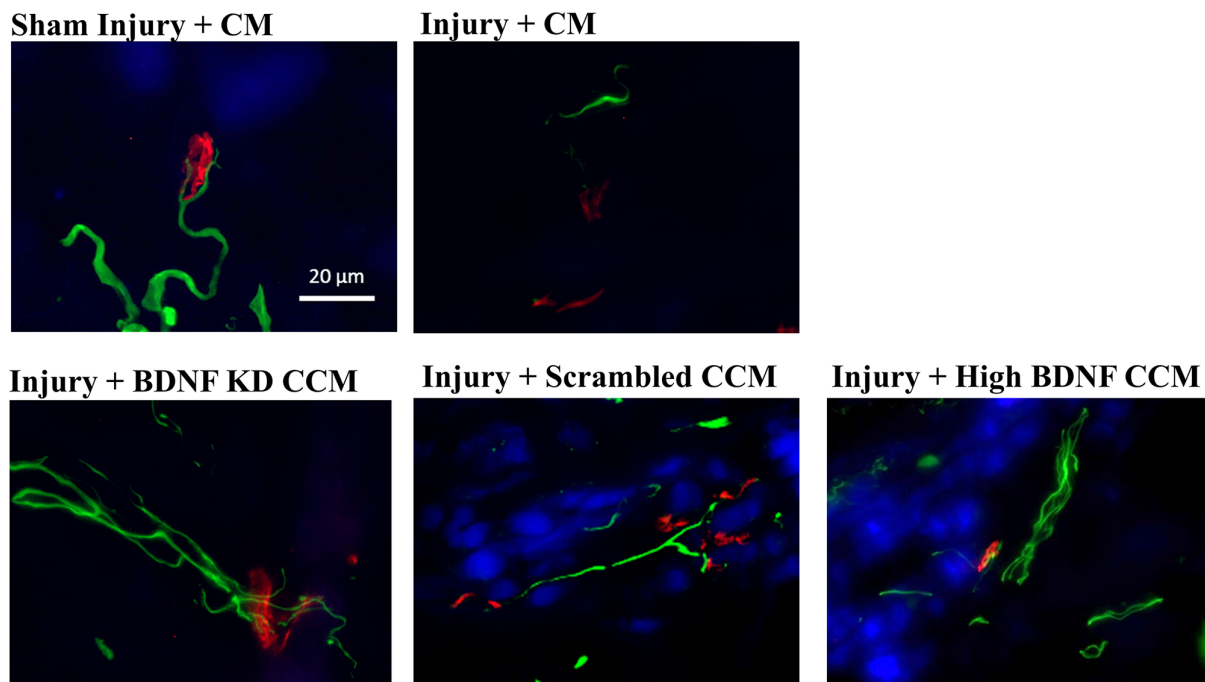


FIGURE 5 | Examples of external urethral sphincter neuromuscular junction staining from each group: Sham Injury + Control Media (CM), Injury (Pudendal Nerve Crush + Vaginal Distension) + CM, Injury + Brain-Derived Neurotrophic Factor Knockdown (BDNF KD) Concentrated Conditioned Media (CCM), Injury + Scrambled CCM, or Injury + High BDNF CCM. Scale bar represents 20 μ m. Green fluorescence shows axons (mouse anti-neurofilament 68 and 200), while red fluorescence indicates neuromuscular junctions (alpha-bungarotoxin stain), and blue indicates muscle (phalloid stain).

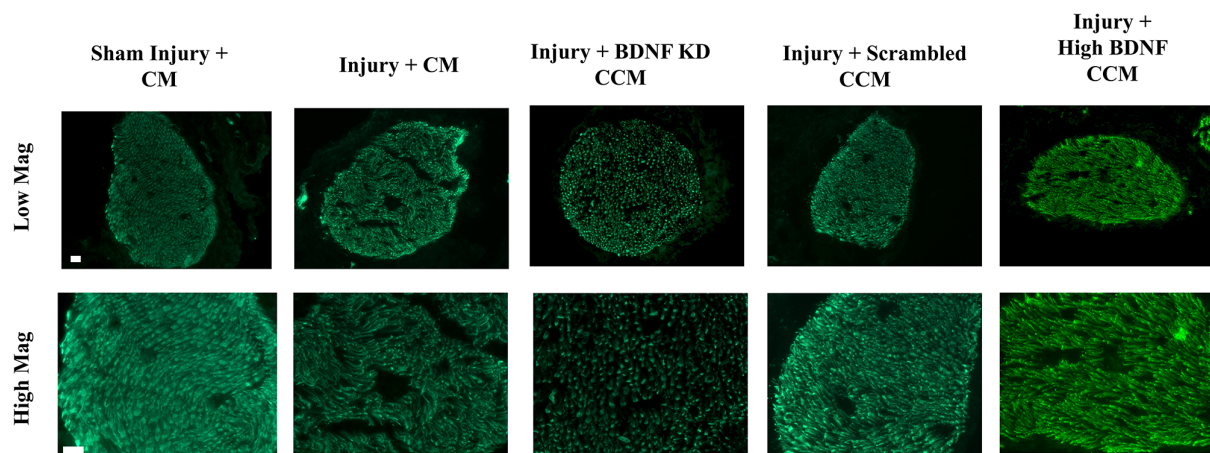


FIGURE 6 | Examples of pudendal nerve sensory branch immunostaining of axons from each group: Sham Injury + Control Media (CM), Injury (Pudendal Nerve Crush + Vaginal Distension) + CM, Injury + Brain-Derived Neurotrophic Factor Knockdown (BDNF KD) Concentrated Conditioned Media (CCM), Injury + Scrambled CCM, or Injury + High BDNF CCM. The white scale bar indicates 20 μ m in both top and bottom rows.

DISCUSSION

SUI is a common condition that affects 50% of women over the age of 60 (Snooks et al., 1990; Augoulea et al., 2017). The primary risk factor for SUI is childbirth, during which the passage of the baby through the birth canal injures both the maternal PN and the muscle it innervates, the EUS, the muscle primarily

responsible for maintenance of urinary continence (Snooks et al., 1986, 1990). This creates a combinatorial neuromuscular injury in which nerve regeneration is impaired due to decreased upregulation of BDNF by the denervated EUS muscle (Pan et al., 2009; Gill et al., 2013b). MSCs and their secretome, or CCM, have been shown to improve regeneration in animal models of this dual neuromuscular injury (Deng et al., 2015;

Janssen et al., 2019). To determine if BDNF is the crucial factor responsible for improved functional recovery *via* CCM treatment, we hypothesized that BDNF is necessary to facilitate functional regeneration *via* secretome from MSCs.

MSCs transduced with a BDNF KD siRNA showed a reduction in BDNF concentration of 50% compared to scrambled CCM BDNF concentration. By selecting high BDNF MSCs to create CCM for comparison, we were able to generate a simple 3-point dose response relation in functional and anatomic outcomes to the dose of BDNF in CCM. The concentration of BDNF in these three different CCM preparations were all significantly different from each other. It is worth noting that lentivirus transduction did not impair the differentiation capabilities of these rat bone marrow derived MSCs.

The differences in LPP between sham injury and injury + CM groups are similar to previously reported values, validating the dual injury model in this study (Deng et al., 2015; Jiang et al., 2018). LPP of the injury + scrambled CCM group was not significantly different from that of the sham injury or injury + CM groups. These results are similar to results presented by Deng et al. (2015) and Janssen et al. (2019) using unmanipulated CCM from rat bone marrow derived MSCs, indicating that lentivirus transduction did not impair the regenerative properties of MSC CCM. Injury + BDNF KD CCM significantly decreased LPP compared to the sham injury and injury + high BDNF CCM groups, demonstrating that BDNF is important to regeneration of the neuromuscular continence mechanism. This is supported by the outcome of our study that LPP of injury + Scrambled CCM was not significantly different from that of sham injury + CM, while LPP of injury + BDNF KD CCM was significantly decreased compared to the sham injury + CM group. This result is similar to prior work with MSCs that over-expressed proteins for angiogenesis or MSC survival given in myocardial infarction models, which found that over-expression of these proteins improved angiogenesis and regeneration (Alfaro and Young, 2012).

LPP is a global measure of the continence mechanism with several other factors contributing to urethral resistance (Jiang et al., 2011). This explains why BDNF KD CCM treatment did not result in significant differences in LPP from scrambled CCM treatment since other factors, e.g., urethral smooth muscles, could compensate for impaired EUS function (Jiang et al., 2011). This result is comparable to a study in which the BDNF regenerative pathway was inhibited after PNC, in which LPP did not change significantly but PN motor branch recordings were significantly affected by BDNF inhibition (Balog et al., 2020).

In the current study, we demonstrated that a 50% decrease in BDNF levels of MSC CCM is sufficient to slow the recovery of the neuromuscular continence mechanism. A greater decrease in CCM BDNF levels may have produced a greater reduction in LPP. Nonetheless, this study demonstrated that decreased BDNF in CCM reduced LPP 3 weeks after the injury.

LPP was the primary outcome for the study, and the study was powered for significant differences in that outcome. As a result, too few animals were studied to power a significant difference in EUS EMG outcomes, due to greater variability in these secondary outcomes. These results are similar to the study by Deng et al.,

which did not show a significant difference in EUS EMG between sham injury and injury + CM (Deng et al., 2015).

We showed a significant difference in PN amplitude and firing rate increase with clitoral brushing between sham injury and injury + CM, validating the dual neuromuscular injury model (Deng et al., 2019). Additionally, CCM treated groups did not have a significantly decreased firing rate compared to sham injured animals, indicating that CCM treatment facilitated axonal regeneration at least partially. While BDNF is important to sensory nerve regeneration, it is essential to motor nerve regeneration, which could explain why no PN sensory branch amplitude differences were observed between the CCM treated groups, while differences were observed between groups in LPP (Geremia et al., 2007; Balog et al., 2020). A limitation of the study is that we did not test pudendal motor branch function. However, we did investigate anatomical reinnervation of EUS NMJs by pudendal motoneurons.

NMJ staining showed healthier NMJs in all CCM treated groups compared to the injury + CM group, similar to previous publications indicating that EUS regeneration was facilitated by factors in the CCM involved in muscle regeneration (Janssen et al., 2019). These results were expected since we did not knock down other CCM components in this experiment. It is likely that by accelerating the regeneration of the EUS, this muscle began producing BDNF to facilitate PN regeneration. Animals in the injury + scrambled CCM and injury + high BDNF CCM groups showed more innervated NMJs than the injury + BDNF KD CCM group, indicating that BDNF was important for reinnervation of NMJs. Additionally, BDNF is not the only neurotrophin present in CCM that could have facilitated the regeneration of nerves, explaining axons present in the BDNF KD CCM group (Crigler et al., 2006; Oskowitz et al., 2011). However, the BDNF KD CCM group demonstrated fewer axons in PN immunofluorescence, similar to the injury + CM group, which could explain the decrease observed in LPP of the injury + BDNF KD CCM group. Martins et al. showed a decrease in axonal elongation and growth rate in neuron cell culture given CCM depleted of BDNF (~25% decrease in BDNF concentration) compared to cells given normal CCM, supporting our finding that BDNF KD CCM treatment reduced axon density (Martins et al., 2017).

One limitation of this study includes not treating rats with exogenous BDNF to determine if the effects seen are due to the BDNF alone. Previous cell culture experiments treated with MSC equivalent BDNF concentration did not see the desired effect (Martins et al., 2017). The fact that MSC levels of BDNF are much lower than the needed amount of exogenous BDNF to induce fiber elongation suggests that BDNF was not solely responsible for fiber elongation (Martins et al., 2017). Additionally, we do not report proteomic analysis of the unmanipulated, BDNF KD, or scrambled CCM to determine if there were any other changes in the CCM due to the transduction or changes in BDNF levels. However, the MSC phenotype was not affected by transduction or the changes in BDNF levels, suggesting that changes, if any, were not substantial. Another limitation is that we did not test multiple time points after injury to determine the time course of recovery or study if the EUS would increase its

BDNF secretion due to the injury and treatments. In addition, quantitative histology may have added to the study but was out of the scope of the project.

Nonetheless, this study supports the theory of SUI, that BDNF is an important factor in the recovery of the neuromuscular continence mechanism (Snooks et al., 1984, 1986; Swash, 1990; Gray, 2004). Gill et al. (2013a) showed that administration of BDNF accelerated LPP recovery, supporting the results of this study. Furthermore, BDNF has been shown to be important to PN recovery since inhibiting the BDNF regenerative pathway delays functional recovery of the PN motor branch, suggesting that the decreased BDNF could result in impaired PN motor branch regeneration (Balog et al., 2020). Electrical stimulation of the PN has been shown to accelerate recovery of the continence mechanism *via* a BDNF-mediated mechanism (Jiang et al., 2018; Balog et al., 2021). The results from this study with that of the studies mentioned above, support the hypothesis that upregulation of BDNF is key for recovery from a combinatorial neuromuscular injury, in childbirth and in other neuromuscular injuries.

CONCLUSION

This study demonstrates that BDNF is an important contributor, but not the only factor in CCM that accelerates neuroregeneration and recovery from a dual muscle and nerve injury. Since the dose of BDNF in CCM is lower than that of exogenous BDNF, other factors in CCM also play an important role in injury repair and recovery from neuromuscular injuries. CCM may therefore provide a regenerative therapy after childbirth and other neuromuscular injuries.

DATA AVAILABILITY STATEMENT

The datasets presented in this article are not readily available because the work was funded by the Department of Veteran's Affairs and the research was conducted at the Louis Stokes

Veteran's Affairs Medical Center and is covered under the Freedom of Information Act. Any request for information must be sent to the Department of Veteran's Affairs and all requests will be honored. Requests to access the datasets should be directed to website: <https://www.va.gov/foia/> email: vacofoiase@va.gov.

ETHICS STATEMENT

The animal study was reviewed and approved by Louis Stokes Cleveland Veterans Affairs Medical Center Institutional Animal Care and Use Committee.

AUTHOR CONTRIBUTIONS

XY: participated in study design, conducting the experiment, statistical analyses, and drafting the manuscript. BB: carried out statistical analyses and drafting the manuscript. DL: participated in conducting the experiment and analyzing the data. BH: participated in conducting the experiment, carrying out statistical analyses, and drafting the manuscript. MK: participated in conducting the experiment and drafting the manuscript. HY: participated in conducting the experiment. SM: participated in analyzing the data and interpretation of results. MD: participated in study design, supervision of training and experiments, interpretation of data, and drafting the manuscript. All authors contributed to the article and approved the submitted version.

FUNDING

This project was supported in part by Dept. of Veterans Affairs RR&D Merit Review A1262R and 1 IK6 RX003843, VA Senior Research Career Scientist Award to MD. This project was also supported in part by Cleveland Clinic Lerner Research Institute.

REFERENCES

- Abrams, P., Cardozo, L., Fall, M., Griffiths, D., Rosier, P., Ulmsten, U., et al. (2002). The standardisation of terminology of lower urinary tract function: report from the standardisation sub-committee of the international continence society. *Neurourol. Urodyn.* 21, 167–178. doi: 10.1002/nau.10052
- Alfaro, M. P., and Young, P. P. (2012). Lessons from genetically altered mesenchymal stem cells (MSCs): candidates for improved MSC-directed myocardial repair. *Cell Transplant.* 21, 1065–1074. doi: 10.3727/096368911X612477
- Augoulea, A., Sioutis, D., Rizos, D., Panoulis, C., Triantafyllou, N., Armeni, E., et al. (2017). Stress urinary incontinence and endogenous sex steroids in postmenopausal women. *Neurourol. Urodyn.* 36, 121–125. doi: 10.1002/nau.22885
- Balog, B. M., Askew, T., Lin, D. L., Kuang, M., Hanzlicek, B., and Damaser, M. S. (2020). The pudendal nerve motor branch regenerates *via* a brain derived neurotrophic factor mediated mechanism. *Exp. Neurol.* 334:113438. doi: 10.1016/j.expneurol.2020.113438
- Balog, B. M., Deng, K., Askew, T., Kuang, M., Hanzlicek, B., and Damaser, M. S. (2021). Brain derived neurotrophic factor mediates accelerated recovery of regenerative electrical stimulation in an animal model of stress urinary incontinence. *Exp. Neurol.* 343:113781. doi: 10.1016/j.expneurol.2021.113781
- Barzilay, R., Sadan, O., Melamed, E., and Offen, D. (2009). Comparative characterization of bone marrow-derived mesenchymal stromal cells from four different rat strains. *Cytotherapy* 11, 435–442. doi: 10.1080/14653240902849796
- Cannon, T. W., and Damaser, M. S. (2001). Effects of anesthesia on cystometry and leak point pressure of the female rat. *Life Sci.* 69, 1193–1202. doi: 10.1016/s0024-3205(01)01182-1
- Chan, K. M., Gordon, T., Zochodne, D. W., and Power, H. A. (2014). Improving peripheral nerve regeneration: from molecular mechanisms to potential therapeutic targets. *Exp. Neurol.* 261, 826–835. doi: 10.1016/j.expneurol.2014.09.006
- Crigler, L., Robey, R. C., Asawachaicharn, A., Gaupp, D., and Phinney, D. G. (2006). Human mesenchymal stem cell subpopulations express a variety of neuro-regulatory molecules and promote neuronal cell survival and neuritogenesis. *Exp. Neurol.* 198, 54–64. doi: 10.1016/j.expneurol.2005.10.029
- Daly, D., Clarke, M., and Begley, C. (2018). Urinary incontinence in nulliparous women before and during pregnancy: prevalence, incidence, type and risk factors. *Int. Urogynecol. J.* 29, 353–362. doi: 10.1007/s00192-018-3554-1
- Delancey, J. O. L., Trowbridge, E. R., Miller, J. M., Morgan, D. M., Guire, K., Fenner, D. E., et al. (2008). Stress urinary incontinence: relative importance of urethral support and urethral closure pressure. *J. Urol.* 179, 2286–2290. doi: 10.1016/j.juro.2008.01.098

- Deng, K., Balog, B. M., Lin, D. L., Hanzlicek, B., Song, Q. X., Zhu, H., et al. (2019). Daily bilateral pudendal nerve electrical stimulation improves recovery from stress urinary incontinence. *Interface Focus* 9:20190020. doi: 10.1098/rsfs.2019.0020
- Deng, K., Lin, D. L., Hanzlicek, B., Balog, B. M., Penn, M. S., Kiedrowski, M. J., et al. (2015). Mesenchymal stem cells and their secretome partially restore nerve and urethral function in a dual muscle and nerve injury stress urinary incontinence model. *Am. J. Physiol. Renal Physiol.* 308, F92–F100. doi: 10.1152/ajprenal.00510.2014
- Dissarajan, C., Cruz, M. A., Kiedrowski, M. J., Balog, B. M., Gill, B. C., Penn, M. S., et al. (2014). Rat mesenchymal stem cell secretome promotes elastogenesis and facilitates recovery from simulated childbirth injury. *Cell Transplant.* 23, 1395–1406. doi: 10.3727/096368913X670921
- Eftekhari, T., Hajibarat, B., Ramezanzadeh, F., and Shariat, M. (2006). Postpartum evaluation of stress urinary incontinence among primiparas. *Int. J. Gynaecol. Obstet.* 94, 114–118. doi: 10.1016/j.ijgo.2006.04.042
- Geremia, N. M., Gordon, T., Brushart, T. M., Al-Majed, A. A., and Verge, V. M. K. (2007). Electrical stimulation promotes sensory neuron regeneration and growth-associated gene expression. *Exp. Neurol.* 205, 347–359. doi: 10.1016/j.expneurol.2007.01.040
- Gill, B. C., Balog, B. M., Dissarajan, C., Jiang, H. H., Steward, J. B., Lin, D. L., et al. (2013a). Neurotrophin therapy improves recovery of the neuromuscular continence mechanism following simulated birth injury in rats. *Neurol. Urodyn.* 32, 82–87. doi: 10.1002/nau.22264
- Gill, B. C., Damaser, M. S., Vasavada, S. P., and Goldman, H. B. (2013b). Stress incontinence in the era of regenerative medicine: reviewing the importance of the pudendal nerve. *J. Urol.* 190, 22–28. doi: 10.1016/j.juro.2013.01.082
- Gray, M. (2004). Stress urinary incontinence in women. *J. Am. Acad. Nurse Pract.* 16, 188–197. doi: 10.1111/j.1745-7599.2004.tb00441.x
- Janssen, K., Lin, D. L., Hanzlicek, B., Deng, K., Balog, B. M., van der Vaart, C. H., et al. (2019). Multiple doses of stem cells maintain urethral function in a model of neuromuscular injury resulting in stress urinary incontinence. *Am. J. Physiol. Renal Physiol.* 317, F1047–F1057. doi: 10.1152/ajprenal.00173.2019
- Jiang, H.-H., Gill, B. C., Dissarajan, C., Zutshi, M., Balog, B. M., Lin, D., et al. (2013). Effects of acute selective pudendal nerve electrical stimulation after simulated childbirth injury. *Am. J. Physiol. Renal Physiol.* 304, F239–F247. doi: 10.1152/ajprenal.00235.2012
- Jiang, H.-H., Pan, H. Q., Gustilo-Ashby, M. A., Gill, B., Glaab, J., Zaszczurynski, P., et al. (2009a). Dual simulated childbirth injuries result in slowed recovery of pudendal nerve and urethral function. *Neurol. Urodyn.* 28, 229–235. doi: 10.1002/nau.20632
- Jiang, H.-H., Gustilo-Ashby, M. A., Salcedo, L. B., Pan, H. Q., Sybert, D. F., Butler, R. S., et al. (2009b). Electrophysiological function during voiding after simulated childbirth injuries. *Exp. Neurol.* 215, 342–348. doi: 10.1016/j.expneurol.2008.10.024
- Jiang, H.-H., Salcedo, L. B., and Damaser, M. S. (2011). Quantification of neurological and other contributors to continence in female rats. *Brain Res.* 1382, 198–205. doi: 10.1016/j.brainres.2011.01.094
- Jiang, H.-H., Song, Q. I., Gill, B. C., Balog, B. M., Juarez, R., Cruz, Y., et al. (2018). Electrical stimulation of the pudendal nerve promotes neuroregeneration and functional recovery from stress urinary incontinence in a rat model. *Am. J. Physiol. Renal Physiol.* 315, F1555–F1564. doi: 10.1152/ajprenal.00431.2017
- Karsy, M., Watkins, R., Jensen, M. R., Guan, J., Brock, A. A., and Mahan, M. A. (2019). Trends and cost analysis of upper extremity nerve injury using the national (nationwide) inpatient sample. *World Neurosurg.* 123, e488–e500. doi: 10.1016/j.wneu.2018.11.192
- Martins, L. F., Costa, R. O., Pedro, J. R., Aguiar, P., Se, S. C., and Fabio, G. (2017). Mesenchymal stem cells secretome-induced axonal outgrowth is mediated by BDNF. *Sci. Rep.* 7:4153. doi: 10.1038/s41598-017-03592-1
- Meyer, S., de Grandi, P., Kuntzer, T., Hurlimann, P., and Schmidt, N. (1993). Birth trauma: its effect on the urine continence mechanisms. *Gynakol. Geburtshilfliche Rundsch.* 33, 236–242. doi: 10.1159/000272115
- Mias, C., Lairez, O., Trouche, E., Roncalli, J., Calise, D., Seguelas, M. H., et al. (2009). Mesenchymal stem cells promote matrix metalloproteinase secretion by cardiac fibroblasts and reduce cardiac ventricular fibrosis after myocardial infarction. *Stem Cells* 27, 2734–2743. doi: 10.1002/stem.169
- Ng, K., Cheung, R. Y., Lee, L. L., Chung, T. K., and Chan, S. S. (2017). An observational follow-up study on pelvic floor disorders to 3–5 years after delivery. *Int. Urogynecol. J.* 28, 1393–1399. doi: 10.1007/s00192-017-3281-z
- Noble, J., Munro, C. A., Prasad, V. S., and Midha, R. (1998). Analysis of upper and lower extremity peripheral nerve injuries in a population of patients with multiple injuries. *J. Trauma* 45, 116–122. doi: 10.1097/00005373-199807000-00025
- Oskowitz, A., McFerrin, H., Gutschow, M., Carter, M. L., and Pochampally, R. (2011). Serum-deprived human multipotent mesenchymal stromal cells (MSCs) are highly angiogenic. *Stem Cell Res.* 6, 215–225. doi: 10.1016/j.scr.2011.01.004
- Pan, H. Q., Kerns, J. M., Lin, D. L., Sybert, D., Steward, J., Hoover, C. R. V., et al. (2009). Dual simulated childbirth injury delays anatomic recovery. *Am. J. Physiol. Renal Physiol.* 296, F277–F283. doi: 10.1152/ajprenal.90602.2008
- Penn, M. S. (2012). Are stem cells the teacher or the student? *Curr. Opin. Organ Transplant.* 17, 663–669. doi: 10.1097/MOT.0b013e32835a5aad
- Peter, S., Evans, C., Ow, S. Y., Scutt, A. M., Wright, P. C., and Biggs, C. A. (2012). Proteomic analysis of the impact of static culturing on the expansion of rat bone marrow mesenchymal stem cells. *Biotechnol. Lett.* 34, 1589–1596. doi: 10.1007/s10529-012-0935-2
- Salam, R. A., Mansoor, T., Mallick, D., Lassi, Z. S., Das, J. K., and Bhutta, Z. A. (2014). Essential childbirth and postnatal interventions for improved maternal and neonatal health. *Reprod. Health* 11:S3. doi: 10.1186/1742-4755-11-S1-S3
- Snooks, S. J., Barnes, P. R., and Swash, M. (1984). Damage to the innervation of the voluntary anal and periurethral sphincter musculature in incontinence: an electrophysiological study. *J. Neurol. Neurosurg. Psychiatry* 47, 1269–1273. doi: 10.1136/jnnp.47.12.1269
- Snooks, S. J., Swash, M., Henry, M. M., and Setchell, M. (1986). Risk factors in childbirth causing damage to the pelvic floor innervation. *Int. J. Colorectal Dis.* 1, 20–24. doi: 10.1007/BF01648831
- Snooks, S. J., Swash, M., Mathers, S. E., and Henry, M. M. (1990). Effect of vaginal delivery on the pelvic floor: a 5-year follow-up. *Br. J. Surg.* 77, 1358–1360. doi: 10.1002/bjs.1800771213
- Swash, M. (1990). The neurogenic hypothesis of stress incontinence. *Ciba Found. Symp.* 151, 156–170. doi: 10.1002/9780470513941.ch9
- Taylor, C. A., Braza, D., Rice, J. B., and Dillingham, T. (2008). The incidence of peripheral nerve injury in extremity trauma. *Am. J. Phys. Med. Rehabil.* 87, 381–385. doi: 10.1097/PHM.0b013e31815e6370
- Tran, C., and Damaser, M. S. (2015). Stem cells as drug delivery methods: application of stem cell secretome for regeneration. *Adv. Drug Deliv. Rev.* 82–83, 1–11. doi: 10.1016/j.addr.2014.10.007
- Zhang, M., Mal, N., Kiedrowski, M., Chacko, M., Askari, A. T., Popovic, Z. B., et al. (2007). SDF-1 expression by mesenchymal stem cells results in trophic support of cardiac myocytes after myocardial infarction. *FASEB J.* 21, 3197–3207. doi: 10.1096/fj.06-6558com

Conflict of Interest: MD has an issued patent on MSC CCM treatment for genitourinary disorders, which is currently optioned for licensing. This study was performed with grant funding prior to optioning the intellectual property and involved no corporate input or influence.

The remaining authors declare that the research was conducted in the absence of any commercial or financial relationships that could be construed as a potential conflict of interest.

Publisher's Note: All claims expressed in this article are solely those of the authors and do not necessarily represent those of their affiliated organizations, or those of the publisher, the editors and the reviewers. Any product that may be evaluated in this article, or claim that may be made by its manufacturer, is not guaranteed or endorsed by the publisher.

Copyright © 2022 Yuan, Balog, Lin, Hanzlicek, Kuang, Yan, Majerus and Damaser. This is an open-access article distributed under the terms of the Creative Commons Attribution License (CC BY). The use, distribution or reproduction in other forums is permitted, provided the original author(s) and the copyright owner(s) are credited and that the original publication in this journal is cited, in accordance with accepted academic practice. No use, distribution or reproduction is permitted which does not comply with these terms.



OPEN ACCESS

EDITED BY
Yongjun Wang,
Nantong University, China

REVIEWED BY
Sheng Yi,
Nantong University, China
Kirsten Haastert-Talini,
Hannover Medical School, Germany

*CORRESPONDENCE
Jared S. Bushman
jbushman@uwyo.edu

SPECIALTY SECTION
This article was submitted to
Cellular Neuropathology,
a section of the journal
Frontiers in Cellular Neuroscience

RECEIVED 27 September 2022
ACCEPTED 28 October 2022
PUBLISHED 14 November 2022

CITATION
Allgood JE, Roballo KCS, Sparks BB
and Bushman JS (2022) The effects
of graft source and orientation on
outcomes after ablation of a
branched peripheral nerve.
Front. Cell. Neurosci. 16:1055490.
doi: 10.3389/fncel.2022.1055490

COPYRIGHT
© 2022 Allgood, Roballo, Sparks and
Bushman. This is an open-access
article distributed under the terms of
the [Creative Commons Attribution
License \(CC BY\)](#). The use, distribution
or reproduction in other forums is
permitted, provided the original
author(s) and the copyright owner(s)
are credited and that the original
publication in this journal is cited, in
accordance with accepted academic
practice. No use, distribution or
reproduction is permitted which does
not comply with these terms.

The effects of graft source and orientation on outcomes after ablation of a branched peripheral nerve

JuliAnne E. Allgood, Kelly C. Santos Roballo,
Bridger B. Sparks and Jared S. Bushman*

Division of Pharmaceutical Sciences, University of Wyoming, Laramie, WY, United States

Segmental peripheral nerve injuries (PNI) are the most common cause of enduring nervous system dysfunction. The peripheral nervous system (PNS) has an extensive and highly branching organization. While much is known about the factors that affect regeneration through sharp bisections and linear ablations of peripheral nerves, very little has been investigated or documented about PNIs that ablate branch points. Such injuries present additional complexity compared to linear segmental defects. This study compared outcomes following ablation of a branch point with branched grafts, specifically examining how graft source and orientation of the branched graft contributed to regeneration. The model system was Lewis rats that underwent a 2.5 cm ablation that started in the sciatic nerve trunk and included the peroneal/tibial branch point. Rats received grafts that were rat sciatic autograft, inbred sciatic allograft, and inbred femoral allograft, each of which was a branched graft of 2.5 cm. Allografts were obtained from Lewis rats, which is an inbred strain. Both branches of the sciatic grafts were mixed motor and sensory while the femoral grafts were smaller in diameter than sciatic grafts and one branch of the femoral graft is sensory and the other motor. All branched grafts were sutured into the defect in two orientations dictated by which branch in the graft was sutured to the tibial vs peroneal stumps in recipients. Outcome measures include compound muscle action potentials (CMAPs) and CatWalk gait analysis throughout the recovery period, with toluidine blue for intrinsic nerve morphometry and retrograde labeling conducted at the 36-week experimental end point. Results indicate that graft source and orientation does play a significant role earlier in the regenerative process but by 36 weeks all groups showed very similar indications of regeneration across multiple outcomes.

KEYWORDS

branched peripheral nerve injury, nerve allograft, immunogenicity, functional outcomes, retrograde labeling

Introduction

Damage to the peripheral nervous system (PNS) is common, with hundreds of thousands of new peripheral nerve injuries (PNIs) occurring in the United States (PNI) each year (Liu et al., 2012; Catala and Kubis, 2013). The most common causes of PNIs are motor vehicle accidents or violent trauma (Pan et al., 2020). Recovery is often slow and incomplete for even simple lacerations (Wang et al., 2019). Outcomes are worse for injuries that ablate sections of the nerves (segmental ablations) and if the PNI is long distances from the innervation target tissues (Cinteza et al., 2015). Permanent disability is common.

One of the reasons that PNIs greater distances from innervation tissues have poorer outcomes is the increasing number of branch points likely to be distal to the injury; there are approximately 80 km of peripheral nerves throughout a human body in an extensively branching organization (Catala and Kubis, 2013). When regenerating axons reach a branch point, the leading axons can sample pathways and appear to initially regenerate randomly into either branch (Madison et al., 1996; Brushhart et al., 1998; Witzel et al., 2005). This dilutes the regenerative effect due to pruning and functional irrelevance of motor neurons that misroute into sensory branches and increases the likelihood that axons do not regenerate to the same target tissue they innervated prior to injury (Brushhart, 1993; Witzel et al., 2005). Plasticity of the central and peripheral nervous systems to compensate for innervation changes is considerable, but is not unlimited (Navarro, 2009).

Unlike linear segmental PNIs that have been extensively studied and addressed with a variety of highly compared techniques and technologies (i.e., autografts, acellular nerve allografts (ANAs), conduits/wraps etc.) (Jones et al., 2016; Safa and Buncke, 2016), very little has been documented for PNIs that ablate a branch point. The process of regeneration at branch points has primarily been investigated in the context of what occurs following segmental or sharp laceration PNIs proximal to branch points, primarily with the rodent femoral nerve model (Irintchev, 2011). The posterior division of the femoral nerve divides into a sensory saphenous branch and a motor branch that innervates the quadriceps muscle, making this a useful model because retrograde labeling can be used to quantify misrouting of regenerating axons (Irintchev, 2011).

Data from these proximal PNIs to the femoral revealed the process of preferential motor reinnervation; where motor neurons are more likely to regenerate into the motor branch and avoid the sensory branch (Brushhart et al., 1998). Preferential motor reinnervation has been attributed to biological cues both within the motor branch as well as cues initiated when the first motor neurons to innervate a distal muscle trigger a process that attracts more slowly regenerating motor neurons down the same path (Brushhart, 1988; Martini et al., 1992). This process reduces the number of motor neurons that regenerate into the sensory branch in the femoral nerve after injury (Madison et al., 2007). It

has been recently observed that sensory axons inhibit extension of motor neuron axons in 3-dimensional organotypic cultures *in vitro* (Brushhart et al., 2020). If this effect is confirmed *in vivo*, it would further support that regeneration of motor neurons at sensorimotor branch points, such as the posterior femoral nerve, is dependent upon both positive and negative cues.

Despite these seminal studies showing the importance of pathfinding of regenerating axons at branch points and the known branching complexity of the PNS, studies on ablated branch points are lacking. Anatomically, ablated branch points present additional complexity simply because there is an increased number of nerve stumps to surgically manage. The lack of comparatively validated methods to manage ablated branch points creates additional uncertainty in the clinical management of these injuries. For example, the attempting to direct regeneration across a branched ablation creates the risk to misdirect a disproportionate number of axons into any of the distal branches. This would potentially leave other branches with too few regenerating axons to mediate function. Disproportionate axonal regeneration at branch points is also a possibility for PNIs to linear segments proximal to branch points, but this would not be a controllable variable in such cases.

We have previously investigated branched ablation PNIs from the perspective that a live nerve graft that matches the anatomy of the defect site would likely be a successful bridging material. Because autografts would not be commonly available for ablated branch points, we investigated the use of live (not decellularized) allografts and developed methods of localized immune suppression to avoid the need for systemic immune suppression (Santos Roballo et al., 2019). Immunosuppression is necessary with mismatched donors and recipients to prevent rejection of the nerve allografts (Siemionow and Sonmez, 2007; Roballo et al., 2022). The model in these previous studies was a 2.0 branched ablation of the sciatic nerve in Lewis rats that included the peroneal/tibial branch point. This defect that bridged with live allografts obtained from major histocompatibility mismatched Sprague Dawley donors (Hurt et al., 2004). 2.0 cm branched autografts, consisting of the same segment cut out and re-sutured into the defect in Lewis rats, were conducted as a control group. Data indicated robust regeneration occurred for autografts and allografts with localized immune suppression into both the tibial and peroneal branches.

Successful regeneration down both branches in this branched ablation PNI model allows for the investigation of more fundamental concepts explored in this report. Specifically, experiments sought to determine how graft source and orientation would affect the regenerative process after a branched ablation PNI of the sciatic nerve. The experimental model is a 2.5 cm ablation of the sciatic nerve that included the tibial and peroneal branch point in rats. A 2.5 cm sciatic or femoral branched graft was sutured into the defect in two

orientations; one where the tibial and motor branches of the sciatic and femoral grafts, respectively, were sutured to the tibial stump in the defect and the peroneal and saphenous branches of the grafts, respectively, sutured to the peroneal stump. The other was a switched orientation where the tibial and motor branches of the sciatic and femoral grafts were respectively sutured to the peroneal stumps and the peroneal and saphenous branches sutured to the tibial stumps. Experiments were conducted with inbred Lewis donors and recipient rats to avoid the need for immune suppression and this potential source of variability (Avramut and Achim, 2003).

Experiments were carried out to 36 weeks and outcome measures included compound muscle action potentials (CMAPs) to distal muscle innervation targets of the tibial and peroneal nerves, CatWalk gait analysis, nerve morphometry from toluidine blue sections of each graft branch and retrograde labeling. Results indicated that the graft source and orientation initially caused some significant differences in CMAPs and CatWalk but that these differences became less evident by the study end point of 36 weeks. Nerve morphometry suggested axon regeneration was robust down both branched with all grafts, with some differences and trends according to graft type and orientation. Retrograde labeling showed that motor axons were more abundant than sensory axons in all groups but switching the orientation of the branches increased the number of sensory axons in the distal peroneal branch compared to the distal tibial branch. Together, this data suggests that regeneration following branched ablation PNI of the sciatic nerve can be reliably achieved with grafts that differ in their size and sensorimotor complexity.

Materials and methods

Animal acquisition and care

Animals for this study were acquired, cared for, and used in accordance with the NIH Guide for the Care and Use of Laboratory Animals under protocols approved by the University of Wyoming IACUC. Rats were housed at ambient temperature with stable humidity on a 12-h day-night cycle and free access to food and water. Lewis and Sprague-Dawley (SD) rats were obtained from Charles River Laboratories, Wilmington, MA, USA. Animals were housed individually from the beginning of CatWalk training. A total of 39 Lewis rats were randomly assigned to one of six surgical groups ($n = 6$) or an uninjured control group ($n = 3$). One rat in the sciatic autograft group developed an ovarian tumor that hindered its ability to walk and was sacrificed at 28 weeks post operatively (PO). Data for this rat was removed from analysis, leaving the Lewis sciatic autograft group with $n = 5$ animals. A total of 12 SD rats were randomly assigned to the sciatic autograft group ($n = 6$) or the sciatic allograft group ($n = 6$). Two rats from the SD sciatic allograft

group had unreparable autophagy and were sacrificed 1 week PO. Data for these rats was removed from analysis leaving the SD sciatic allograft group with $n = 4$ animals.

Harvest and storage of allografts

Male Lewis rats were used as donors to obtain inbred allografts in Lewis-to-Lewis. Male Sprague Dawley rats were used as donors in the outbred Sprague Dawley to Sprague Dawley experiments. Rats were sacrificed by isoflurane overdose followed by cervical dislocation. After euthanasia, both the right and left sciatic and femoral nerves were harvested, carefully stripped of connective tissue, and stored in $1\times$ PBS on ice for between 1 and 5 h prior to implantation.

Surgical procedure and post-operative care

Surgery and post-operative care was as previously described (Santos Roballo et al., 2019). Briefly, female Lewis rats weighing an average of 219 ± 13 g were anesthetized with 2% inhaled isoflurane, their left hind limb shaved, and the incision site sterilized with $3\times$ wipes with betadine (VWR, BDH7207-4) and 100% isopropyl alcohol (Sam's West, 645081). Vaseline was placed over the eyes to prevent drying, and rats were administered 2 mg/kg bupivacaine (VetOne, 510212) subcutaneously at the incision site and 5 mg/kg Baytril (Bayer, 84744158) and 0.03 mg/kg buprenorphine (PAR pharmaceuticals, 42023-179-05) subcutaneously in the opposite hind limb. Rats were placed on a 38°C circulating water temperature-controlled surface, with toe pinch used to confirm sufficient anesthesia, and the surgical site draped with sterile pads. Using sterile no-touch technique, a ~ 3 cm incision was made to the skin above the femur and the fascia between the gluteus superficialis and biceps femoris were gently separated to expose the sciatic nerve. A 2.5 cm section of the sciatic nerve was removed beginning ~ 1 mm distal to the external obturator tendon and extending distally, which was 1 cm or more past the peroneal-tibial branch point. Grafts were trimmed to 2.5 cm and implanted with 9-0 sutures (esutures, AA-2628). Musculature and skin were closed with 6-0 sutures (esutures, A697N) and animals were allowed to recover on the heated surface before being placed into individual cages. Experiments with Sprague Dawley rats used the same procedure, but had 2.0 cm defects and grafts implanted instead of 2.5 cm.

For post-operative care, rats received 0.03 mg/kg buprenorphine twice daily subcutaneously for 3 days after surgery and one dose of 5 mg/kg Baytril subcutaneously for 7 days after surgery. Animals were monitored at least twice per day for signs of distress or autophagy for the first 7 days and at least once per day thereafter. Six of the recipient Lewis rats

were found to have disrupted the sutures in their skin within 4 days of surgery but without any tissue autophagy or autotomy. After resuturing when required, these rats were fitted with Elizabethan collars (Kent Scientific, EC404VS) until 10 days after surgery and remained in the study.

Gait analysis

The Noldus Catwalk XT system was used to evaluate behavioral recovery following sciatic nerve injury as we previously described (Osimanjiang et al., 2022). Briefly, animals were placed on one end of an open-ended tunnel with overhead red-light illumination and green light walkway illumination (0.12 intensity). Animals were acclimated and conditioned to the system for four weeks prior to surgery. Baseline data was collected when animals voluntarily ran three times across the platform in compliance with the set parameters, 60% or less speed variation and less than 15 s duration, while a camera fixed at 42 cm below the platform recorded foot placement. Lewis rats ran the CatWalk for data collection every two weeks for 36 weeks with each animal requiring a minimum of three compliant runs per trial. Data was auto classified by the CatWalk software and a follow-up performed by individuals blinded to experimental groups to correct any misidentified steps. The cadence in steps/second, max contact mean intensity, and right front (RF)/Left Hind (LH) coupling were calculated using the CatWalk software after classification was complete. Additionally, toe spread, print length, and intermediate toe spread were also manually measured according to previously published protocols for all left hind feet to allow for the CatWalk software to calculate sciatic functional index (SFI) (De Medinaceli et al., 1984; Bozkurt et al., 2011; Isvoranu et al., 2021).

Electrophysiology

Recovery down each sciatic nerve branch was assessed with electrophysiological recordings from needle electrodes in the foot muscles innervated by the tibial and peroneal branches as previously described (Werdin et al., 2009; Roballo and Bushman, 2019; Santos Roballo et al., 2019). Using the Viking NCS EMG EP IOM System, Compound Muscle Action Potentials (CMAPs) were collected using five electrodes (Natus, 019-476600): ground, reference, recording, and an anode/cathode pair for stimulating the muscle. Placement of the ground and reference electrodes were subcutaneously placed on the lateral side of the 5th metatarsal running dorsal through the heel, and on the lateral side of the 5th metatarsal running to the anterior, respectively. Subcutaneously the recording electrode was inserted on the dorsal foot muscle between the 2nd and 3rd metatarsals for peroneal branch stimulation and on the plantar

muscle between the 2nd and 3rd metatarsal for stimulation of the tibial branch. Stimulation using the anode/cathode pair was done percutaneously at the ankle in the space between the tibia and calcaneal tendon. The top three highest amplitudes and top three lowest latencies were averaged and used for analysis at each time point for each animal. CMAPs recordings were taken prior to surgery and every 4 weeks post operatively (PO) for the duration of the 36-week study.

Retrograde labeling

Two days prior to euthanasia, animals were anesthetized with 2% isoflurane, the nerve exposed, and microinjection syringes fitted with Nanofil 36 G needles (World Precision Instruments, NF36BV-2) inserted under the epineurium. Cholera Toxin subunit B (CTb) was slowly injected into each branch. The tibial branch was injected with 4 μ l CTb conjugated with Alexa Fluor 488 (ThermoFisher, C22841) diluted 1:100 in 1 \times PBS (ThermoFisher, 14190235) and the peroneal branch was injected with 2–3 μ l CTb conjugated with Alexa Fluor 555 (ThermoFisher, C22843) diluted 1:100 in 1 \times PBS. Needles were left inserted into nerves for 60 s following injection. The muscle and skin were then sutured using 6-0 sutures, and the animals were allowed to recover on the heated pad. Animals were also administered 0.03 mg/kg buprenorphine twice daily until sacrifice.

Euthanasia and tissue collection

At the end point, animals were euthanized via perfusion with 4% paraformaldehyde (PFA) in 1 \times PBS (Cat. No. 14200075, Life Technologies). Briefly, animals were anesthetized via isoflurane, the chest cavity opened, and animals were intracardially perfused with 40 ml 0.9% saline (Intermountain life sciences, Z1377) followed by 25 ml of 4% PFA. After perfusion, the left sciatic nerve and the right and left gastrocnemius and tibialis anterior muscles were removed, weighed, and stored in 4% PFA. The spinal cord from T12 to L6 was removed and stored in 4% PFA for retrograde analysis.

Toluidine blue staining

2 mm of the distal most portions of the branches in the grafts were cut via scalpel for toluidine blue staining. Toluidine blue staining was performed for each branch according to the previously described protocol (Ghnenis et al., 2018). Each distal graft branch was put in 2% osmium tetroxide (Sigma-Aldrich, 75632) diluted 1:1 in Trump's fixative for 2 h. Nerve segments were then removed and placed in 1 \times PBS for 10 min to wash remaining osmium and Trump's. Nerve sections then

underwent dehydration using 30, 60, 90, and 100% acetone while the epoxy embedding medium (Sigma-Aldrich, 45359) was prepared. After the dehydration process, the nerves were acclimated to the epoxy using a 1:1 100% acetone:epoxy mixture for 30 min followed by a 1:2 100% acetone:epoxy mixture for another 30 min. Segments were then placed in molds (VWR, cat. no. 103302-482) and submerged in epoxy in a 60 °C oven overnight. Once polymerized an ultramicrotome fitted with a glass knife was used to cut the nerve into semithin sections before they were placed on glass slides. 1% toluidine blue (ThermoFisher, 348601000) was prepared and used to stain the sections for 30 seconds before washing. Slides were then cover slipped and prepared for imaging.

Cryosectioning

Spinal cords were removed from 4% PFA and stored in 30% sucrose solution in PBS (ThermoFisher, J65148.A1) overnight. Spinal cords were cut into smaller sections to allow for cross sectional cutting. Samples from between L3-L5, where the sciatic nerve enters the spinal cord, were embedded in Tissue-Tek® O.C.T. Compound, Sakura® Finetek (VWR, cat. no. 25608–930) and frozen at –20°C. 20 µm thick sections were cut on a cryostat and placed on Superfrost glass slides (VWR, 48311-703). Slides were then cover slipped using Fluoroshield (Sigma-Aldrich, cat. no. F6182-20ML) and allowed to dry at 4°C overnight.

Imaging and counting

Toluidine blue stained sciatic nerves were imaged using a Zeiss Axio Scan Z.1 which allowed for brightfield images of whole nerves (10× magnification), used for total nerve axon counts and axonal density, and high magnification images (60× magnification), required for axon diameter and G-ratio calculation. Qupath software was used to obtain total nerve axon counts and axonal density and ImageJ was used to obtain average axonal diameter and G-ratio measurements as described (Bankhead et al., 2017; Roballo and Bushman, 2019). Total axon counts were taken by manually marking each identifiable axon. Axonal density was obtained by manually counting each identifiable axon in a 20,000 µm² section of the nerve. Average axonal diameter was obtained by measuring the inner, unmyelinated, x and y diameter of a randomly selected subset of axons. G-ratio was calculated by dividing the axon diameter by the diameter of the axon plus the myelin sheath of a randomly selected subset of axons.

A Zeiss 980 inverted confocal microscope was used to obtain fluorescent images of retrograde labeled spinal cords. Whole spinal cord images were obtained at 10× using the tile function of the microscope. Higher magnification (20×) images were also

acquired in the ventral and dorsal horns. Qupath software was used to manually count all labeled neurons in the ventral and dorsal horns of the spinal cords. Labeled neurons were only counted if they were contained in the dorsal or ventral horn. The dorsal and ventral sides of the spinal cord were identified by locating the median fissure and anterior spinal artery as landmarks (Watson et al., 2009; Toossi et al., 2021). Dorsal and ventral horns were separated by identifying the lateral spinal nucleus and drawing lines slightly ventral to that point at approximately the division of the 5 and 6 laminae, according to Watson et al. (2009). Only clearly identifiable neurons outlined in stain were counted (Toossi et al., 2021). The number of dorsal horn labeled neurons were then divided by the number of ventral horn labeled neurons to obtain a ratio of dorsal horn (sensory) neurons to ventral horn (motor) neurons.

Statistical analysis

Rats were randomly sorted into experimental groups. Experimenters assessing sensorimotor and histological outcomes were blinded to the experimental groups during data collection. IBM SPSS software was used to run all statistical analysis. One-way repeated measures ANOVA with Tukey *post-hoc* analysis was performed for all Catwalk and CMAPs data. Two-way ANOVAs with Tukey *post-hoc* analysis were performed for all toluidine blue data. A Wilcoxon signed rank test was used to compare tibial and peroneal retrograde labeling data. Paired T tests were used to compare muscle wet weights in the left gastrocnemius group to the right gastrocnemius group and the left tibialis anterior to the right tibialis anterior group.

Results

Study design

This study was designed to determine how graft source and orientation influenced regeneration in a branched ablation PNI. 2.5 cm defects of the rat sciatic nerve were created that included the peroneal-tibial bifurcation. The sciatic nerve is a useful model as a result of its mixed sensory and motor nerve morphology in the trunk as well as the peroneal and tibial branches (Irintchev, 2011). For surgical groups, the 2.5 cm defect was bridged with sciatic autografts, inbred sciatic allografts (Figure 1A), or inbred femoral allografts (Figure 1B). Each graft type was tested in two orientations; an original orientation where the tibial and motor branches of sciatic and femoral grafts were sutured to the tibial stump and the peroneal and saphenous were sutured to the peroneal stump; or a switched orientation where the peroneal and saphenous branches in the sciatic and femoral grafts, respectively, were sutured to the tibial stump and the tibial

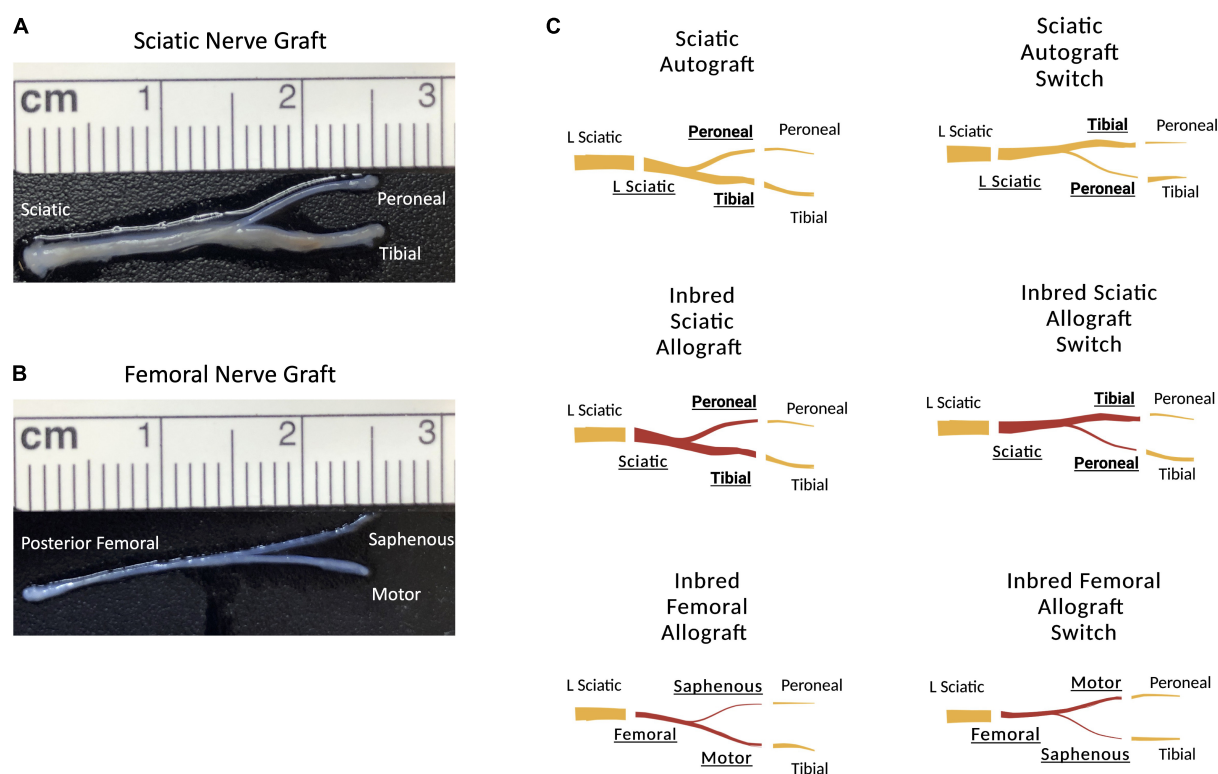


FIGURE 1

Schematic representation of the surgical groupings and graft types. (A) 2.5 cm sciatic nerve graft with peroneal and tibial branches. (B) 2.5 cm femoral nerve graft with saphenous and motor branches. (C) Schematic representation showing the orientation of the grafts. Original sciatic nerve orientation with the peroneal branch of the graft sutured to the distal peroneal site and the tibial branch of the graft sutured to the distal tibial site. The sciatic switch groups with the opposite, with the peroneal branch of the graft sutured to the distal tibial site and the tibial branch of the graft sutured to the distal peroneal site. Inbred sciatic allografts depicting the same orientations as shown for sciatic autografts. Inbred femoral allografts in the original orientation with the motor branch of the graft sutured to the distal tibial site and the saphenous branch of the graft sutured to the distal peroneal site. In the switched orientation, the motor branch of the graft was sutured to the distal peroneal site and the saphenous branch of the graft was sutured to the distal tibial site.

and motor branches of the grafts were sutured to the peroneal stump (Figure 1C). The femoral nerve graft is useful to explore what effect the distinct sensorimotor branch point in this graft would have on regeneration where both the distal branches are mixed (Irintchev, 2011). Both host and donor animals were inbred Lewis rats to minimize immunogenicity as no immunosuppressive treatment was administered.

At the initiation of the study, rats underwent 4 weeks of CatWalk acclimatization and training followed by sciatic nerve surgery with functional and behavioral assessments every 2- or 4-weeks PO (Figure 2). All animals started to show CMAPs and Catwalk recovery by 13 weeks PO. At the study endpoint of 36 weeks, retrograde labeling was performed, muscle wet weight was measured, and nerve cross sections were stained with toluidine blue and analyzed for morphometry of each branch within the graft (Figure 2). Due to the quantity of data gathered, results are shown comparing each graft type by orientation to facilitate analysis and interpretation. Comparisons of the same outcome measures between all groups were also made and can be seen in Supplementary Figures 2–4. Data indicated in the

tibial branch represents measures on the branch connected to the tibial stump irrespective of whether the nerve branch within the graft was tibial or peroneal of the sciatic branched grafts or saphenous or motor of the femoral branched grafts. Vis a versa for data for the peroneal branch.

Regeneration by orientation of sciatic autografts

The tibial and peroneal nerves are of significantly different sizes (Figure 1A) and switching the orientation of these branches causes incongruity of graft diameter during surgical coaptation. As graft diameter and autograft harvesting are common surgical considerations in treatment of segmental nerve injuries, experiments sought to determine if graft orientation (i.e., switching the branches) affected outcomes in the 2.5 cm branched ablation model.

Compound muscle action potential data showed that amplitudes increased in the peroneal branch of the sciatic nerve

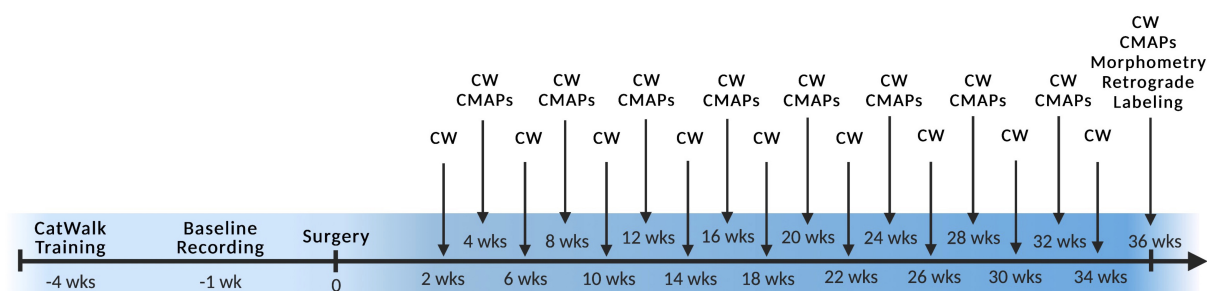


FIGURE 2

Experimental timeline. Surgery was performed at week 0 with preoperative training and baseline recordings labeled with negative numbers and all postoperative timepoints labeled with positive numbers. CW, Catwalk; CMAPs, compound muscle action potentials. $n = 5$ for sciatic autograft group, $n = 6$ for sciatic autograft, inbred sciatic autografts, and inbred femoral autografts groups.

in the switched orientation (2.03 ± 0.314 mV, 2.03 ± 0.206 mV) at many time points, significantly so at 16- and 28- weeks PO ($p = 0.03$, $p = 0.004$), respectively (Figure 3A). Latencies for the peroneal branch were also decreased in the autograft switch group (1.19 ± 0.072 ms, 1.26 ± 0.0879 ms, 1.32 ± 0.0891 ms) at many time points, significantly at 20-, 24- and 28-weeks PO, respectively ($p = 0.011$, $p = 0.024$, $p \leq 0.001$) (Figure 3B). Peroneal CMAP amplitudes suggest that the number of reinnervating fibers to distal musculature was improved at early timepoint when the orientation of the graft was switched compared to the non-switched orientation. Decreased peroneal latency in the switched orientation suggests a more rapid conduction speed at these time points, closer to the conduction speed at baseline. Conversely, CMAP amplitudes and latencies for the tibial branch were equivalent at all time points in the autograft group compared to the switched orientation (Figures 3C,D).

CatWalk was performed to assess functional reinnervation as well as behavioral recovery of gait following injury. Catwalk recordings in the sciatic autograft group showed significantly less disruption to their cadence at 12- and 36-weeks PO (9.84 ± 0.60 steps/s, 9.3 ± 1.13 steps/s) compared to the sciatic autograft switch group at these same time points (6.3 ± 0.46 steps/s, 6.3 ± 0.96 steps/s) ($p \leq 0.001$, $p = 0.015$), indicating injury accommodations were initially made for the sciatic autograft group to maintain a high cadence (Figure 3E). Right front-left hind (RF-LH) coupling is an indication of inter-paw coordination and in uninjured rats for this study, the LH was placed first, and stayed placed 20% longer during a step sequence, than the RF (Figure 3F). Changes in the RF-LH coupling pattern indicate a disruption to inter-paw coordination that can be caused by a reduction in the number of steps from the LH or that LH is on the platform for a longer portion of the step sequence. Increased RF-LH coupling can be seen in both the sciatic autograft and sciatic autograft switch group 4 weeks PO. By 8 weeks PO the sciatic autograft switch group reduced their RF-LH coupling compared to the sciatic autograft group, which increased their RF-LH coupling further. Both groups steadily

reduced their RF-LH coupling following 8 weeks PO indicating steady recovery of inter-paw coordination. Max contact mean intensity is presented as a measure of LH/RH*100 and is a measure of the amount of weight borne on the LH foot relative to an intact (RH) control. The sciatic autograft group had significantly less weight borne on the LH compared to the sciatic autograft switch group at all timepoints after injury, although the difference was only significant at 12 weeks PO (76 ± 4 , 95.1 ± 4.01 , $p = 0.001$), correlating with the cadence results (Figure 3G). This reduction in weight borne on the LH is one of the accommodations made by the sciatic autograft rats to allow for cadence to remain relatively unchanged. Sciatic functional index (SFI) assesses the functional recovery of the sciatic nerve and its contribution to overall gait (Bozkurt et al., 2008). The sciatic autograft and sciatic autograft switch groups had the same functional SFI recovery despite any gait accommodations made by each group (Figure 3H).

Retrograde labeling was performed to identify any changes in sensory and motor reinnervation through the grafts. Sectioning of the spinal cord showed the distribution of labeled neuronal soma from the peroneal (magenta) and tibial (green) labels (Figure 4A). Localization of sensory (dorsal horn) and motor (ventral) neurons were determined by their location in relation to the median fissure and anterior spinal artery as described previously (Watson et al., 2009; Toossi et al., 2021) (Figure 4A, merged). As expected of mixed sensory and motor nerves, images show an abundance of both magenta and green label in the dorsal and ventral horns for both groups (Figure 4A). A large portion of labeled neurons can be seen in the ventral horn, indicating a majority of tagged neurons were motor neurons. Quantification of the ratio of sensory to motor neurons showed no significant differences between branches or compared to uninjured controls, where the ratio of motor/sensory in both branches was approximately 0.2 (Figure 4B).

Morphological analysis of the nerve size, total axon counts, axonal appearance, and axonal density were performed on toluidine-blue semithin cross sections. Sections were taken

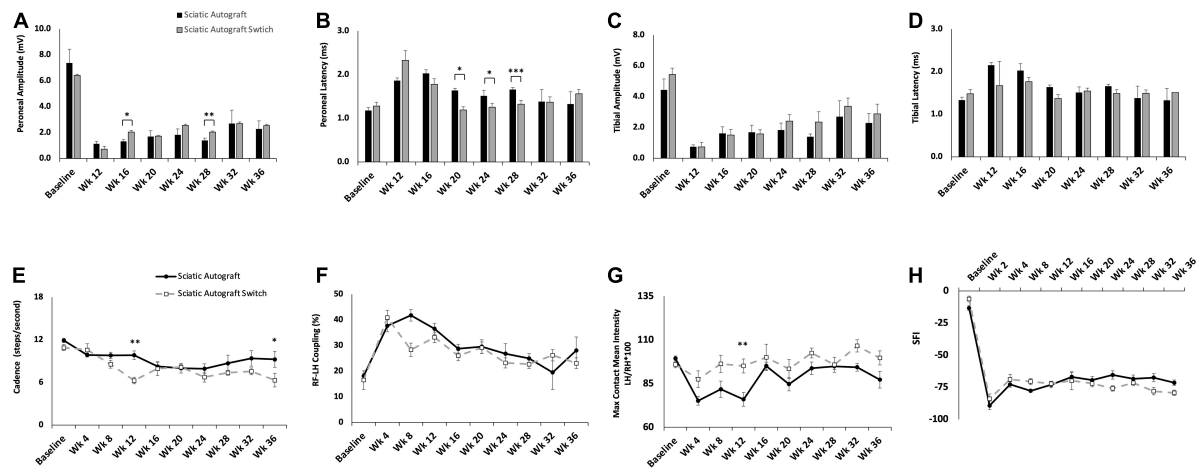


FIGURE 3

Compound muscle action potentials (CMAP) and gait analysis of the sciatic autograft and sciatic autograft switch groups. **(A)** Amplitude recordings of the peroneal branch of the sciatic nerve. **(B)** Latency recordings of the peroneal branch of the sciatic nerve. **(C)** Amplitudes recorded from the tibial branch of the sciatic nerve. **(D)** Latencies of the tibial branch of the sciatic nerve. * $p < 0.05$, ** $p < 0.01$, *** $p < 0.001$ by repeated measures ANOVA with Tukey *post-hoc* test. **(E)** Cadence in steps per second as calculated by the CatWalk software. **(F)** RF-LH coupling showing the percentage of time the left hind (LH) paw preceded the right front (RF) paw in the step cycle. **(G)** Measure of the maximum intensity at the point of maximum contact for the left hind paw/right hind paw*100. **(H)** Sciatic functional index (SFI) recordings as calculated by the CatWalk software. $n = 5$ for sciatic autograft, $n = 6$ for sciatic autograft switch, * $p < 0.05$, ** $p < 0.01$ by repeated measures ANOVA with Tukey *post-hoc* test. Error bars are standard error of the mean (SEM).

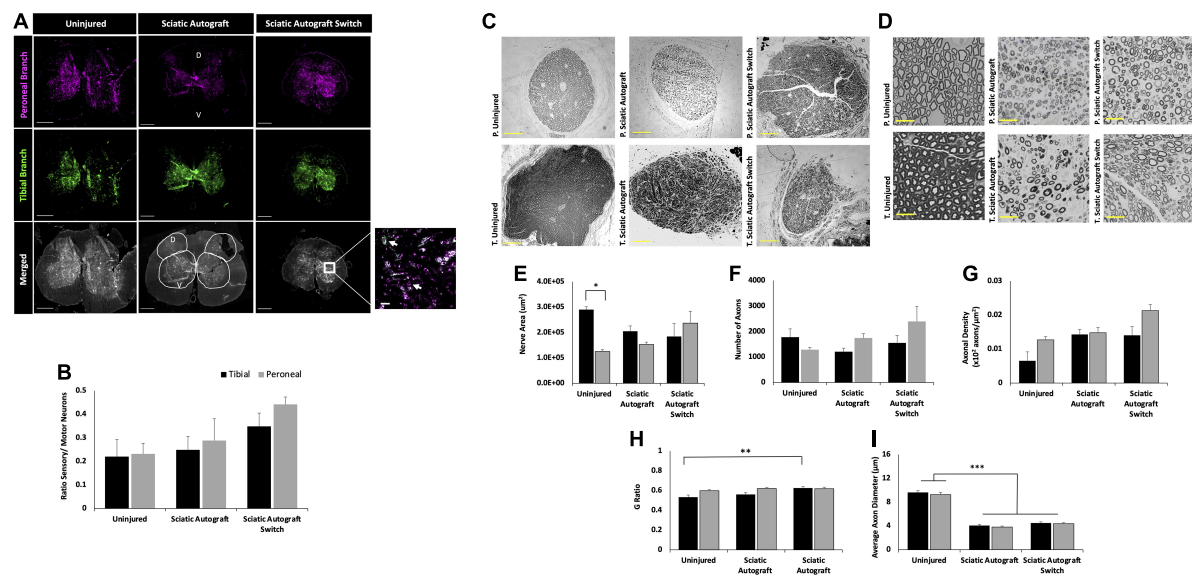


FIGURE 4

Sciatic autograft and sciatic autograft switch retrograde labeling and nerve morphometry. **(A)** Retrograde labeled spinal cords showing peroneal (magenta) and tibial (green) branch labeling. The dorsal and ventral horns are outlined in the merged image for the sciatic autograft group. Box in the merged image of the sciatic autograft switch column shows a 20 \times magnification, scale bar is 20 μ m. Arrows indicate labeled neurons. Scale bars are 500 μ m. **(B)** Ratio of sensory/motor neurons counted from the peroneal (magenta) and tibial (green) nerves. Scale bars are 200 μ m. **(C)** Cross section images of the peroneal and tibial nerves taken at 10 \times . Scale bars are 200 μ m. **(D)** 40 \times images of the toluidine blue stained sections from within the grafts; labeling of images is based on connection of the branch in the graft to the hosts peroneal or tibial distal nerve stump. Scale bars are 20 μ m. **(E)** Total cross sectional nerve area taken for the tibial and peroneal branches. **(F)** Total number of axons. **(G)** Axonal density. **(H)** G-ratio. **(I)** Average inner x and y plane axon diameter. $n = 5$ for sciatic autograft, $n = 6$ for sciatic autograft switch, * $p < 0.05$, ** $p < 0.01$, *** $p < 0.001$ by two-way ANOVA with Tukey *post-hoc* test. Error bars are SEM.

within each branch of the graft and the notation in the figures signifies what distal nerve structure the branch in graft was sutured to (i.e., peroneal switch is within the tibial branch of the graft that is connected to the peroneal stump). **Figures 4C,D** show representative low and high magnification images of the nerve and axons. Nerve area of the tibial branch of uninjured animals was significantly larger than the peroneal branch ($2.9 \times 10^5 \pm 1.1 \times 10^4 \mu\text{m}^2$ vs. $1.3 \times 10^5 \pm 7.2 \times 10^3 \mu\text{m}^2$, $p = 0.005$) which is to be expected based on the visibly noticeable size difference of the tibial and peroneal branches seen in **Figure 1A** (**Figure 4E**). This significant difference was not preserved in the branches of the sciatic autograft and sciatic autograft switch groups, but there was a trend for larger nerve area within the tibial portions of grafts irrespective of if the tibial portion of the graft was sutured to the tibial or peroneal nerve. No significant differences were observed for total number of axons and axon density (**Figures 4F,G**). While not significantly different, the sciatic autograft switch group had a larger nerve area, total number of axons, and axonal density in the peroneal branch than the uninjured or sciatic autograft groups. Considering that the distal peroneal branch was connected to the tibial branch of the graft, where the sample was taken from, it is notable that this was not significant. The G-ratio of the sciatic autograft switch tibial branch (0.627 ± 0.014) was found to be significantly higher than the uninjured tibial branches (0.533 ± 0.021 , $p = 0.007$) (**Figure 4H**). Both tibial and peroneal branches in the uninjured control had significantly larger average axon diameters than both sciatic autograft groups ($p \leq 0.001$) (**Figure 4I**). These results indicate that even by 36 weeks PO, that autografts did not replicate the larger axon diameter of uninjured animals but did display G-ratios consistent with their smaller axon diameters.

Regeneration by orientation of inbred sciatic allografts

Evaluation of inbred sciatic allografts was included primarily as an intermediary to the inbred femoral allografts. Sciatic allografts from inbred Lewis rats allows for direct comparison to sciatic autografts to determine the extent that immunogenicity factored into this inbred model. **Figures 5, 6** show CMAPs, CatWalk, retrograde labeling and nerve morphometry of the sciatic allograft, sciatic allograft switch and the sciatic autograft groups to facilitate comparison. Peroneal amplitudes and latencies both recovered at a steady state for the sciatic allograft and sciatic allograft switch groups (**Figures 5A,B**). Some significant differences in peroneal amplitudes were observed at week 12 where sciatic autograft (1.13 ± 0.19 mV, $p = 0.028$) and sciatic allograft (1.22 ± 0.517 mV, $p = 0.003$) were significantly greater than the sciatic allograft switch (0.80 ± 0.333 mV); at week 24 where sciatic allograft (2.71 ± 0.384 mV) was significantly greater than the sciatic

autograft (1.83 ± 0.455 mV, $p = 0.018$) and sciatic allograft switch (1.66 ± 0.263 mV, $p = 0.002$); and at week 28 where the sciatic autograft (1.40 ± 0.173 mV) was significantly inferior to sciatic allograft (2.47 ± 0.262 mV, $p \leq 0.001$) and sciatic allograft switch (2.42 ± 0.184 mV, $p \leq 0.001$). Peroneal latencies in the sciatic allograft [1.57 ± 0.22 ms ($p = 0.003$), 1.47 ± 0.150 ms ($p \leq 0.001$), 1.39 ± 0.104 ms ($p = 0.014$)] and sciatic allograft switch groups [2.68 ± 0.429 ms ($p = 0.028$), 1.52 ± 0.173 ms ($p = 0.003$), 1.29 ± 0.043 ms ($p \leq 0.001$)] showed some differences from sciatic autograft (1.87 ± 0.06 ms, 2.03 ± 0.08 ms, 1.66 ± 0.044 ms) at 12-, 16-, and 28-weeks PO, respectively, but equalized by the last two time points (**Figure 5B**).

Tibial amplitudes suggest inferior reinnervation in the sciatic autograft (1.69 ± 0.45 mV, 1.40 ± 0.173 mV) compared to sciatic allograft (2.57 ± 0.509 mV, $p = 0.002$) at 20 weeks PO and between the sciatic allograft (3.61 ± 0.295 mV, $p \leq 0.001$) and sciatic allograft switch groups (3.57 ± 0.692 mV, $p \leq 0.001$) at 28 weeks PO. The sciatic allograft group also had significantly higher tibial amplitudes than the sciatic allograft switch group (1.44 ± 0.382 , $p = 0.002$) at 20 weeks PO before the switch group recovered to higher amplitudes at 24 weeks PO (**Figure 5C**). Tibial latencies similarly showed some significant differences at 28 weeks PO between the sciatic autograft group (1.66 ± 0.0439 ms) and sciatic allograft group (1.45 ± 0.062 ms, $p = 0.007$) (**Figure 5D**). Taken together, these results suggest that initially more reinnervation of distal muscle groups occurred for the sciatic allograft group before equalizing at later time points to the reinnervation seen in other groups.

CatWalk measurements of cadence and RF-LH coupling showed equivalent recovery between the sciatic autograft group and both sciatic allograft groups (**Figures 5E,F**). Max contact mean intensity was significantly higher 12 weeks PO in the sciatic allograft (96.2 ± 3.15 , $p \leq 0.001$) and sciatic allograft switch groups (96.5 ± 2.29 , $p \leq 0.001$) compared to the sciatic autograft group (76 ± 4) (**Figure 5G**). These patterns are similar to **Figure 3** and show that gait accommodations to the injury were unique for the sciatic autograft group. There was no difference in SFI scores between sciatic autograft and allograft groups until 28- and 32-weeks PO when the sciatic allograft group (-81.7 ± 1.39 , -81.1 ± 1.44) became significantly worse than the sciatic allograft switch group (-63.5 ± 5.77 , $p = 0.004$; -68.7 ± 2.90 , $p = 0.015$) and the sciatic autograft group (-68.5 ± 2.98 , $p = 0.02$; -67.5 ± 3.22 , $p = 0.004$) (**Figure 5H**). This correlates with the CMAPs data and indicates reinnervation plateaued around 28 weeks PO in the sciatic allograft group.

Retrograde labeling data indicates a retention in mixed nerve morphology in all groups with equivalent ratios of sensory to motor neurons in the uninjured, sciatic autograft and sciatic allograft switch group. However, the sciatic allograft group regenerated significantly more sensory neurons in the peroneal branch (0.75 ± 0.14) than in the tibial branch (0.38 ± 0.25 ,

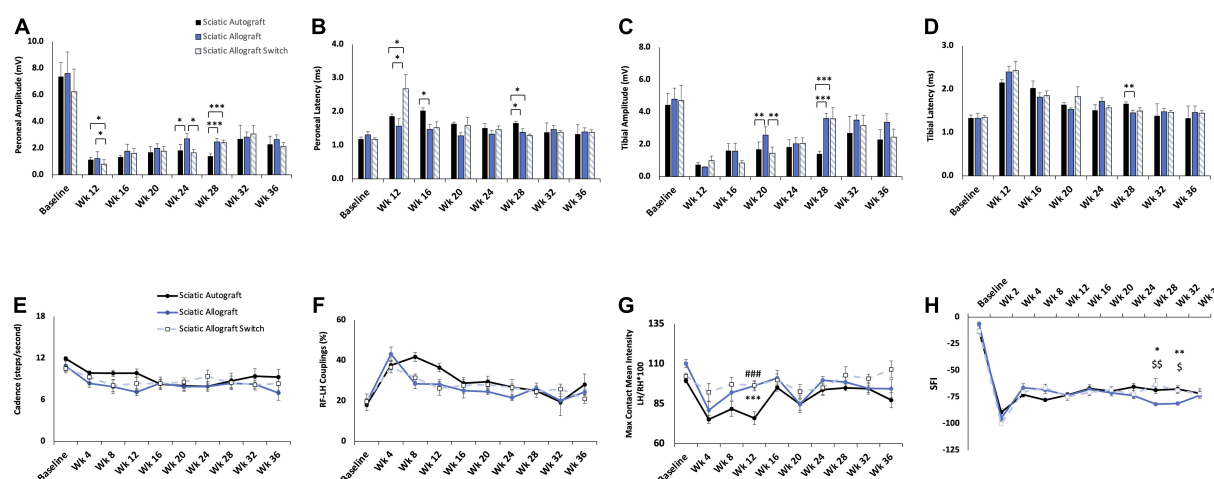


FIGURE 5

Compound muscle action potential (CMAP) and gait analysis of inbred Lewis to Lewis sciatic allograft and sciatic allograft switch groups. Sciatic autograft is included for reference. (A) Amplitude recordings of the peroneal branch of the sciatic nerve. (B) Latency recordings of the peroneal branch of the sciatic nerve. (C) Amplitudes recorded from the tibial branch of the sciatic nerve. (D) Latencies of the tibial branch of the sciatic nerve. * $p < 0.05$, ** $p < 0.01$, *** $p < 0.001$. (E) Cadence in steps per second as calculated by the CatWalk software. (F) RF-LH coupling showing the percentage of time the left hind (LH) paw preceded the right front (RF) paw in the step cycle. (G) Measure of the maximum intensity at the point of maximum contact for the left hind paw/right hind paw*100. (H) Sciatic functional index (SFI) recordings as calculated by the CatWalk software. $n = 5$ for autograft group and $n = 6$ for inbred sciatic allografts in both orientations. * $p < 0.05$, ** $p < 0.01$ between sciatic autograft and sciatic allograft, ### $p < 0.001$ between sciatic autograft and sciatic allograft switch, \$ $p < 0.05$, \$\$ $p < 0.01$, \$\$\$ $p < 0.001$ between sciatic allograft and sciatic allograft switch. All statistical analysis were repeated measures ANOVA with Tukey post hoc test. Error bars are SEM.

$p = 0.034$) indicating differences in axonal guidance down each branch (Figures 6A,B). This pattern was not retained in the switch surgery which could indicate a complexity in axonal guidance introduced by the switch surgery.

Representative nerve images for morphometry seen in Figure 6C show the general trend that the tibial branch was larger in the groups that were not switched, while the sciatic allograft group that was switched had a higher nerve area (sections from inside the tibial branch of the graft) in the peroneal branch, as expected (Figure 6E). The total number of axons was larger in the peroneal branch of the sciatic allograft switch group despite having similar axon density in both the peroneal and tibial branches suggesting that the increase nerve area seen in this nerve branch accounted for the increased number of axons when axonal density was calculated (Figure 6F). Representative higher magnification images in Figure 6D show the differences in nerve appearance across groups. G-ratio was significantly higher in the tibial branch of the sciatic allograft group (0.66 ± 0.013) compared to the uninjured (0.533 ± 0.021 , $p \leq 0.001$), sciatic autograft (0.56 ± 0.020 , $p \leq 0.001$), and sciatic allograft switch groups (0.59 ± 0.013 , $p \leq 0.001$) (Figure 6H). The average axonal diameter was also significantly higher in the tibial branch of the sciatic allograft group ($4.97 \pm 0.233 \mu\text{m}$) compared to the autograft ($4.07 \pm 0.211 \mu\text{m}$, $p = 0.02$) and allograft switch group ($3.78 \pm 0.217 \mu\text{m}$, $p \leq 0.001$), but not compared to the uninjured control (9.64 ± 0.28), which had significantly higher average axon diameter in both branches compared to

all groups ($p \leq 0.001$) (Figure 6I). The tibial branch of the sciatic allograft group showed the best regeneration across groups as indicated by a larger number of axons that had significantly more myelination and axon diameter than other groups.

These results with Lewis to Lewis inbred sciatic allografts, obtained without any immunosuppressive therapy, support that immunogenicity did not play a significantly deleterious role in regeneration in transplants between inbred Lewis rats. The results can be contrasted with our previous findings with nerve allografts from Sprague Dawley donors into Lewis recipients, where the lack of immune suppression significantly decreased regeneration without immune suppression (Santos Roballo et al., 2019). As a basis of comparison, we also conducted a pilot cohort of 2.0 cm branched sciatic autografts and sciatic allografts without any immune suppression, where donor and host animals were outbred Sprague Dawley rats. Significant differences were observed for peroneal and tibial CMAPs at 20 ($p = 0.017$, $p \leq 0.001$) and 26 weeks ($p = 0.008$, $p = 0.009$) PO, respectively (Supplementary Figures 1A,B). The CMAPs results are corroborated by the total axons counts, which indicate that the total number of axons in the tibial branch ($1.7 \times 10^3 \pm 196$ axons) of the sciatic autograft was significantly larger than the tibial branch ($1.1 \times 10^3 \pm 153$ axons, $p = 0.012$) of the outbred sciatic allograft group (Supplementary Figures 1C,D). The G-ratio in the Sprague Dawley rats was identical across both branches of both groups (Supplementary Figure 1E). This data suggests that immunogenicity is a

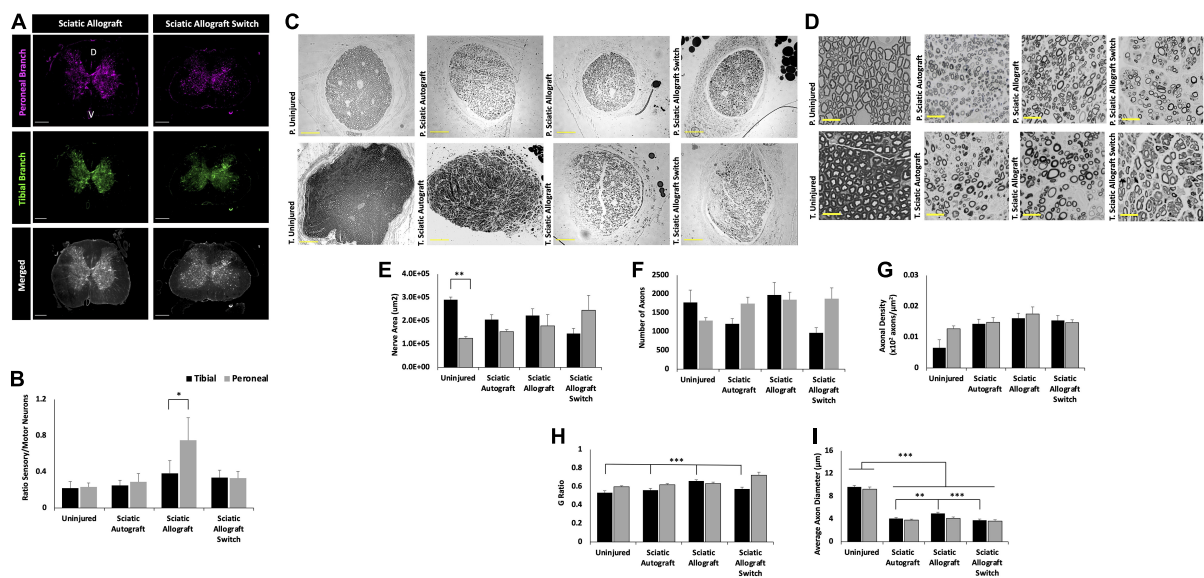


FIGURE 6

Inbred Lewis to Lewis sciatic allograft and sciatic allograft switch group retrograde labeling and nerve morphometry. Sciatic autograft is included for reference. (A) Retrograde labeled spinal cords showing peroneal (magenta) and tibial (green) branch labeling. Scale bars are 500 μm . (B) Ratio of sensory/motor neurons counted from the peroneal (magenta) and tibial (green) nerves. * $p < 0.05$ by Wilcoxon Signed Rank Test comparing tibial and peroneal ratios. (C) Cross section images of the peroneal and tibial nerves taken at 10 \times . Scale bars are 200 μm . (D) 40 \times images of the toluidine blue stained sections from within the grafts; labeling of images is based on connection of the branch in the graft to the hosts peroneal or tibial distal nerve stump. Scale bars are 20 μm . (E) Total cross sectional nerve area taken for the tibial and peroneal branches. (F) Total number of axons. (G) Axonal density. (H) G-ratio. (I) Average inner x and y plane axon diameter. $n = 5$ for sciatic autograft, $n = 6$ for sciatic allografts in both orientations, * $p < 0.05$, ** $p < 0.01$, *** $p < 0.001$ by two-way ANOVA with Tukey *post-hoc* test. Error bars are SEM.

significant factor for allografting conducted with this outbred strain of Sprague Dawley rats compared to the inbred Lewis rats.

Regeneration with inbred femoral allografts

Preferential motor reinnervation has been partly attributed to intrinsic factors within the motor branch of the femoral nerve that guide regenerating motor axons into the motor branch (Morita et al., 2008). Femoral allografts were tested in both orientations to determine if this would affect regeneration into the tibial and peroneal branches of the sciatic nerve, which are both mixed sensory and motor (Irintchev, 2011). This was tested by transplanting femoral allografts in the Lewis to Lewis inbred model.

Femoral allografts showed a plateau in reinnervation by 28 weeks PO that can be seen in CMAPs. CMAPs recording of the peroneal branch show a significantly higher peroneal amplitude in the femoral allograft group (1.98 ± 0.297 mV) compared to the sciatic autograft (1.40 ± 0.173 mV, $p = 0.009$) at 28 weeks PO, but amplitudes in the femoral allograft group plateaued after this point (Figure 7A). Peroneal amplitudes in the femoral allograft switch group also plateaued after 28 weeks PO. Peroneal latency did not differ significantly between groups at any time point but taken with peroneal amplitude,

also showed a peak in peroneal branch recovery at 28 weeks PO in the femoral allograft and femoral allograft switch group (Figure 7B). A similar pattern was seen in the tibial branch where tibial amplitude was found to be significantly higher in the sciatic autograft group (1.40 ± 0.173 mV) at 28 weeks PO in comparison to the femoral allograft group (2.96 ± 0.461 mV, $p = 0.005$) with both the femoral allograft and femoral allograft switch group plateauing after this time point (Figure 7C). Tibial latency in the sciatic autograft group was significantly larger in the sciatic autograft (2.15 ± 0.06 ms) compared to the femoral allograft switch group (1.62 ± 0.218 ms, $p \leq 0.001$) at 12 weeks PO but there were no differences in any group at later time points (Figure 7D). This suggests a threshold of recovery was reached in the femoral allografts regardless of their orientation.

The femoral allograft group showed divergent behavioral recovery at early time points. Cadence was significantly reduced in the femoral allograft group (7.3 ± 0.85 steps/s, $p = 0.017$) at 8 weeks PO compared to the femoral allograft switch group (9.6 ± 0.49 steps/s) (Figure 7E). This normalized to the sciatic autograft and femoral allograft switch groups by 16 weeks PO (Figure 7E). In addition to reduced cadence, the femoral group also had RF-LH coupling percentages that were lower than the other groups but not significantly so (Figure 7F). As the experiment progressed, the femoral allograft group regained a cadence that was in accordance with the other groups, but continued to show a reduced percentage of RF-LH coupling

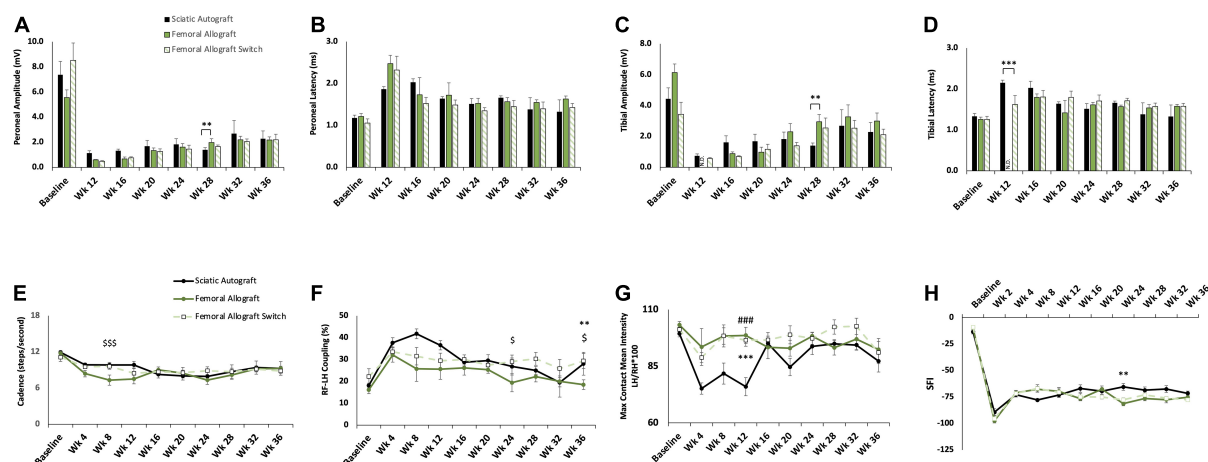


FIGURE 7

Compound muscle action potential (CMAP) and gait analysis of inbred Lewis to Lewis femoral allograft and femoral allograft switch groups. Sciatic autograft is included for reference. (A) Amplitude recordings of the peroneal branch of the sciatic nerve. (B) Latency recordings of the peroneal branch of the sciatic nerve. (C) Amplitudes recorded from the tibial branch of the sciatic nerve. (D) Latencies of the tibial branch of the sciatic nerve. $**p < 0.01$, $***p < 0.001$, N.D. indicates fewer than 3 rats responded. (E) Cadence in steps per second as calculated by the CatWalk software. (F) RF-LH coupling showing the percentage of time the left hind (LH) paw preceded the right front (RF) paw in the step pattern. (G) Measure of the maximum intensity at the point of maximum contact for the left hind paw/right hind paw*100. (H) Sciatic functional index (SFI) recordings as calculated by the CatWalk software. $n = 5$ for autograft group and $n = 6$ for inbred femoral allografts in both orientations. $**p < 0.01$, $***p < 0.001$ between sciatic autograft and femoral allograft, $###p < 0.001$ between sciatic autograft and femoral allograft switch, $\$p < 0.05$, $$$$p < 0.001$ between femoral allograft and femoral allograft switch. All statistical analysis are a repeated measures ANOVA with Tukey post hoc test. Error bars are SEM.

that was significantly lower ($19.4 \pm 4.13\%$) than the femoral allograft switch group ($29.1 \pm 2.95\%$, $p = 0.037$) at week 24 and was significantly lower ($18.5 \pm 2.22\%$) than the femoral allograft switch ($29.4 \pm 3.38\%$, $p = 0.016$) and sciatic autograft ($28.1 \pm 5.24\%$, $p = 0.003$) at 36 weeks PO.

Mean intensity recordings for the femoral allograft group (98.6 ± 3.58 , $p \leq 0.001$) and femoral allograft switch group (96.5 ± 2.65 , $p \leq 0.001$) were consistent across the duration of the study and were significantly higher than the sciatic autograft group (76 ± 4) 12 weeks PO (Figure 7G). This pattern is unique because it implies that the femoral allograft group were able to maintain their RF-LH coordination and relative weight borne on the LH, but this had to be compensated for by reducing their cadence. SFI measurements were also consistent across group for a large portion of the study, with the femoral allograft group (-81.2 ± 2.04) being significantly different from the sciatic autograft group (-65.4 ± 3.20 , $p = 0.004$) only at week 24 before increasing to be in line with the sciatic autograft and femoral allograft switch group at 28 weeks PO (Figure 7H). CatWalk data support CMAPs data showing that functional reinnervation reached completion by 28 weeks in both femoral allograft groups. Additionally, the femoral allograft group made significant gait accommodations after injury that did not resolve as the study progressed.

While not significant, spinal cord images of the femoral allograft group show more sensory axons in the peroneal branch compared to the tibial branch, which is consistent with the pattern seen in the sciatic allograft group (Figure 8A). The

femoral allograft switch group had equal ratios of sensory/motor neurons in the tibial and peroneal branch (Figure 8B). This data indicates that while reinnervation was largely mixed sensory and motor axons, there could be some indications that graft origin impacts axonal guidance in branched injuries if placed in a nerve of complementary size.

The difference in cross sectional area can be seen in the representative images in Figures 8C,D. The greatest differences in total cross sectional nerve area were between the tibial branch of the uninjured control and the femoral allograft switch group, where nerves were taken from the saphenous graft attached to the distal tibial branch (Figure 8E). While not significant, this pattern was also seen in the reduced number of axons in the femoral allograft switch group (844 ± 136 axons) compared to the uninjured control (1777 ± 326 axons) and indicates that the significantly smaller nerve area in the saphenous branch compared to the tibial branch cannot accommodate as many axons (Figure 8F). However, despite the total area and axonal count differences seen in the saphenous branch, there are not any differences in the axonal density between groups (Figure 8G). Myelin thickness was significantly greater in the tibial branch of the femoral allograft group (0.670 ± 0.013) compared to the sciatic autograft (0.560 ± 0.020 , $p = 0.001$) and uninjured controls (0.533 ± 0.021 , $p \leq 0.001$). This is consistent with the results seen in the sciatic allograft tibial branch and indicates more robustly myelinated axons in grafts attached to the distal tibial stump regardless of the graft origin. G-ratio in the peroneal branch was significantly smaller in the

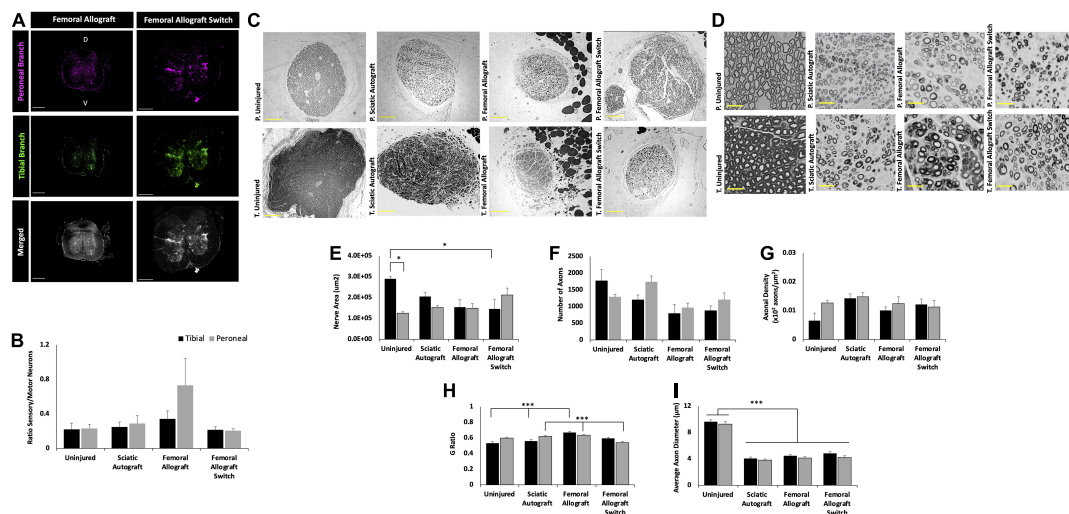


FIGURE 8
Inbred Lewis to Lewis femoral allograft and femoral allograft switch group retrograde labeling and nerve morphometry. Sciatic autograft is included for reference. **(A)** Retrograde labeled spinal cords showing peroneal (magenta) and tibial (green) branch labeling. Scale bars 500 μm . **(B)** Ratio of sensory/motor neurons counted from the peroneal (magenta) and tibial (green) nerves. **(C)** Cross section images of the peroneal and tibial nerves taken at 10 \times . Scale bars are 200 μm . **(D)** 40 \times images of the toluidine blue stained sections from within the grafts; labeling of images is based on connection of the branch in the graft to the hosts peroneal or tibial distal nerve stump. Scale bars are 20 μm . **(E)** Total cross sectional nerve area taken for the tibial and peroneal branches. **(F)** Total number of axons. **(G)** Axonal density. **(H)** G-ratio. **(I)** Average inner x and y plane axon diameter. $n = 5$ for sciatic autograft, $n = 6$ for femoral allografts in both orientations, $*p < 0.05$, $***p < 0.001$ by two-way ANOVA with Tukey *post-hoc* test. Error bars are SEM.

femoral allograft switch group (0.6335 ± 0.012) compared to the sciatic autograft (0.620 ± 0.013 , $p = 0.022$) and femoral allograft groups (0.542 ± 0.015 , $p = 0.01$) indicating that it is not the motor branch of the femoral nerve that is responsible for greater myelination in grafts attached to the distal tibial branch (Figure 8H). As expected with no nerve injury, the uninjured control retained significantly greater average axon diameter in both branches compared to the experimental treatment groups while there were no differences between both of the femoral allograft or sciatic autograft groups ($p \leq 0.001$) (Figure 8I).

Comparison across all groups

The same data presented in Figures 3–8 is shown for all groups by each outcome in Supplementary Figures 2–4 to facilitate direct comparison across all groups. CMAP data indicated that the femoral allograft group showed lower amplitudes than the sciatic allograft group at multiple time points across peroneal amplitude, peroneal latency, and tibial amplitude (Supplementary Figures 2A–C). The peroneal amplitude was larger in the sciatic allograft group compared to the femoral allograft group at all time points, significantly so at 16-, and 24-weeks PO ($p = 0.002$, and $p = 0.001$), respectively. The peroneal latency was initially significantly larger ($p = 0.049$) in the femoral allograft group compared to the sciatic allograft group before equalizing at 28 weeks PO. Tibial amplitude was less in the femoral allograft group compared to the sciatic

allograft group at all time points, significantly so at 20 weeks PO ($p \leq 0.001$). Tibial latency was larger in the femoral allograft group at multiple time points, but not significantly so. The significance found across the CMAPs recordings indicates a greater level of reinnervation in the sciatic allograft group in both the peroneal and tibial branches.

CMAP trends between switched orientations were also present at multiple time points. The peroneal amplitude in the sciatic autograft switch group was larger than the femoral allograft switch group at all time points, significantly so at 16- and 24-weeks PO ($p \leq 0.001$, $p \leq 0.001$). Peroneal latencies showed more fluctuation over time and were only smaller than femoral allograft switch groups from 20 to 28 weeks PO. Tibial amplitudes were larger in the autograft switch group at a majority of time points, significantly so at 16- and 24-weeks PO ($p = 0.001$, $p = 0.021$). Tibial latencies were less in the autograft switch group compared to the femoral allograft switch group at all later time points, significantly so at 28 weeks PO ($p \leq 0.001$). These trends indicate greater recovery in the sciatic autograft switch group compared to the femoral allograft switch group. While recovery in the distal peroneal branch of the femoral allograft switch group was consistent across time points, peroneal latencies and tibial amplitude and latencies indicate poor reinnervation to the dorsal muscles of the feet. Recovery in the peroneal and tibial branch of the autograft switch showed greater indications of reinnervation to the dorsal muscles of the feet through larger magnitude amplitudes and smaller latencies.

Additionally, CMAPs taken from the sciatic allograft switch group had larger peroneal and tibial amplitudes at all time points compared to femoral allograft switch group, but only significantly so at 28 weeks PO ($p \leq 0.001$) in the peroneal branch. Tibial and peroneal latencies were high at early time points in the sciatic allograft switch group before showing improvement and reducing to be equivalent to the femoral allograft switch group, which plateaued at week 16 in each branch. These results, taken in combination with the sciatic autograft switch group could indicate that an incongruous nerve alignment in congruent graft tissue allows for greater reinnervation of distal muscles compared to grafts that are not congruent with the original injury.

When comparing differences for CatWalk across all groups, cadence was the only measure that showed significant differences outside of what was previously discussed. Cadence was significantly larger in the sciatic allograft switch (8.35 ± 0.92 steps/s) compared to the sciatic autograft switch (6.27 ± 0.46 steps/s, $p = 0.033$) 12 weeks PO (Supplementary Figure 3A). The cadence in the femoral allograft switch (8.88 ± 0.64 steps/second, $p = 0.017$) and sciatic allograft switch groups (9.35 ± 0.93 steps/s, $p = 0.005$) were significantly higher than the autograft switch group (6.76 ± 0.70 steps/s) 24 weeks PO. The sciatic autograft switch group had a lower cadence at multiple time points compared to multiple groups, which could point to reduced functional motor reinnervation, and thus reduced movement ability, with the switched autograft nerves at early time points.

Significant comparisons can also be made between groups when looking at nerve morphometry, specifically axonal density. The peroneal branch in the sciatic autograft switch group (0.014 ± 0.003 axons/ μm^2) had a significantly higher axonal density than the femoral allograft switch group (0.012 ± 0.002 axons/ μm^2 , $p = 0.015$) which is also seen represented in the higher peroneal amplitudes at week 36 in the sciatic autograft switch group (Supplementary Figure 4C). This correlates with the CMAPs data and suggests that a greater number of axons reinnervated the peroneal branch of the sciatic autograft switch group compared to the femoral allograft switch group. No other significant differences were found between groups.

In addition, the sciatic allograft switch group (0.643 ± 0.018 , $p = 0.001$) had a significantly larger G-ratio in the peroneal branch compared to the femoral allograft switch group (0.542 ± 0.015) indicating a more robust recovery of myelination backed up by functional tests (Supplementary Figure 4D). G-ratio was also found to be significantly smaller in the tibial branch of the femoral allograft switch group (0.595 ± 0.013) compared to the sciatic allograft group (0.660 ± 0.013 , $p = 0.002$) while the femoral allograft group (0.670 ± 0.013) G-ratio was significantly higher compared to the sciatic allograft switch group (0.574 ± 0.019 , $p = 0.012$). This data indicated reduced myelination in switched nerve branches with smaller graft branches compared to larger

original orientation branches. Average axonal diameter was significantly higher in the peroneal branch of the sciatic autograft switch group ($4.37 \pm 0.19 \mu\text{m}$) compared to the sciatic allograft switch group ($3.65 \pm 0.23 \mu\text{m}$, $p = 0.018$) which is also in line with CMAPs recordings which show more robust recovery with larger axons in autograft switch groups (Supplementary Figure 4E).

Muscle wet weight measurements compared between groups show no significant muscle loss in either the left gastrocnemius or left tibialis anterior muscles (Supplementary Figure 5). As expected, the right-side gastrocnemius and tibialis anterior were significantly larger than the left (injured) side for all groups showing muscle loss as a result of the injury. The amount of muscle lost was consistent with allografts done in previous reports, indicating there was motor reinnervation that occurred (Roballo and Bushman, 2019).

Discussion

Previous studies of PNIs have focused on regeneration following lacerations and linear segmental nerve defects, where there is relatively little known about regeneration of segmental nerve defects that ablate entire branch points. Regeneration following ablation of branch points presents a complex scenario for clinicians. The present study was designed to investigate how the orientation and source of branched nerve grafts affects outcomes following an ablation of the branch point where both distal branches are mixed motor and sensory. 2.5 cm ablations of the sciatic nerve in rats, that included the peroneal and tibial branch point (Figure 1A), were bridged with 2.5 cm branched sciatic nerve autografts, inbred sciatic nerve allografts, and inbred femoral nerve allografts. Each type of branched graft was tested in two orientations, with each branch sutured to the distal stump of either the peroneal or tibial nerve of the host animal (Figure 1B). Outcome measures included behavioral, functional, electrophysiological, immunohistochemical and morphometric measures out to 36 weeks.

The primary advancement from this study is that graft source and orientation did not have broad significant effects on outcomes in the long term and experimental end point of 36 weeks. CMAP amplitudes for both sciatic autograft groups were equivalent for both orientations measured from muscles within the foot innervated by the tibial and peroneal nerves (Figures 3A,C). This was also the case for sciatic and femoral allografts in each orientation (Figures 5A,C, 7A,C). CMAP amplitudes recovered to similar extents across all graft types and orientations (Supplementary Figures 2A,C). Nerve morphometry revealed no significant differences in numbers of total axons or axonal density within each branch in either orientation at 36 weeks (Supplementary Figures 4B,C). CatWalk behavioral assessments of max contact mean intensity

and SFI, the main assessments used to determine functional recovery of the injury, were equivalent for graft type and orientation (**Supplementary Figures 3C,D**). There were end point differences in RF-LH coupling and cadence at 36 weeks. However, these are assessments of gait that can indicate injury accommodation based on coordination and speed and may not be direct indications of functional recovery compared to baseline (Deumens et al., 2007; Parkkinen et al., 2013). Therefore, this data collectively indicates that long-term indications of recovery for a 2.5 cm defect of the sciatic nerve that ablated the peroneal/tibial branch point did not show significant differences across multiple outcomes by 36 weeks PO if the defect was bridged with sciatic autograft, sciatic allograft, or femoral allograft in either orientation. This suggests that axon regeneration is robust through branched nerve grafts over the long-term provided that the grafts have matching branching anatomy, somewhat irrespective of how closely matched the diameters of the graft are to the injured nerves.

A secondary advancement of this study was that electrophysiological and behavioral outcome measures did show differences at earlier time points based on inbred graft source and orientation, despite that the differences had largely equalized by the study endpoint. It must be noted that this study's end point of 36 weeks is longer than most other studies in rat sciatic nerve, typically ranging from 12 to 20 weeks (Deleonibus et al., 2021). CMAP amplitudes for sciatic autograft switch were significantly higher than the original orientation in the peroneal branch at 16 and 28 weeks, with similar (non-significant) trends at 24 weeks. Peroneal latencies were likewise improved in the switched orientation, indicating that regeneration to tissues innervated by the peroneal branch were enhanced when connected to the tibial branch of the graft (**Figure 3D**). In comparing all groups together, peroneal, and tibial CMAPs for sciatic autografts and allografts in either orientation were significantly superior to femoral allografts at several earlier time points (**Supplementary Figure 2**).

CatWalk parameters were also affected in all groups at early time points. The cadence was significantly higher for the sciatic autograft group compared to the sciatic autograft switch group at 8 weeks PO and femoral allograft group at 12 weeks PO (**Figures 3E, 7E**). Additionally, RF-LH couplings showed that there were differences in RF-LH coordination in the sciatic autograft group compared to all groups at early time points (**Figures 3F, 5F, 7F**). Max contact mean intensity is a measure of weight borne on a foot at the time of maximum contact with the CatWalk platform. It's worth noting that max contact mean intensity has been used as an indicator of pain in previous studies of diabetic neuropathy, and much smaller sciatic crush/transection injuries, but has not been confirmed as an indicator of pain in large transection studies such as this study (Vrinten and Hamers, 2003; Deumens et al., 2007; Vieira et al., 2020). Max contact mean intensity is here used as a measure of weight borne on the foot as an indicator

of LH function. Lesser intensity equates to less weight borne on the LH compared to the RH. The sciatic autograft group showed the largest fluctuation in weight borne on their LH foot which, in addition with cadence and RF-LH coupling indicates a pattern of injury accommodation in which their LH foot was used sparingly and only as an anchor to allow for balance and speed of crossing (**Figure 3G**). Other experimental groups showed a different pattern of injury accommodation in which the LH initially appeared to be used only for balance, which slowed down their overall cadence. As the nerve regenerated, and cadence improved, the RF-LH coordination improved, and more weight was able to be placed on the LH. Functional recovery of the sciatic nerve, through measurement of SFI, only started to change between groups at 24 weeks PO when the femoral allograft was significantly worse than the sciatic autograft and at 28- and 32-weeks PO where the sciatic allograft was significantly reduced. These SFI changes correlate with significant differences in tibial CMAPs data and indicate a time of significant remodeling to motor innervation that equalized by 36 weeks.

Data from the femoral nerve allografts was of particular interest as it diverged from the sciatic grafts in several ways. The femoral nerve branch is such that the cutaneous branch is exclusively sensory while the motor branch innervates the quadriceps muscle and lacks sensory fibers, whereas both the peroneal and tibial branches of the sciatic nerve contain both sensory and motor neurons (Irintchev, 2011). Preferential motor reinnervation at sensorimotor branch points was established in the femoral nerve and found to be partially mediated by carbohydrate epitopes expressed on motor-associated Schwann cells (Löw et al., 1994; Martini et al., 1994; Morita et al., 2008). It was therefore a possibility that regeneration of motor fibers would be enhanced down the motor branch of the femoral allograft irrespective of whether it was sutured to the tibial or peroneal stump.

Motor reinnervation in the femoral allograft group appears to be different based on branch and time point in this study. While CMAP tibial amplitudes and latencies were improved compared to the peroneal branch after 24 weeks PO in the original orientation femoral allograft group, there were only two rats at 12 weeks PO that responded to tibial stimulation compared to the peroneal branch where all rats responded (**Figure 7**). This suggests the possibility of early motor reinnervation occurring down the peroneal branch, followed by a later wave of additional motor axons down the tibial branch from 16 to 24 weeks PO. CatWalk recordings support this observation; there was very little disruption to RF-LH coordination and weight bearing on the LH at all time points, but cadence was significantly reduced around 8 weeks PO and SFI was reduced at 24 weeks PO. This could be caused by peroneal motor innervation, which controls dorsiflexion of the foot, occurring early and allowing the animal to coordinate LH stepping and weight bearing with a transient reduction

in cadence. Late tibial reinnervation or pruning of incorrectly innervated motor axons accounts for the changes in SFI, which requires innervation of both branches of the sciatic nerve to impact toe spread. An interesting follow up study might use a similar branched grafting procedure but into a femoral nerve branched defect rather than the sciatic to determine if end-organ innervation can still drive preferential motor reinnervation when using mixed branched grafts. We are not aware of any such studies.

Potential reasons that outcomes at earlier time points differed by graft and orientation are not certain but may include factors related to the grafts as well as the defect site. Within this study, where the defect site was standard for all groups, it appears that size disparity in the branches within the graft correlates with earlier differences in outcomes. For example, sciatic autografts show lower peroneal CMAP amplitudes at the earlier time points when the peroneal branch within the graft was sutured to the peroneal stump compared to the switched orientation when the tibial branch within the graft was sutured to the peroneal stump (Figure 3A). The tibial branch in the graft is larger than the peroneal branch (Figure 1A), potentially indicating that axon regeneration at early time points may have facilitated more axons entering the larger (tibial) branch within the graft. Similar trends were observed comparing sciatic allograft to sciatic allograft switch (Figure 5A) and femoral allograft to femoral allograft switch (Figure 7C), where the motor branch within the femoral is larger than the saphenous branch (Figure 1B). Early differences in regeneration may become less evident over time as additional regeneration, remodeling and collateralization occur. As discussed in more detail below, cross sectional area of nerve branches and axon number within the grafts appears to have altered depending on which distal branch it was connected to. Conducting morphometry on nerves at earlier time points when CMAPs and CatWalk differed by graft source and orientation would be beneficial.

A third advancement of this is some of the intriguing findings of nerve morphometry. As stated previously, the cross sections of the tibial branch of the sciatic nerve is larger than the peroneal branch in uninjured animals ($1.2 \times 10^5 \pm 7.2 \times 10^3 \mu\text{m}^2$ for peroneal, $2.9 \times 10^5 \pm 1.1 \times 10^4 \mu\text{m}^2$ for tibial, $p = 0.005$) (Figure 4E). Thirty-six weeks following treatment with sciatic autografts, the cross-sectional area of the tibial branch within autografts that were sutured to the tibial stump was $2.1 \times 10^5 \pm 2.1 \times 10^4 \mu\text{m}^2$ and the tibial branches with grafts sutured to the peroneal stump (switched orientation) were slightly larger $2.4 \times 10^5 \pm 4.7 \times 10^4 \mu\text{m}^2$, both smaller than in uninjured tibial nerves (Figure 4E). The opposite trend was observed for the smaller peroneal branch, where the cross-sectional area of the peroneal section of the graft sutured to the tibial ($1.8 \times 10^5 \pm 5.0 \times 10^4$) was now larger than in uninjured peroneal ($1.5 \times 10^5 \pm 9.2 \times 10^3 \mu\text{m}^2$). This

trend was less clear in sciatic and femoral allograft groups, where direct comparison is complicated by donor nerves being obtained from age-matched males that were generally larger than the female recipients (275 g vs. 219 g) and therefore not directly comparable. While differences for autografts did not reach statistical significance, these data suggest that branches within branched autografts may increase or decrease in size depending on what distal nerve branch they are connected to.

Trends in the total number of regenerated axons is also of interest. Axon number in uninjured tibial branches was 1777 ± 326 compared to 1205 ± 140 when the tibial branch of sciatic autografts was sutured to the tibial stump and 2398 ± 588 when the tibial branch within the graft was sutured to the peroneal stump (Figure 4F). Axonal density accordingly increased after injury as the areas of the nerve branches within the autografts became smaller (Figure 4G). Axon number in the tibial branches of sciatic allografts sutured to the tibial distal stump was 1846 ± 200 and was maintained at similarly high numbers, 1875 ± 287 of axons in tibial graft branches sutured to peroneal stumps. The larger motor branch of the femoral nerve similarly attracted regeneration of additional axons when sutured to the peroneal stump (1208 ± 199) compared to when the saphenous nerve in the graft was sutured to the peroneal stump (968 ± 135). We would suggest that future studies on branched ablations should consider using additional animals/group to account for increased variability likely caused by the branching.

A potentially complicating factor in this study is the immunogenicity of the inbred sciatic and inbred femoral allografts as no immunosuppressive therapy was applied. We had previously found that regeneration with both 1 cm and 2.0 cm branched allografts from Sprague Dawley donors into Lewis rats was poor when no immunosuppression was provided (Roballo and Bushman, 2019; Santos Roballo et al., 2019). Results shown in Supplementary Figure 1 indicate that there is still immunogenicity when both donor and host are Sprague Dawley animals, as evidenced by reductions in regeneration in allograft groups. This is likely explained by the outbred nature of the Sprague Dawley strain, having shown immunogenicity in other reports of nerve allotransplantation (Mikesh et al., 2018). Addressing immunogenicity with immunosuppressive therapy is not without complications as validated immunosuppressants tacrolimus and cyclosporin have positive effects on axonal extension and Wallerian degeneration independent of their mechanisms suppressing immune cells (Sunio and Bittner, 1997; Avramut and Achim, 2003). We therefore chose inbred Lewis rats to mitigate immunogenicity of allografts rather than immunosuppressive treatment. Comparison of outcomes for sciatic autografts and inbred sciatic allografts in both orientations show highly comparable outcomes for these groups, suggesting that immunogenicity was not a significant factor

for allografts within inbred Lewis rats (Figures 5, 6). The finding that sciatic autografts and inbred allografts show equivalency long-term is meaningful because it allows for direct comparison with the femoral nerve, which has the sensorimotor divisions in branches that is not within the peroneal and tibial branches of the sciatic that both contain sensory and motor neurons.

Retrograde labeling using Alexa Flour conjugated CTb is a method used to trace the motor and sensory neurons in a given nerve and can be used to identify the regeneration nerve morphology (Hirakawa et al., 1992; Zhao et al., 2020; Cui et al., 2022). The retrograde labeling done in this study shows that there were more motor axons compared to sensory axons in all groups, seen in the higher number of labeled neurons in the ventral horn compared to the dorsal horn. When the number of neurons in each horn are counted and compared as a ratio of sensory to motor neurons for each nerve branch, some interesting trends appear. As expected of a nerve with mixed morphology, the uninjured control shows nearly identical ratios of sensory/motor neurons in both the tibial and peroneal branches. This trend is also true for the sciatic autograft group indicating that injury did not meaningfully change the number of sensory and motor neurons. Interestingly, the sciatic allograft switch group also had a nearly identical sensory/motor ratio of neurons while the sciatic allograft group showed significantly more sensory neurons in the peroneal branch compared to the tibial branch. The pattern of reinnervation seen in the sciatic allograft group could possibly support the assertion that sensory axons are more robustly regenerated down the peroneal branch early, followed by motor axons that were diverted to the tibial branch. This pattern was not retained in the switch surgery, which we hypothesize is caused by the added complexity of the size disparity in the graft and distal stump affecting axonal growth cone guidance. The same pattern occurred in the femoral allograft where, while not significantly so, the saphenous branch was innervated by more sensory neurons than the motor branch. Again, when the graft orientation was switched, the pattern did repeat and there were similar ratios of sensory/motor neurons in each branch. This pattern needs to be explored by further study, particularly with more femoral grafts in opposing orientations implanted into the sciatic nerve and femoral nerve to determine if this pattern holds true with more replicates and if it is caused by size disparity in the branches.

SFI is a measure of functional recovery in the sciatic nerve and is calculated using the overall toe spread, the intermediate toe spread and the print length of the injured foot. SFI has yet to be assessed in an injury of the 2.5 cm size and branching the CatWalk. The current study saw initial recovery between 2- and 4-weeks PO before there were only minor fluctuations in recovery. Previous reports using the CatWalk to assess SFI following injury have highlighted limitations of this technology which may impact the SFI scores (Bozkurt et al., 2008).

Specifically, Bozkurt et al. (2008), discussed that SFI values can be significantly diminished when rats move with faster speed, which impacts gait (Koopmans et al., 2007). This is a large consideration for this study in which rats moved quickly across the CatWalk platform and achieved what appeared to be relatively little sciatic function according to SFI scores. Additionally, calculating SFI early after injury is challenging and can be inaccurate due to paresis of the injured paw (Monte-Raso et al., 2008). Previous studies that utilize SFI have also found little improvement in later time points following injury in rat models that are much less severe (5 mm nerve gap with direct neurorrhaphy, 1 cm autograft, and 5 mm autograft) and complex (linear grafts) than the current study (Shenag et al., 1989; Lin et al., 2010; Nagao et al., 2011). The static sciatic index, which assesses function while standing still, would be a complementary measure to SFI to better dissect differences in behavioral outcomes.

Conclusion

This study compared the efficacy with which branched nerve grafts promote repair after ablation of a branch point. Results support that the use of branched grafts is a viable technique for the repair of branched nerve injuries as evidenced by regeneration down individual branches. Long term regeneration is not impacted by the harvest location of the graft or the orientation. This is a promising indication for the use of branched grafts to repair branched nerve defects.

Data availability statement

The raw data supporting the conclusions of this article will be made available by the authors, without undue reservation.

Ethics statement

This animal study was reviewed and approved by University of Wyoming IACUC.

Author contributions

JA helped design the study, performed the surgeries and animals care, collected data, analyzed data, and wrote and edited the manuscript. KR performed some surgeries, training, data acquisition, and edited the manuscript. BS assisted with animal care, acquired CMAPs and CatWalk data, and wrote and edited the manuscript. JB devised experiments, provided supplies and lab space, analyzed data, and wrote and edited the manuscript. All authors contributed to the article and approved the submitted version.

Funding

This work was supported by US Department of Defense grant W81XWH-17-1-0402, the University of Wyoming Sensory Biology COBRE under National Institutes of Health (NIH) Award Number 5P20GM121310, and the National Institute of General Medical Sciences of the NIH under the Award Number P20GM103432.

Acknowledgments

We thank Zhaojie Zhang, Director of the Jenkins Microscopy Facility for his assistance with imaging and BioRender for the use of their program to create **Figures 1, 2**.

Conflict of interest

The authors declare that the research was conducted in the absence of any commercial or financial relationships that could be construed as a potential conflict of interest.

References

- Avramut, M., and Achim, C. L. (2003). Immunophilins in nervous system degeneration and regeneration. *Curr. Top. Med. Chem.* 3, 1376–1382. doi: 10.2174/1568026033451871
- Bozkurt, A., Deumens, R., Scheffel, J., O'dey, D., Weis, J., Joosten, E., et al. (2008). Catwalk gait analysis in assessment of functional recovery after sciatic nerve injury. *J. Neurosci. Methods* 173, 91–98. doi: 10.1016/j.jneumeth.2008.05.020
- Bozkurt, A., Scheffel, J., Brook, G., Joosten, E., Suschek, C., O'dey, D., et al. (2011). Aspects of static and dynamic motor function in peripheral nerve regeneration: SSI and CatWalk gait analysis. *Behav. Brain Res.* 219, 55–62. doi: 10.1016/j.bbr.2010.12.018
- Brushart, T., Kebaish, F., Wolinsky, R., Skolasky, R., Li, Z., and Barker, N. (2020). Sensory axons inhibit motor axon regeneration in vitro. *Exp. Neurol.* 323:113073. doi: 10.1016/j.expneurol.2019.113073
- Brushart, T. M. (1988). Preferential reinnervation of motor nerves by regenerating motor axons. *J. Neurosci.* 8, 1026–1031. doi: 10.1523/JNEUROSCI.08-03-01026.1988
- Brushart, T. M. (1993). Motor axons preferentially reinnervate motor pathways. *J. Neurosci.* 13, 2730–2738. doi: 10.1523/JNEUROSCI.13-06-02730.1993
- Brushart, T. M., Gerber, J., Kessens, P., Chen, Y. G., and Royall, R. M. (1998). Contributions of pathway and neuron to preferential motor reinnervation. *J. Neurosci.* 18, 8674–8681. doi: 10.1523/JNEUROSCI.18-21-08674.1998
- Catala, M., and Kubis, N. (2013). Gross anatomy and development of the peripheral nervous system. *Handb. Clin. Neurol.* 115, 29–41. doi: 10.1016/B978-0-444-52902-2.00003-5
- Cinteza, D., Persinaru, I., Maciuceanu Zarnescu, B. M., Ionescu, D., and Lascar, I. (2015). Peripheral nerve regeneration - an appraisal of the current treatment options. *Maedica (Bucur)* 10, 65–68.
- Cui, J.-J., Wang, J., Xu, D.-S., Wu, S., Guo, Y.-T., Su, Y.-X., et al. (2022). Alexa fluor 488-conjugated cholera toxin subunit B optimally labels neurons 3–7 days after injection into the rat gastrocnemius muscle. *Neural Regen. Res.* 17:2316. doi: 10.4103/1673-5374.337055
- De Medinaceli, L., Derenzo, E., and Wyatt, R. J. (1984). Rat sciatic functional index data management system with digitized input. *Comput. Biomed. Res.* 17, 185–192. doi: 10.1016/0010-4809(84)90031-4
- Deleonibus, A., Rezaei, M., Fahradyan, V., Silver, J., Rampazzo, A., and Bassiri Gharb, B. (2021). A meta-analysis of functional outcomes in rat sciatic nerve injury models. *Microsurgery* 41, 286–295. doi: 10.1002/micr.30713
- Deumens, R., Jaken, R. J., Marcus, M. A., and Joosten, E. A. (2007). The CatWalk gait analysis in assessment of both dynamic and static gait changes after adult rat sciatic nerve resection. *J. Neurosci. Methods* 164, 120–130. doi: 10.1016/j.jneumeth.2007.04.009
- Ghnenis, A. B., Czaikowski, R. E., Zhang, Z. J., and Bushman, J. S. (2018). Toluidine blue staining of resin-embedded sections for evaluation of peripheral nerve morphology. *J. Vis. Exp.* 137:e58031. doi: 10.3791/58031
- Hirakawa, M., McCabe, J., and Kawata, M. (1992). Time-related changes in the labeling pattern of motor and sensory neurons innervating the gastrocnemius muscle, as revealed by the retrograde transport of the cholera toxin B subunit. *Cell Tissue Res.* 267, 419–427. doi: 10.1007/BF00319364
- Hurt, P., Walter, L., Sudbrak, R., Klages, S., Muller, I., Shiina, T., et al. (2004). The genomic sequence and comparative analysis of the rat major histocompatibility complex. *Genome Res.* 14, 631–639. doi: 10.1101/gr.1987704
- Irintchev, A. (2011). Potentials and limitations of peripheral nerve injury models in rodents with particular reference to the femoral nerve. *Ann. Anat.* 193, 276–285. doi: 10.1016/j.aanat.2011.02.019
- Isvoranu, G., Manole, E., and Neagu, M. (2021). Gait analysis using animal models of peripheral nerve and spinal cord injuries. *Biomedicine* 9:1050. doi: 10.3390/biomedicine9081050
- Jones, S., Eisenberg, H. M., and Jia, X. (2016). Advances and future applications of augmented peripheral nerve regeneration. *Int. J. Mol. Sci.* 17:1494. doi: 10.3390/ijms17091494
- Koopmans, G. C., Deumens, R., Brook, G., Gerver, J., Honig, W. M., Hamers, F. P., et al. (2007). Strain and locomotor speed affect over-ground locomotion in intact rats. *Physiol. Behav.* 92, 993–1001. doi: 10.1016/j.physbeh.2007.07.018
- Lin, K.-L., Yang, D.-Y., Chu, I.-M., Cheng, F.-C., Chen, C.-J., Ho, S.-P., et al. (2010). DuraSeal as a ligature in the anastomosis of rat sciatic nerve gap injury. *J. Surg. Res.* 161, 101–110. doi: 10.1016/j.jss.2008.10.020

Publisher's note

All claims expressed in this article are solely those of the authors and do not necessarily represent those of their affiliated organizations, or those of the publisher, the editors and the reviewers. Any product that may be evaluated in this article, or claim that may be made by its manufacturer, is not guaranteed or endorsed by the publisher.

Author disclaimer

The content is solely the responsibility of the authors and does not necessarily represent the official views of the US Department of Defense, NIH, or the University of Wyoming.

Supplementary material

The Supplementary Material for this article can be found online at: <https://www.frontiersin.org/articles/10.3389/fncel.2022.1055490/full#supplementary-material>

- Liu, W., Ren, Y., Bossert, A., Wang, X., Dayawansa, S., Tong, J., et al. (2012). Allotransplanted neurons used to repair peripheral nerve injury do not elicit overt immunogenicity. *PLoS One* 7:e31675. doi: 10.1371/journal.pone.0031675
- Löw, K., Orberger, G., Schmitz, B., Martini, R., and Schachner, M. (1994). The L2/Hnk-1 carbohydrate is carried by the myelin associated glycoprotein and sulphated glucuronyl glycolipids in muscle but not cutaneous nerves of adult mice. *Eur. J. Neurosci.* 6, 1773–1781. doi: 10.1111/j.1460-9568.1994.tb00570.x
- Madison, R. D., Archibald, S. J., and Brushart, T. M. (1996). Reinnervation accuracy of the rat femoral nerve by motor and sensory neurons. *J. Neurosci.* 16, 5698–5703. doi: 10.1523/JNEUROSCI.16-18-05698.1996
- Madison, R. D., Robinson, G. A., and Chadaram, S. R. (2007). The specificity of motor neurone regeneration (preferential reinnervation). *Acta Physiol.* 189, 201–206. doi: 10.1111/j.1748-1716.2006.01657.x
- Martini, R., Schachner, M., and Brushart, T. M. (1994). The L2/Hnk-1 carbohydrate is preferentially expressed by previously motor axon-associated Schwann cells in reinnervated peripheral nerves. *J. Neurosci.* 14, 7180–7191. doi: 10.1523/JNEUROSCI.14-11-07180.1994
- Martini, R., Xin, Y., Schmitz, B., and Schachner, M. (1992). The L2/Hnk-1 carbohydrate epitope is involved in the preferential outgrowth of motor neurons on ventral roots and motor nerves. *Eur. J. Neurosci.* 4, 628–639. doi: 10.1111/j.1460-9568.1992.tb00171.x
- Mikesh, M., Ghergherechi, C. L., Ramesh, S., Jagannath, K., Ali, A., Sengelaub, D. R., et al. (2018). Polyethylene glycol treated allografts not tissue matched nor immunosuppressed rapidly repair sciatic nerve gaps, maintain neuromuscular functions, and restore voluntary behaviors in female rats. *J. Neurosci. Res.* 96, 1243–1264. doi: 10.1002/jnr.24227
- Monte-Raso, V. V., Barbieri, C. H., Mazzer, N., Yamasita, A. C., and Barbieri, G. (2008). Is the sciatic functional index always reliable and reproducible? *J. Neurosci. Methods* 170, 255–261. doi: 10.1016/j.jneumeth.2008.01.022
- Morita, I., Kizuka, Y., Kakuda, S., and Oka, S. (2008). Expression and function of the Hnk-1 carbohydrate. *J. Biochem.* 143, 719–724. doi: 10.1093/jb/mvm221
- Nagao, R. J., Lundy, S., Khaing, Z. Z., and Schmidt, C. E. (2011). Functional characterization of optimized acellular peripheral nerve graft in a rat sciatic nerve injury model. *Neurol. Res.* 33, 600–608. doi: 10.1179/1743132810Y.0000000023
- Navarro, X. (2009). “Neural plasticity after nerve injury and regeneration,” in *International review of neurobiology*, eds G. Stefano, T. Pierluigi, and B. Bruno (Cambridge MA: Academic Press). doi: 10.1016/S0074-7742(09)87027-X
- Osimanjiang, W., Allgood, J. E., Van Sandt, R. L., Burns, D. T., and Bushman, J. S. (2022). Sexual dimorphism in lesion size and sensorimotor responses following spinal cord injury. *Front. Neurol.* 13:1308.
- Pan, D., Mackinnon, S. E., and Wood, M. D. (2020). Advances in the repair of segmental nerve injuries and trends in reconstruction. *Muscle Nerve* 61, 726–739. doi: 10.1002/mus.26797
- Parkkinen, S., Ortega, F. J., Kuptsova, K., Huttunen, J., Tarkka, I., and Jolkonen, J. (2013). Gait impairment in a rat model of focal cerebral ischemia. *Stroke Res. Treat.* 2013:410972. doi: 10.1155/2013/410972
- Bankhead, P., Loughrey, M. B., Fernández, J. A., Dombrowski, Y., McArt, D. G., and Dunne, P. D. (2017). Qupath: Open source software for digital pathology image analysis. *Sci. Rep.* 7:16878. doi: 10.1038/s41598-017-17204-5
- Roballo, K. C. S., and Bushman, J. (2019). Evaluation of the host immune response and functional recovery in peripheral nerve autografts and allografts. *Transpl. Immunol.* 53, 61–71. doi: 10.1016/j.trim.2019.01.003
- Roballo, K. C. S., Gigley, J. P., Smith, T. A., Bittner, G. D., and Bushman, J. S. (2022). Functional and immunological peculiarities of peripheral nerve allografts. *Neural Regen. Res.* 17, 721–727. doi: 10.4103/1673-5374.322445
- Safa, B., and Buncke, G. (2016). Autograft substitutes: Conduits and processed nerve allografts. *Hand Clin.* 32, 127–140. doi: 10.1016/j.hcl.2015.12.012
- Santos Roballo, K. C., Dhungana, S., Jiang, Z., Oakey, J., and Bushman, J. S. (2019). Localized delivery of immunosuppressive regulatory T cells to peripheral nerve allografts promotes regeneration of branched segmental defects. *Biomaterials* 209, 1–9. doi: 10.1016/j.biomaterials.2019.04.015
- Shenaq, J. M., Shenaq, S. M., and Spira, M. (1989). Reliability of sciatic function index in assessing nerve regeneration across a 1 cm gap. *Microsurgery* 10, 214–219. doi: 10.1002/micr.1920100315
- Siemionow, M., and Sonmez, E. (2007). Nerve allograft transplantation: A review. *J. Reconstr. Microsurg.* 23, 511–520. doi: 10.1055/s-2007-1022694
- Sunio, A., and Bittner, G. D. (1997). Cyclosporin A retards the wallerian degeneration of peripheral mammalian axons. *Exp. Neurol.* 146, 46–56. doi: 10.1006/exnr.1997.6484
- Toossi, A., Bergin, B., Marefatallah, M., Parhizi, B., Tyreman, N., Everaert, D. G., et al. (2021). Comparative neuroanatomy of the lumbosacral spinal cord of the rat, cat, pig, monkey, and human. *Sci. Rep.* 11, 1–15. doi: 10.1038/s41598-021-81371-9
- Vieira, W. F., Malange, K. F., De Magalhães, S. F., Dos Santos, G. G., De Oliveira, A. L. R., Da Cruz-Höfling, M. A., et al. (2020). Gait analysis correlates mechanical hyperalgesia in a model of streptozotocin-induced diabetic neuropathy: A CatWalk dynamic motor function study. *Neurosci. Lett.* 736:135253. doi: 10.1016/j.neulet.2020.135253
- Vrinten, D. H., and Hamers, F. F. (2003). ‘CatWalk’ automated quantitative gait analysis as a novel method to assess mechanical allodynia in the rat; A comparison with von Frey testing. *Pain* 102, 203–209. doi: 10.1016/s0304-3959(02)00382-2
- Wang, M. L., Rivlin, M., Graham, J. G., and Beredjikian, P. K. (2019). Peripheral nerve injury, scarring, and recovery. *Connect. Tissue Res.* 60, 3–9. doi: 10.1080/03008207.2018.1489381
- Watson, C., Paxinos, G., Kayalioglu, G., and Heise, C. (2009). Atlas of the rat spinal cord. *Spinal Cord* 238–306. doi: 10.1016/B978-0-12-374247-6.50019-5
- Werden, F., Grüssinger, H., Jaminet, P., Kraus, A., Manoli, T., Danker, T., et al. (2009). An improved electrophysiological method to study peripheral nerve regeneration in rats. *J. Neurosci. Methods* 182, 71–77. doi: 10.1016/j.jneumeth.2009.05.017
- Witzel, C., Rohde, C., and Brushart, T. M. (2005). Pathway sampling by regenerating peripheral axons. *J. Comp. Neurol.* 485, 183–190. doi: 10.1002/cne.20436
- Zhao, Y., Maharjan, S., Sun, Y., Yang, Z., Yang, E., Zhou, N., et al. (2020). Red fluorescent aunds with conjugation of cholera toxin subunit B (Ctb) for extended-distance retro-nerve transporting and long-time neural tracing. *Acta Biomater.* 102, 394–402. doi: 10.1016/j.actbio.2019.11.045



OPEN ACCESS

EDITED BY

Melissa R. Andrews,
University of Southampton,
United Kingdom

REVIEWED BY

Assunta Virtuoso,
University of Campania Luigi
Vanvitelli, Italy
Nathalie Sol-Foulon,
INSERM U1127 Institut du Cerveau et
de la Moelle épinière (ICM), France

*CORRESPONDENCE

Yan Wang
swallow-1113@163.com

SPECIALTY SECTION

This article was submitted to
Neurotrauma,
a section of the journal
Frontiers in Neurology

RECEIVED 26 April 2022

ACCEPTED 17 November 2022

PUBLISHED 16 December 2022

CITATION

Yuan Y, Wang Y, Wu S and Zhao MY
(2022) Review: Myelin clearance is
critical for regeneration after
peripheral nerve injury.
Front. Neurol. 13:908148.
doi: 10.3389/fneur.2022.908148

COPYRIGHT

© 2022 Yuan, Wang, Wu and Zhao.
This is an open-access article
distributed under the terms of the
[Creative Commons Attribution License
\(CC BY\)](https://creativecommons.org/licenses/by/4.0/). The use, distribution or
reproduction in other forums is
permitted, provided the original
author(s) and the copyright owner(s)
are credited and that the original
publication in this journal is cited, in
accordance with accepted academic
practice. No use, distribution or
reproduction is permitted which does
not comply with these terms.

Review: Myelin clearance is critical for regeneration after peripheral nerve injury

YiMing Yuan¹, Yan Wang^{1,2*}, ShanHong Wu¹ and
Ming Yue Zhao^{1,2}

¹Laboratory of Brain Function and Neurorehabilitation, Heilongjiang University of Chinese Medicine, Harbin, China, ²Department of Rehabilitation, The Second Affiliated Hospital of Heilongjiang University of Chinese Medicine, Harbin, China

Traumatic peripheral nerve injury occurs frequently and is a major clinical and public health problem that can lead to functional impairment and permanent disability. Despite the availability of modern diagnostic procedures and advanced microsurgical techniques, active recovery after peripheral nerve repair is often unsatisfactory. Peripheral nerve regeneration involves several critical events, including the recreation of the microenvironment and remyelination. Results from previous studies suggest that the peripheral nervous system (PNS) has a greater capacity for repair than the central nervous system. Thus, it will be important to understand myelin and myelination specifically in the PNS. This review provides an update on myelin biology and myelination in the PNS and discusses the mechanisms that promote myelin clearance after injury. The roles of Schwann cells and macrophages are considered at length, together with the possibility of exogenous intervention.

KEYWORDS

Schwann cell, myelin clearance, peripheral nerve injury, demyelination, autophagy, macrophages

Introduction

Injury to peripheral nerves leads to a series of molecular, cellular, and microstructural responses that promote their regeneration and functional recovery. Peripheral nerve regeneration may be hindered by slow organizational growth, degeneration of its distal segments, and impediments to its reinnervation. Regeneration is frequently insufficient and accompanied by negative clinical sequelae (1). While there has been substantial focus on clinical interventions designed to improve this process, the contributions associated with myelin clearance remain comparatively unexplored.

Lipid-rich myelin formed by Schwann cells (SCs) facilitates saltatory impulse transmission and provides trophic support to the peripheral nervous system (PNS) via radial sorting of its axons. SCs associate with and wrap around larger axons late in embryonic development to facilitate myelination that will be initiated postnatally. Regeneration of myelin is a critical aspect of any effective treatment for peripheral nerve injury (PNI). Remyelination is critical for effective repair after PNI and will be needed to provide new support for the PNS. Furthermore, myelin breakdown has been recognized as a key contributor to various peripheral nerve diseases.

Fragments generated by myelin breakdown obstruct axon regeneration. Myelin ovoids resulting from the destruction of the myelin sheath can be detected in SCs associated with degenerating axons (22). These ovoids contain numerous factors, including myelin-related glycoprotein (MAG) which can inhibit axon development (23, 24). Myelin debris at the lesion site results in local pressure and also impedes nerve repair (25). Jessen et al. reported that the PNS was able to undergo repair more effectively than the central nervous system (CNS) (26). This may be explained at least in part by its superior capacity for myelin removal (27). The results of several recent studies suggested that the removal of myelin debris is a prerequisite for effective nerve regeneration (28–30). Thus, an understanding of the mechanisms contributing to myelin removal from injured nerves will have broad implications for this process.

Earlier work has established that myelin breakdown occurs during the early stages immediately following nerve injury and is followed by the clearance of myelin debris. In this review, we will begin with a discussion of myelin formation. We will then discuss previous research and consider the results of recent studies that address the mechanisms involved in myelin removal. We will conclude with a discussion of the therapeutic implication of these findings.

The accumulation of myelin debris has a significant impact on nerve regeneration; this material is no longer useful and contains many inhibitory signals that prevent repair. Interestingly, and in contrast to the PNS, the CNS does not have satisfied mechanisms that promote effective myelin degradation (31). Myelin fragments can persist at the site of a CNS injury for months or even years where they serve to inhibit essential repair mechanisms (32). For example, Fujita et al. reported that MAG detected in CNS inhibits regeneration *via* its capacity to suppress tropomyosin receptor kinase (Trk) activity (33). In the nerve system, there is undoubtedly a balance between the

clearance of myelin and detrimental consequences that impede regeneration, and this relationship seems to be better regulated in PNS.

In this review, we focus on new insights directed at the earliest responses to nerve injury (Figure 1); established mechanisms and conventional insights into this process have been reviewed elsewhere (37). The article highlights new findings that address various mechanisms that drive myelin removal and concentrates on new perspectives of peripheral nerve regeneration based on the construction of a suitable microenvironment. We also discuss the potential impact of myelin removal in other neurological diseases.

The formation and function of myelin

Before discussing clearance, we need to have a full understanding of the mechanisms underlying myelin formation and function in PNS. Myelin is a lipid–protein complex derived from membranes of SCs (in the PNS) and oligodendrocytes (in the CNS) that forms a sheath that supports and protects individual axons (38), facilitates rapid transit of electrical signals, and provides critical nourishment. Myelin-providing (pro-myelin) SCs are generated from precursors that undergo three developmental shifts, including transitions from crest cells to SC precursors (SCPs), from SCPs to immature SCs, and from immature SCs to either pro-myelin SCs or non-myelinating (Remak) SCs. The pro-myelin SCs then undergo radial sorting; some of these cells go on to generate myelin sheaths (39, 40).

Myelin in the PNS is comprised of both lipids (70–80%) and proteins (20–30%) (41), the latter group including primarily myelin protein zero (MPZ), as well as myelin basic protein

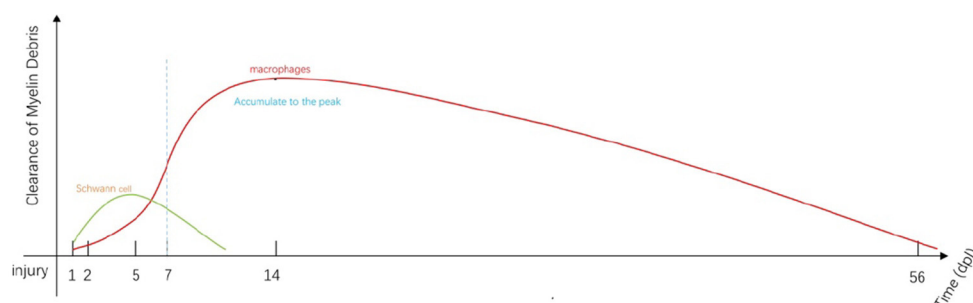


FIGURE 1

Immediately after injury, SCs and macrophages (including resident and early-stage infiltrating macrophages) begin to remove myelin debris (34). SC-mediated phagocytosis reaches a peak at approximately 5 days post-injury (dpi; green line). Most of the engulfment results from macrophage activity that increases from 5 to 7 dpi (red line). Macrophage-mediated phagocytosis reaches a peak at approximately 14 dpi and remains detectable at day 56 (35). Fibroblasts and neutrophils also contribute to myelin clearance at this stage (35, 36). The myelin fragments are ultimately cleared by localized apoptosis followed by transport by the lymphatics to the spleen.

(MBP) and peripheral myelin proteins 2 and 22 (PMP2/PMP22). Those proteins undergo upregulation at the start of myelination and provide the myelin sheath with a unique membrane structure. The interactions between these proteins and the phospholipid bilayer result in compact cytoplasmic leaflets. Upregulated expression of these myelin genes is regulated by the POU-associated transcription factor, Oct6 (SCIP), Brn2, the high-mobility group protein Sox10, and the protein Krox20/Egr2 (42).

Both extrinsic and intracellular signals regulate the process of myelination. Among these signals, neuregulin (Nrg)1 regulates nearly all aspects and functions of SCs (40). Similarly, laminin and laminin receptors modulate myelination *via* their role in promoting essential autocrine signals (43). Likewise, Gpr126 provides critical signals that promote myelination *via* its role in regulating signaling by cyclic adenosine monophosphate (cAMP) (44, 45). Myelination also relies on several downstream intracellular signaling pathways involving PI3K, PLC- γ , focal adhesion kinase (FAK), mitogen-activated protein kinase (MAPK), and Wnt/ β -Catenin (46–48). In addition, cAMP promotes and maintains myelination *via* both intracellular signaling as well as mechanisms that regulate its expression (49, 50).

Results from previous reports revealed that iron was required for myelin production and its maintenance in the CNS (51, 52). Results from more recent studies revealed that iron homeostasis is also required for myelin formation in the PNS; Santiago González et al. reported the divalent metal transporter 1 (DMT1) (53), heavy ferritin chain (Fth), and the transferrin receptor 1 (TfR1), which are factors that regulate iron absorption and storage, provide crucial contributions to SC maturation and myelin formation. Iron outflow also has an impact on myelin formation. The ferroxidase enzyme, ceruloplasmin (Cp), protects the PNS and regulates iron efflux, thereby modulating the maturation of SCs and axon myelination (54). Disorders of iron homeostasis can induce oxidative stress and SC injury (53, 54).

A comprehensive understanding of the composition of myelin and the mechanisms involved in its formation will be essential for our assessment of myelin clearance that takes place in response to nervous system injuries. We note that the factors and signals described earlier also play critical roles in regulating myelin removal after injury. Furthermore, the connections linking myelin formation and removal have important implications with respect to the treatment of PNI.

Negative regulation of myelination

Demyelination is a characteristic response to a peripheral nerve injury. Pro-myelin SCs activate a cellular program that leads to the disintegration of the myelin sheath.

Demyelination of injured peripheral nerves typically takes place *via* Wallerian degeneration (WD) that both negatively regulates myelination and leads to myelin degradation. Reduced expression of myelin-associated proteins may also contribute to rapid demyelination, as this response promotes SC proliferation, clearance of myelin debris, and nerve regeneration (9). We will thus review this process as the first step of the clearance program, as this approach can help us to understand the molecular mechanisms that promote the clearance of myelin sheath fragments (Figure 2).

Factors that regulate myelination

c-Jun

The transcription factor, c-Jun, is found at the core of the AP-1 complex and is involved in the formation of the myelin sheath (55). More recent evidence has elucidated the role of c-Jun-mediated activities that regulate the responses of denervated SCs after injury, notably the formation of regeneration tracks, support of neuronal survival, promotion of axon regrowth, and myelin clearance (56). Furthermore, c-Jun deletion resulted in diminished clearance of myelin fragments and delayed regeneration (56). Additional evidence revealed that diminished quantities of O-GlcNAc transferase (OGT), which is an enzyme associated with post-translational modifications that suppress c-Jun, also impaired the process of remyelination (57); this result also suggested that activated c-Jun was an essential component of the regeneration process. Results from additional studies revealed that AMP-activated protein kinase (AMPK) attenuated myelin gene expression and thus reduced myelin formation, which is also a response to the activation of c-Jun signaling (58). SC dedifferentiation, myelin clearance, and regeneration were all impaired in the absence of c-Jun (56, 59). While overexpression of c-Jun can also harm the repair, process, and moderate activation is required (60).

Sox2

The Sox2 transcription factor regulates the activities of Schwann cells. Earlier *in vitro* studies revealed that Sox2 negatively regulated both crest and stem cells and thus regulated the formation of myelin (61). Recent findings have revealed that Sox2 may have a specific impact on myelin produced in the PNS. Interestingly, sustained expression of negative regulators, including Sox2 and Id2, protected mice modeling Charcot-Marie-Tooth (CMT) 1B disease from both dysmyelination and the deleterious impact of mutated myelin-related proteins, including MPZ (62). Activation of SC-autonomous and SC-nonautonomous protective functions may be a key mechanism underlying this result.

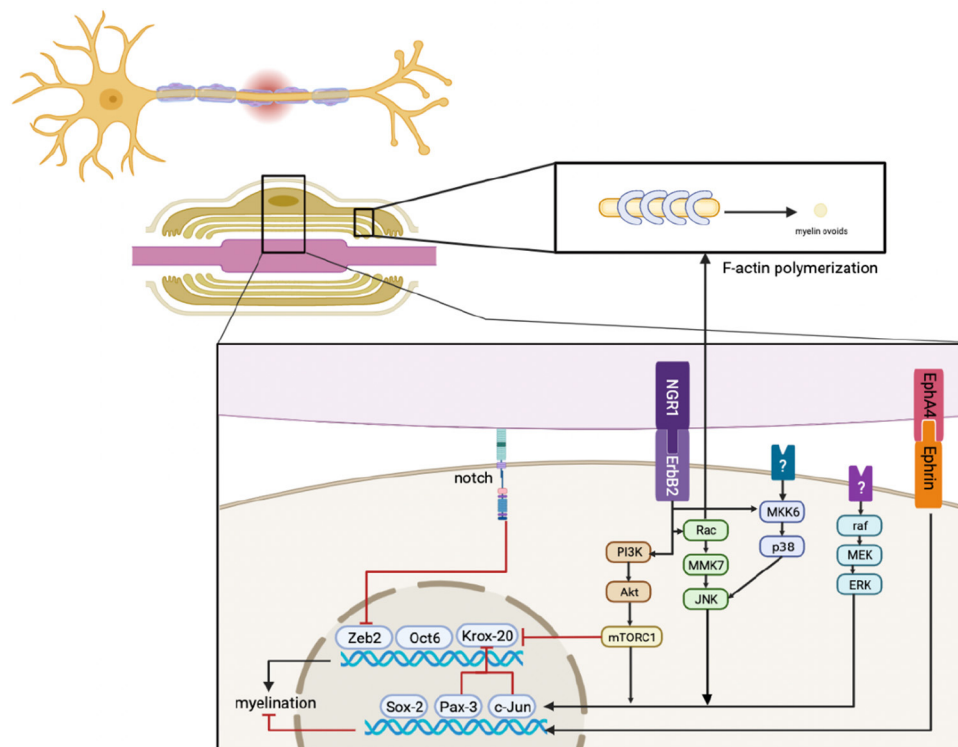


FIGURE 2

Immediately after injury, ErbB2, MAPK, PI3K, Notch, and EphA4 signals respond in SCs, their crosstalk, and the downstream signaling pathways that regulate factors that mediate myelination. This results in the downregulation of pro-myelinating genes, including Zeb2, Oct6, and Krox20, and the upregulation of negative regulatory factors, including Sox-2, Pax-3, and c-Jun. In addition, activated Rac promotes F-actin polymerization to generate myelin ovoids. Myelin is also cleared during this stage.

Pax-3

Pax-3 is a paired domain transcription factor expressed in the PNS and SCs that represses the induction of MBP by preventing the activation of the MBP promoter by cAMP (63, 64). Furthermore, Doddrell et al. (65) reported that Pax-3 strongly inhibited the cAMP-mediated induction of both Krox20 and Oct-6 in SCs as well as the expression of Sox-10. Interestingly, Pax-3 inhibited the expression of c-Jun and enhanced Notch-1 expression (65); collectively, these results suggested that Pax-3 inhibited Krox20 in a c-Jun-independent manner. However, while these factors are all involved in the repression of myelination, the precise mechanisms will need to be elucidated by further research.

Pathways regulating myelin gene expression after injury

MAPK and NRG1

ERK signaling is strongly and rapidly activated approximately 4 h after insult at both injured and distal sites (66, 67). Harrisingh et al. (67) described the role of the

Raf-ERK pathway in promoting SC dedifferentiation. As a first step, Raf activation suppresses the expression of myelin-associated proteins induced by cAMP (67, 68). Moreover, results from another previous study revealed that Raf overexpression generated in response to tamoxifen strongly activates Raf-ERK signaling and downregulates myelin-related gene expression in an uninjured nerve (69). Sustained activation of ERK also resulted in morphological defects, restricted regeneration, and impaired functional recovery, although rapid demyelination was observed (70).

Crosstalk between NRG1 and MAPK signaling pathways promotes demyelination and is a crucial factor involved in the migration of crest cells and the generation of mature SCs, as well as maintaining appropriate myelin thickness (71–73). Although NRG1 promotes both proliferation and the formation of myelin (50), recent results suggest that NRG1 may also promote reductions in the concentration of myelin fragments (73). The role of Rac-MAPK in the processes underlying demyelination is somewhat better clarified and is regulated by Ngr1/ErbB2 signaling (74, 75). Its intracellular target, MAPKK7 (MKK7), is upstream of JNK and was reported to induce the expression of c-Jun as opposed to ERK (76). The net result was the

downregulation of myelin gene expression at the distal site of an injured nerve.

Yang et al. reported that p38 MAPK was responsible for NRG1-mediated downregulation of myelin as well as the blockade of Krox20 expression. Results from this report also revealed that activated MKK6, which is a direct and specific upstream activator of p38 MAPK, also promoted demyelination (77).

Several additional factors related to this pathway were also found to delay myelination. Among these, bone morphogenetic protein (BMP)7 limited the formation of myelin sheath during development (78). Dummula et al. reported that the inhibition of BMP expression resulted in myelin preservation in the CNS; these events also had an immediate impact on the maturation of oligodendrocyte precursor cells and myelin formation (78). Recent evidence suggests that BMP family proteins exhibit a similar function in PNS. Results in this report revealed that BMP4 was upregulated beginning at 12h after injury and reached peak expression at 24h; expression then decreases continuously thereafter (79), paralleling demyelination. Further analysis revealed that BMP resulted in reductions in cAMP-induced expression of myelin genes, potentially due to its capacity to target the p38MAPK/c-Jun axis. Similarly, fibroblast growth factor 21 (FGF21) was originally identified as a factor that promoted remyelination in CNS (80). However, recent results suggest that FGF21 has completely different functions in PNS, specifically those resulting in the repression of myelin-related genes (81). The results from this report revealed that negative regulation secondary to FGF21 was mediated by the p38 mitogen-activated protein kinase (MAPK)/c-Jun axis. Zhang et al. reported that the expression of FGF21 in developing SCs was diminished in the presence of dibutyl-cAMP, thus suggesting dynamic regulation of myelin production (81). SCs in the PNS can synthesize and secrete FGF21 which extends its impact beyond the paracrine observed in the liver. Therefore, FGF21 and BMP7 may be among the critical negative regulatory factors involved in myelination after nerve injury. Interestingly, Wang et al. reported the increased expression of genes associated with immature SCs and decreased expression of genes associated with mature SCs in FGF9-gene-deleted mice (82). Overall, these results suggest that FGF9 may also seem to be involved in the process of myelin degeneration.

The intracellular GTPase Rac regulates actin polymerization and is a component of an essential pathway involved in the fragmentation of myelin (74, 83). Myelin ovoids formed during the early stages of WD may be responsible for the SC-mediated removal of compact myelin sheath material (84). After an injury, WD begins with the stereotypic fragmentation of myelin sheath into myelin ovoids at the Schmidt–Lanterman cleft (SLC), which is an area that contains non-compact myelin sheath material. Then, the structure of the SC cytoskeleton changes considerably. Although the SLC features atypical adherens junctions (AJs) (48, 85), the molecular nature of SLC appears to parallel those,

and polymerization of new actin filaments occurs after injury and promotes the degeneration of both AJs and E-cadherin, thereby inducing the myelin fragmentation (74). Activated Rac GTPase localizes to the SLC and regulates actin polymerization. By contrast, inhibition of actin polymerization also suppressed the formation of myelin ovoids and the degeneration of E-cadherin. Thus, we conclude that new F-actin that polymerizes after WD promotes the clearance of myelin sheath material (83).

Notch signaling

Notch is a transmembrane receptor protein that is cleaved to generate a Notch intracellular domain (NICD) after combining it with its ligand, Jagged-1. Notch signaling is a central pathway in developing invertebrates that are upregulated in response to Sox-2 and downregulated in response to Krox20 signaling. NICD preserves myelination and induces its expression (50).

Results from previous research revealed that activated Notch pathways regulated demyelination and proliferation of SCs (86); engineered overexpression of NCID results in rapid demyelination of injured nerves (87). Wang et al. reported that forced overexpression of NCID promotes peripheral nerve regeneration *via* pathways that promote accelerated demyelination (82). Moreover, Notch acts as the inhibitor of Zeb2 (88) and is thus involved in another essential pathway associated with myelin regeneration (89).

A recent study reported that post-translational sumoylation negatively regulates angiogenesis *via* its impact on Notch signaling (90). Accordingly, one might speculate that sumoylation might also have a negative impact on myelination *via* its capacity to target the Notch signaling pathway in SCs (91). Sumoylation may also inhibit Oct6 and Krox20 (11), although the impact of these modifications on myelination remains unexplored.

PI3K-Akt-mTORC1

mTORC1 is a central modulator of numerous anabolic reactions and promotes myelination in the PNS (60). Interestingly, mTORC1 undergoes transient activation after injury and suppresses myelination (92). mTORC1 is activated in SCs after injury *via* NRG1-PI3K-Akt signaling that suppresses myelination rather than promoting regeneration (53, 93, 94). Activated mTORC1 has no impact on macrophage recruitment (60). mTORC1 also promotes demyelination by inhibiting Krox20 and activating c-Jun (60, 93). However, mTORC1-mediated demyelination was not enhanced *via* the additional activation; this may be due to feedback inhibition on the PI3K-Akt pathway (94). Over-activation of mTORC1 also resulted in delayed regeneration; this dual function may be a new target for therapeutics designed to combat nervous system diseases.

Neuregulin1

Neuregulin1/ErbB2 signaling pathways are involved in crosstalk with MAPK and PI3K and regulate demyelination. NRG1 is crucial to the formation of glia and the migration of crest cells as well as the formation of mature SCs and mechanisms that control myelin thickness (71–73). The results of several previous studies revealed that NRG1/ErbB signaling could target the bZIP transcription factor Maf, thereby limiting the formation of myelin *via* its impact on cholesterol levels (57, 95). Therefore, NRG1 signaling is strongly connected to myelin clearance.

Recent reports have revealed that the expression of soluble NRG1 changes in response to peripheral nerve injury and ultimately downregulates the expression of myelin-related genes including Pmp22, Serinc5, Ndr1, Fa2h, Mal, Rxrg, and Krox20, in response to injury and activation of c-Jun (96). NRG1 responses during the first stage of clearance regulated myelin-associated gene expression. By contrast, NRG1 promotes myelin regeneration during the following stages (and also during development); these results suggest that NRG1 also acts as a dynamic regulator that stabilizes these processes with respect to the pathophysiological responses of the PNS. The interactions between these mechanisms permit myelin clearance to proceed.

The NRG1 type III (NRG1 III) isoform positively regulates the formation of myelin and radial sorting together with input from laminin $\alpha 2\beta 1\gamma 1$ (Lm211) (97, 98). Recently, laminin $\alpha 2\beta 1\gamma 1$ was identified as playing a negative role in the regulation of myelin formation in SCs (99). Likewise, tumor necrosis factor (TNF)- α -converting enzyme (TACE; also known as ADAM17) was found to cleave NRG1 III within its epidermal growth factor domain which then negatively regulates the formation of the myelin sheath (100).

EphA4

Eph/Ephrin is an important neuronal mediator that is responsible for glial activation, axon guidance and regeneration, and synapse plasticity and formation (101), as well as the regulation of myelin formation (102). EphA4 regulates CNS myelination *via* the ephrin-A1-EphA4 pathway (103). More recent research suggests that Eph4 negatively regulates the formation of myelin in SCs (104). The results of this study revealed upregulation of EphA4 until 14 days after injury; expression of both MAG and MPZ decreased after peripheral nerve injury, consistent with a role for EphA4 in inhibiting myelin sheath formation. The observed suppression of remyelination may be the result of SC proliferation during the early phases after injury and suppression of the differentiation of SCs at a later stage (40, 104, 105). Although this mechanism inhibits regeneration for an extended period (until 28 days) after injury, its potential to accelerate myelin clearance must also be considered. Collectively, these results suggest that appropriate negative regulation of myelination is beneficial to

the regenerative process. Although the mechanisms remain to be clarified, factors that regulate the expression of EphA4 may emerge as new targets for drugs designed to promote myelin removal.

Transient receptor potential vanilloid 4 channels

Transient receptor potential vanilloid 4 is a non-specific calcium-permeable cation channel that is expressed widely and activated throughout the nervous system. One recent study revealed that TRPV4 promoted regeneration *via* demyelination of static nerves 2 to 14 days after injury (106). Interestingly, Remak SCs express high levels of TRPV4. Notably, TRPV4 gene-deleted mice exhibit delayed demyelination, thereby repressing nerve regeneration and delaying functional recovery. Moreover, the expression of TRPV4 undergoes a significant increase and returns to normal levels at 21 days due to the rapid myelination that takes place during the stage to follow (106). TRPV4-mediated alterations in calcium flux may have an impact on this process (107, 108). Therefore, TRPV4 and/or related calcium channels may be new targets used to treat PNI.

Because demyelination and regeneration are temporally correlated to one another, demyelination may be one factor contributing to the mechanism underlying nerve regeneration. WD and inhibition of myelin regeneration at early stages both have a positive impact on myelin clearance. Furthermore, some signals are dual-functioning with respect to myelin generation; these signals might be explored as a means to promote more effective regeneration. However, the basis of these interactions and/or synergy needs to be investigated further to promote effective treatments of neurological diseases.

Autophagy and myelin clearance

Autophagy is an important pathway used to dispose of and ultimately recycle disordered proteins and discarded cellular structures and is critical for maintaining cell stability (109). At its most basic level, autophagy is necessary to preserve the integrity of cellular structures. The process involves five main steps, including (1) initiation and nucleation, (22) elongation of the membrane, (23) cargo sorting, (24) fusion of the mature autophagosome with lysosomes, and (25) nutrient recycling and renewal (110). Autophagy is one of the critical processes used by SCs to clear tissue debris that accumulates after PNI.

Autophagy in SCs: A crucial process

The results of a recent study by Jang et al. (111) revealed that the primary myelin ovoid contains a fluid-filled axoplasm with a compact myelin sheath and scanty abaxonal cytoplasm

that form P (proximal)-fibers. The P-fibers were eventually overtaken by D(degeneration)-fibers, which have been described as hypertrophic SCs that contain several small myelin vesicles associated with the process of degeneration. Agents that inhibit the function of lysosomes delay the transition from P- to D-fibers. These findings revealed that autophagy is essential for the timely clearance of the myelin sheath after PNI; interestingly, this process cannot be completely accomplished by macrophages recruited from circulation. Thus, autophagic SCs are needed to promote the earliest stages of myelin clearance, myelin regeneration, and scar reduction (112).

Autophagy in SCs is activated during development and suppressed once the cells reach a mature stage (111, 113). Although autophagy will be suppressed at maturity, SCs still utilize this function to eliminate unnecessary cytoplasm, thereby maintaining homeostasis (Figure 3).

SCs will rapidly switch their transcriptional program to a repair state that promotes the early stages of myelin clearance in response to PNI. Activation of autophagy is a critical component of this transformation (114). Autophagic clearance mechanisms improve the microenvironment, provide basal energy for SC survival (104), and prevent the emergence and recurrence of neuropathic pain (115). Notably, lipids represent 70–80% of the composition of peripheral myelin (116) and lipid droplets have been detected as autophagic cargo (117). Therefore, autophagy is a crucial process involved in nerve repair; impaired autophagy results in reductions in both myelin degradation and remyelination (118).

Main regulators of autophagy and autophagic flux

Nerve growth factor

Li et al. reported that levels of autophagy-related (ATG)-7, ATG-5, Beclin-1, and LC3 proteins all increased in response to treatment with exogenous nerve growth factor (NGF) (119). In contrast to the traditional perspective, recent results suggest that the administration of NGF upregulates autophagic activity in SCs, most likely *via* the p75NTR/AMPK/mTOR pathway. In addition, NGF binds to p75NTR and activates small GTPases to increase the expression of c-Jun. Augmented expression of c-Jun might inhibit the myelination as described earlier. Therefore, the pathways linking NGF and autophagy specifically in SCs may represent novel therapeutic targets for drugs designed to promote nerve regeneration.

SIRT1/Hypoxia-inducible factor 1 α

The NAD-dependent deacetylase, Sirt1, plays a critical role in regulating autophagy (120). Recent evidence suggests that

overexpression of Sirt1 promotes regeneration and functional recovery *via* the activation of autophagy (121). Sirt1 promotes mTOR-independent autophagy *via* the activation of the downstream factor, Hif1 α (121). Interestingly, these results suggest that Sirt1 might drive autophagy directly *via* its capacity to inhibit both mTOR and FOXO (122). Although the precise mechanism involved in this pathway requires further elucidation, it may also represent a target for one or more novel treatment strategies.

CXCL12

CXCL12 is one of the most widely studied chemokines and binds to its specific receptor, CXCR4/7. Administration of CXCL12 elicited positive therapeutic effects in various nervous system diseases (123–126). Of note, CXCL12 enhances autophagy after nerve injury and thus promotes nerve regeneration (126). Specifically, recombinant CXCL12 enhances autophagy in SCs in a time-dependent manner and inhibits the PI3K/AKT/mTOR pathway. Thus, the increased levels of autophagy induced by CXCL12 may be related to its capacity to inhibit mTOR (126).

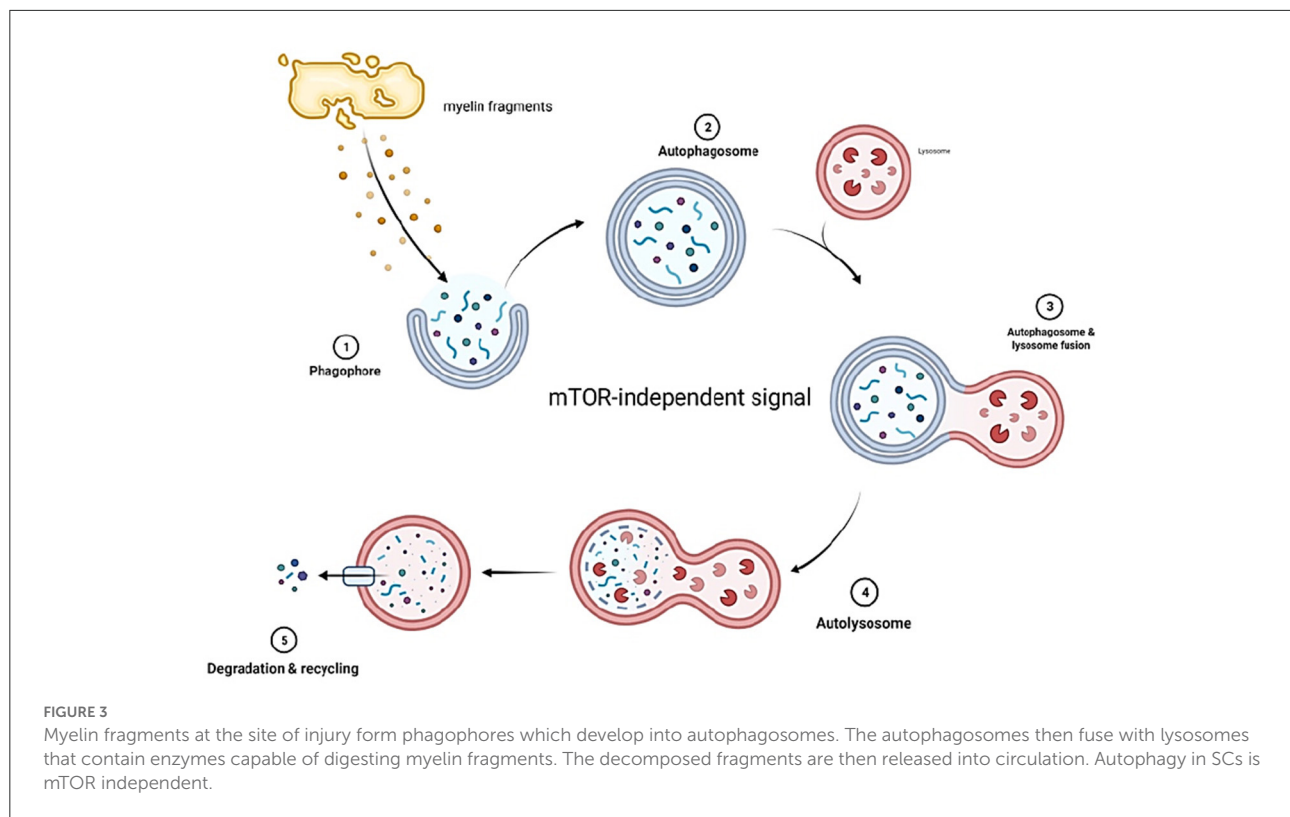
Calcineurin

Calcineurin is a calcium-dependent serine/threonine protein phosphatase that is composed of calcineurin A (CnA) and calcineurin B (CnB). Cn was originally identified as a regulator of autophagy in lysosomal biogenesis (127). Recent findings reveal that Cn regulates autophagy *via* the activation of a calcium signaling pathway and transcriptional factor EB (TFEB) (127, 128). Additional evidence documented the role of exogenous trehalose in inducing autophagy in models of motor neuron degeneration (129); Reed et al. reported that CnB might play a critical role in this pathway. Furthermore, CnB gene-deleted mice exhibited a reduced autophagic influx, delayed myelination, and altered radial sorting (130). CnB ablation also impaired translocation to the nucleus, suggesting that Cn was capable of activating autophagy in SCs *via* the actions of TFEB.

Interestingly, Cn had no significant impact on the development of myelin (130); likewise, most of the other factors that regulate myelin clearance are also not closely associated with the process of myelin formation.

Vacuolar protein sorting family

PI3K vacuolar protein sorting 32 (Pik3c3) contributes to the synthesis of PI3P and is thus crucial for membrane transport and autophagy. The complex nature of PI3P regulation has been considered one of the mechanisms associated with CMT



disease. In one recent study, Logan et al. found that mature autophagosomes could not be formed in Vps34-deficient SCs in the absence of PI3P, and thus the process of autophagy would be destroyed (131).

Wang et al. have recently suggested the existence of an ESCRT-Vps4-autophagy pathway that regulates the clearance of cellular debris (132). Vps4 is an ESCRT accessory protein that plays a vital role in regulating axonal autophagic flux. Cellular levels of Vps4 were found to influence the autophagic flux in experiments performed in *Drosophila melanogaster*. Subsequent studies performed in mammalian models revealed that Vps4 provided support to the autophagic flux but was not critical for its induction (132). Vps4 was consumed rapidly after injury and may induce the accumulation of autophagosomes and thus impair cellular organization. Therefore, we speculate that Vps4 may have the capacity to promote nerve regeneration via the regulation of autophagy and thus the clearance of myelin debris.

FGF

The basic fibroblast growth factor (bFGF) is a major neurotrophic factor secreted by SCs as well as neuronal cell populations. High levels of bFGF expression can promote numerous functions associated with PNI, including

neuroprotection, neurogenesis, and the generation of an appropriate microenvironment (133, 134). Notably, recent studies revealed that the upregulation of bFGF promotes myelin clearance *in vitro* via the maintenance of an effective autophagic flux at the early stages after PNI (135). Additional studies suggested that bFGF most likely targets the TFEB pathway (135).

In addition, recent evidence suggests that fibroblast growth factor 1 (FGF1) elicits its protective and regenerative effects on SCs due to its capacity to regulate autophagy via peroxiredoxin (PRDX1), possibly in association with the Wnt pathway (136).

Unlike the classical activation of autophagy, which relies on the inhibition of the mTOR pathway, autophagy in SCs is activated by an mTOR-independent mechanism that is regulated by the actions of ceramides on the JNK/c-Jun pathway (114, 118, 137). Activation of this pathway may be synergistic with the inhibitory effect of c-Jun on myelin-associated protein expression in response to acute injury. Interestingly, mTORC1 is necessary for myelin clearance during the post-injury period via its role in promoting the dedifferentiation of SCs and increasing the expression of c-Jun, thereby inhibiting the expression of myelin-related proteins (60). Collectively, these findings may explain how SC-mediated autophagy occurs via an mTOR-independent mechanism.

Other SC-associated mechanisms that promote myelin clearance

TAM receptor tyrosine kinases

Tyros3, AXL, and Mer are among the TAM receptors. Members of this family of receptor tyrosine kinases promote SC-mediated phagocytosis *via* mechanisms that are similar to those used by macrophages. Interestingly, mouse model strains with defective autophagy remain capable of debris clearance over an extended period. These observations imply the existence of other pathways that can compensate for one or more autophagic defects. Recent evidence from mouse models of PNI suggests that SCs may promote clearance *via* TAM receptor (Axl/Mertk)-mediated phagocytosis (138). Clearance of myelin debris was impaired in mice devoid of these receptors.

Transcription factor nuclear factor erythroid-2-related factor 2

Transcription factor Nrf2 is activated in response to oxidative stress that develops after PNI. Oxidative stress typically results from a crush injury or chronic neuronal constriction; reactive oxygen species (ROS) are also produced after a transection injury (139–141). Nrf2 is held in the cytoplasm by its Kelch-like ECH-associated protein 1 (Keap1) inhibitor domain. Gene expression is activated *via* its antioxidant response elements (AREs) (142). When compared to wild-type mice, Nrf2-deficient strains were present with more myelin residue, lower levels of macrophage infiltration, and weak recovery of the neuromuscular junction. Thus, there may be a critical role for a Keap1-Nrf2-ARE pathway (143), and Nrf2 may be a crucial factor involved in promoting the timely clearance of myelin fragments.

Macrophages

After PNI, SCs will call on local macrophages and recruit cells from the peripheral circulation to assist with cleaning the microenvironment. Both resident and infiltrating macrophages provide critical contributions to this process (144) (Figure 4).

Contribution of resident and infiltrating macrophages

Resident macrophages

Macrophages that are resident cells in peripheral nerves respond to injury and also play an active role in the early stages of peripheral nerve diseases (35, 145). Similar to SCs, resident macrophages are capable of phagocytosis, albeit to a more limited degree (23, 34). However, it is critical to recognize

that all resident macrophages do not respond to all injuries. For example, a recent study by Ydens et al. revealed that primarily endoneurial macrophages respond to nerve crush injury (146). In addition to debris removal, resident macrophages secrete monocyte-attracting chemokines and can thus recruit additional macrophages and enhance debris clearance (36).

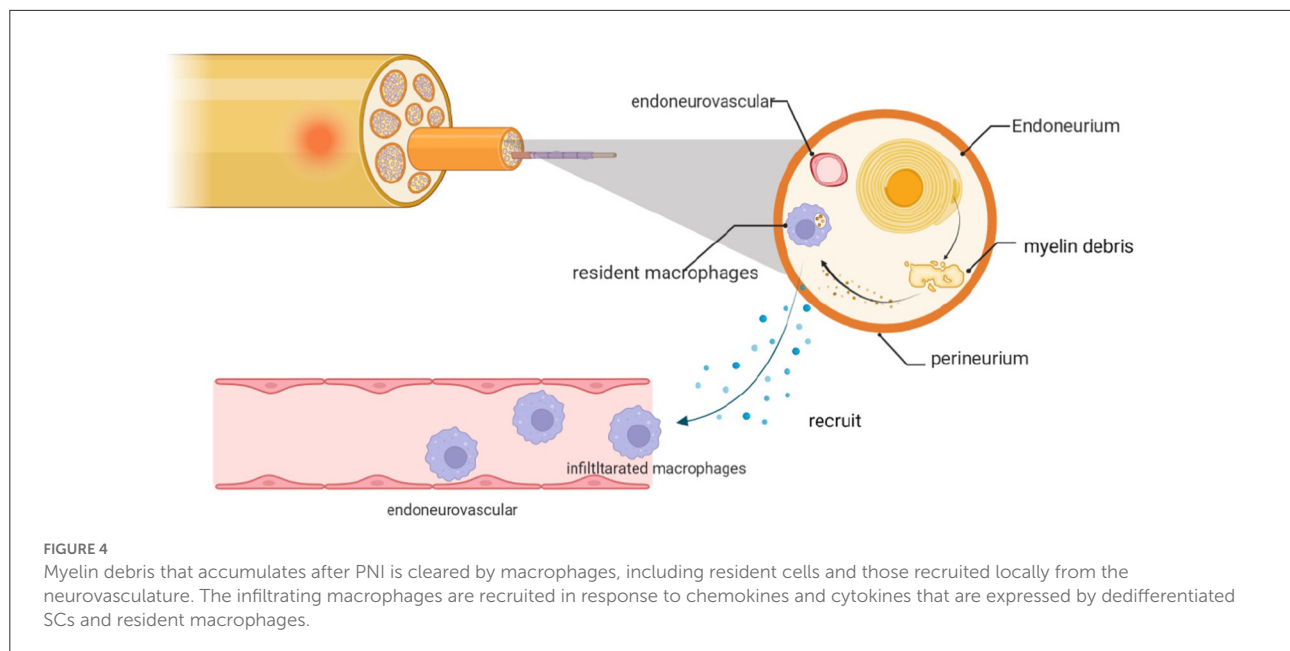
Infiltrating macrophages

More efficient macrophage recruitment and activation results in improved myelin clearance. Within the first 2 to 3 days after the disruption of the endoneurovascular, macrophages are recruited to and infiltrate the injury site. Macrophage accumulation reaches a peak at approximately 14 days post-injury (36). Circulating macrophages are attracted to the site of injury by inflammatory cytokines and chemokines, including TNF- α , interleukin (IL)-1 α , IL-1 β , chemokine C-C motif ligand 2 (CCL2), leukemia inhibitory factor (LIF), and pancreatitis-associated protein III (PAP-III) (36, 138, 147). Galectin-1 and galectin-3 are also critical factors involved in macrophage accumulation (147, 148); these mediators are expressed in SCs, nerves, and fibroblasts. Infiltrating macrophages also produce CCL2, TNF α , IL-1 α , and IL-1 β that collectively serve to augment recruitment and phagocytosis. Decomposition of the blood-nerve barrier (BNB) which isolates the nerve following the recruitment of macrophages is induced by Raf/ERK signaling in dedifferentiated SCs (69). A full discussion of several related mechanisms involved in the regulation of macrophage recruitment and activation is included in the sections to follow.

Macrophages associated mechanisms promoting myelin clearance

Complement system

The complement system plays a critical role in modulating the impact of macrophages responding to a PNI. After an injury, the complement system can be activated through either classical or alternative pathways (149, 150). Complement component 3 (C3) and its receptor, complement receptor 3 (CR3), are central mediators of myelin clearance. CR3 expressed on the macrophage surface binds to the degenerating myelin sheaths and initiates phagocytosis (151). Phagocytosis is delayed in cells that have been treated with soluble (s)CR1, which is an inhibitor of both the classical and alternative pathways of complement activation (150). Recruitment and activation of macrophages are also suppressed in C3- (152), C5-, and C6-deficit mice (150, 153); myelin seems to remain intact in the C6-deficient strain (150). Collectively, these results suggest that the complement system contributes directly to SC- and macrophage-mediated myelin clearance.



Calcium-binding proteins S100A8 and S100A9

Calcium-binding proteins S100A8 and S100A9 activate inflammation and may initiate an acute phase response and a chemotactic gradient that precedes the main inflammatory response (154). Both S100A8 and S100A9 are upregulated in response to injury, specifically in both proximal and distal segments in nerve transection models. As these proteins are both toll-like receptor (TLR)4 ligands (155), their expression results in the induction of additional pro-inflammatory genes in SCs, including partial chemokines, inflammatory cytokines, and matrix metalloproteinases. These factors result in the infiltration of circulating macrophages at the injured site (154).

Toll-like receptors

Toll-like receptors (TLRs) are strongly induced in response to acute injury and play essential roles in the PNS (29). TLRs are expressed on the surface of resident macrophages and can be activated by endogenous ligands that initiate an innate immune response. Mice devoid of TLR2, TLR4, or myeloid differentiation factor 88 (MyD88) exhibited diminished macrophage recruitment due to impaired expression of CCL2 and IL-1 β compared with their respective wild-type strains (156). The activation and recruitment of macrophages are augmented in response to the administration of TLR agonists, although this mechanism is impaired in mice that are TLR or TLR-signaling deficient. For example, Vallières et al. (157) reported that systemic injections of the TLR4 agonist, lipopolysaccharide (LPS), increased

both macrophage recruitment and phagocytosis. TLRs respond to both pathogen-associated molecular patterns (PAMPs) (158) and to nonpathogenic ligands, including necrotic cells, heat shock proteins (HSPs 60 and 70), and extracellular matrix (ECM) components (159) that typically accumulate and promote inflammation at the site of a nerve injury site (160). TLR3, TLR4, and TLR7 also contribute to the immune surveillance of the PNS (29). Overall, TLRs provide critical signals that permit the PNS to respond to injury by activating macrophages and initiating myelin clearance.

G protein-coupled receptor Gpr126/Adgrg6

Gpr126/Adgrg6 has been characterized as a critical mediator of nerve development (161) and a regulator of myelin sheath formation (162). However, recent evidence suggests that this receptor plays an essential role in the recruitment of macrophages and ultimately myelin regeneration. Mogha et al. reported that Gpr126 contributed to the regulation of chemokines and TNF- α ; levels of downstream targets, including CCL2, CCL3, and CXCL10, are reduced in Gpr126 deficit mice (163). These results suggest that the relationship between Gpr126 and chemokines has a significant impact on the regulation of macrophage recruitment. Notably, c-Jun, a factor known to be involved in regeneration, is upregulated in Gpr126-deficient mice. Therefore, we speculate that efforts to regulate Gpr126 may lead to new strategies for the treatment of PNI (27, 164) and that the Gpr126/Adgrg6 receptor may be targeted to

promote the recruitment of macrophages and clearance of myelin debris.

Serum amyloid A

Serum amyloid A is a major component of the acute phase response to injury and infection that induces the production of pro-inflammatory chemokines. While SAA is synthesized primarily in the liver, the generation of SAA at extrahepatic sites may serve to regulate local inflammatory responses (165). SAA can be synthesized in SCs in response to injury and can induce the production of chemokines CCL2 and CCL12. SAA also has functions that are similar to those of chemokines and provides crucial contributions to macrophage recruitment. Expression of SAA is suppressed in IL-6-deficit mice in association with reduced levels of CCL2; these results suggest that SAA may be a key modulator of IL-6-mediated induction of this chemokine. Results from recent reports reveal that SAA is upregulated in SCs 3 days after injury (166) and that this response is significantly diminished in IL-6 gene-deleted mice. Collectively, these results suggest that IL-6 plays an essential role in SAA expression induced in response to injury (166) and that the IL-6-SAA-CCL2 pathway may be a new target that can be exploited therapeutically to regulate macrophage recruitment.

Apolipoprotein D

Apolipoprotein D is a glia-derived apolipoprotein that is required for a timely and effective response to injury (167, 168). As reported in a previous study, the role played by ApoD in response to nerve injury is associated with the dedifferentiation SCs (169). Myelin clearance and regeneration are delayed in injured nerves from ApoD-deficient mice; these results suggest that ApoD may play a crucial role in promoting myelin clearance. The report further demonstrated that the number of macrophages at the injury site was related to levels of ApoD, which in turn had a substantial impact on myelin clearance (169). The rates of both macrophage recruitment and myelin clearance were reduced in ApoD gene-deleted mice. Expression of the effector molecule, galectin-3, was also influenced by ApoD (169). The results of this study suggested a negative feedback mechanism in which ApoD regulated the production of factors associated with TLR activation, including CCL2 and TNF- α , and thus controlled for the potential over-recruitment of circulating macrophages (169). ApoD also helps to promote efficient myelin degradation; while myelin-positive ApoD-deficient macrophages accumulate more rapidly, these cells accumulate larger myelin particles and require more time to degrade MBP and MAG (169). Overall, the main impact of ApoD on myelin clearance relates to its capacity to recruit and activate macrophages and to promote autophagy *via* Becl1 (168). Thus, ApoD is another potential target that might be developed for new treatment strategies.

Sox2

The transcription factor, Sox2, limits the myelination of SCs both *in vitro* and *in vivo* *via* its capacity to suppress Krox20 (170). Sox2 also promotes clearance of myelin debris *via* its capacity to promote macrophage recruitment of macrophages. Long-term expression of Sox2 results in a persistent inflammatory state. Interestingly, while overexpression of Sox2 promotes both proliferation and radial sorting of SCs, it also limits SC-mediated myelination and thus inhibits functional recovery in the PNS (171). While these findings may seem contradictory, they can be understood in light of the development of PNS. Thus, Sox2 may also be a critical therapeutic target *via* strategies that precisely regulate its expression based on the time elapsed after the acute injury.

Fibroblast growth factor 9

Fibroblast growth factor 9 contributes to the recruitment of M1 macrophages and macrophage recruitment is diminished in FGF9-deficient mice. Ablation of FGF9 also limited the accumulation of CD68-positive and CD86-positive macrophages (172). Consequently, we speculate that FGF9 is a critical factor involved in clearing myelin debris after a PNI.

Phospholipase A2 family

The phospholipase A2 enzyme family includes a calcium-dependent group IVA (GIVA cPLA2) and a calcium-independent group VIA (GVIA iPLA 2). PLA2s regulate phospholipid metabolism, membrane turnover, host defense, and signal transduction (61, 173); these activities have been characterized in the PNS (174). PLA2s play important roles in regulating the metabolic activities of infiltrated macrophages. SCs express both group IVA and group VIA PLAs approximately 6 h after injury. López-Vales et al. (175) reported diminished expression of IL-1 β and CCL2 mRNA in nerves devoid of group IVA and group VIA PLA2s in association with a reduction in the number of macrophages. Therefore, this mechanism also needs to be considered as a way to regulate macrophages.

Adhesion molecules

Intercellular cell adhesion molecule-1 (ICAM-1) is a member of the immunoglobulin superfamily that is upregulated in SCs and venous endothelial cells in the nerve tissue that promotes macrophage recruitment (176). ICAM-1 is upregulated in the early stages immediately after injury. Ablation of ICAM-1 results in decreased recruitment of macrophages in response to a transection injury as well as the accumulation of more myelin debris (177). However, this result was not confirmed in experiments performed using a different strain of ICAM-1 gene-deleted mice (178). Further study will be needed to confirm or refute the original findings.

P-selectin is another cell adhesion molecule that is expressed both on blood vessel endothelial cells and activated platelets. The interaction between P-selectin and its ligand, P-selectin ligand (PSGL-1), may promote macrophage recruitment and sustain this cell population at a later stage after injury (179). The expression of TNF- α , IL-6, and other pro-inflammatory cytokines was significantly attenuated in injured nerves from P-selectin-deficient mice (179). These results imply that P-selectin may be an essential mediator of macrophage infiltration.

Microvascular endothelial cells

Results from several recent studies revealed that microvascular endothelial cells are also crucial for the recruitment of macrophages and engulfing myelin debris that accumulates in response to injury (35, 180).

Macrophages are the cells that are primarily responsible for clearing myelin debris that accumulates in response to acute PNI. The processes involved in macrophage recruitment and activation are complex and in need of further research. Among the points not considered in this review, additional consideration of macrophage classification and the unique roles of M1 and M2 macrophages might be warranted. However, the M1 and M2 macrophage phenotypes cannot be determined accurately in cells and tissues from experiments performed *in vivo* (146). Here, we focused our attention on the activation and recruitment of macrophages under conditions that have been closely associated with myelin clearance. Interestingly, although macrophages are typically the primary mode of myelin clearance, disruption of macrophage recruitment has no clear impact on this process. Results from several studies revealed that neutrophils can also clear myelin debris and can compensate for the absence of macrophages in these circumstances (35). Fibroblasts may also have the capacity to remove tissue debris along with SCs during the early stages of the injury (4, 181).

Exogenous interventions

Numerous exogenous approaches, listed in Table 1, may be used to promote the clearance of myelin fragments. These approaches are based on the mechanisms associated with myelination (including negative regulation), autophagy, and the role of resident and infiltrating macrophages. These strategies will be discussed at length in the following article and may provide one or more new directions for research undertakings.

Inhibition of NF- κ B

Nuclear factor κ B (NF- κ B) is a master regulator of the inflammatory response and a mediator in many disease processes. While activation and translocation of NF- κ B are

essential to promote SC myelination and differentiation *in vitro* (182, 183), this factor is dispensable for myelination *in vivo* (3). Previous evidence suggested that NF- κ B might be an essential mediator of PNI and that compact remyelination is delayed by short-term suppression of this transcription factor (2). Interestingly, NF- κ B inhibition was found to promote regeneration after PNI (2). Therefore, factors that regulate NF- κ B activation and translocation may be critical factors associated with the process of myelin removal.

Ascorbic acid

Ascorbic acid, also known as vitamin C, is an essential micronutrient. Recent reports suggest that AA was also important for repairing nerve injury, specifically, both morphological and functional recovery of injured peripheral nerves (184). Other researchers reported that the administration of AA resulted in enhanced levels of c-Jun level and diminished levels of MAG during the early stages of PNI; collectively, these responses all repress myelin formation (4). AA also plays a critical role in macrophage recruitment. The results revealed that AA could enhance macrophage migration and infiltration and thus provide support for a suitable microenvironment (4). Interestingly, AA was also capable of promoting myelination *via* the activation of DNA demethylation (185). Collectively, these results suggest that AA may be an effective means to promote repair throughout the entire period after nerve injury.

Inhibition of Wnt/ β -catenin

The Wnt/ β -catenin pathway regulates the expression of myelin-related genes (48). Wnt promotes the myelin gene expression by suppressing glycogen synthase kinase 3 β (GSK3 β); this will preserve β -catenin which then enters the nucleus. Once in the nucleus, β -catenin interacts with T-cell factor/lymphoid-enhancer factors (TCF/LEF or TCFs) that regulate the expression of myelin-related genes (79).

Notably, GSK3 β is an essential factor in the pathway that regulates myelin-related gene expression. In addition, recent evidence suggests that early clearance of myelin debris is enhanced in response to lithium chloride (LiCl) which is a characterized inhibitor of the enzymatic activity of GSK3 β (6). An evaluation of the subsequent phase revealed that myelin regeneration occurred in parallel with the findings described in the previous study (5). Thus, GSK3 β may be another critical target for therapeutic strategies designed to promote the clearance of myelin debris and ultimately myelin regeneration. Accordingly, the GSK3 β inhibitor LiCl may be applied in peripheral nerves as a bidirectional regulator of myelin synthesis. The roles of other GSK3 β inhibitors remain to be explored.

TABLE 1 Exogeneous interventions.

Name	Intervention ways	Mechanism	References
Nuclear factor κ B (NF- κ B)	Exogenous inhibition	Suppress myelination	(2, 3)
Ascorbic acid	Exogenous inhibition	Suppress myelination; Promote macrophage infiltration	(4)
Wnt/ β -catenin	Exogenous inhibition	Suppress myelination	(5, 6)
Oxysterols	Treat with LXRs	Suppress myelination	(7)
Low-density lipoprotein receptor-related protein 4(Lrp4)	Exogenous inhibition	Suppress myelination	(8, 9)
LKB1 Liver kinase B1(LKB1)	Exogenous inhibition	Suppress myelination	(10)
HDAC1/2	Exogenous inhibition	Suppress myelination	(11)
SnRNA715	Not mentioned <i>in vivo</i>	Suppress myelination	(12)
circRNA.2837	Exogenous inhibition	Promote autophagy	(13)
Resveratrol (RSV)	Given exogenously	Promote autophagy	(14)
Rapamycin	Given exogenously	Promote autophagy	(15)
Epothilone B (EropB)	Given exogenously	Promote autophagy	(16)
Metformin	Given exogenously	Promote autophagy	(17)
β -Site amyloid precursor protein (APP) cleaving enzyme 1 (BACE1)	Exogenous inhibition	Promote the macrophages phagocytosis	(18, 19)
E6020	Given exogenously	Promote the macrophages phagocytosis	(20)
Signal regulatory protein- α (SIRP α)	Exogenous inhibition	Promote the macrophages phagocytosis	(21)

Oxysterols

Oxysterol is known for its impact on cholesterol homeostasis and in neurodegenerative disorders including Alzheimer's disease (186) and multiple sclerosis (187, 188). Oxysterol produced in SCs of PNS suppresses the expression of myelin-related genes, Pmp22, and MPZ in experiments performed *in vitro* (5). Oxysterol treatment of cells expressing high levels of liver X receptors (LXRs) also resulted in significant suppression; these results suggested that these inhibitory effects may be mediated by LXR ligands. Additional evidence revealed that LXR-mediated suppression might be the result of inhibition of the classical Wnt pathway (7). LXRs are likely to be involved in many pathways that promote both physiological and pathological responses in the PNS (189). The aforementioned mechanism might be clarified with additional research.

Low-density lipoprotein receptor-related protein 4

Low-density lipoprotein receptor-related protein 4 is a critical protein that contributes directly to the Agrin-Lrp4-MuSK signaling pathway and is an essential regulator in nervous system development (8). Recent evidence revealed that Lrp4 expressed in SCs may be crucial for the regeneration of

axons *via* an extrinsic mechanism (190). Moreover, Krox20 is downregulated in Lrp4 conditional gene-deleted mice together with low levels of MPZ (9). In this study, mutant mice exhibited superior repair properties and benefitted from the rapid clearance of myelin and proliferation of SCs that resulted from Krox20 downregulation after injury. Exploring a more defined mechanism of inhibition, Krox20 may support a new target for regenerating axons.

Inhibition of liver kinase B1

Liver kinase B1 is asymmetrically localized at the SC-axon interface; this specific localization is dependent on PKA-mediated phosphorylation at Ser-431. LKB1 may be the central regulator of cellular asymmetry in SCs which is a property required to initiate myelination. Accordingly, the expression of Krox20 and MPZ is suppressed in LKB1 gene-deleted mice in association with delayed myelination (10). The LKB1-mutant mice demonstrated hypomyelination and limb handicaps (10, 191). In addition, the LKB1 deficit limits the activation of the tricarboxylic acid cycle (TCA) and thus reduces the production of citrate. Citrate is a six-carbon precursor to many cellular lipids; thus, changes in its intracellular concentration will have an immediate impact on normal myelination (191, 192). Therefore, we hypothesize that in the early stages after injury,

LKB1 localization might be modulated by targeting PKA-mediated phosphorylation of Ser431, thereby regulating the process of myelin removal.

Epigenetic modulators

Epigenetic modulators may have an impact on myelin-related gene expression and clearance. For example, the expression of histone deacetylase (HDAC)1/2 was strongly upregulated after PNI. The high expression levels of HDAC1/2 resulted in delayed demyelination and axon degeneration (11). Conversely, deletion of the genes encoding HDAC1/2 delayed the expression of Oct6 and enhanced c-Jun. These events helped to transform SCs into a pro-repair state and to reduce the expression of both Krox20 and MPZ. Moreover, recent results revealed that a brief period of HDAC1/2 inhibition promotes nerve regeneration together with the increased thickness of myelin. Thus, we conjecture that early inhibition of HDAC1/2 promotes regeneration by accelerating phenotype conversion and suppressing myelination during the early stages.

Recently, it has been found that histone deacetylase 3 (HDAC3, a histone-modifying enzyme) acts as an inhibitor of SC myelination (193). HDAC3 was proved with a high-level expression after injury in SCs to suppress the process of remyelination. This overexpression represses the activation of PI3K-AKT and ERK. HDAC3 cooperates with histone acetyltransferase (HAT) targeting TEAD4, described as a new inhibitor of SC myelin growth, which is shown by genomic occupancy analyses (193). Although partial inhibition of HDAC3 led to faster neurological and functional recovery, we currently do not know the contribution of HDAC3 to myelin clearance in the early phase after injury. Still, this possibility function cannot be denied. HDAC3 may play a bidirectional regulatory role in the process of neurological recovery, which needs to be demonstrated by further studies.

Noncoding RNA

Small non-coding RNA 715 (sncRNA 715) originates from ribosomal DNA (rDNA) and was identified as an early inhibitor of demyelination and MBP translation in the CNS (194). Recent results documented that sncRNA 715 was expressed in pro-myelin SCs in PNS where it regulates MBP translation via a mechanism similar to that described in the CNS (12). Although we are not aware of any alterations in sncRNA715 expression in response to injury, we hypothesize that myelin removal might be regulated by exogenous interventions that target sncRNA715. Therefore, strategies that target noncoding RNA may be used to stabilize the microenvironment during the early stages of injury.

Circular RNAs (circRNAs) are non-coding RNAs found in the cytoplasm that regulate transcriptional and

posttranscriptional gene expression. While there is little evidence available that documents the role of circRNA in the PNS, recent evidence suggests that they may be functionally associated with processes that regulate autophagy. Zhou et al. (13) reported significant discrepancies in the expression of circRNAs immediately after PNI; the elimination of circRNA.2837 resulted in the amplification of autophagy in primary spinal nerves. Likewise, the downregulation of circRNA *in vitro* could block static nerve injury by promoting autophagy *via* targeting miR-34a (13).

Resveratrol

Resveratrol activates autophagy and thus has an impact on many signals that promote or alleviate pathology, including those contributing to nerve injury and CNS/PNS diseases. Although its mechanism of action remains unclear, RSV is believed to promote autophagy *via* its interactions with signaling pathways associated with mTOR, AMPK, SIRT1, PI3K/Akt, and MAPK. RSV also suppresses the TLR4/NF- κ B signaling to activate autophagy, thereby accelerating clearance and promoting regeneration (14). Administration of RSV may thus be an effective strategy for the treatment of PNS and CNS injury.

Rapamycin

In mammals, mTOR is a downstream factor of PI3K/Akt signaling (195) and regulates the formation of myelin and the growth of axons. Results from previous studies revealed that mTOR inhibition activates autophagy and thus promotes the clearance of damaged cellular components and preserves homeostasis (196–198). A study of PNI in rats reported that treatment with the mTOR inhibitor, rapamycin, promotes peripheral nerve regeneration and functional recovery after injury (15). While this may appear to be paradoxical given the role of mTOR in promoting negative regulation of myelin formation, autophagy detected in SCs under these circumstances may be the result of an mTOR-independent pathway. We suspect that this is likely given the timing of intervention after injury; in other words, timely intervention with mTOR inhibitors might enhance myelin clearance.

Epothilone B

While EropB was initially used to treat cancer, additional studies revealed that this agent could promote recovery from CNS diseases (199, 200). The results of recent research suggest that EropB can aid with the structural and functional repair of damaged peripheral nerves (16). In contrast to the

aforementioned strategy, EropB enhances autophagy in the PNS and promotes the migration of SCs. This process can be suppressed in the presence of the autophagy inhibitor, 3-MA. Additional research suggests that EropB may provide crucial regulation of this response by suppressing the PI3K/Akt pathway.

Metformin

Metformin is a first-line anti-hyperglycemic agent used to treat type II diabetes mellitus. Metformin has also been used to relieve neurological problems, including neuropathic pain in the spine (201), cognitive decline, and memory loss (202). The results of a recent study reveal that metformin can induce autophagy in the early stages after injury and enhance the number of autophagosomes. This facilitates recovery by increasing the rate and extent of autophagy which results in more effective removal of myelin fragments (17).

Inhibition of β -Site amyloid precursor protein cleaving enzyme 1

β -Site amyloid precursor protein cleaving enzyme 1 is an aspartyl protease known for its role in producing amyloid- β peptides in association with Alzheimer's disease. In the PNS, BACE1 cleaves neuregulin 1 type III (72) and, indirectly, APP (203). Reductions in BACE1 activity in gene-deleted rats enhance the clearance of myelin debris and promote axon regeneration compared to the wild-type (204, 205). By contrast, BACE1 over-expression leads to significant reductions in the length of the regenerated axons as well as the number of neuromuscular junctions (19). Treatment with a BACE1 inhibitor results in improved nerve regrowth and clearance of debris 7 days after a crushing injury (206). This rapid clearance is facilitated by the earlier influx of macrophages that are capable of more effective phagocytosis (79). The mechanisms underlying this response involve the upregulation of both tumor necrosis factor receptor 1 (TNFR1) and its downstream transcription factor, NF- κ B, at the distal site of the injury.

E6020

E6020 is a lipid A mimetic and TLR4 agonist that promotes macrophage-mediated phagocytosis of accumulated debris. E6020 also induced cytokine production, activation of intracellular NF- κ B signaling, and an overall "activated" macrophage morphology in experiments performed *in vitro*. Treatment with E6020 resulted in a larger macrophage infiltrate. Although these results cannot be paralleled with LPS, E6020-induced clearance might be controlled in the appropriate range and thus used to limit over-clearance (20).

Inhibition of signal regulatory protein α

A SIRP α -dependent mechanism suppressed macrophage activation and thus impeded myelin clearance *in vivo*. Earlier studies revealed that CD47 associated with myelin interacted with SIRP α on macrophages to downregulate phagocytosis in the CNS (207). This interaction, combined with IL-10, constraints inflammation-induced macrophage phagocytosis and thus may protect healthy cells (208). Recent studies have characterized this interaction in the PNS. Injured rats undergoing SIRP α inhibition respond with rapid clearance of myelin, axon regeneration, and repair of the affected nerve. This effect results from blocking the binding between SIRP α and CD47 and removing CD47 from myelin fragments (21).

Conclusion

Regeneration after PNI is influenced by many factors and molecular mechanisms. The extent of the injury and the ability to establish and provide ongoing support for a microenvironment that supports regeneration are among these critical features. Previous studies and clinical strategies have focused primarily on interventions that might promote axonal and myelin regeneration after injury; there has been little to no attention paid to the process of myelin clearance. Here, we discuss several strategies that might be used to promote myelin clearance. Collectively, current evidence suggests that clearance of myelin debris is beneficial for the process of regeneration during the early stages yet harmful if the process has been delayed. An improved understanding of mechanisms associated with myelin clearance after a PNI might contribute to new and effective therapeutic strategies to promote regeneration after injury. These findings will also provide essential contributions to our understanding of demyelinating neural disorders, degenerative diseases, and diseases of the CNS.

There are still many issues that need to be investigated, including the key pathways and the potential range of intervention strategies, as well as the aforementioned paradoxes and negative influences, among others. For example, one study features a nerve regeneration strategy involving partial enzymatic digestion of myelin debris. This mechanism facilitates the rapid removal of debris and creates a favorable microenvironment that has promoted the regeneration of damaged nerves in experimental rat models. However, as reported by Tsuang et al. (108), repair exhibited by the high-dose group was significantly less than that observed among those treated with lower doses. These results also suggest that treatment should be decided on a per-case basis and might focus on the rapid removal of cellular debris. Additional experiments will be needed to re-evaluate and optimize these strategies.

Author contributions

Conceptualization: YY and YW. Investigation: YY and SW. Writing—original draft preparation: YY and MZ. Writing—review and editing, project administration, funding acquisition, and Supervision: YW. All authors have read and agreed to the published version of the manuscript.

Funding

This research was funded by the National Natural Science Foundation of China (Grant: 81973926), the Provincial Natural Science Foundation (Grant: LH2021H090), and the Outstanding Innovative Talents Support Program of Heilongjiang University of Chinese Medicine (2018RCL10).

References

- Huebner EA, Strittmatter SM. Axon regeneration in the peripheral and central nervous systems. *Results Probl Cell Differ.* (2009) 48:339–51. doi: 10.1007/400_2009_19
- Morton PD, Johnstone JT, Ramos AY, Liebl DJ, Bunge MB, Bethea JR. Nuclear factor- κ B activation in Schwann cells regulates regeneration and remyelination. *Glia.* (2012) 60:639–50. doi: 10.1002/glia.22297
- Morton PD, Dellarole A, Theus MH, Walters WM, Berge SS, Bethea JR. Activation of NF- κ B in Schwann cells is dispensable for myelination in vivo. *J Neurosci.* (2013) 33:9932–6. doi: 10.1523/JNEUROSCI.2483-12.2013
- Qu W-R, Zhu Z, Liu J, Song D-B, Tian H, Chen B-P, et al. Interaction between Schwann cells and other cells during repair of peripheral nerve injury. *Neural Regen Res.* (2021) 16:93–8. doi: 10.4103/1673-5374.286956
- Makoukji J, Belle M, Meffre D, Stassart R, Grenier J, Shackleford G, et al. Lithium enhances remyelination of peripheral nerves. *Proc Natl Acad Sci U S A.* (2012) 109:3973–8. doi: 10.1073/pnas.1121367109
- Chen Y, Weng J, Han D, Chen B, Ma M, Yu Y, et al. GSK3 β inhibition accelerates axon debris clearance and new axon remyelination. *Am J Transl Res.* (2016) 8:5410–20.
- Makoukji J, Shackleford G, Meffre D, Grenier J, Liere P, Lobaccaro J-MA, et al. Interplay between LXR and Wnt/ β -catenin signaling in the negative regulation of peripheral myelin genes by oxysterols. *J Neurosci.* (2011) 31:9620–9. doi: 10.1523/JNEUROSCI.0761-11.2011
- Wu H, Lu Y, Shen C, Patel N, Gan L, Xiong WC, et al. Distinct roles of muscle and motoneuron LRP4 in neuromuscular junction formation. *Neuron.* (2012) 75:94–107. doi: 10.1016/j.neuron.2012.04.033
- Hui T-K, Lai X-S, Dong X, Jing H, Liu Z, Fei E, et al. Ablation of Lrp4 in Schwann cells promotes peripheral nerve regeneration in mice. *Biology (Basel).* (2021) 10:452. doi: 10.3390/biology10060452
- Shen Y-AA, Chen Y, Dao DQ, Mayoral SR, Wu L, Meijer D, et al. Phosphorylation of LKB1/Par-4 establishes Schwann cell polarity to initiate and control myelin extent. *Nat Commun.* (2014) 5:4991. doi: 10.1038/ncomms5991
- Brügger V, Duman M, Bochud M, Mürner E, Heller M, Ruff S, et al. Delaying histone deacetylase response to injury accelerates conversion into repair Schwann cells and nerve regeneration. *Nat Commun.* (2017) 8:14272. doi: 10.1038/ncomms14272
- Müller C, Hochhaus NM, Fontana X, Luhmann HJ, White R. SncRNA715 inhibits schwann cell myelin basic protein synthesis. *PLoS ONE.* (2015) 10:e0136900. doi: 10.1371/journal.pone.0136900
- Zhou Z-B, Niu Y-L, Huang G-X, Lu J-J, Chen A, Zhu, L. Silencing of circRNA.2837 plays a protective role in sciatic nerve injury by sponging the miR-34 family via regulating neuronal autophagy. *Mol Ther Nucleic Acids.* (2018) 12:718–29. doi: 10.1016/j.omtn.2018.07.011

Conflict of interest

The authors declare that the research was conducted in the absence of any commercial or financial relationships that could be construed as a potential conflict of interest.

Publisher's note

All claims expressed in this article are solely those of the authors and do not necessarily represent those of their affiliated organizations, or those of the publisher, the editors and the reviewers. Any product that may be evaluated in this article, or claim that may be made by its manufacturer, is not guaranteed or endorsed by the publisher.

- Zhang J, Ren J, Liu Y, Huang D, Lu L. Resveratrol regulates the recovery of rat sciatic nerve crush injury by promoting the autophagy of Schwann cells. *Life Sci.* (2020) 256:117959. doi: 10.1016/j.lfs.2020.117959
- Huang H-C, Chen L, Zhang H-X, Li S-F, Liu P, Zhao T-Y, et al. Autophagy promotes peripheral nerve regeneration and motor recovery following sciatic nerve crush injury in rats. *J Mol Neurosci.* (2016) 58:416–23. doi: 10.1007/s12031-015-0672-9
- Zhou J, Li S, Gao J, Hu Y, Chen S, Luo X, et al. Epothilone B facilitates peripheral nerve regeneration by promoting autophagy and migration in schwann cells. *Front Cell Neurosci.* (2020) 14:143. doi: 10.3389/fncel.2020.00143
- Liu L, Tian D, Liu C, Yu K, Bai J. Metformin enhances functional recovery of peripheral nerve in rats with sciatic nerve crush injury. *Med Sci Monit.* (2019) 25:10067–76. doi: 10.12659/MSM.918277
- Liu L, Fissel JA, Tasnim A, Borzan J, Gocke A, Calabresi PA, et al. Increased TNFR1 expression and signaling in injured peripheral nerves of mice with reduced BACE1 activity. *Neurobiol Dis.* (2016) 93:21–7. doi: 10.1016/j.nbd.2016.04.002
- Tallon C, Rockenstein E, Masliah E, Farah MH. Increased BACE1 activity inhibits peripheral nerve regeneration after injury. *Neurobiol Dis.* (2017) 106:147–57. doi: 10.1016/j.nbd.2017.07.003
- Church JS, Milich LM, Lerch JK, Popovich PG, McTigue DM. E6020, a synthetic TLR4 agonist, accelerates myelin debris clearance, Schwann cell infiltration, and remyelination in the rat spinal cord. *Glia.* (2017) 65:883–99. doi: 10.1002/glia.23132
- Elberg G, Liraz-Zaltsman S, Reichert F, Matozaki T, Tal M, Rotshenker S. Deletion of SIRP α (signal regulatory protein- α) promotes phagocytic clearance of myelin debris in Wallerian degeneration, axon regeneration, and recovery from nerve injury. *J Neuroinflammation.* (2019) 16:277. doi: 10.1186/s12974-019-1679-x
- Stoll G, Griffin JW, Li CY, Trapp BD. Wallerian degeneration in the peripheral nervous system: participation of both Schwann cells and macrophages in myelin degradation. *J Neurocytol.* (1989) 18:671–83. doi: 10.1007/BF01187086
- Shen ZL, Lassner F, Bader A, Becker M, Walter GF, Berger A. Cellular activity of resident macrophages during Wallerian degeneration. *Microsurgery.* (2000) 20:255–61. doi: 10.1002/1098-2752(2000)20:5<255::aid-micr6>3.0.co;2-a
- Rao SNR, Pearse DD. Regulating axonal responses to injury: the intersection between signaling pathways involved in axon myelination and the inhibition of axon regeneration. *Front Mol Neurosci.* (2016) 9:33. doi: 10.3389/fnmol.2016.00033
- Pereira JA, Lebrun-Julien F, Suter U. Molecular mechanisms regulating myelination in the peripheral nervous system. *Trends Neurosci.* (2012) 35:123–34. doi: 10.1016/j.tins.2011.11.006
- Jessen KR, Mirsky R, Lloyd AC. Schwann cells: development and role in nerve repair. *Cold Spring Harb Perspect Biol.* (2015) 7:a020487. doi: 10.1101/cshperspect.a020487

27. Brosius Lutz A, Barres BA. Contrasting the glial response to axon injury in the central and peripheral nervous systems. *Dev Cell*. (2014) 28:7–17. doi: 10.1016/j.devcel.2013.12.002
28. Chen Z-L, Yu W-M, Strickland S. Peripheral regeneration. *Annu Rev Neurosci*. (2007) 30:209–33. doi: 10.1146/annurev.neuro.30.051606.094337
29. Goethals S, Ydens E, Timmerman V, Janssens S. Toll-like receptor expression in the peripheral nerve. *Glia*. (2010) 58:1701–9. doi: 10.1002/glia.21041
30. Namgung U. The role of Schwann cell-axon interaction in peripheral nerve regeneration. *Cells Tissues Organs*. (2014) 200:6–12. doi: 10.1159/000370324
31. Schwab ME. Nogo and axon regeneration. *Curr Opin Neurobiol*. (2004) 14:118–24. doi: 10.1016/j.conb.2004.01.004
32. Vargas ME, Barres BA. Why is Wallerian degeneration in the CNS so slow? *Annu Rev Neurosci*. (2007) 30:153–79. doi: 10.1146/annurev.neuro.30.051606.094354
33. Fujita Y, Endo S, Takai T, Yamashita T. Myelin suppresses axon regeneration by PIR-B/SHP-mediated inhibition of Trk activity. *EMBO J*. (2011) 30:1389–401. doi: 10.1038/emboj.2011.55
34. Mueller M, Wacker K, Ringelstein EB, Hickey WF, Imai Y, Kiefer R. Rapid response of identified resident endoneurial macrophages to nerve injury. *Am J Pathol*. (2001) 159:2187–97. doi: 10.1016/S0002-9440(10)63070-2
35. Lindborg JA, Mack M, Zigmund RE. Neutrophils are critical for myelin removal in a peripheral nerve injury model of wallerian degeneration. *J Neurosci*. (2017) 37:10258–77. doi: 10.1523/JNEUROSCI.2085-17.2017
36. Zigmund RE, Echevarria FD. Macrophage biology in the peripheral nervous system after injury. *Prog Neurobiol*. (2019) 173:102–21. doi: 10.1016/j.pneurobio.2018.12.001
37. Balakrishnan A, Belfiore L, Chu T-H, Fleming T, Midha R, Biernaskie J, et al. Insights into the role and potential of schwann cells for peripheral nerve repair from studies of development and injury. *Front Mol Neurosci*. (2020) 13:608442. doi: 10.3389/fnmol.2020.608442
38. Nave K-A. Myelination and support of axonal integrity by glia. *Nature*. (2010) 468:244–52. doi: 10.1038/nature09614
39. Feltri ML, Poitelon Y, Previtali SC. How Schwann cells sort axons: new concepts. *Neuroscientist*. (2016) 22:252–65. doi: 10.1177/1073858415572361
40. Jessen KR, Mirsky R. The success and failure of the schwann cell response to nerve injury. *Front Cell Neurosci*. (2019) 13:33. doi: 10.3389/fncel.2019.00033
41. Liu B, Xin W, Tan J-R, Zhu R-P, Li T, Wang D, et al. Myelin sheath structure and regeneration in peripheral nerve injury repair. *Proc Natl Acad Sci U S A*. (2019) 116:22347–52. doi: 10.1073/pnas.1910292116
42. Svarén J, Meijer D. The molecular machinery of myelin gene transcription in Schwann cells. *Glia*. (2008) 56:1541–51. doi: 10.1002/glia.20767
43. Chernousov MA, Yu W-M, Chen Z-L, Carey DJ, Strickland S. Regulation of Schwann cell function by the extracellular matrix. *Glia*. (2008) 56:1498–507. doi: 10.1002/glia.20740
44. Monk KR, Oshima K, Jörs S, Heller S, Talbot WS. Gpr126 is essential for peripheral nerve development and myelination in mammals. *Development*. (2011) 138:2673–80. doi: 10.1242/dev.062224
45. Glenn TD, Talbot WS. Signals regulating myelination in peripheral nerves and the Schwann cell response to injury. *Curr Opin Neurobiol*. (2013) 23:1041–8. doi: 10.1016/j.conb.2013.06.010
46. Heller BA, Ghidinelli M, Voelkl J, Einheber S, Smith R, Grund E, et al. Functionally distinct PI 3-kinase pathways regulate myelination in the peripheral nervous system. *J Cell Biol*. (2014) 204:1219–36. doi: 10.1083/jcb.201307057
47. Newbern J, Birchmeier C. Nrg1/ErbB signaling networks in Schwann cell development and myelination. *Semin Cell Dev Biol*. (2010) 21:922–8. doi: 10.1016/j.semdb.2010.08.008
48. Tawak M, Makoukji J, Belle M, Fonte C, Trousson A, Hawkins T, et al. Wnt/beta-catenin signaling is an essential and direct driver of myelin gene expression and myelinogenesis. *J Neurosci*. (2011) 31:3729–42. doi: 10.1523/JNEUROSCI.4270-10.2011
49. Jessen KR, Mirsky R. The origin and development of glial cells in peripheral nerves. *Nat Rev Neurosci*. (2005) 6:671–82. doi: 10.1038/nrn1746
50. Arthur-Farraj P, Wanek K, Hantke J, Davis CM, Jayakar A, Parkinson DB, et al. Mouse schwann cells need both NRG1 and cyclic AMP to myelinate. *Glia*. (2011) 59:720–33. doi: 10.1002/glia.21144
51. Beard JL, Wiesinger JA, Connor JR. Pre- and postweaning iron deficiency alters myelination in Sprague-Dawley rats. *Dev Neurosci*. (2003) 25:308–15. doi: 10.1159/000073507
52. Cheli VT, Santiago González DA, Marziali LN, Zamora NN, Guitart ME, Spreuer V, et al. The divalent metal transporter 1 (DMT1) is required for iron uptake and normal development of oligodendrocyte progenitor cells. *J Neurosci*. (2018) 38:9142–59. doi: 10.1523/JNEUROSCI.1447-18.2018
53. Santiago González DA, Cheli VT, Wan R, Paez PM. Iron metabolism in the peripheral nervous system: the role of DMT1, ferritin, and transferrin receptor in schwann cell maturation and myelination. *J Neurosci*. (2019) 39:9940–53. doi: 10.1523/JNEUROSCI.1409-19.2019
54. Santiago González DA, Cheli VT, Rosenblum SL, Denaroso G, Paez PM. Ceruloplasmin deletion in myelinating glial cells induces myelin disruption and oxidative stress in the central and peripheral nervous systems. *Redox Biol*. (2021) 46:102118. doi: 10.1016/j.redox.2021.102118
55. Jessen KR, Mirsky R. Negative regulation of myelination: relevance for development, injury, and demyelinating disease. *Glia*. (2008) 56:1552–65. doi: 10.1002/glia.20761
56. Arthur-Farraj PJ, Latouche M, Wilton DK, Quintes S, Chabrol E, Banerjee A, et al. c-Jun reprograms Schwann cells of injured nerves to generate a repair cell essential for regeneration. *Neuron*. (2012) 75:633–47. doi: 10.1016/j.neuron.2012.06.021
57. Kim M, Wende H, Walcher J, Kühnemund J, Cheret C, Kempa S, et al. Maf links Neurogranin signaling to cholesterol synthesis in myelinating Schwann cells. *Genes Dev*. (2018) 32:645–57. doi: 10.1101/gad.310490.117
58. Liu X, Peng S, Zhao Y, Zhao T, Wang M, Luo L, et al. AMPK negatively regulates peripheral myelination via activation of c-Jun. *Mol Neurobiol*. (2017) 54:3554–64. doi: 10.1007/s12035-016-9913-3
59. Fontana X, Hristova M, Da Costa C, Patodia S, Thei L, Makwana M, et al. c-Jun in Schwann cells promotes axonal regeneration and motoneuron survival via paracrine signaling. *J Cell Biol*. (2012) 198:127–41. doi: 10.1083/jcb.201205025
60. Norrmén C, Figlia G, Pfister P, Pereira JA, Bachofner S, Suter U. mTORC1 is transiently reactivated in injured nerves to promote c-Jun elevation and Schwann cell dedifferentiation. *J Neurosci*. (2018) 38:4811–28. doi: 10.1523/JNEUROSCI.3619-17.2018
61. Dennis EA. The growing phospholipase A2 superfamily of signal transduction enzymes. *Trends Biochem Sci*. (1997) 22:1–2. doi: 10.1016/s0968-0004(96)20031-3
62. Florio F, Ferri C, Scapin C, Feltri ML, Wrabetz L, D'Antonio M. Sustained expression of negative regulators of myelination protects schwann cells from dysmyelination in a charcot-marie-tooth 1B mouse model. *J Neurosci*. (2018) 38:4275–87. doi: 10.1523/JNEUROSCI.0201-18.2018
63. Kiousi C, Gross MK, Gruss P. Pax3: a paired domain gene as a regulator in PNS myelination. *Neuron*. (1995) 15:553–62. doi: 10.1016/0896-6273(95)90144-2
64. Blanchard AD, Sinanan A, Parmantier E, Zwart R, Broos L, Meijer D, et al. Oct-6 (SCP/Tst-1) is expressed in Schwann cell precursors, embryonic Schwann cells, and postnatal myelinating Schwann cells: comparison with Oct-1, Krox-20, and Pax-3. *J Neurosci Res*. (1996) 46:630–40. doi: 10.1002/(SICI)1097-4547(19961201)46:5<630::AID-JNR11>3.0.CO;2-0
65. Doddrell RDS, Dun X-P, Moate RM, Jessen KR, Mirsky R, Parkinson DB. Regulation of Schwann cell differentiation and proliferation by the Pax-3 transcription factor. *Glia*. (2012) 60:1269–78. doi: 10.1002/glia.22346
66. Sheu JY, Kulhanek DJ, Eckenstein FP. Differential patterns of ERK and STAT3 phosphorylation after sciatic nerve transection in the rat. *Exp Neurol*. (2000) 166:392–402. doi: 10.1006/exnr.2000.7508
67. Harrisingh MC, Perez-Nadales E, Parkinson DB, Malcolm DS, Mudge AW, Lloyd AC. The Ras/Raf/ERK signalling pathway drives Schwann cell dedifferentiation. *EMBO J*. (2004) 23:3061–71. doi: 10.1038/sj.emboj.7600309
68. Morgan L, Jessen KR, Mirsky R. The effects of cAMP on differentiation of cultured Schwann cells: progression from an early phenotype (04+) to a myelin phenotype (P0+, GFAP-, N-CAM-, NGF-receptor-) depends on growth inhibition. *J Cell Biol*. (1991) 112:457–67. doi: 10.1083/jcb.112.3.457
69. Napoli I, Noon LA, Ribeiro S, Kerai AP, Parrinello S, Rosenberg LH, et al. A central role for the ERK-signaling pathway in controlling Schwann cell plasticity and peripheral nerve regeneration in vivo. *Neuron*. (2012) 73:729–42. doi: 10.1016/j.neuron.2011.11.031
70. Cervellini I, Galino J, Zhu N, Allen S, Birchmeier C, Bennett DL. Sustained MAPK/ERK activation in adult schwann cells impairs nerve repair. *J Neurosci*. (2018) 38:679–90. doi: 10.1523/JNEUROSCI.2255-17.2017
71. Michailov GV, Sereda MW, Brinkmann BG, Fischer TM, Haug B, Birchmeier C, et al. Axonal neurotrophin-1 regulates myelin sheath thickness. *Science*. (2004) 304:700–3. doi: 10.1126/science.1095862

72. Taveggia C, Zanazzi G, Petrylak A, Yano H, Rosenbluth J, Einheber S, et al. Neuregulin-1 type III determines the ensheathment fate of axons. *Neuron*. (2005) 47:681–94. doi: 10.1016/j.neuron.2005.08.017
73. Fricker FR, Bennett DL. The role of neuregulin-1 in the response to nerve injury. *Future Neurol*. (2011) 6:809–22. doi: 10.2217/fnl.11.45
74. Jung J, Cai W, Lee HK, Pellegatta M, Shin YK, Jang SY, et al. Actin polymerization is essential for myelin sheath fragmentation during Wallerian degeneration. *J Neurosci*. (2011) 31:2009–15. doi: 10.1523/JNEUROSCI.4537-10.2011
75. Shin YK, Jang SY, Park JY, Park SY, Lee HJ, Suh DJ, et al. The Neuregulin-Rac-MKK7 pathway regulates antagonistic c-jun/Krox20 expression in Schwann cell dedifferentiation. *Glia*. (2013) 61:892–904. doi: 10.1002/glia.22482
76. Parkinson DB, Bhaskaran A, Arthur-Farraj P, Noon LA, Woodhoo A, Lloyd AC, et al. c-Jun is a negative regulator of myelination. *J Cell Biol*. (2008) 181:625–37. doi: 10.1083/jcb.200803013
77. Yang DP, Kim J, Syed N, Tung Y-J, Bhaskaran A, Mindos T, et al. p38 MAPK activation promotes denervated Schwann cell phenotype and functions as a negative regulator of Schwann cell differentiation and myelination. *J Neurosci*. (2012) 32:7158–68. doi: 10.1523/JNEUROSCI.5812-11.2012
78. Dummula K, Vinukonda G, Chu P, Xing Y, Hu F, Mailk S, et al. Bone morphogenetic protein inhibition promotes neurological recovery after intraventricular hemorrhage. *J Neurosci*. (2011) 31:12068–82. doi: 10.1523/JNEUROSCI.0013-11.2011
79. Liu X, Zhao Y, Peng S, Zhang S, Wang M, Chen Y, et al. BMP7 retards peripheral myelination by activating p38 MAPK in Schwann cells. *Sci Rep*. (2016) 6:31049. doi: 10.1038/srep31049
80. Kuroda M, Muramatsu R, Maedera N, Koyama Y, Hamaguchi M, Fujimura H, et al. Peripherally derived FGF21 promotes remyelination in the central nervous system. *J Clin Invest*. (2017) 127:3496–509. doi: 10.1172/JCI94337
81. Zhang Y, Jiang K, Xie G, Ding J, Peng S, Liu X, et al. FGF21 impedes peripheral myelin development by stimulating p38 MAPK/c-Jun axis. *J Cell Physiol*. (2021) 236:1345–61. doi: 10.1002/jcp.29942
82. Wang J, Ren K-Y, Wang Y-H, Kou Y-H, Zhang P-X, Peng J-P, et al. Effect of active Notch signaling system on the early repair of rat sciatic nerve injury. *Artif Cells Nanomed Biotechnol*. (2015) 43:383–9. doi: 10.3109/21691401.2014.896372
83. Park HT, Feltri ML. Rac1 GTPase controls myelination and demyelination. *Bioarchitecture*. (2011) 1:110–3. doi: 10.4161/bioa.1.3.16985
84. Tricaud N, Park HT. Wallerian demyelination: chronicle of a cellular cataclysm. *Cell Mol Life Sci*. (2017) 74:4049–57. doi: 10.1007/s00018-017-2565-2
85. Fannon AM, Sherman DL, Ilyina-Gragerova G, Brophy PJ, Friedrich VL, Colman DR. Novel E-cadherin-mediated adhesion in peripheral nerve: Schwann cell architecture is stabilized by autotypic adherens junctions. *J Cell Biol*. (1995) 129:189–202. doi: 10.1083/jcb.129.1.189
86. Woodhoo A, Alonso MBD, Droggiti A, Turmaine M, D'Antonio M, Parkinson DB, et al. Notch controls embryonic Schwann cell differentiation, postnatal myelination and adult plasticity. *Nat Neurosci*. (2009) 12:839–47. doi: 10.1038/nn.2323
87. Jessen KR, Mirsky R. Control of Schwann cell myelination. *F1000 Biol Rep*. (2010) 2:19. doi: 10.3410/B2-19
88. Boerboom A, Dion V, Chariot A, Franzen R. Molecular mechanisms involved in schwann cell plasticity. *Front Mol Neurosci*. (2017) 10:38. doi: 10.3389/fnmol.2017.00038
89. Brinkmann BG, Quintes S. Zeb2: Inhibiting the inhibitors in Schwann cells. *Neurogenesis (Austin)*. (2017) 4:e1271495. doi: 10.1080/23262133.2016.1271495
90. Zhu X, Ding S, Qiu C, Shi Y, Song L, Wang Y, et al. SUMOylation negatively regulates angiogenesis by targeting endothelial NOTCH signaling. *Circ Res*. (2017) 121:636–49. doi: 10.1161/CIRCRESAHA.117.310696
91. Fergani IF, Frick LR. Wrestling and wrapping: a perspective on SUMO proteins in schwann cells. *Biomolecules*. (2021) 11:1055. doi: 10.3390/biom11071055
92. Taveggia C. Schwann cells-axon interaction in myelination. *Curr Opin Neurobiol*. (2016) 39:24–9. doi: 10.1016/j.conb.2016.03.006
93. Figlia G, Gerber D, Suter U. Myelination and mTOR. *Glia*. (2018) 66:693–707. doi: 10.1002/glia.23273
94. Figlia G, Norrmén C, Pereira JA, Gerber D, Suter U. Dual function of the PI3K-Akt-mTORC1 axis in myelination of the peripheral nervous system. *Elife*. (2017) 6:e29241. doi: 10.7554/eLife.29241
95. Saher G, Quintes S, Möbius W, Wehr MC, Krämer-Albers E-M, Brügger B, et al. Cholesterol regulates the endoplasmic reticulum exit of the major membrane protein P0 required for peripheral myelin compaction. *J Neurosci*. (2009) 29:6094–104. doi: 10.1523/JNEUROSCI.0686-09.2009
96. El Soury M, Fornasari BE, Morano M, Grazio E, Ronchi G, Incarnato D, et al. Soluble neuregulin1 down-regulates myelination genes in Schwann cells. *Front Mol Neurosci*. (2018) 11:157. doi: 10.3389/fnmol.2018.00157
97. Chen Z-L, Strickland S. Laminin gamma1 is critical for Schwann cell differentiation, axon myelination, and regeneration in the peripheral nerve. *J Cell Biol*. (2003) 163:889–99. doi: 10.1083/jcb.200307068
98. Yu W-M, Chen Z-L, North AJ, Strickland S. Laminin is required for Schwann cell morphogenesis. *J Cell Sci*. (2009) 122:929–36. doi: 10.1242/jcs.033928
99. Ghidinelli M, Poitelon Y, Shin YK, Ameroso D, Williamson C, Ferri C, et al. Laminin 211 inhibits protein kinase A in Schwann cells to modulate neuregulin 1 type III-driven myelination. *PLoS Biol*. (2017) 15:e2001408. doi: 10.1371/journal.pbio.2001408
100. La Marca R, Cerri F, Horiuchi K, Bachi A, Feltri ML, Wrabetz L, et al. TACE (ADAM17) inhibits Schwann cell myelination. *Nat Neurosci*. (2011) 14:857–65. doi: 10.1038/nn.2849
101. Linneberg C, Harboe M, Laursen LS. Axo-glia interaction preceding CNS myelination is regulated by bidirectional eph-ephrin signaling. *ASN Neuro*. (2015) 7:1759091415602859. doi: 10.1177/1759091415602859
102. Iwasato T, Katoh H, Nishimaru H, Ishikawa Y, Inoue H, Saito YM, et al. Rac-GAP alpha-chimerin regulates motor-circuit formation as a key mediator of EphrinB3/EphA4 forward signaling. *Cell*. (2007) 130:742–53. doi: 10.1016/j.cell.2007.07.022
103. Harboe M, Torvund-Jensen J, Kjaer-Sorensen K, Laursen LS. Ephrin-A1-EphA4 signaling negatively regulates myelination in the central nervous system. *Glia*. (2018) 66:934–50. doi: 10.1002/glia.23293
104. Chen R, Yang X, Zhang B, Wang S, Bao S, Gu Y, et al. EphA4 negatively regulates myelination by inhibiting schwann cell differentiation in the peripheral nervous system. *Front Neurosci*. (2019) 13:1191. doi: 10.3389/fnins.2019.01191
105. Salzer JL. Schwann cell myelination. *Cold Spring Harb Perspect Biol*. (2015) 7:a020529. doi: 10.1101/cshperspect.a020529
106. Feng X, Takayama Y, Ohno N, Kanda H, Dai Y, Sokabe T, et al. Increased TRPV4 expression in non-myelinating Schwann cells is associated with demyelination after sciatic nerve injury. *Commun Biol*. (2020) 3:716. doi: 10.1038/s42003-020-01444-9
107. Miller RH. Calcium control of myelin sheath growth. *Nat Neurosci*. (2018) 21:2–3. doi: 10.1038/s41593-017-0043-7
108. Tsuang F-Y, Chen M-H, Lin F-H, Yang M-C, Liao C-J, Chang W-H, et al. Partial enzyme digestion facilitates regeneration of crushed nerve in rat. *Transl Neurosci*. (2020) 11:251–63. doi: 10.1515/tnsci-2020-0112
109. Mizushima N, Levine B, Cuervo AM, Klionsky DJ. Autophagy fights disease through cellular self-digestion. *Nature*. (2008) 451:1069–75. doi: 10.1038/nature06639
110. Dikic I, Elazar Z. Mechanism and medical implications of mammalian autophagy. *Nat Rev Mol Cell Biol*. (2018) 19:349–64. doi: 10.1038/s41580-018-0003-4
111. Jang SY, Shin YK, Park SY, Park JY, Rha S-H, Kim JK, et al. Autophagy is involved in the reduction of myelinating Schwann cell cytoplasm during myelin maturation of the peripheral nerve. *PLoS ONE*. (2015) 10:e0116624. doi: 10.1371/journal.pone.0116624
112. Ko P-Y, Yang C-C, Kuo Y-L, Su F-C, Hsu T-I, Tu Y-K, et al. Schwann-cell autophagy, functional recovery, and scar reduction after peripheral nerve repair. *J Mol Neurosci*. (2018) 64:601–10. doi: 10.1007/s12031-018-1056-8
113. Belgrad J, De Pace R, Fields RD. Autophagy in myelinating glia. *J Neurosci*. (2020) 40:256–66. doi: 10.1523/JNEUROSCI.1066-19.2019
114. Gomez-Sanchez JA, Carty L, Iruarrizaga-Lejarreta M, Palomo-Irigoyen M, Varela-Rey M, Griffith M, et al. Schwann cell autophagy, myelinophagy, initiates myelin clearance from injured nerves. *J Cell Biol*. (2015) 210:153–68. doi: 10.1083/jcb.201503019
115. Marinelli S, Nazio F, Tinari A, Ciarlo L, D'Amelio M, Pieroni L, et al. Schwann cell autophagy counteracts the onset and chronification of neuropathic pain. *Pain*. (2014) 155:93–107. doi: 10.1016/j.pain.2013.09.013
116. Chrast R, Saher G, Nave K-A, Verheijen MHG. Lipid metabolism in myelinating glial cells: lessons from human inherited disorders and mouse models. *J Lipid Res*. (2011) 52:419–34. doi: 10.1194/jlr.R009761
117. Singh R, Kaushik S, Wang Y, Xiang Y, Novak I, Komatsu M, et al. Autophagy regulates lipid metabolism. *Nature*. (2009) 458:1131–5. doi: 10.1038/nature07976

118. Lüningschrör P, Slotta C, Heimann P, Briese M, Weikert UM, Massih B, et al. Absence of Plekhg5 results in myelin infoldings corresponding to an impaired schwann cell autophagy, and a reduced t-cell infiltration into peripheral nerves. *Front Cell Neurosci.* (2020) 14:185. doi: 10.3389/fncel.2020.00185
119. Li R, Li D, Wu C, Ye L, Wu Y, Yuan Y, et al. Nerve growth factor activates autophagy in Schwann cells to enhance myelin debris clearance and to expedite nerve regeneration. *Theranostics.* (2020) 10:1649–77. doi: 10.7150/thno.40919
120. Lee IH, Cao L, Mostoslavsky R, Lombard DB, Liu J, Bruns NE, et al. A role for the NAD-dependent deacetylase Sirt1 in the regulation of autophagy. *Proc Natl Acad Sci U S A.* (2008) 105:3374–9. doi: 10.1073/pnas.0712145105
121. Romeo-Guitart D, Leiva-Rodriguez T, Forés J, Casas C. Improved motor nerve regeneration by SIRT1/Hif1 α -mediated autophagy. *Cells.* (2019) 8:E1354. doi: 10.3390/cells8111354
122. Hubbard BP, Sinclair DA. Small molecule SIRT1 activators for the treatment of aging and age-related diseases. *Trends Pharmacol Sci.* (2014) 35:146–54. doi: 10.1016/j.tips.2013.12.004
123. Carbajal KS, Schaumburg C, Strieter R, Kane J, Lane TE. Migration of engrafted neural stem cells is mediated by CXCL12 signaling through CXCR4 in a viral model of multiple sclerosis. *Proc Natl Acad Sci U S A.* (2010) 107:11068–73. doi: 10.1073/pnas.1006375107
124. Ardelit AA, Bhattacharyya BJ, Belmadani A, Ren D, Miller RJ. Stromal derived growth factor-1 (CXCL12) modulates synaptic transmission to immature neurons during post-ischemic cerebral repair. *Exp Neurol.* (2013) 248:246–53. doi: 10.1016/j.expneurol.2013.06.017
125. Zendedel A, Johann S, Mehrabi S, Joghataei M-T, Hassanzadeh G, Kipp M, et al. Activation and regulation of NLRP3 inflammasome by intrathecal application of sdf-1a in a spinal cord injury model. *Mol Neurobiol.* (2016) 53:3063–75. doi: 10.1007/s12035-015-9203-5
126. Gao D, Tang T, Zhu J, Tang Y, Sun H, Li S. CXCL12 has therapeutic value in facial nerve injury and promotes Schwann cells autophagy and migration via PI3K-AKT-mTOR signal pathway. *Int J Biol Macromol.* (2019) 124:460–8. doi: 10.1016/j.ijbiomac.2018.10.212
127. Medina DL, Di Paola S, Peluso I, Armani A, De Stefani D, Venditti R, et al. Lysosomal calcium signalling regulates autophagy through calcineurin and TFEB. *Nat Cell Biol.* (2015) 17:288–99. doi: 10.1038/ncb3114
128. Tong Y, Song F. Intracellular calcium signaling regulates autophagy via calcineurin-mediated TFEB dephosphorylation. *Autophagy.* (2015) 11:1192–5. doi: 10.1080/15548627.2015.1054594
129. Rusmini P, Cortese K, Crippa V, Cristofani R, Cicardi ME, Ferrari V, et al. Trehalose induces autophagy via lysosomal-mediated TFEB activation in models of motoneuron degeneration. *Autophagy.* (2019) 15:631–51. doi: 10.1080/15548627.2018.1535292
130. Reed CB, Frick LR, Weaver A, Sidoli M, Schlant E, Feltri ML, et al. Deletion of calcineurin in schwann cells does not affect developmental myelination, but reduces autophagy and delays myelin clearance after peripheral nerve injury. *J Neurosci.* (2020) 40:6165–76. doi: 10.1523/JNEUROSCI.0951-20.2020
131. Logan AM, Mammal AE, Robinson DC, Chin AL, Condon AF, Robinson FL. Schwann cell-specific deletion of the endosomal PI 3-kinase Vps34 leads to delayed radial sorting of axons, arrested myelination, and abnormal ErbB2-ErbB3 tyrosine kinase signaling. *Glia.* (2017) 65:1452–70. doi: 10.1002/glia.23173
132. Wang H, Wang X, Zhang K, Wang Q, Cao X, Wang Z, et al. Rapid depletion of ESCRT protein Vps4 underlies injury-induced autophagic impediment and Wallerian degeneration. *Sci Adv.* (2019) 5:eaav4971. doi: 10.1126/sciadv.aav4971
133. Pollak DD, Minh BQ, Cicvaric A, Monje FJ. A novel fibroblast growth factor receptor family member promotes neuronal outgrowth and synaptic plasticity in aplysia. *Amino Acids.* (2014) 46:2477–88. doi: 10.1007/s00726-014-1803-2
134. Moncion A, Lin M, O'Neill EG, Franceschi RT, Kripfgans OD, Putnam AJ, et al. Controlled release of basic fibroblast growth factor for angiogenesis using acoustically-responsive scaffolds. *Biomaterials.* (2017) 140:26–36. doi: 10.1016/j.biomaterials.2017.06.012
135. Jiang Y, Liang J, Li R, Peng Y, Huang J, Huang L. Basic fibroblast growth factor accelerates myelin debris clearance through activating autophagy to facilitate early peripheral nerve regeneration. *J Cell Mol Med.* (2021) 25:2596–608. doi: 10.1111/jcmm.16274
136. Li R, Li D-H, Zhang H-Y, Wang J, Li X-K, Xiao J. Growth factors-based therapeutic strategies and their underlying signaling mechanisms for peripheral nerve regeneration. *Acta Pharmacol Sin.* (2020) 41:1289–300. doi: 10.1038/s41401-019-0338-1
137. Ravikumar B, Sarkar S, Davies JE, Futter M, Garcia-Arencibia M, Green-Thompson ZW, et al. Regulation of mammalian autophagy in physiology and pathology. *Physiol Rev.* (2010) 90:1383–435. doi: 10.1152/physrev.00030.2009
138. Brosius Lutz A, Chung W-S, Sloan SA, Carson GA, Zhou L, Lovelett E, et al. Schwann cells use TAM receptor-mediated phagocytosis in addition to autophagy to clear myelin in a mouse model of nerve injury. *Proc Natl Acad Sci U S A.* (2017) 114:E8072–80. doi: 10.1073/pnas.1710566114
139. Bhattacharya A, Muller FL, Liu Y, Sabia M, Liang H, Song W, et al. Denervation induces cytosolic phospholipase A2-mediated fatty acid hydroperoxide generation by muscle mitochondria. *J Biol Chem.* (2009) 284:46–55. doi: 10.1074/jbc.M806311200
140. Tan ECTH, Bahrami S, Kozlov AV, Kurvers HAJM, Ter Laak HJ, Nohl H, et al. The oxidative response in the chronic constriction injury model of neuropathic pain. *J Surg Res.* (2009) 152:84–8. doi: 10.1016/j.jss.2008.03.035
141. Abruzzo PM, di Tullio S, Marchionni C, Belia S, Fanó G, Zampieri S, et al. Oxidative stress in the denervated muscle. *Free Radic Res.* (2010) 44:563–76. doi: 10.3109/10715761003692487
142. Kensler TW, Wakabayashi N, Biswal S. Cell survival responses to environmental stresses via the Keap1-Nrf2-ARE pathway. *Annu Rev Pharmacol Toxicol.* (2007) 47:89–116. doi: 10.1146/annurev.pharmtox.46.120604.141046
143. Zhang L, Johnson D, Johnson JA. Deletion of Nrf2 impairs functional recovery, reduces clearance of myelin debris and decreases axonal remyelination after peripheral nerve injury. *Neurobiol Dis.* (2013) 54:329–38. doi: 10.1016/j.nbd.2013.01.003
144. Griffin JW, George R, Ho T. Macrophage systems in peripheral nerves. A review. *J Neuropathol Exp Neurol.* (1993) 52:553–60. doi: 10.1097/00005072-199311000-00001
145. Müller M, Stenner M, Wacker K, Ringelstein EB, Hickey WF, Kiefer R. Contribution of resident endoneurial macrophages to the local cellular response in experimental autoimmune neuritis. *J Neuropathol Exp Neurol.* (2006) 65:499–507. doi: 10.1097/01.jnen.0000229239.43866.d1
146. Ydens E, Amann L, Asselbergh B, Scott CL, Martens L, Sichien D, et al. Profiling peripheral nerve macrophages reveals two macrophage subsets with distinct localization, transcriptome and response to injury. *Nat Neurosci.* (2020) 23:676–89. doi: 10.1038/s41593-020-0618-6
147. Gaudet AD, Popovich PG, Ramer MS. Wallerian degeneration: gaining perspective on inflammatory events after peripheral nerve injury. *J Neuroinflammation.* (2011) 8:110. doi: 10.1186/1742-2094-8-110
148. Narciso MS, Mietto B, de S, Marques SA, Soares CP, Mermelstein C, et al. Sciatic nerve regeneration is accelerated in galectin-3 knockout mice. *Exp Neurol.* (2009) 217:7–15. doi: 10.1016/j.expneurol.2009.01.008
149. Ramaglia V, King RHM, Nourallah M, Wolterman R, de Jonge R, Ramkema M, et al. The membrane attack complex of the complement system is essential for rapid Wallerian degeneration. *J Neurosci.* (2007) 27:7663–72. doi: 10.1523/JNEUROSCI.5623-06.2007
150. Ramaglia V, Wolterman R, de Kok M, Vigar MA, Wagenaar-Bos I, King RHM, et al. Soluble complement receptor 1 protects the peripheral nerve from early axon loss after injury. *Am J Pathol.* (2008) 172:1043–52. doi: 10.2353/ajpath.2008.070660
151. Brück W. The role of macrophages in Wallerian degeneration. *Brain Pathol.* (1997) 7:741–52. doi: 10.1111/j.1750-3639.1997.tb01060.x
152. Dailey AT, Avellino AM, Benthem L, Silver J, Kliot M. Complement depletion reduces macrophage infiltration and activation during Wallerian degeneration and axonal regeneration. *J Neurosci.* (1998) 18:6713–22.
153. Liu L, Lioudyno M, Tao R, Eriksson P, Svensson M, Aldskogius H. Hereditary absence of complement C5 in adult mice influences Wallerian degeneration, but not retrograde responses, following injury to peripheral nerve. *J Peripher Nerv Syst.* (1999) 4:123–33.
154. Chernov AV, Dolkas J, Hoang K, Angert M, Srikrishna G, Vogl T, et al. The calcium-binding proteins S100A8 and S100A9 initiate the early inflammatory program in injured peripheral nerves. *J Biol Chem.* (2015) 290:11771–84. doi: 10.1074/jbc.M114.622316
155. Schiopu A, Cotoi OS. S100A8 and S100A9: DAMPs at the crossroads between innate immunity, traditional risk factors, and cardiovascular disease. *Mediators Inflamm.* (2013) 2013:828354. doi: 10.1155/2013/828354
156. Boivin A, Pineau I, Barrette B, Filali M, Vallières N, Rivest S, et al. Toll-like receptor signaling is critical for Wallerian degeneration and functional recovery after peripheral nerve injury. *J Neurosci.* (2007) 27:12565–76. doi: 10.1523/JNEUROSCI.3027-07.2007
157. Vallières N, Berard JL, David S, Lacroix S. Systemic injections of Blipopolysaccharide accelerates myelin phagocytosis during Wallerian degeneration in the injured mouse spinal cord. *Glia.* (2006) 53:103–13. doi: 10.1002/glia.20266
158. Nguyen MD, Julien J-P, Rivest S. Innate immunity: the missing link in neuroprotection and neurodegeneration? *Nat Rev Neurosci.* (2002) 3:216–27. doi: 10.1038/nrn752

159. Takeda K, Kaisho T, Akira S. Toll-like receptors. *Annu Rev Immunol.* (2003) 21:335–76. doi: 10.1146/annurev.immunol.21.120601.141126
160. Willis D, Li KW, Zheng J-Q, Chang JH, Smit AB, Smit A, et al. Differential transport and local translation of cytoskeletal, injury-response, and neurodegeneration protein mRNAs in axons. *J Neurosci.* (2005) 25:778–91. doi: 10.1523/JNEUROSCI.4235-04.2005
161. Langenhan T, Piao X, Monk KR. Adhesion G protein-coupled receptors in nervous system development and disease. *Nat Rev Neurosci.* (2016) 17:550–61. doi: 10.1038/nrn.2016.86
162. Mogha A, Benesh AE, Patra C, Engel FB, Schöneberg T, Liebscher I, et al. Gpr126 functions in Schwann cells to control differentiation and myelination via G-protein activation. *J Neurosci.* (2013) 33:17976–85. doi: 10.1523/JNEUROSCI.1809-13.2013
163. Mogha A, Harty BL, Carlin D, Joseph J, Sanchez NE, Suter U, et al. Gpr126/Adgrg6 has schwann cell autonomous and nonautonomous functions in peripheral nerve injury and repair. *J Neurosci.* (2016) 36:12351–67. doi: 10.1523/JNEUROSCI.3854-15.2016
164. Martini R, Fischer S, López-Vales R, David S. Interactions between Schwann cells and macrophages in injury and inherited demyelinating disease. *Glia.* (2008) 56:1566–77. doi: 10.1002/glia.20766
165. Upgragarin N, Landman WJM, Gastra W, Gruys E. Extrahepatic production of acute phase serum amyloid A. *Histol Histopathol.* (2005) 20:1295–307. doi: 10.14670/HH-20.1295
166. Jang SY, Shin YK, Lee HY, Park JY, Suh DJ, Kim JK, et al. Local production of serum amyloid A is implicated in the induction of macrophage chemoattractants in Schwann cells during wallerian degeneration of peripheral nerves. *Glia.* (2012) 60:1619–28. doi: 10.1002/glia.22382
167. Spreyer P, Schaal H, Kuhn G, Rothe T, Unterbeck A, Olek K, et al. Regeneration-associated high level expression of apolipoprotein D mRNA in endoneurial fibroblasts of peripheral nerve. *EMBO J.* (1990) 9:2479–84
168. Ganfornina MD, Do Carmo S, Martínez E, Tolivia J, Navarro A, Rassart E, et al. ApoD, a glia-derived apolipoprotein, is required for peripheral nerve functional integrity and a timely response to injury. *Glia.* (2010) 58:1320–34. doi: 10.1002/glia.21010
169. García-Mateo N, Ganfornina MD, Montero O, Gijón MA, Murphy RC, Sanchez D. Schwann cell-derived Apolipoprotein D controls the dynamics of post-injury myelin recognition and degradation. *Front Cell Neurosci.* (2014) 8:374. doi: 10.3389/fncel.2014.00374
170. Roberts SL, Dun X, Doddrell RDS, Mindos T, Drake LK, Onaitis MW, et al. Sox2 expression in Schwann cells inhibits myelination in vivo and induces influx of macrophages to the nerve. *Development.* (2017) 144:3114–25. doi: 10.1242/dev.150656
171. Parrinello S, Napoli I, Ribeiro S, Wingfield Digby P, Fedorova M, Parkinson DB, et al. EphB signaling directs peripheral nerve regeneration through Sox2-dependent Schwann cell sorting. *Cell.* (2010) 143:145–55. doi: 10.1016/j.cell.2010.08.039
172. Deng B, Lv W, Duan W, Liu Y, Li Z, Song X, et al. FGF9 modulates Schwann cell myelination in developing nerves and induces a pro-inflammatory environment during injury. *J Cell Biochem.* (2018) 119:8643–58. doi: 10.1002/jcb.27105
173. Brown WJ, Chambers K, Doody A. Phospholipase A2 (PLA2) enzymes in membrane trafficking: mediators of membrane shape and function. *Traffic.* (2003) 4:214–21. doi: 10.1034/j.1600-0854.2003.00078.x
174. Yaksh TL, Kokotos G, Svensson CI, Stephens D, Kokotos CG, Fitzsimmons B, et al. Systemic and intrathecal effects of a novel series of phospholipase A2 inhibitors on hyperalgesia and spinal prostaglandin E2 release. *J Pharmacol Exp Ther.* (2006) 316:466–75. doi: 10.1124/jpet.105.091686
175. Lopez-Vales R, Navarro X, Shimizu T, Baskakis C, Kokotos G, Constantinou-Kokotou V, et al. Intracellular phospholipase A(2) group IVA and group VIA play important roles in Wallerian degeneration and axon regeneration after peripheral nerve injury. *Brain.* (2008) 131:2620–31. doi: 10.1093/brain/awn188
176. Yang J, Gu Y, Huang X, Shen A, Cheng C. Dynamic changes of ICAM-1 expression in peripheral nervous system following sciatic nerve injury. *Neurol Res.* (2011) 33:75–83. doi: 10.1179/016164110X12714125204353
177. Vougioukas VI, Roeske S, Michel U, Brück W. Wallerian degeneration in ICAM-1-deficient mice. *Am J Pathol.* (1998) 152:241–9.
178. Avellino AM, Dailey AT, Harlan JM, Sharar SR, Winn RK, McNutt LD, et al. Blocking of up-regulated ICAM-1 does not prevent macrophage infiltration during Wallerian degeneration of peripheral nerve. *Exp Neurol.* (2004) 187:430–44. doi: 10.1016/j.expneurol.2004.02.004
179. Liou J-T, Lee C-M, Lin Y-C, Chen C-Y, Liao C-C, Lee H-C, et al. P-selectin is required for neutrophils and macrophage infiltration into injured site and contributes to generation of behavioral hypersensitivity following peripheral nerve injury in mice. *Pain.* (2013) 154:2150–9. doi: 10.1016/j.pain.2013.06.042
180. Zhou T, Zheng Y, Sun L, Badea SR, Jin Y, Liu Y, et al. Microvascular endothelial cells engulf myelin debris and promote macrophage recruitment and fibrosis after neural injury. *Nat Neurosci.* (2019) 22:421–35. doi: 10.1038/s41593-018-0324-9
181. Hall SE, Savill JS, Henson PM, Haslett C. Apoptotic neutrophils are phagocytosed by fibroblasts with participation of the fibroblast vitronectin receptor and involvement of a mannose/fucose-specific lectin. *J Immunol.* (1994) 153:3218–27.
182. Yoon C, Korade Z, Carter BD. Protein kinase A-induced phosphorylation of the p65 subunit of nuclear factor-kappaB promotes Schwann cell differentiation into a myelinating phenotype. *J Neurosci.* (2008) 28:3738–46. doi: 10.1523/JNEUROSCI.4439-07.2008
183. Chen Y, Wang H, Yoon SO, Xu X, Hottiger MO, Svaren J, et al. HDAC-mediated deacetylation of NF-κB is critical for Schwann cell myelination. *Nat Neurosci.* (2011) 14:437–41. doi: 10.1038/nn.2780
184. Li L, Li Y, Fan Z, Wang X, Li Z, Wen J, et al. Ascorbic acid facilitates neural regeneration after sciatic nerve crush injury. *Front Cell Neurosci.* (2019) 13:108. doi: 10.3389/fncel.2019.00108
185. Huff TC, Sant DW, Camarena V, Van Booven D, Andrade NS, Mustafi S, et al. Vitamin C regulates Schwann cell myelination by promoting DNA demethylation of pro-myelinating genes. *J Neurochem.* (2021) 157:1759–73. doi: 10.1111/jnc.15015
186. Lütjohann D, Papassotiropoulos A, Björkhem I, Locatelli S, Bagli M, Oehring RD, et al. Plasma 24S-hydroxycholesterol (cerebrosterol) is increased in Alzheimer and vascular demented patients. *J Lipid Res.* (2000) 41:195–8.
187. Leoni V, Masterman T, Diczfalussy U, De Luca G, Hillert J, Björkhem I. Changes in human plasma levels of the brain specific oxysterol 24S-hydroxycholesterol during progression of multiple sclerosis. *Neurosci Lett.* (2002) 331:163–6. doi: 10.1016/s0304-3940(02)00887-x
188. Teunissen CE, Dijkstra CD, Polman CH, Hoogervorst ELJ, von Bergmann K, Lütjohann D. Decreased levels of the brain specific oxysterol 24S-hydroxycholesterol in serum of multiple sclerosis patients. *Neurosci Lett.* (2003) 347:159–62. doi: 10.1016/s0304-3940(03)00667-0
189. Sundaram VK, Massaad C, Grenier J. Liver X receptors and their implications in the physiology and pathology of the peripheral nervous system. *Int J Mol Sci.* (2019) 20:E4192. doi: 10.3390/ijms20174192
190. Gribble KD, Walker LJ, Saint-Amant L, Kuwada JY, Granato M. The synaptic receptor Lrp4 promotes peripheral nerve regeneration. *Nat Commun.* (2018) 9:2389. doi: 10.1038/s41467-018-04806-4
191. Pooya S, Liu X, Kumar VBS, Anderson J, Imai F, Zhang W, et al. The tumour suppressor LKB1 regulates myelination through mitochondrial metabolism. *Nat Commun.* (2014) 5:4993. doi: 10.1038/ncomms5993
192. Beirowski B, Babetto E, Golden JB, Chen Y-J, Yang K, Gross RW, et al. Metabolic regulator LKB1 is crucial for Schwann cell-mediated axon maintenance. *Nat Neurosci.* (2014) 17:1351–61. doi: 10.1038/nn.3809
193. He X, Zhang L, Queme LF, Liu X, Lu A, Waclaw RR, et al. A histone deacetylase 3-dependent pathway delimits peripheral myelin growth and functional regeneration. *Nat Med.* (2018) 24:338–51. doi: 10.1038/nm.4483
194. Bauer NM, Moos C, van Horssen J, Witte M, van der Valk P, Altenhein B, et al. Myelin basic protein synthesis is regulated by small non-coding RNA 715. *EMBO Rep.* (2012) 13:827–34. doi: 10.1038/embor.2012.97
195. Sherman DL, Krols M, Wu L-MN, Grove M, Nave K-A, Gangloff Y-G, et al. Arrest of myelination and reduced axon growth when Schwann cells lack mTOR. *J Neurosci.* (2012) 32:1817–25. doi: 10.1523/JNEUROSCI.4814-11.2012
196. Xue Z, Zhang S, Huang L, He Y, Fang R, Fang Y. Increased expression of Beclin-1-dependent autophagy protects against beta-amyloid-induced cell injury in PC12 cells [corrected]. *J Mol Neurosci.* (2013) 51:180–6. doi: 10.1007/s12031-013-9974-y
197. Dunlop EA, Tee AR. mTOR and autophagy: a dynamic relationship governed by nutrients and energy. *Semin Cell Dev Biol.* (2014) 36:121–9. doi: 10.1016/j.semdcb.2014.08.006
198. Carroll B, Dunlop EA. The lysosome: a crucial hub for AMPK and mTORC1 signalling. *Biochem J.* (2017) 474:1453–66. doi: 10.1042/BCJ20160780
199. Ballatore C, Brunden KR, Huryn DM, Trojanowski JQ, Lee VM-Y, Smith AB. Microtubule stabilizing agents as potential treatment for Alzheimer's disease and related neurodegenerative tauopathies. *J Med Chem.* (2012) 55:8979–96. doi: 10.1021/jm301079z
200. Ruschel J, Hellal F, Flynn KC, Dupraz S, Elliott DA, Tedeschi A, et al. Axonal regeneration. Systemic administration of epothilone B promotes axon regeneration

after spinal cord injury. *Science*. (2015) 348:347–52. doi: 10.1126/science.aaa2958

201. Weng W, Yao C, Poonit K, Zhou X, Sun C, Zhang F, et al. Metformin relieves neuropathic pain after spinal nerve ligation via autophagy flux stimulation. *J Cell Mol Med*. (2019) 23:1313–24. doi: 10.1111/jcmm.14033

202. Rotermund C, Machetanz G, Fitzgerald JC. The therapeutic potential of metformin in neurodegenerative diseases. *Front Endocrinol (Lausanne)*. (2018) 9:400. doi: 10.3389/fendo.2018.00400

203. Nikolaev A, McLaughlin T, O'Leary DDM, Tessier-Lavigne M. N-APP binds DR6 to cause axon pruning and neuron death via distinct caspases. *Nature*. (2009) 457:981–9. doi: 10.1038/nature07767

204. Farah MH, Pan BH, Hoffman PN, Ferraris D, Tsukamoto T, Nguyen T, et al. Reduced BACE1 activity enhances clearance of myelin debris and regeneration of axons in the injured peripheral nervous system. *J Neurosci*. (2011) 31:5744–54. doi: 10.1523/JNEUROSCI.6810-10.2011

205. Farah MH. BACE1 influences debris clearance and axonal regeneration in injured peripheral nerve. *J Peripher Nerv Syst*. (2012) 17:30–3. doi: 10.1111/j.1529-8027.2012.00428.x

206. Tallon C, Farah MH. Beta secretase activity in peripheral nerve regeneration. *Neural Regen Res*. (2017) 12:1565–74. doi: 10.4103/1673-5374.217319

207. Gitik M, Liraz-Zaltsman S, Oldenborg P-A, Reichert F, Rotshenker S. Myelin down-regulates myelin phagocytosis by microglia and macrophages through interactions between CD47 on myelin and SIRPα (signal regulatory protein-α) on phagocytes. *J Neuroinflammation*. (2011) 8:24. doi: 10.1186/1742-2094-8-24

208. Bian Z, Shi L, Guo Y-L, Lv Z, Tang C, Niu S, et al. Cd47-Sirpα interaction and IL-10 constrain inflammation-induced macrophage phagocytosis of healthy self-cells. *Proc Natl Acad Sci U S A*. (2016) 113:E5434–5443. doi: 10.1073/pnas.1521069113



OPEN ACCESS

EDITED BY
Peter John Shortland,
Western Sydney University, Australia

REVIEWED BY
Xavier Navarro,
Universitat Autònoma de Barcelona, Spain
Ria Arnold,
University of Wollongong, Australia

*CORRESPONDENCE
Mohammed Barham
✉ barham.mohammed@uk-koeln.de


SPECIALTY SECTION
This article was submitted to
Neurotrauma,
a section of the journal
Frontiers in Neurology

RECEIVED 22 September 2022
ACCEPTED 23 December 2022
PUBLISHED 19 January 2023

CITATION
Barham M, Andermahr J, Majczyński H,
Stawińska U, Vogt J and Neiss WF (2023)
Treadmill training of rats after sciatic nerve graft
does not alter accuracy of muscle
reinnervation. *Front. Neurol.* 13:1050822.
doi: 10.3389/fneur.2022.1050822

COPYRIGHT
© 2023 Barham, Andermahr, Majczyński,
Stawińska, Vogt and Neiss. This is an
open-access article distributed under the terms
of the [Creative Commons Attribution License](#)
(CC BY). The use, distribution or reproduction
in other forums is permitted, provided the
original author(s) and the copyright owner(s)
are credited and that the original publication in
this journal is cited, in accordance with
accepted academic practice. No use,
distribution or reproduction is permitted which
does not comply with these terms.

Treadmill training of rats after sciatic nerve graft does not alter accuracy of muscle reinnervation

Mohammed Barham^{1*}, Jonas Andermahr ², Henryk Majczyński³,
Urszula Stawińska³, Johannes Vogt^{1,4} and Wolfram F. Neiss⁵

¹Department II of Anatomy, University of Cologne and University Hospital of Cologne, Cologne, Germany, ²Kreiskrankenhaus Mechernich, Mechernich, Germany, ³Nencki Institute of Experimental Biology, Polish Academy of Sciences, Warszawa, Poland, ⁴Cluster of Excellence for Aging Research (CECAD) and Center of Molecular Medicine Cologne (CMMC), University of Cologne, Cologne, Germany, ⁵Department I of Anatomy, University of Cologne and University Hospital of Cologne, Cologne, Germany

Background and purpose: After peripheral nerve lesions, surgical reconstruction facilitates axonal regeneration and motor reinnervation. However, functional recovery is impaired by aberrant reinnervation.

Materials and methods: We tested whether training therapy by treadmill exercise (9 × 250 m/week) before (run–idle), after (idle–run), or both before and after (run–run) sciatic nerve graft improves the accuracy of reinnervation in rats. Female Lewis rats (LEW/SsNHsd) were either trained for 12 weeks (run) or not trained (kept under control conditions, idle). The right sciatic nerves were then excised and reconstructed with 5 mm of a congenic allograft. One week later, training started in the run–run and idle–run groups for another 12 weeks. No further training was conducted in the run–idle and idle–idle groups. Reinnervation was measured using the following parameters: counting of retrogradely labeled motoneurons, walking track analysis, and compound muscle action potential (CMAP) recordings.

Results: In intact rats, the common fibular (peroneal) and the soleus nerve received axons from 549 ± 83 motoneurons. In the run–idle group, 94% of these motoneurons had regenerated 13 weeks after the nerve graft. In the idle–run group, 81% of the normal number of motoneurons had regenerated into the denervated musculature and 87% in both run–run and idle–idle groups. Despite reinnervation, functional outcome was poor: walking tracks indicated no functional improvement of motion in any group. However, in the operated hindlimb of run–idle rats, the CMAP of the soleus muscle reached 11.9 mV (normal 16.3 mV), yet only 6.3–8.1 mV in the other groups.

Conclusion: Treadmill training neither altered the accuracy of reinnervation nor the functional recovery, and pre-operative training (run–idle) led to a higher motor unit activation after regeneration.

KEYWORDS

motoneuron, sciatic nerve, nerve regeneration, misdirected reinnervation, physical exercise, recovery of function

1. Introduction

The ultimate goal of nerve repair is the morphological and functional recovery of the motor and sensory systems. Numerous investigations were conducted in either the sciatic nerve or the common fibular [peroneal] nerve to estimate the quality and quantity of regeneration and recovery of function using retrograde neuronal labeling, stereology, and electrophysiology (1–13), walking track measurements (5, 13–18), and video analysis of gait methodologies (10, 19–22).

Accuracy of motor and sensory reinnervation remains a major challenge after peripheral nerve transection. The regenerating axons tend to re-grow incorrectly and thus miss the original target (23, 24). Although motoneurons preferentially reinnervate motor nerves (25, 26), they do not reinnervate the motor endplates of the original muscle fibers. This misdirection of reinnervation in cranial and spinal nerves dramatically changes the myotopic organization of central motor nuclei (3, 4, 27–34). This results in an auto-paralytic syndrome (24, 35, 36) or other permanent functional deficiencies (3, 4, 35, 37, 38). Since the pioneering work of Otto von Büngner (39), there is considerable, yet contradictory, evidence that rehabilitation after peripheral nerve injury by *adequate* exercise may contribute to functional recovery (40, 41).

Several researchers have reported a positive effect of training following nerve crush or injury. This training included both an elevated source of drinking water (17, 39, 40, 42, 43) and balance and coordination training (44–46). However, no significant training effect on sensorimotor function was observed after sciatic nerve crush followed by endurance training (47). A detrimental training effect was even reported by van Meeteren et al. (48).

Following *nerve axotomy*, a beneficial training effect has been described (49–53). No training effect using forearm stimulation or whole-body vibration was seen by Sinis et al. (54) and de Oliveira Marques et al. (55), respectively. A *negative training effect*, that is, better recovery of the SFI (sciatic functional index) in idle than in trained rats was reported by Rustemeyer et al. (56).

Treadmill training has been used in several previous studies of sciatic nerve transection (45, 52) or sciatic nerve graft (56). This investigation differs from those markedly in two ways: First, no one has previously studied the training effect on healthy animals before a nerve lesion. Does better fitness at the onset of neuronal regeneration make a difference in recovery? Second, we have trained rats until 13 weeks after surgery; only two other investigations report a similar duration of treadmill training. Rustemeyer et al. (56) trained rats for 16 weeks after sciatic nerve graft but only animals with FK506 therapy. Maqueste et al. (49) trained for 10 weeks after peroneal nerve suture but focused on axonal regeneration of mechano- and metabosensitive muscle afferents. For these reasons, this study was designed to analyze the effects of treadmill training on the onset of neuronal regeneration in healthy animals before a nerve lesion and the effects of prolonged treadmill training on functional recovery after sciatic nerve graft.

2. Materials and methods

2.1. Experimental design

All experimental procedures were performed according to the guidelines of the European Union Council (86/609/EU), and all experimental protocols were approved by the Local Animal Protection Committee (Bezirksregierung Köln, Az. 50.203.2-K35, 34/2001). Thirty-two adult, female, and Lewis rats (175–200 g; LEW/SsNHsd, Harlan, Bicester, England) were used for experimentation, and eight age-matched, male Lewis rats were used as congenic nerve donors. Throughout the study, all animals were fed standard laboratory food (Ssniff, D-59494 Soest, Germany) and tap water *ad libitum*. All animals were maintained on an artificial light–dark cycle of 12 h on and 12 h off.

The experimental animals were divided into four groups of eight rats each: *run–run*, *run–idle*, *idle–run*, and *idle–idle*. All groups received identical surgery but different physical exercises. They either received treadmill training (*run*) or no training (*idle*) for 12 weeks before and/or 12 weeks after the nerve transplant, starting 1 week after surgery. During the 12-week training, walking track analyses were performed to assess the differences in recovery of function. The evoked compound muscle action potential (CMAP) was recorded directly before nerve transection and once again 13 weeks post-transplantation. After the second set of CMAP recordings, retrograde fluorescent labeling was applied to count the number of regenerated sciatic motoneurons and assess the accuracy of reinnervation.

2.2. Physical exercise before surgery

Sixteen experimental rats (*run–run* and *run–idle* groups) were trained on a 5-lane treadmill (Panlab LE 8710R; www.panlab.com) for 12 weeks. During the first 4 weeks, each training session (two times per day at 08.00 and 16.00; nine sessions/week) began at a speed of 3 m/min that was gradationally increased to 6, 9, 12, 15, and 18 m/min, and then decreased by the same increments. The animals ran 75 m/session during the first week, 100 m during the second, 125 m in the third week, and 150 m during the fourth week. During weeks 5–12, the animals ran 250 m/session (9 × 250 m/week), reaching up to 30 m/min. All rats adapted to the treadmill well (see results). Pending the 12 weeks, the other 16 experimental rats (*idle–run* and *idle–idle* groups) and the eight age-matched donor rats were kept sedentary. Namely, two rats per cage were kept—and allowed to ambulate—in type IIIH cages [L425 mm x W265 mm x H180 mm with 800 cm² floor area (Bioscape, Raulx, 44579 Germany)] in the same animal room as the rats in training.

2.3. Sciatic nerve graft

The microsurgery was performed under an operating microscope (Carl Zeiss) after an intraperitoneal injection of 0.05 ml Ketanest/Rompun per 10 g body weight [100 mg Ketanest (WDT, D-30827 Garbsen, Germany) plus 10 mg Rompun (Bayer AG, 51368 Leverkusen, Germany) per kg body weight, that is, 1.0 ml Ketanest 100 mg/ml plus 0.5 ml Rompun 20 mg/ml mixed with 3.5 ml NaCl 0.9%]. In all 32 experimental rats, the CMAP of the sciatic nerve was measured on both the left and the right sides. On the right experimental side, after exposure of the sciatic nerve, a 5-mm long segment of the nerve was excised between the greater trochanter and the sciatic trifurcation. The continuity of the nerve was reconstructed with a 5-mm long fresh sciatic nerve graft from an age-matched, congenic donor rat by applying two 11–0 atraumatic sutures (Ethicon EH 7438G, D-22851 Norderstedt, Germany). For reconstructive surgery, each donor rat was anesthetized (see above), and four 5-mm long segments, that is, two of the left and two of the right sciatic nerve were successively excised and later implanted into four experimental animals. After the excision of the nerve grafts, the donor rats were immediately euthanized by cervical dislocation.

LEW/SsNHsd is an inbred rat strain in which congenic heterologous transplants behave like autologous transplants. Neither in this nor in a previous study (5), we have encountered immune

reactions up to 12 weeks after the sciatic nerve transplant. Similarly, automutilation did not occur in the LEW/SsNHsd rats (16, 57, 58).

2.4. Physical exercise after surgery

The run-idle and idle-idle groups were kept sedentary for 13 weeks of axonal regeneration. The run-run and idle-run groups were also kept sedentary for 1-week post-operation to allow for undisturbed wound healing. Then, training was resumed in run-run group (9×250 m/week) and was initiated in idle-run group for 12 weeks.

The rats with preoperative training promptly started running again and did not require reinforcement by the electric grid. Training of the idle-run rats was started gradually, exactly as the training in the run-run and run-idle groups before the surgery. All training sessions were closely supervised by Dr. Barham as the veterinarian, and animals that occasionally showed signs of fatigue were excepted from the session.

2.5. Walking track analysis

To estimate the functional recovery of gait, we have analyzed walking tracks strictly identical as described by Barham et al. (5). We used the program FOOTPRINTS [version 1.22, free university license (59)] for measuring the walking tracks and FOOTPRINTS STATISTICS (Robert A. Neiss; version 13-1, free license: neiss.anatomie@uni-koeln.de) for mathematical processing.

The Sciatic Functional Index (SFI) (14, 60) of each rat was calculated from walking tracks obtained 10 times before injury (normal values), immediately after nerve graft (paralysis values), and then a further 12 times post-operation (recovery values). For the recording of walking tracks, we used a 1-m long wooden ramp (30° inclination) with a small dark chamber at the top end. The track was covered with a white paper strip. The plantar surfaces of both hind paws were painted with a solution of black food coloring (mixture of European food colors E135, E104, E110, and E125) made sticky with powdered sugar (15 ml of food coloring + 120 g of sugar powder), and then the rat walked or in the case of lesioned animals rather crawled up the ramp into the top chamber. Footprints of hind paws left a stark contrast on white paper (21, 61); one strip contained seven to eight prints of each paw. The walking tracks were digitized, binarized, and converted to a resolution of 75 dpi as required for FOOTPRINTS.

Using FOOTPRINTS Print Length (PL), Total Spreading (TS, distance from the first to the fifth toe) and Intermediary Spreading (IS, distance from the second to the fourth toe) were measured for each normal (N) left and each experimental (E) right footprint (see [Supplementary material 1](#)). For each track, the mean value of 7–8 footprints of the normal side (NPL, NTS, and NIS) and the mean of the experimental side (EPL, ETS, and EIS) were calculated. In addition, the most important factor of the SFI (62), the normal step length, was measured from the left to the right, i.e., the distance from a stance on the normal left hind limb to the forward movement of the experimental right hind limb [Normal To Opposite Foot (NTOF)], and the experimental step length was measured from right to left [Experimental To Opposite Foot (ETOF)]. The lesioned hind limb is

weakened and cannot support the body weight during stance as well as the normal hind limb, resulting in an often much smaller ETOF than NTOF. ETOF minus NTOF is a direct measure of limping. The maximal values of NTOF and ETOF of each track were used for the SFI, not the mean (62). Using the average of means of eight tracks, the Sciatic Functional Index (14) was calculated as follows:

$$SFI = \left(\frac{ETOF - NTOF}{NTOF} + \frac{NPL - EPL}{EPL} + \frac{ETS - NTS}{NTS} + \frac{EIS - NIS}{NIS} \right) \div 4 \times 220$$

The measurements of ~4,100–4,700 footprints of the 616 walking tracks were carried out by specially trained technicians. To prevent observer bias, all mathematical processing was performed by another person, and only after raw data collection of walking tracks and the counting of labeled motoneurons on coded sections had been completed.

2.6. Motor nerve conduction test

Using Neuropack 2 (www.nihonkohden.com), the evoked compound muscle action potential of the soleus muscle was measured on both sides first, immediately before nerve graft (normal CMAP) and second, directly before neuronal labeling (regenerated/contralateral CMAP). Under Ketanest/Rompun anesthesia, the sciatic nerve was exposed at the mid-thigh through a gluteal muscle-splitting incision. A muscle pouch was formed and filled with 3–4 ml of paraffin oil as an electrical isolator. Then, a bipolar needle electrode was inserted into the soleus muscle laterally bypassing the gastrocnemius muscle [see Figures 100, 101 in Greene (63)]. Great care was taken that both uninsulated tips of the electrode had no contact with the gastrocnemius muscle but exclusively positioned in the soleus muscle. A flush-tip monopolar stimulator was placed onto the sciatic nerve directly proximal to the transplant, 5 mm distal to the spine on the control side. The duration of the stimulus was 0.2 ms at the supramaximal intensity of 2.6 mA. The recording analysis time was 20 ms with 10–1,000 μ V sensitivity and filters of 20–3,000 Hz. We measured the amplitude (the peak-to-peak height of the main evoked electromyography waveform, excluding late waves) and latency of muscle contraction (delay of the peak wave). All measurements were repeated 10 times.

2.7. Retrograde fluorescent neuronal labeling

Thirteen weeks post-transplantation, sufficient time for sciatic nerve regeneration and muscle reinnervation in rats (1, 3–5), the final walking track was recorded. The animals were re-anesthetized and the second set of CMAP data was recorded on the left and right sides. In addition, on the right side, the common fibular (peroneal) nerve was transected 10 mm proximal to the fibular head, and the soleus branch of the tibial nerve was close to its entrance into the soleus muscle. A few crystals of DiI (1,1'-Diocetadecyl-3,3,3',3'-Tetramethylindocarbocyanine Perchlorate; Molecular Probes, The Netherlands; cat. no. D-282) were applied to the proximal stump

of the common fibular nerve and some crystals of Fast-Blue (FB; EMS-Chemie, D-64823 Groß-Umstadt, Germany) were applied to the proximal stump of the soleus nerve. Both fluorescent tracers were always applied distal to the transplant site. Care was taken to avoid bleeding and thus blood diffusion of the fluorescent dyes. **Figure 1** (intact rat) shows that cross-diffusion of tracers did not occur. Fourteen days later, all rats were transcardially perfused with 4% formaldehyde in 0.1M phosphate buffer of pH 7.4. The lumbosacral spinal cord [L2-S2; the rat sciatic nerve that originates from L4-L6 (64)] was removed and postfixed overnight at 4°C by immersion in the same fixative. The spinal cord was longitudinally cut into a complete series of 36–40 vibratome sections of 50 µm thickness (Leica VT 1000-S), as the fibular communal nerve nucleus and the soleus nerve nucleus encompass 22–30 sections of 50 µm thickness. Then, all sections were collected, mounted, air-dried, and stored in the dark at 4°C until microscopy. Images for neuron counting (1,300 × 1,030-pixel, 3.8 MB) were recorded within the first 24 h after cutting with a Zeiss Axioskop plus ProgResC14 CCD camera (D-07743 Jena, Germany, www.jenoptik.com), using a Zeiss Plan-Neofluar 10x.

Sections were observed through shift-free AHF filter sets: www.ahf.de F11-013 for Fast Blue (FB; blue) and F41-003 for DiI (yellow/orange). Two TIFF images were recorded per field of view. The full length of the labeled motoneuron columns was covered by tiling the image frames. Using Image-Pro Plus 6.3 (www.mediacy.com; Rockville, Maryland USA 20852) and employing the physical fractionator (65), all retrogradely labeled motoneurons with a visible cell nucleus were counted in every second section (66), throughout the spinal cord. The counting of labeled neurons was performed on the operated side in separate and superimposed image files (4, 67). For a detailed discussion of the stereology, see Note on cell counting in: Valero-Cabré et al. (3).

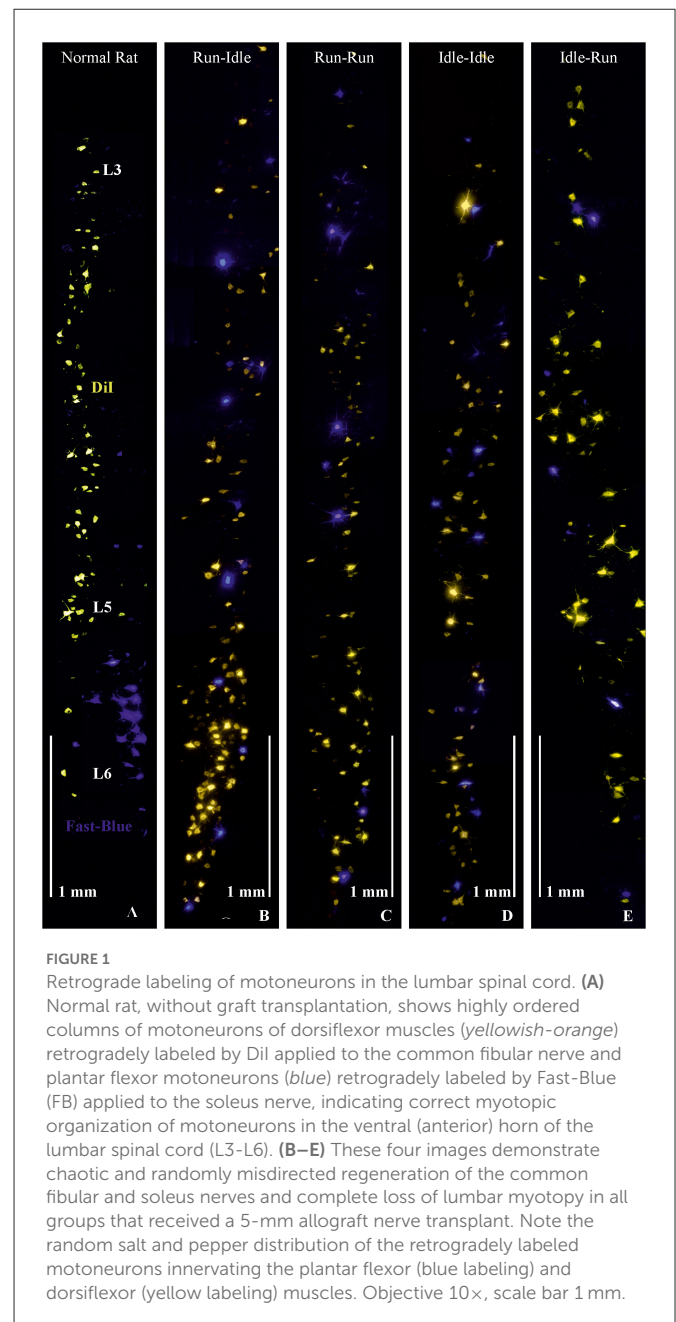
2.8. Statistical evaluation

All values are expressed as the mean ± standard deviation. Separate one-way ANOVA tests were used to analyze the effect of the training groups on the number of spinal motoneurons innervating the dorsiflexor muscles (DiI-label), respectively, the plantar flexor muscle (FB-label) of double-labeled motoneurons (DiI + FB label), as well as the total number of labeled neurons per animal. The training effects on SFI and of the motor nerve conduction tests were analyzed with a repeated measure two-way ANOVA with two factors: (1) Pre- and post-nerve graft and (2) type of training, followed by *post hoc* Fisher's LSD tests. In all tests, $p < 0.05$ was considered significant.

3. Results

3.1. General observations on treadmill training

All rats, those with training before nerve injury (run-run and run-idle groups), as well as those with training exclusively after nerve transection and repair (idle-run group), were accustomed to the treadmill. Most of the rats required a single contact with the electric grid before perpetually running on the treadmill during subsequent



sessions (except when exhausted, see below). When lifted to the treadmill, the animals jumped rather eagerly into their lanes. The distance of 250 meters per track was performed at a maximal 30 m/min, that is, ~11-min run, including a lower speed of warm-up, a procedure, which was manageable for all rats. However, after two sessions per day, a few trained rats showed signs of exhaustion. These signs included ceasing to run and resting on the disconnected electric grid, especially in the afternoon sessions. With 16 rats in training, that is, 16×9 runs = 144 training runs per week, this occurred to ~3–5 rats per week. These rats were immediately returned to the cage, and in all cases of exhaustion, they resumed running—without problems—on the following day. In daily controls by a veterinarian specialist in experimental animal husbandry, exercised rats seemed less prone to obesity and appeared more vigilant than idle animals.

TABLE 1 Number of retrogradely labeled spinal motoneurons.

Animal groups	DiI-labeled neurons innervating dorsiflexor muscles	FB-labeled neurons innervating plantar flexor muscles	Double-labeled neurons	Total (DiI+FB)	Number of neurons (% of normal count)
Normal rats*	443 ± 74	106 ± 23	Zero	549 ± 83	100%
Run-idle	352 ± 139	126 ± 53	37 ± 28	515 ± 193	93.9%
Run-run	379 ± 99	86 ± 36	10 ± 5	476 ± 99	86.6%
Idle-idle	364 ± 54	101 ± 39	15 ± 10	480 ± 94	87.4%
Idle-run	352 ± 68	85 ± 23	10 ± 7	453 ± 76	82.4%

DiI-labeled motoneurons of the dorsiflexor muscles projecting through the common fibular nerve and Fast Blue-labeled motoneurons of the plantar flexor muscles projecting through the soleus nerve in untreated animals and rats that had or had not received 12 weeks of treadmill-training before and/or after sciatic nerve graft (mean ± SD). Double-labeled motoneurons innervating dorsiflexor and plantar flexor muscles at the same time (mis-sprouting) were found in all rats that had received nerve surgery but not in intact animals. The right column shows the total number of motoneurons that were regenerated 91 days after nerve surgery. *Our previous data from six normal Lewis rats (5).

3.2. Regeneration of motoneurons

Ninety-one days after the nerve graft, the animals were reoperated for the placement of electrodes for the second set of motor nerve conduction measurements (see Section 3.4), and subsequently the application of neuronal tracers. During this surgery, no signs of neuroma formation were observed at or distal to the site of the nerve graft.

As in our previous studies (3–5), we retrogradely labeled the transected soleus nerve with Fast Blue (FB) and the cut common fibular nerve with DiI. Hereby, we stained all spinal motoneurons innervating the soleus muscle as an important plantar flexor (FB blue labeling in Figure 1), while DiI (yellow/orange labeling in Figure 1) labeled the motoneurons of most dorsiflexor muscles of the foot and toes (anterior tibialis, extensor digitorum longus and brevis, and extensor hallucis longus muscles).

In normal female Lewis rats, 443 ± 74 motoneurons projecting through the common fibular nerve innervating the dorsiflexor muscles, and 106 ± 23 motoneurons projecting through the soleus nerve innervating the plantar flexor muscles can be labeled by this tracer application (5). In all operated groups, the number of dorsiflexor motoneurons dropped to ~350–380, while that of motoneurons innervating soleus muscle decreased to ~85–125 (details see Table 1). In addition, we counted 37 ± 28 double-labeled neurons per rat in the run-idle group but only 10–15 in the other three experimental groups (Table 1). Such double-labeled neurons simultaneously innervate both dorsiflexor and plantar flexor muscles, that is, antagonistic muscles were never observed in normal, non-operated animals—only after nerve injury and regeneration. The change in neuron numbers after nerve lesion and regeneration coincides with dramatic changes in the myotopic organization of neurons.

In non-operated rats, the perikarya of motoneurons of the dorsiflexor muscles projecting through the common fibular nerve are localized in the lumbar segments L3–L5 as a cylinder-shaped nucleus in the ventral horn close to the white matter. The perikarya of plantar flexor motoneurons projecting through the soleus nerve are found in lumbar segments L5–L6, as a shorter column, more ventrally overlapping the motoneurons of the dorsiflexor muscles (Figure 1, normal rat).

In all operated rats—regardless of the training modality—the myotopic organization was replaced by a chaotic innervation, as previously shown in tracing studies of the regenerated sciatic nerve (3–5). Due to a misdirection of reinnervation, rats of all experimental groups showed evidence of a complete loss of myotopic localization of flexor and extensor motoneurons in the anterior horn of the spinal cord (Figure 1). There was no difference in the number and localization of misinnervating neurons among the run-idle, run-run, idle-idle, and idle-run groups. Separate one-way ANOVA tests showed no significant differences among all training types regarding the number of (1) DiI-labeled motoneurons, (2) FB-labeled motoneurons, and (3) the total number of labeled neurons per animal.

In summary, neither the numbers (Table 1) nor the distribution of labeled motoneurons along the lumbar spinal cord (Figure 1) indicates any effect of treadmill training on the morphological outcome of neural regeneration.

3.3. Recovery of gait

A total of 616 walking tracks of 32 rats were condensed into the dimensionless Sciatic Functional Index (14). In all rats, the SFI was around zero (−0.2 to 1.4) with a symmetric normal gait (Figure 2, uppermost track) before the lesion of the sciatic nerve. Immediately after axotomy, the total and intermediate toe spreading (ETS and EIS) on the injured side were greatly reduced in all experimental groups. The print length (EPL) was increased compared with data from the intact hind limb (NTS, NIS, and NPL). The animals severely limped with a step length from right to left (ETOF) of almost zero (Figure 2, lower tracks). Immediately after the graft, the SFI dropped to ~−60 (Figure 3), indicating complete paralysis of the transected nerve (14). During regeneration, the SFI should increase with the gradual restoration of muscle innervation (62); however, this did not occur as expected. The SFI remained at a low level, ranging from −35 to −69 (run-idle), −27 to −69 (run-run), −30 to −64 (idle-idle), and −16 to −63 (idle-run), as measured 13 times in a 3–91 day period after nerve reconstruction (Figure 3). There was no indication of recovery of motor function after nerve repair (Figures 2, 3). This holds true for all animals, either trained or kept idle. Repeated measure two-way ANOVA showed (1) no significant difference in SFI

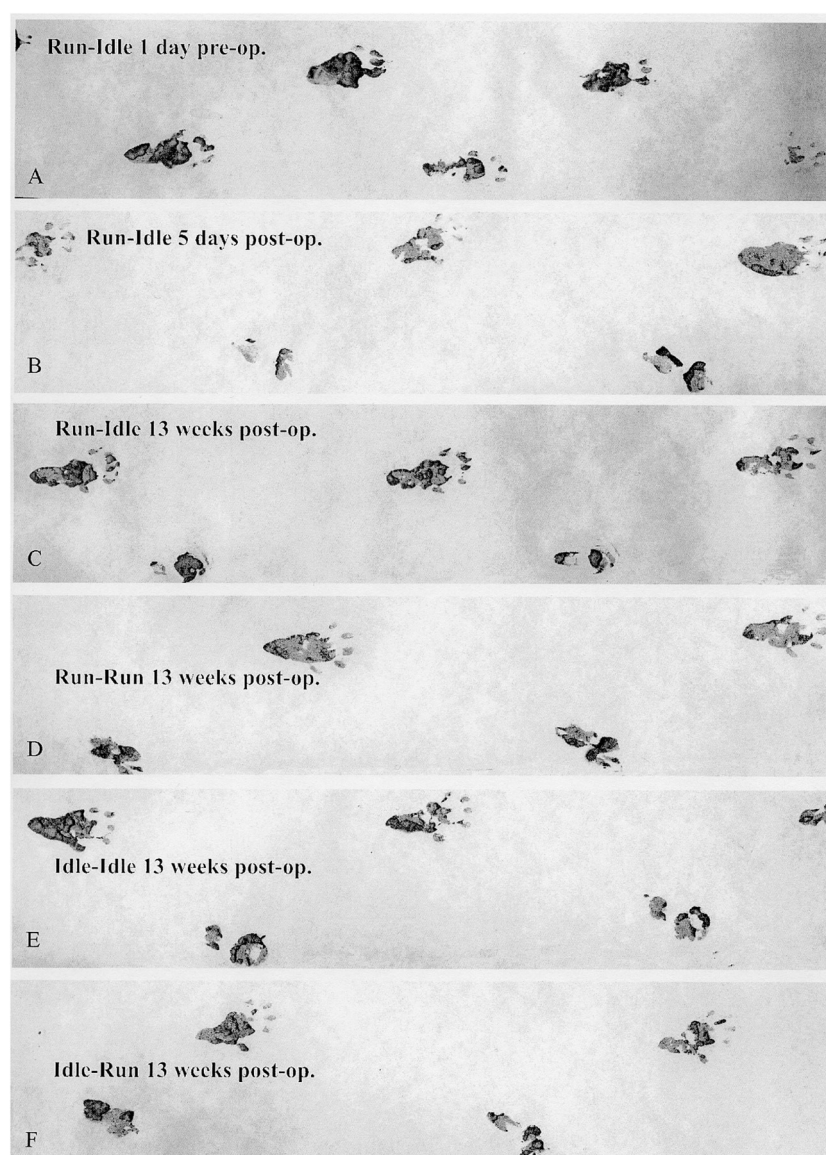


FIGURE 2

Walking track analysis. Representative sets of footprints running from left to right. (A) This track was made by a trained normal rat (run–idle 1 day before nerve transplant), with a symmetrical gait and well-splayed toes. (B) The second track presents the completely paralyzed right (operated) hind paw 5 days after the sciatic nerve transplant. The four lowest tracks (C–F) were recorded 13 weeks after sciatic nerve surgery. The upper prints from the second to the last track stem are from the intact left hind paw, and the lower are prints from the misdirectly reinnervated right hind paw. A comparison of the run–idle tracks at 5 and 91 days after nerve transplantation shows no improvement in the motor control of the right foot and the gait pattern. For details on the measurement of footprints, see [Supplementary Figure 1](#).

values during regeneration from 7 to 91 days after nerve graft and (2) no significant difference between the four training types.

3.4. Motor nerve conduction test measurements

The evoked compound muscle action potential on both, the right and left sides, was recorded in all experimental animals immediately before and 91 days after sciatic nerve reconstruction. In a pilot study in our laboratory, the CMAP amplitude of the soleus muscle was 16.5 ± 2.1 mV and the latency of muscle contraction was

2.1 ± 0.2 ms in six normal Lewis rats. The mean preoperative value of all 32 rats in the present study was 16.6 ± 2.5 mV amplitude and the latency was 2.3 ± 0.2 ms (average of means \pm SD). Within each group, there was no apparent difference in the amplitude of CMAP and the latency of muscle contraction between the right and left sides of each animal before sciatic axotomy ([Table 2](#)).

Thirteen weeks after allograft transplantation, both CMAP amplitude and latency on the left control side were about the same as before the surgery ([Table 2](#)). On the right operated side, the amplitude in the run–idle rats reduced to 73% of the preoperative value, but this dropped to 37, 54, or 43% in the run–run, idle–idle, and idle–run, respectively ([Table 2](#) and [Figure 4](#)). The latency of muscle

contraction on the right operated side was prolonged to 117–134% of the preoperative value (Table 2).

On the left side, that is, the unoperated side repeated measure two-way ANOVA showed (1) no significant difference in CMAP amplitude and latency before and after nerve graft and (2) no significant difference between the four training types.

On the right side, that is, the side of the nerve graft the same tests showed for latency (1) a very significant difference before and after the nerve graft, but (2) no significant difference between the four training types. With regard to CMAP amplitude, the repeated measure two-way ANOVA showed (1) a very significant difference before and after the nerve graft and also (2) a significant difference between the four training types. 91 days after the nerve graft, *Post hoc* Fisher's test showed no significant differences between idle-run and

the three other training groups, but rather surprisingly a significantly higher CMAP amplitude after run-idle training than after run-run ($p = 0.012$) or idle-idle ($p = 0.011$).

None of these data indicate a noticeable positive effect of treadmill training on the accuracy of muscle regeneration (Figure 1) and regain of function (Figures 2, 3)—with the exception of the increased CMAP amplitude in run-idle rats ($p = 0.04$).

4. Discussion

The ideal goal of any peripheral nerve reconstruction by end-to-end suture is to achieve a correct realignment of nerve fascicles and—theoretically—of the proximal and distal stumps of the same axons. While the former is very difficult (68–71), the latter appears impossible. There is no precise guide for the resprouting growth cones of ~7,100 myelinated and 51,000 non-myelinated axons comprising the regenerated sciatic nerve of an adult rat (66). Inadequate pathfinding leads to motor synkinesis, uncoordinated muscle movement, and/or sensory discrimination (36, 72). Previously, we found that the rat sciatic nerve regenerates almost as well with reconstructions delayed up to 1-year post-injury as with immediate nerve repair (5).

4.1. Neuronal regeneration after nerve graft

In the present study, we created a major lesion, that is, 5 mm allograft transplantation, in contrast to the crush lesion of the sciatic nerve performed in other studies (40, 43, 55). After regeneration, the number of spinal motoneurons demonstrated with retrograde labeling in the run-idle group was 94% of the normal values (549) in intact rats, 87% in each run-run and idle-idle, or 81% in idle-run. Hence, the training did not increase the number of regenerated motoneurons 13 weeks after nerve surgery—contrary to reports that are more favorable with shorter regeneration times. Molteni et al. (73) reported that after 3 days of sciatic nerve crush and regeneration, there were ~2× as many labeled neurons in the trained

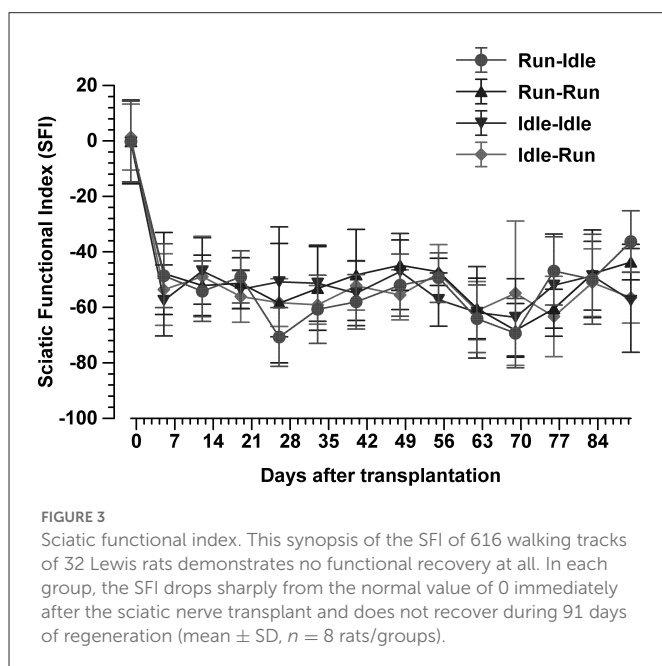


TABLE 2 Motor nerve conduction test measurements.

Animal groups	Normal intact rats		91 days after nerve graft	
	Right side	Left side	Operated side (right)	Control side (left)
Amplitude of compound muscle action potential [mV]				
Run-idle	16.3 \pm 3.6	17.2 \pm 5.0	11.9 \pm 4.9 (73%)	18.8 \pm 7.9
Run-run	17.3 \pm 4.2	17.3 \pm 5.2	6.3 \pm 3.4 (37%)	18.7 \pm 7.8
Idle-idle	12.1 \pm 3.3	13.6 \pm 2.5	6.5 \pm 2.2 (54%)	19.3 \pm 5.6
Idle-run	18.9 \pm 3.9	20.1 \pm 3.9	8.1 \pm 2.0 (43%)	18.0 \pm 7.2
Latency of compound muscle action potential [ms]				
Run-idle	2.3 \pm 0.7	2.1 \pm 0.4	3.1 \pm 0.7 (134%)	2.4 \pm 0.6
Run-run	2.6 \pm 0.5	2.1 \pm 0.2	3.2 \pm 0.6 (124%)	2.4 \pm 0.7
Idle-idle	2.7 \pm 0.5	2.1 \pm 0.5	3.2 \pm 0.6 (117%)	2.1 \pm 0.5
Idle-run	2.4 \pm 0.3	2.3 \pm 0.5	3.1 \pm 0.4 (134%)	2.0 \pm 0.3

CMAP amplitude and latency of the soleus muscle were measured in the same rats immediately before the transection of the sciatic nerve and again 91 days after the nerve graft (mean \pm SD, $n = 8$ rats/group). Data in brackets are the percent of the preoperative value.

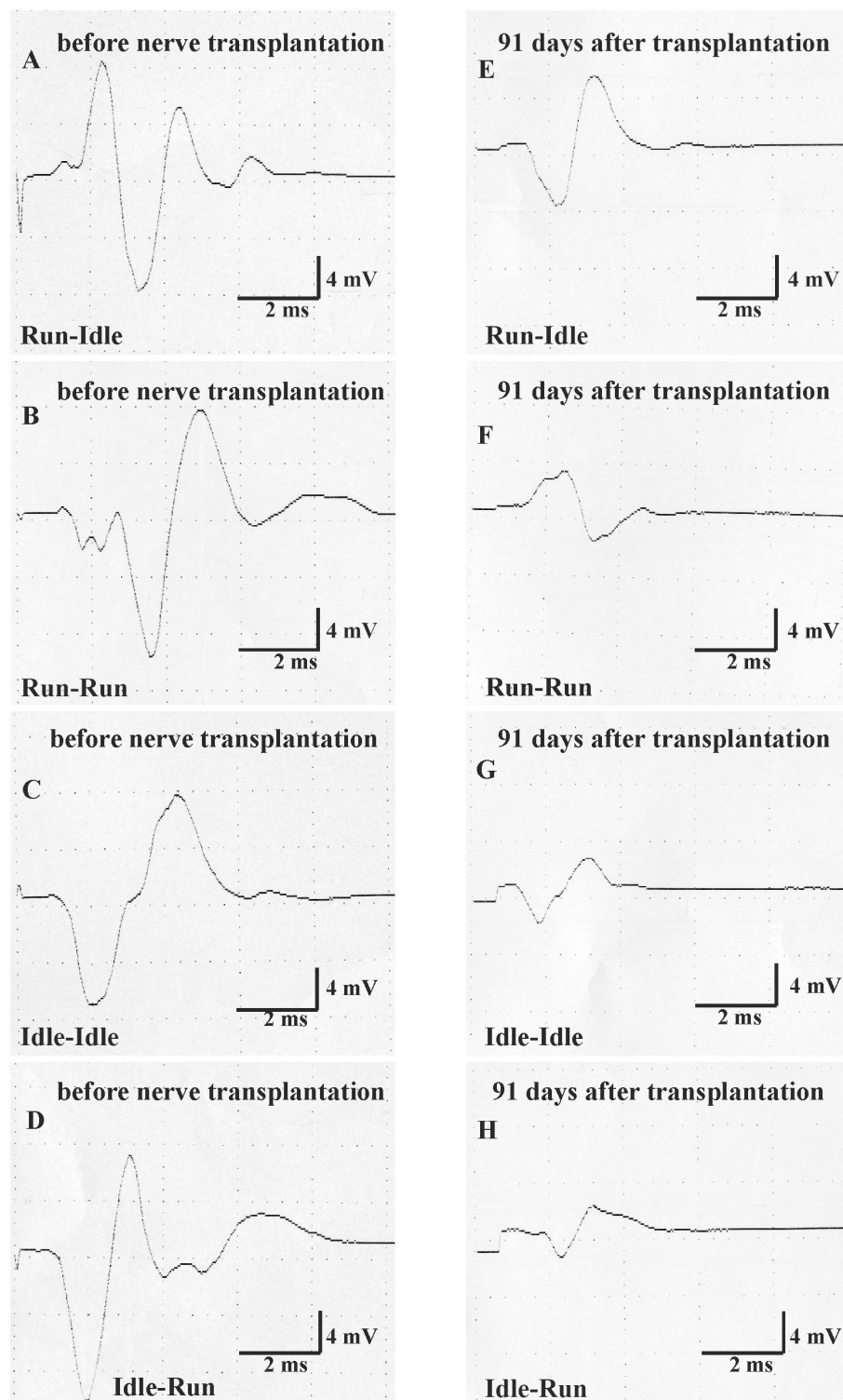


FIGURE 4

Motor nerve conduction test (MNCT). The evoked compound muscle action potential of the soleus muscle was measured first immediately before nerve transplantation in all four groups (normal CMAP, A–D), and second 91 days after sciatic nerve transplantation (regenerated CMAP, E–H).

mice as in the sedentary animals. English et al. (52) concluded that following transection and application of fibrin glue on the sciatic nerve, after 2 and 4 weeks of regeneration, ~120–240 labeled motoneurons were counted in treadmill-trained mice and 20–150 in

untrained mice. Overall, these data sets, in combination with ours, suggest that training “enhances” or “accelerates” axon regeneration in the early phase of regeneration but does not improve the final functional outcome.

4.2. Accuracy of muscle reinnervation and assessment of functional outcome

In our study, the quantitative regrowth of motoneuron axons distal to the sciatic nerve graft through the soleus and common fibular nerves was distinctly successful in all rats after nerve repair. However, the qualitative accuracy of reinnervation (Figure 1) and the recovery of motor function (Figures 2, 3) proved unsuccessful. The functional outcome, judged by SFI, was equally poor in all rats, run-idle, idle-run, run-run, or idle-idle. Neither allograft nerve graft (present study), end-to-end nerve suture, or artificial nerve conduit have achieved correct myotopic reinnervation (2, 3, 7, 31–34). Even cut and immediate suture of the thin (<0.2 mm) buccal branch of the facial nerve in rats in close proximity to its target muscle causes severe misdirection of reinnervation (34). The greatest benefit of motor reinnervation is the restoration of muscle tonus and the reduction of muscle atrophy.

In contrast to our present experiment, a crush lesion of the nerve is a relatively minor injury that does not change the myotopic organization of motoneurons in rats (3) and allows full recovery of the SFI (74). After crush axons presumably resprout rather correctly along with the bands of Büngner (39) back to their original targets due to the guidance of basal lamina tubes (68). Nerve transection, however, interrupts all basal lamina tubes, leads to the mis-sprouting of axonal branches, and destroys myotopic reinnervation (Figure 1) that cannot be compensated by central plasticity (75). In particular, double-labeled neurons, that were never observed in intact animals, simultaneously innervate fibers of the flexor and extensor muscles, and thus cause an antagonistic inhibition, also referred to as auto- or post-paralytic syndrome (3–6, 24, 27, 28, 76).

In several regeneration studies after sciatic nerve crush, forced or voluntary exercise has been reported to improve functional recovery, enhance the return of a sensorimotor function (40), increase sensory axon regeneration (73), promote remyelination of the injured nerve (77), and enlarge myofibril cross-sectional areas and diminish collagen around muscle fibers (46). Staircase training has improved task-specific performance as well as nonspecific motor and sensorimotor activities following the contusion of the rat spinal cord (78). Our long-term data after nerve graft that entail complete transection of all nerve fibers greatly differ from these more favorable results after sciatic nerve crush (40, 46, 73, 77). But why? If our training regime had negatively influenced regeneration, the animals in the idle-idle and the run-idle groups should have yielded better outcomes than run-run and idle-run rats. This was definitively not the case (Figure 3 and Table 2). Our neuronal labeling data prove that neural regeneration was complete and poor functional recovery due to neither lack of repair [compare also (79)] nor overt errors during the procedure. Hence, treadmill training, apparently independent of stress, does not alter the recovery of function after complete transection and regeneration of the sciatic nerve. The only favorable new data of the present study is the beneficial effect of preoperative training on the CMAP of the reinnervated muscle. The amplitude of CMAP was about 16.4 mV in healthy intact rats. This value was dramatically decreased and the difference was statistically significant after 91 days of regeneration in all experimental groups with the exception of the run-idle group. The run-idle group exhibited better contractility and strength of the

soleus muscle compared with other groups. Our data prove that physical fitness due to exercise before nerve injury has a beneficial effect on healing—indeed a better effect than physical exercise during regeneration.

5. Conclusion

Our data confirm with long observation times, ensuring complete regeneration, that treadmill training after sciatic nerve injury has neither beneficial nor harmful effects on muscle reinnervation and recovery of motor function. We obtained no evidence that treadmill training improves the accuracy of reinnervation.

Data availability statement

The raw data supporting the conclusions of this article will be available by the corresponding author, without undue reservation.

Ethics statement

The experimental animal study was reviewed and approved by the Bezirksregierung Köln (Az. 50.203.2-K35, 34/2001) based on the guidelines of the European Union Council (86/609/EU) and according to § 8 Tierschutzgesetz (German Federal Law for the Protection of Animals). Written informed consent was obtained from the owners for the participation of their animals in this study.

Author contributions

MB, JA, and WN: study concept and design. MB, JA, and HM: data acquisition. MB, HM, US, JV, and WN: analysis and interpretation of data. MB and JV: drafting of the manuscript. JV, US, and WN: critical revision of the manuscript for important intellectual content. US and WN: obtained funding. WN: study supervision. All authors had full access to all the data in the study and take responsibility for the integrity of the data and the accuracy of the data analysis. All authors contributed to the article and approved the submitted version.

Funding

This work was supported by the European Union COST Action B30: Neural Regeneration and Plasticity. This study was supported by the CRC 1451 to JV and MB and Cluster of Excellence for Aging Research (CECAD), University of Cologne, 50931 Cologne, Germany.

Acknowledgments

We sincerely thank Dr. H. Stützer, Institute for Medical Statistics, Informatics and Epidemiology, and Dr. M. Bekisz from the Nencki Institute, for their statistical data analysis and Mrs. I. Rohrmann for

her skillful technical assistance in our laboratory. We also thank A. Fulgham-Scott for her assistance in writing the manuscript and M. Mohammed for his technical assistance.

Conflict of interest

The authors declare that the research was conducted in the absence of any commercial or financial relationships that could be construed as a potential conflict of interest.

Publisher's note

All claims expressed in this article are solely those of the authors and do not necessarily represent those of their affiliated organizations, or those of the publisher, the editors and the reviewers.

References

- Meek MF, Den Dunnen WF, Schakenraad JM, Robinson PH: Long-term evaluation of functional nerve recovery after reconstruction with a thin-walled biodegradable poly (DL-lactide-epsilon-caprolactone) nerve guide, using walking track analysis and electrostimulation tests. *Microsurgery*. (1999) 19:247–253. doi: 10.1002/(SICI)1098-2752(1999)19:5<247::AID-MICR7>3.0.CO;2-E
- Valero-Cabré A, Navarro X. Functional impact of axonal misdirection after peripheral nerve injuries followed by graft or tube repair. *J Neurotrauma*. (2002) 19:1475–85. doi: 10.1089/089771502320914705
- Valero-Cabré A, Tsironis K, Skouras E, Navarro X, Neiss WF. Peripheral and spinal motor reorganization after nerve injury and repair. *J Neurotrauma*. (2004) 21:95–108. doi: 10.1089/089771504772695986
- Valero-Cabré A, Tsironis K, Skouras E, Perego G, Navarro X, Neiss WF: Superior muscle reinnervation after autologous nerve graft or poly-L-lactide-epsilon-caprolactone (PLC) tube implantation in comparison to silicone tube repair. *J Neurosci Res*. (2001) 63:214–223. doi: 10.1002/1097-4547(20010115)63:2<214::AID-JNRI1014>3.0.CO;2-D
- Barham M, Andermahr J, Lee J-I, Neiss WF. Successful reinnervation but poor recovery of motor function following sciatic nerve transplant delayed up to one year after axotomy in rats. *Int J Neuroprotect Neuroregener*. (2007) 3:225–38.
- Barham M, Streppel M, Guntinas-Lichius O, Fulgham-Scott N, Vogt J, Neiss WF. Treatment with nimodipine or FK506 after facial nerve repair neither improves accuracy of reinnervation nor recovery of mimetic function in rats. *Front Neurosci*. (2022) 16:895076. doi: 10.3389/fnins.2022.895076
- Hamilton SK, Hinkle ML, Nicolini J, Rambo LN, Rexwinkle AM, Rose SJ, et al. Misdirection of regenerating axons and functional recovery following sciatic nerve injury in rats. *J Comp Neurol*. (2011) 519:21–33. doi: 10.1002/cne.22446
- Udina E, Cobiánchi S, Allodi I, Navarro X. Effects of activity-dependent strategies on regeneration and plasticity after peripheral nerve injuries. *Ann Anat*. (2011) 193:347–53. doi: 10.1016/j.aanat.2011.02.012
- Udina E, Puigdemasa A, Navarro X. Passive and active exercise improve regeneration and muscle reinnervation after peripheral nerve injury in the rat. *Muscle Nerve*. (2011) 43:500–9. doi: 10.1002/mus.21912
- Jang SH, Lee JH. Effects of physical exercise on the functional recovery of rat hindlimbs with impairments of the sciatic nerve as assessed by 2D video analysis. *J Phys Ther Sci*. (2015) 27:935–8. doi: 10.1589/jpts.27.935
- Catapano J, Willand MP, Zhang JJ, Scholl D, Gordon T, Borschel GH. Retrograde labeling of regenerating motor and sensory neurons using silicone caps. *J Neurosci Methods*. (2016) 259:122–8. doi: 10.1016/j.jneumeth.2015.11.020
- Mackinnon SE, Hudson AR, Hunter DA. Histologic assessment of nerve regeneration in the rat. *Plast Reconstr Surg*. (1985) 75:384–8. doi: 10.1097/0006534-198503000-00014
- Bain JR, Mackinnon SE, Hunter DA. Functional evaluation of complete sciatic, peroneal, and posterior tibial nerve lesions in the rat. *Plast Reconstr Surg*. (1989) 83:129–38. doi: 10.1097/0006534-198901000-00025
- de Medinaceli L, Freed WJ, Wyatt RJ. An index of the functional condition of rat sciatic nerve based on measurements made from walking tracks. *Exp Neurol*. (1982) 77:634–43. doi: 10.1016/0014-4886(82)90234-5
- de Medinaceli L, Leblanc AL, Merle M. Functional consequences of isolated nerve stretch: experimental long-term static loading. *J Reconstr Microsurg*. (1997) 13:185–92. doi: 10.1055/s-2007-1006403
- Hare GM, Evans PJ, Mackinnon SE, Best TJ, Bain JR, Szalai JP, et al. Walking track analysis: a long-term assessment of peripheral nerve recovery. *Plast Reconstr Surg*. (1992) 89:251–8. doi: 10.1097/0006534-199202000-00009
- Ilha J, Araujo RT, Malysz T, Hermel EE, Rigon P, Xavier LL, et al. Endurance and resistance exercise training programs elicit specific effects on sciatic nerve regeneration after experimental traumatic lesion in rats. *Neurorehabil Neural Repair*. (2008) 22:355–66. doi: 10.1177/1545968307313502
- Casal D, Mota-Silva E, Iria I, Pais D, Farinho A, Alves S, et al. Functional and physiological methods of evaluating median nerve regeneration in the rat. *J Vis Exp*. (2020) 158:e59767. doi: 10.3791/59767
- Hruska RE, Kennedy S, Silbergeld EK. Quantitative aspects of normal locomotion in rats. *Life Sci*. (1979) 25:171–9. doi: 10.1016/0024-3205(79)90389-8
- Westerga J, Gramsbergen A. The development of locomotion in the rat. *Brain Res Dev Brain Res*. (1990) 57:163–74. doi: 10.1016/0165-3806(90)90042-W
- Dijkstra JR, Meek MF, Robinson PH, Gramsbergen A. Methods to evaluate functional nerve recovery in adult rats: walking track analysis, video analysis and the withdrawal reflex. *J Neurosci Methods*. (2000) 96:89–96. doi: 10.1016/S0165-0270(99)00174-0
- Rui J, Runge MB, Spinner RJ, Yaszemski MJ, Windebank AJ, Wang H. Gait cycle analysis: parameters sensitive for functional evaluation of peripheral nerve recovery in rat hind limbs. *Ann Plast Surg*. (2014) 73:405–11. doi: 10.1097/SAP.0000000000000008
- Langley JN, Hashimoto M. On the suture of separate nerve bundles in a nerve trunk and on internal nerve plexuses. *J Physiol*. (1917) 51:318–46. doi: 10.1113/jphysiol.1917.sp001805
- Esslen E. Electromyographic findings on two types of misdirection of regenerating axons. *Electroencephalogr Clin Neurophysiol*. (1960) 12:738–41. doi: 10.1016/0013-4694(60)90120-6
- Brushart TM. Preferential reinnervation of motor nerves by regenerating motor axons. *J Neurosci*. (1988) 8:1026–31. doi: 10.1523/JNEUROSCI.08-03.01026.1988
- Brushart TM, Seiler WA. Selective reinnervation of distal motor stumps by peripheral motor axons. *Exp Neurol*. (1987) 97:289–300. doi: 10.1016/0014-4886(87)90090-2
- Angelov DN, Skouras E, Guntinas-Lichius O, Streppel M, Popratiloff A, Walther M, et al. Contralateral trigeminal nerve lesion reduces polyneuronal muscle innervation after facial nerve repair in rats. *Eur J Neurosci*. (1999) 11:1369–78. doi: 10.1046/j.1460-9568.1999.00545.x
- Dohm S, Streppel M, Guntinas-Lichius O, Pesheva P, Probstmeier R, Walther M, et al. Local application of extracellular matrix proteins fails to reduce the number of axonal branches after varying reconstructive surgery on rat facial nerve. *Restor Neurol Neurosci*. (2000) 16:117–26.
- Udina E, Rodriguez FJ, Verdu E, Espejo M, Gold BG, Navarro X. FK506 enhances regeneration of axons across long peripheral nerve gaps repaired with collagen guides seeded with allogeneic Schwann cells. *Glia*. (2004) 47:2120–9. doi: 10.1002/glia.20025

Any product that may be evaluated in this article, or claim that may be made by its manufacturer, is not guaranteed or endorsed by the publisher.

Supplementary material

The Supplementary Material for this article can be found online at: <https://www.frontiersin.org/articles/10.3389/fneur.2022.1050822/full#supplementary-material>

SUPPLEMENTARY FIGURE 1

Footprints. The left side (A) shows the footprints of a normal, intact rat 1 day before sciatic nerve graft; the right side (B) shows the footprints of a rat 13 weeks after 5-mm sciatic nerve graft on the right experimental side. EIS, Experimental Intermediary Toe-Spreading; EPL, Experimental Print Length; ETOF, Experimental To Opposite Foot; ETS, Experimental Total Toe-Spreading; NIS, Normal Intermediary Toe-Spreading; NPL, Normal Print Length; NTOF, Normal To Opposite Foot; NTS, Normal Total Toe-Spreading.

30. de Ruiter GC, Malessy MJ, Alaid AO, Spinner RJ, Engelstad JK, Sorenson EJ, et al. Misdirection of regenerating motor axons after nerve injury and repair in the rat sciatic nerve model. *Exp Neurol*. (2008) 211:339–50. doi: 10.1016/j.expneurol.2007.12.023
31. Sabatier MJ, To BN, Nicolini J, English AW. Effect of axon misdirection on recovery of electromyographic activity and kinematics after peripheral nerve injury. *Cells Tissues Organs*. (2011) 193:298–309. doi: 10.1159/000323677
32. de Ruiter GC, Spinner RJ, Verhaagen J, Malessy MJ. Misdirection and guidance of regenerating axons after experimental nerve injury and repair. *J Neurosurg*. (2014) 120:493–501. doi: 10.3171/2013.8.JNS122300
33. Ozsoy U, Demirel BM, Hizay A, Ozsoy O, Ankerne J, Angelova S, et al. Manual stimulation of the whisker pad after hypoglossal-facial anastomosis (HFA) using a Y-tube conduit does not improve recovery of whisking function. *Exp Brain Res*. (2014) 232:2021–33. doi: 10.1007/s00221-014-3892-2
34. Harris GR, Breazzano MP, Shyu I, Donahue SP, Lavin PJM. Oculomotor Synkinesis (Aberrant Reinnervation of the Third Cranial Nerve) Associated with Atypical Tolosa-Hunt Syndrome. *Neuroophthalmology*. (2019) 44:262–6. doi: 10.1080/01658107.2019.1576738
35. Montserrat L, Benito M. Facial synkinesis and aberrant regeneration of facial nerve. *Adv Neurol*. (1988) 49:211–24.
36. Sumner AJ. Aberrant reinnervation. *Muscle Nerve*. (1990) 13:801–3. doi: 10.1002/mus.880130905
37. Guntinas-Lichius O, Glowka TR, Angelov DN, Irintchev A, Neiss WF. Improved functional recovery after facial nerve reconstruction by temporary denervation of the contralateral mimic musculature with botulinum toxin in rats. *Neurorehabil Neural Repair*. (2011) 25:15–23. doi: 10.1177/1545968310376058
38. Seitz M, Grosheva M, Skouras E, Angelova SK, Ankerne J, Jungnickel J, et al. Poor functional recovery and muscle polyinnervation after facial nerve injury in fibroblast growth factor-2/- mice can be improved by manual stimulation of denervated vibrissal muscles. *Neuroscience*. (2011) 182:241–7. doi: 10.1016/j.neuroscience.2011.03.032
39. Büngner Ov: Über die Degenerations- und Regenerationsvorgänge am Nerven nach Verletzungen. *Beiträge zur Pathologischen Anatomie und zur Pathologie*. (1891) 10:321–93
40. van Meeteren NL, Brakkee JH, Hamers FP, Helders PJ, Gispen WH. Exercise training improves functional recovery and motor nerve conduction velocity after sciatic nerve crush lesion in the rat. *Arch Phys Med Rehabil*. (1997) 78:70–7. doi: 10.1016/S0003-9993(97)90013-7
41. Milicic C, Sirbu E. A comparative study of rehabilitation therapy in traumatic upper limb peripheral nerve injuries. *Neuro Rehabil*. (2018) 42:113–9. doi: 10.3233/NRE-172220
42. Seo TB, Han IS, Yoon JH, Hong KE, Yoon SJ, Namgung U. Involvement of Cdc2 in axonal regeneration enhanced by exercise training in rats. *Med Sci Sports Exerc*. (2006) 38:1267–76. doi: 10.1249/01.mss.0000227311.00976.68
43. Bonetti LV, Korb A, Da Silva SA, Ilha J, Marcuzzo S, Achaval M, et al. Balance and coordination training after sciatic nerve injury. *Muscle Nerve*. (2011) 44:55–62. doi: 10.1002/mus.21996
44. Bobinski F, Martins DF, Bratti T, Mazzardo-Martins L, Winkelmann-Duarte EC, Guglielmo LG, et al. Neuroprotective and neuroregenerative effects of low-intensity aerobic exercise on sciatic nerve crush injury in mice. *Neuroscience*. (2011) 194:337–48. doi: 10.1016/j.neuroscience.2011.07.075
45. Boeltz T, Ireland M, Mathis K, Nicolini J, Poplavski K, Rose SJ, et al. Effects of treadmill training on functional recovery following peripheral nerve injury in rats. *J Neurophysiol*. (2013) 109:2645–57. doi: 10.1152/jn.00946.2012
46. Bonetti LV, Malysz T, Ilha J, Barbosa S, Achaval M, Faccioni-Heuser MC. The effects of two different exercise programs on the ultrastructural features of the sciatic nerve and soleus muscle after sciatic crush. *Anat Rec (Hoboken)*. (2017) 300:1654–61. doi: 10.1002/ar.23611
47. Bonetti LV, Schneider AP, Barbosa S, Ilha J, Faccioni-Heuser MC. Balance and coordination training and endurance training after nerve injury. *Muscle Nerve*. (2015) 51:83–91. doi: 10.1002/mus.24268
48. van Meeteren NL, Brakkee JH, Helders PJ, Gispen WH. The effect of exercise training on functional recovery after sciatic nerve crush in the rat. *J Peripher Nerv Syst*. (1998) 3:277–82.
49. Marqueste T, Alliez JR, Alluin O, Jammes Y, Decherchi P. Neuromuscular rehabilitation by treadmill running or electrical stimulation after peripheral nerve injury and repair. *J Appl Physiol*. (2004) 96:1988–95. doi: 10.1152/jappphysiol.00775.2003
50. Sabatier MJ, Redmon N, Schwartz G, English AW. Treadmill training promotes axon regeneration in injured peripheral nerves. *Exp Neurol*. (2008) 211:489–93. doi: 10.1016/j.expneurol.2008.02.013
51. Asensio-Pinilla E, Udina E, Jaramillo J, Navarro X. Electrical stimulation combined with exercise increase axonal regeneration after peripheral nerve injury. *Exp Neurol*. (2009) 219:258–65. doi: 10.1016/j.expneurol.2009.05.034
52. English AW, Cucoranu D, Mulligan A, Sabatier M. Treadmill training enhances axon regeneration in injured mouse peripheral nerves without increased loss of topographic specificity. *J Comp Neurol*. (2009) 517:245–55. doi: 10.1002/cne.22149
53. English AW, Wilhelm JC, Sabatier MJ. Enhancing recovery from peripheral nerve injury using treadmill training. *Ann Anat*. (2011) 193:354–61. doi: 10.1016/j.aanat.2011.02.013
54. Sinis N, Guntinas-Lichius O, Irintchev A, Skouras E, Kuerten S, Pavlov SP, et al. Manual stimulation of forearm muscles does not improve recovery of motor function after injury to a mixed peripheral nerve. *Exp Brain Res*. (2008) 185:469–83. doi: 10.1007/s00221-007-1174-y
55. de Oliveira Marques C, Amaro Espindula I, Kwame Karikari Darko E, Viçosa Bonetti L, Souza A, Aparecida Partata W, et al. Whole-body vibration therapy does not improve the peripheral nerve regeneration in experimental model. *J Musculoskelet Neuronal Interact*. (2021) 21:68–78.
56. Rustemeyer J, Krajacic A, Dicke U. Histomorphological and functional impacts of postoperative motor training in rats after allograft sciatic nerve transplantation under low-dose FK 506. *Muscle Nerve*. (2009) 39:480–8. doi: 10.1002/mus.21251
57. Carr MM, Best TJ, Mackinnon SE, Evans PJ. Strain differences in autotomy in rats undergoing sciatic nerve transection or repair. *Ann Plast Surg*. (1992) 28:538–44. doi: 10.1097/0000637-199228060-00008
58. Chamberlain LJ, Yannas IV, Hsu HP, Strichartz GR, Spector M. Near-terminus axonal structure and function following rat sciatic nerve regeneration through a collagen-GAG matrix in a ten-millimeter gap. *J Neurosci Res*. (2000) 60:666–77. doi: 10.1002/(SICI)1097-4547(20000601)60:5<666::AID-JNR12>3.0.CO;2-0
59. Klapdor K, Dülfer BG, Hammann A, Van der Staay FJ. A low-cost method to analyse footprint patterns. *J Neurosci Methods*. (1997) 75:49–54. doi: 10.1016/S0165-0270(97)00042-3
60. Cação-Benedini LO, Ribeiro PG, Gomes AR, Ywazaki JL, Monte-Raso VV, Prado CM, et al. Remobilization through stretching improves gait recovery in the rat. *Acta Histochem*. (2013) 115:460–9. doi: 10.1016/j.acthis.2012.11.001
61. Johnston RB, Zachary L, Dellon AL, Seiler WA, Teplica DM: Improved imaging of rat hindfoot prints for walking track analysis. *J Neurosci Methods*. (1991) 38:111–4. doi: 10.1016/0165-0270(91)90161-R
62. de Medinaceli L, Seaber AV. Experimental nerve reconnection: importance of initial repair. *Microsurgery*. (1989) 10:56–70. doi: 10.1002/micr.1920100111
63. Greene EC. Anatomy of the rat. *Transac Am Philos Soc New Ser*. (1935) 27:1–370. doi: 10.2307/1005513
64. Schmalbruch H: Fiber composition of the rat sciatic nerve. *Anat Rec*. (1986) 215:71–81. doi: 10.1002/ar.1092150111
65. Gundersen HJ: Stereology of arbitrary particles. A review of unbiased number and size estimators and the presentation of some new ones, in memory of William R. Thompson. *J Microsc*. (1986) 143:3–45. doi: 10.1111/j.1365-2818.1986.tb02764.x
66. Auer M, Allodi I, Barham M, Udina E, Neiss WF, Navarro X, et al. C3 exoenzyme lacks effects on peripheral axon regeneration in vivo. *J Peripher Nerv Syst*. (2013) 18:30–6. doi: 10.1111/jns.12004
67. Neiss WF, Guntinas Lichius O, Angelov DN, Gunkel A, Stennert E. The hypoglossal-facial anastomosis as model of neuronal plasticity in the rat. *Ann Anat*. (1992) 174:419–33. doi: 10.1016/S0940-9602(11)80266-9
68. Lundborg G. *Nerve Injury and Repair: Regeneration, Reconstruction, and Cortical Remodeling 2nd edn*. Philadelphia: Elsevier/Churchill Livingstone (2004). p. 248.
69. Evans PJ, Bain JR, Mackinnon SE, Makino AP, Hunter DA. Selective reinnervation: a comparison of recovery following microsuturing and conduit nerve repair. *Brain Res*. (1991) 559:315–21. doi: 10.1016/0006-8993(91)90018-Q
70. Millesi H. *Chirurgie der peripheren Nerven*. München, Wien, Baltimore: Urban & Schwarzenberg (1992). p. 232.
71. Amara B, de Medinaceli L, Lane GB, Merle M. Functional assessment of misdirected axon growth after nerve repair in the rat. *J Reconstr Microsurg*. (2000) 16:563–7. doi: 10.1055/s-2000-8396
72. Aldskogius H, Molander C. Specificity in regenerative outgrowth and target reinnervation by mammalian peripheral axons. *Restor Neurol Neurosci*. (1990) 1:275–80. doi: 10.3233/RNN-1990-13415
73. Molteni R, Zheng JQ, Ying Z, Gómez-Pinilla F, Twiss JL. Voluntary exercise increases axonal regeneration from sensory neurons. *Proc Natl Acad Sci U S A*. (2004) 101:8473–8. doi: 10.1073/pnas.0401443101
74. Malysz T, Ilha J, Nascimento PS, De Angelis K, Schaan BD, Achaval M. Beneficial effects of treadmill training in experimental diabetic nerve regeneration. *Clinics (São Paulo)*. (2010) 65:1329–37. doi: 10.1590/S1807-59322010001200017
75. Gruart A, Streppel M, Guntinas-Lichius O, Angelov DN, Neiss WF, Delgado-García JM. Motoneuron adaptability to new motor tasks following two types of facial-facial anastomosis in cats. *Brain*. (2003) 126:115–133. doi: 10.1093/brain/awg008
76. Akulov MA, Orlova OR, Tabashnikova TV, Karnaukhov VV, Orlova AS. Facial nerve injury in neurosurgery: a rehabilitation potential of botulinum therapy. *Zh Vopr Neurokhir Im N N Burdenko*. (2018) 82:111–8. doi: 10.17116/neiro2018821111-118
77. Kim J-O, Seo T, Yoon J-H. Effects of treadmill training on axonal regeneration, spinal cord motor neuron, GAP-43 & GLUT-4 protein expression after sciatic nerve injury in the streptozotocin-induced diabetic rats. *Int J Applied Sports Sci*. (2007) 19:117–33.
78. Singh A, Murray M, Houle JD. A training paradigm to enhance motor recovery in contused rats: effects of staircase training. *Neurorehabil Neural Repair*. (2011) 25:24–34. doi: 10.1177/1545968310378510
79. Streppel M, Angelov DN, Guntinas-Lichius O, Hilgers RD, Rosenblatt JD, Stennert E, et al. Slow axonal regrowth but extreme hyperinnervation of target muscle after suture of the facial nerve in aged rats. *Neurobiol Aging*. (1998) 19:83–8. doi: 10.1016/S0197-4580(97)00163-2



OPEN ACCESS

EDITED BY

Edgar Richard Kramer,
University of Plymouth,
United Kingdom

REVIEWED BY

Kirsten Haastert-Talini,
Hannover Medical School, Germany
Justin C. Burrell,
University of Pennsylvania,
United States

*CORRESPONDENCE

George D. Bittner
✉ bittner@austin.utexas.edu

SPECIALTY SECTION

This article was submitted to
Cellular Neuropathology,
a section of the journal
Frontiers in Cellular Neuroscience

RECEIVED 02 November 2022

ACCEPTED 20 December 2022

PUBLISHED 19 January 2023

CITATION

Lopez S, Bittner GD and Treviño RC
(2023) Rapid and effective fusion repair
of severed digital nerves using
neurorrhaphy and bioengineered
solutions including polyethylene
glycol: A case report.
Front. Cell. Neurosci. 16:1087961.
doi: 10.3389/fncel.2022.1087961

COPYRIGHT

© 2023 Lopez, Bittner and Treviño.
This is an open-access article
distributed under the terms of the
[Creative Commons Attribution License](#)
(CC BY). The use, distribution or
reproduction in other forums is
permitted, provided the original
author(s) and the copyright owner(s)
are credited and that the original
publication in this journal is cited, in
accordance with accepted academic
practice. No use, distribution or
reproduction is permitted which does
not comply with these terms.

Rapid and effective fusion repair of severed digital nerves using neurorrhaphy and bioengineered solutions including polyethylene glycol: A case report

Stephen Lopez¹, George D. Bittner^{2*} and Richard C. Treviño³

¹Canton Plastic Surgery, Canton, OH, United States, ²Department of Neuroscience, University of Texas at Austin, Austin, TX, United States, ³WellSpan Medical Group, York, PA, United States

Peripheral nerve injuries (PNIs) that consist of simple nerve severance often result in severe motor impairment and permanent loss of function. Such patients face significant costs and pose major burdens to healthcare systems. Currently, the most promising surgical technique to achieve the best clinical outcome after such PNIs is immediate primary coaptation of severed nerve ends by microsutures (neurorrhaphy). However, recovery is often poor and delayed for many months due to Wallerian degeneration (WD) and slow (1–2 mm/day) axonal outgrowths from severed proximal axons that may not properly reinnervate denervated afferent/efferent targets that have atrophied. In contrast, recent pre-clinical studies using polyethylene glycol (PEG) to facilitate primary nerve repair have greatly improved the rate and extent of sensory and motor recovery and prevented much WD and muscle atrophy. That is, PEG-fused axons rapidly establish proximal–distal axoplasmic/axolemmal continuity, which do not undergo WD and maintain the structure and function of neuromuscular junction (NMJ). PEG-fused axons rapidly reinnervate denervated NMJs, thereby preventing muscle atrophy associated with monthslong denervation due to slowly regenerating axonal outgrowths. We now describe PEG-mediated fusion repair of a digital nerve in each of two patients presenting with a digital laceration resulting in total loss of sensation. The first patient's tactile perception improved markedly at 3 days postoperatively (PO). Two-point discrimination improved from greater than 10 mm at initial presentation to 4 mm at 11-week PO, and the Semmes–Weinstein monofilament score improved from greater than 6.65 to 2.83 mm, a near-normal level. The second patient had severe PO edema and scar development requiring a hand compression glove and scar massage, which began improving at 11-week PO. The sensory function then improved for 4 months PO, with both two-point discrimination and Semmes–Weinstein scores approaching near-normal levels at the final follow-up. These case

study data are consistent with data from animal models. All these data suggest that PEG-fusion technologies could produce a paradigm shift from the current clinical practice of waiting days to months to repair ablation PNIs with autografts, anucleated nerve allografts, or conduits in which the patient outcome is solely dependent upon axon regeneration over months or years.

KEYWORDS

peripheral nerve injury, polyethylene glycol, repair digital nerves, Wallerian degeneration, Semmes–Weinstein monofilament test, two point discrimination test

Introduction

Peripheral nerve injuries (PNIs) often produce impairments leading to long-term disabilities (Ruijs et al., 2005). Continued advances in surgical devices and procedures for nerve repair have had marginal success with patient satisfaction in motor recovery as low as 51.6% (Ruijs et al., 2005). Although limited data are available on their incidence, PNIs can lead to significant motor impairment and permanent loss of function, resulting in extraordinary costs and burdens to healthcare systems (Lundborg, 2005; Rosberg et al., 2005; Campbell, 2008; Brushart, 2011). Primary coaptations of severed proximal and distal nerve ends using microsutures (neurorrhaphy) currently produce the best outcomes clinically and in experimental animals, but recovery is still markedly delayed and poor due to Wallerian degeneration (WD) and slow nerve outgrowth at 1–2 mm per day often producing non-specific (if any) reinnervation of original sensory and motor target tissues (Mailander et al., 1989; al-Ghazal et al., 1994; Campbell, 2008; Brushart, 2011). This delayed reinnervation also limits recovery after neurorrhaphy due to muscle atrophy and loss of denervated end organs (Donaldson et al., 2002; Brushart, 2011). For example, an M3 motor grade (against gravity without resistance) and less than 15 mm two-point discrimination qualify as successful clinical outcomes.

Polyethylene glycol (PEG) has been used for its membrane fusogenic properties for many decades to make cell hybrids (Roos et al., 1983) and as an intravenous treatment for hemophiliacs (Johnson et al., 1971). Its fusogenic properties have successfully been applied to invertebrate giant axons and mammalian PNS and CNS axons *ex vivo* and *in vivo* (Bittner et al., 1986, 2012, 2016, 2022; Krause and Bittner, 1990; Lore et al., 1999; Donaldson et al., 2002). PEG-fusion repair of severed axons combined with primary nerve coaptation immediately and randomly joins (fuses/repairs) severed distal and proximal axonal ends to re-establish the structural and functional/electrophysiological continuity of 40–60% of severed myelinated axons across the lesion site. Successfully, PEG-fused axons do not undergo WD and exhibit minimal delamination or other changes in their myelin sheaths. PEG-fusion repair

of singly cut PNIs immediately reinnervates many muscle fibers and sensory receptor endings. This rapid reinnervation is non-specific and produces immediate functional recovery of compound (nerve) action potentials and compound muscle action potentials but not immediate recovery of voluntary behaviors. Recovery of useful sensory/motor functions and voluntary behaviors takes 2–6 weeks and extensively involves many PNS and CNS plasticities (Mikesh et al., 2018a,b; Ghergherehchi et al., 2019; Bittner et al., 2022). The 40–60% of axons *not* PEG-fused undergo WD within 7 days and regenerating outgrowths arise from the severed ends of surviving proximal axons connected to their sensory cell bodies in dorsal root ganglia or motor cell bodies in the spinal ventral horn.

In this case study report, we apply the success of PEG-fusion previously demonstrated in animal models (Lore et al., 1999; Bittner et al., 2012, 2016, 2022; Bamba et al., 2016; Mikesh et al., 2018a,b) to present one of the first patient series in 2017–2018 in the United States to undergo FDA-approved PEG-fusion of human peripheral nerves.

Case presentation

The trial was approved by the WellSpan Health Institutional Review Board. Trial registrations, www.clinicaltrials.gov NCT03236064. IND 118873 for PEG, were approved by the FDA. All participants provided written informed consent. The patients presented here are the first cases in our study series. Selection criteria were patients with a sharp, clean laceration and the ability for primary repair without tension within 24 h of the injury. Exclusion criteria were patients with traction injuries, inability to repair the nerve within 24 h, and the inability to primary repair without tension. We used two-point discrimination (2PD) and Semmes–Weinstein monofilament (SWM) tests (Bell-Krotoski et al., 1995; Silva et al., 2014). In brief, the normal range of digital 2PD is 2–8 mm, and 2.83–3.61 SWM sizes constitute a normal response.

All patients that met the inclusion criteria were given the opportunity to participate in our study. Patients were

TABLE 1 Polyethylene glycol (PEG)-fusion protocol for repairing singly cut peripheral nerve injuries (PNIs).

Protocol Steps #1–5	Completely sever and trim nerve ends	Additive distress/toxicity: None Purpose: Prepare nerve ends for neurorrhaphy and PEG repair/fusion.
1. Priming Solution #1	Irrigation of surgical field with hypotonic Ca ²⁺ -free saline for 1–2 min	Additive distress/toxicity: None Purpose: Increase axoplasmic volume. Open cut axonal ends. Expel intracellular vesicles/organelles to enhance PEG-fusion.
2. Protection Solution #2	Administer 0.5% methylene blue (MB; an antioxidant) in distilled water for 1–2 min to opened cut ends	Additive distress/toxicity: None Purpose: Prevent formation of intracellular vesicles/organelles that interfere with PEG-fusion of cut ends and can seal-off each apposed cut end rather joining/fusing them.
3. Closely appose cut, opened, nerve ends	Perform neurorrhaphy	Additive distress/toxicity: None Purpose: Join nerve ends together for axonal sealing. Provide mechanical strength at each site of PEG-fusion.
4. PEG-fuse many axons Solution #3	Apply 50% w/w 3.35 kDa PEG in ddH ₂ O for 1–2 min to the coaptation site	Additive distress/toxicity: None Purpose: Remove bound cell water to induce closely apposed, open, axonal membranes to non-specifically fuse.
5. Membrane repair Solution #4	Irrigation of coaptation site with isotonic Ca ²⁺ -containing saline	Additive distress/toxicity: None Purpose: Induce vesicle formation to plug/seal any axolemmal holes after PEG-induced annealing of open cut axonal ends.

administered standard general anesthesia. The wounds were explored using loupe magnification. The nerve repairs were performed under the operating microscope. For our PEG-fusion protocol as published for the repair of singly cut rat sciatic nerves (Table 1), we irrigated the repair site with a calcium-free hypotonic solution (50% v/v normal saline in water) and used 9-0 nylon epineurial sutures to coapt the nerves. Methylene blue (1%, Faulding, Aguadilla, Puerto Rico) was then applied to the coapted site. PEG 50% w/w in sterile distilled water was subsequently added for 2 min to promote the fusion of the axolemmal leaflets. The lesion site was then irrigated with Lactated Ringer's Injection solution (Hospira, Lake Forest, IL, USA) to completely remove the PEG and enhance axonal repair, that is, Lactated Ringer's solution contains calcium, which helps seal any remaining holes in PEG-fused axons and seal the cut ends of any axons that did not successfully fuse (Table 1). The wounds were then closed with 4-0 nylon sutures, and the patients were splinted to facilitate recovery.

Patient #1: A 35-year-old, right hand dominant, female patient lacerated her left index finger on a broken mirror at 1,500 h on 18 February 2017 and went to the emergency room secondary to a loss of sensation on the radial aspect of her left index finger. The laceration was on the radial side of the metacarpophalangeal flexion crease 7.5 cm from the tip of the finger. Her previous medical history included a storage pool defect, endometriosis, polycystic ovarian disease, and an adrenal mass. She smoked approximately half pack per day. The evaluation in the emergency room demonstrated no sensation present on the radial side of the index finger from the point of the laceration to the distal tip of the finger, with a 2PD response of greater than 10 mm and SWM response of greater than 6.65 mm. Noxious stimuli were applied by a 25-gauge needle and stabbed along with the radial aspect of the finger, including the pulp, without any perceived sensation. The sensation was intact

and normal on the ulnar aspect of the index finger with 4 mm 2PD of 4 mm and 3.61 mm SWM.

Informed consent was obtained from patient #1 for PEG-fusion repair of the digital nerve, and the patient was then taken to the operating room at 0830 on 18 February 2017, i.e., within 24 h of injury. As observed under operating microscope high powered magnification, 50% of the radial digital nerve was lacerated, and the radial half had two clean-cut fascicles with a separation of less than 2 mm. Both the proximal and distal ends were easily identified and could be perfectly aligned. The epineurium was easily approximated, creating a direct fascicle-to-fascicle contact without bunching or axonal escape. The radial digital artery and flexor tendon sheath were intact. Post-surgery, the patient was placed in a protective dorsal blocking splint maintaining the index and middle fingers in the intrinsic plus position. The total time elapsed from the laceration to repair was 17.5 h.

Patient #1 had subjective feeling in the tip of her index finger and responded to noxious stimuli at the time of discharge 1–2 h PO, and the results were notably better than her pre-operative evaluation. By 3 days PO, the largest type A fibers of the fingertip had some recordable sensation using SWM of 4.56 at the distal tip [The SWM examination demonstrated no sensation prior to intervention]. However, at 3-day PO, she initially complained of dull aching, some hypersensitivity, and lacked normal thermoreception, perceiving cold as wet. Her 2PD continued to improve over the next 70 days (Figure 1A). Her 2PD and SWM scores returned to near baseline levels by 80-day PO, which remained stable for 2 years PO (Figures 1A, B). At the last postoperative visit, the patient experienced cold stimuli as wet, suggesting that the smaller type A δ and C fibers were altered, resulting in a lack of thermoreception.

Patient #2: A 35-year-old male patient lacerated the palmar aspect of his left hand when cleaning a teapot, when it shattered

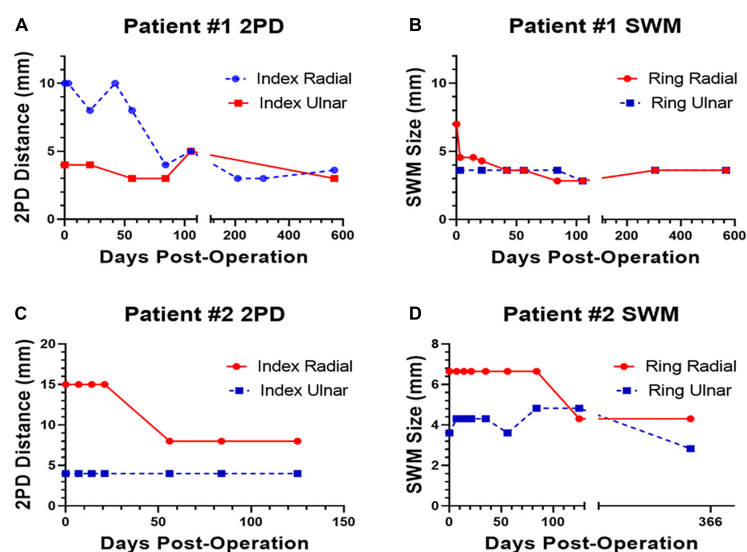


FIGURE 1

Polyethylene glycol (PEG)-fusion 2PD and Semmes–Weinstein monofilament (SWM) scores on the injured site (red, solid line) and on the uninjured site (blue, dotted line) plotted versus postoperatively (PO) days for Patient #1 (A,B) and Patient #2 (C,D).

(15 October 2017). Patient #2 reported copious bleeding that could not be controlled with a towel wrap. He called EMS and was brought into the emergency department with two forearm tourniquets in place. His past medical history was significant for anxiety and depression. His current medications were Paxil. The evaluation in the ER revealed a 3 cm transverse laceration at the base of the thenar eminence. Allen's test was abnormally consistent with ulnar artery laceration. There was no sensation in the thumb, index, or middle fingers with 2PD greater than 10 mm. His 2PD on the small finger and ulnar aspect of the ring finger was 5 mm.

Informed consent was obtained from Patient #2 for PEG-fusion repair of the digital nerve, and he was taken to the operating room within 24 h of the injury. Exploration was performed under loupe magnification. The ulnar artery was completely lacerated and repaired with 8-0 nylon suture. The median nerve was completely lacerated within the carpal tunnel just proximal to its branching. Intraoperative nerve stimulation confirmed motor branch laceration and location. Accurate fascicular alignment was achieved, and epineural repair was performed under the operating microscope with three 8-0 nylon sutures. Tension-free repair was noted with the wrist in 20° of flexion and full finger extension; he was placed in a posterior splint maintaining wrist flexion of 20° but allowed finger motion.

At 6 days PO, the 2PD of the thumb, index, and middle fingers was all greater than 10 mm. Thumb palmar abduction was weak. At 13-day PO, pinprick sensation was intact on the palmar aspect over the proximal phalanx of the index and middle fingers; 2PD was still greater than 10 mm at the finger pulps. At 21-day PO, Patient #2 demonstrated no improvement. At 35-day PO, his 2PD was 8 mm on the radial aspect of the

ring finger and greater than 10 mm for the thumb, index, and middle fingers. His splint was discontinued and therapy (hand compression and glove and scar massage) commenced due to significant edema and scar development PO. At 8-week PO, Patient #2 reported painful stimuli from a splinter in one of his fingers and was able to perceive heat. His 2PD was 8 mm for the ring finger and greater than 8 mm for the thumb, index, and ring fingers (Figures 1C, D). At 4-month PO, Patient #2 reported continued improvement in sensation to affected digits, but his 2PD remained greater than 8 mm; his SWM was 6.65. At 11-month final follow-up, his SWM was 4.31 for the thumb, index, and middle fingers and 2.83 for the ring and small fingers (Figures 1C, D). There were no documented adverse events related to the PEG-fusion procedure through 11-month PO.

Discussion

Patient #1 had a clean partial laceration to a pure sensory nerve. This minimally traumatic injury to an unfunctional nerve made PO assessments easier than if a mixed motor and sensory nerves were severed. This injury also allowed us to observe the outcomes of various sensory nerve fiber types, for example, mechanoreceptors, thermoreceptors, and nociceptors. At a rate of ~1 mm per day, the proximal portion of the nerve should have taken 75 days to regenerate to begin to reinnervate terminal end organs. However, Patient #1 showed marked improvement in recovery time with recordable SWM and 2PD values as early as 0–20 days PO and a return to normal values by 70 days PO.

Patient #2 had a complete laceration of a mixed sensory and motor nerves. His motor recovery was more difficult to

assess since he had weak abductor pollicis brevis function on presentation (indicating dual innervation). Patient #2 was lost to hospital follow-up for almost 4 months PO but was tested independently at 11 months by a nurse practitioner educated in proper SWM assessments. His 2PD was not collected, but his SWM was 4.31 at the thumb, index, and middle fingers and radial half of the ring finger. The ulnar half of the ring finger was 2.83. Subjectively, the patient was pleased with his result and continued to note improvement in sensation.

To our knowledge, there is only one other published international case study of PEG-fusion (Bamba et al., 2016) performed on four digital nerve transections in two patients, one boy (aged 16 years) and one girl (aged 17 years). All four nerve injuries were sharp complete transections and repaired without complications within 12 h post-injury. In both patients, gross sensation was observed within 1–3 weeks, comparable to our digital nerve laceration in which gross sensation was perceived almost immediately.

Human and experimental pre-clinical data on the repair of severance type PNIs by neurorrhaphy alone are remarkably similar, as human and experimental pre-clinical data are on the repair of severance type PNIs by neurorrhaphy with PEG-fusion technology. That is, the repair of severance type PNIs with neurorrhaphy alone produces (Campbell, 2008; Brushart, 2011; Bittner et al., 2012, 2016, 2022; Mikesch et al., 2018a,b):

- (1) **Immediate loss of axonal integrity** so that action potentials are no longer conducted from the CNS to the periphery or from the periphery to the CNS across the injury site (s).
- (2) **Immediate loss of sensation and muscle function** in the affected area, for example, the region of the limb previously innervated by the severed nerve distal to the injury site.
- (3) **Irreversible WD** within 3–7 days of axons distal to the injury site.
- (4) **Atrophy of muscle in the region of the limb previously innervated by the severed nerve distal to the injury site** often occurs before reinnervation.
- (5) **Poor behavioral recovery after months/years.** Any sensation/functional recovery exclusively occurs using natural regeneration from surviving proximal axonal stumps that grow out at 1–2 mm/day. These phenomena are very similar to those observed for humans in clinical settings.

In contrast to (1)–(5) listed above, experimental animals having cuts repaired by neurorrhaphy and PEG-fusion exhibit (Bittner et al., 2012, 2016, 2022; Mikesch et al., 2018a,b):

- 1*) **Axonal integrity rapidly (within minutes) restored** as assessed by (a) conduction of extracellularly recorded compound action potentials (CAPs) intracellular dye diffusion in both directions across the lesion site(s), (b) conduction of compound muscle action potentials

(CMAPs) to muscle groups distal to the lesion, (c) retrograde fast axonal transport restored 0–2 days postoperatively (PO) following PEG-fused single cut lesions or 14–17 days PO following PEG-fused ablation lesions.

- 2*) **Neuromuscular junctions (NMJs) continuously maintained**, as measured by CMAPs confocal immunohistochemistry, TEM, counts of innervated muscle fibers, and evoked muscle twitches.
- 3*) **No WD of distal segments of many host or donor graft axons**, as assessed by photon microscopy and TEM of cross and longitudinal sections.
- 4*) **Reduced atrophy (compared with controls) of muscle fibers**, as assessed by TEM.
- 5*) **Functional/behavioral recovery restored within days to weeks to levels that can approach that of unoperated animals**, as measured by the Sciatic Functional Index (SFI), a commonly used behavioral measure primarily determined by fine sensory and motor control of distal muscle masses responsible for toe spread and foot placement.

The sensory aspects of phenomena in experimental animals are similar to those reported for our two patients and those of Bamba et al. (2016).

One potential drawback to PEG-fusion is its lack of initial specificity in mixed nerve repairs. That is, motor axons can be fused with sensory. While this efferent/afferent mismatch is possible, the degree could be limited by two mechanisms. The first would be accurate fascicle alignment. Knowledge of peripheral nerve topography has revealed motor/sensory segregation. While it is not possible to 100% accurately align the fascicles, the use of the operating microscope and nerve surface landmarks should achieve alignment sufficient to allow motor/sensory nerve groups enough overlap to achieve target success. The other mechanism is 40–60% of axons in a nerve are typically repaired by PEG-fusion (Mikesch et al., 2018a,b). The axons that do not fuse can regenerate in the usual fashion and produce improvement in sensory perceptions, as observed in both patients, that is, Patient #2 demonstrated marked improvement in sensation at 11-month PO, and Patient #1 showed rapid improvement in SWM values but slow improvement in 2PD values.

Conclusion

Our clinical data suggest that PEG-fusion repairs of PNIs have the potential for much improved clinical outcomes when compared with traditional coaptation repairs, especially in proximal mixed motor/sensory nerves. The adoption of PEG-fusion to treat PNIs would constitute a paradigm shift not only in functional outcomes but also in clinical care. While there is no consensus on the post-injury timing for addressing

transection PNIs (Pan et al., 2020), current clinical practices with PNIs are often to wait days or weeks following the PNI before repairing (Campbell, 2008). This practice of waiting to address the PNI is not a clinical necessity and outcomes with PNIs addressed at different times within weeks of the injury do not differ (Jones et al., 2018). Thus, while delayed repair (days–weeks post-PNI) can be helpful for more clearly assessing the extent of nerve damage and more favorable scheduling of procedures, it is not a necessary clinical practice—particularly for those patients with complete lesions where the need for surgery is already certain, which is the initial target patient population for the PEG-fusion technology. While outcomes with current technologies do not require early intervention, the benefits of immediate reinnervation through PEG-fused axons in patients would warrant a shift in clinical practices toward treatment within 72 h or less (determined by experiments on experimental animals). Most other clinical practices associated with the treatment of PNIs, such as controlling neuropathic pain, would likely be the same (Dworkin et al., 2003).

Data availability statement

The original contributions presented in this study are included in the article/supplementary material, further inquiries can be directed to the corresponding author.

Ethics statement

The studies involving human participants were reviewed and approved by WellSpan Health Institutional Review Board. Trial registrations, www.clinicaltrials.gov NCT03236064. IND 118873 for PEG was approved by the FDA. The patients/participants provided their written informed consent to participate in this study. Written informed consent was obtained from the individual(s) for the publication of any potentially identifiable images or data included in this article.

Author contributions

SL and RT performed the surgeries and oversaw patient follow-up. All authors helped design the study, analyzed data,

wrote and edited various drafts of the manuscript, and approved the submitted version.

Funding

This trial was funded and sponsored by grants from the Lone Star Paralysis Foundation to RT and GB (www.lonestarparalysis.org). Some medical writing support to RT and SL was funded by Neuraptive Therapeutics Inc. The funder was not involved in the study design, collection, analysis, interpretation of data, the writing of this article or the decision to submit it for publication. Funding of the cost of the article will be covered by a gift from The Lone Star Paralysis Foundation.

Acknowledgments

Judith N. Steenbergen and Sascha Strait (Scientific and Medical Affairs Consulting at WellSpan) provided medical writing support as did Chelsea Bush, clinical research manager at Lumata Health. We thank Dr. Cathy Yang for help with illustrations and Liwen Zhou with help on references.

Conflict of interest

The authors declare that the research was conducted in the absence of any commercial or financial relationships that could be construed as a potential conflict of interest.

Publisher's note

All claims expressed in this article are solely those of the authors and do not necessarily represent those of their affiliated organizations, or those of the publisher, the editors and the reviewers. Any product that may be evaluated in this article, or claim that may be made by its manufacturer, is not guaranteed or endorsed by the publisher.

References

- al-Ghazal, S. K., McKiernan, M., Khan, K., and McCann, J. (1994). Results of clinical assessment after primary digital nerve repair. *J. Hand Surg. Br.* 19, 255–257. doi: 10.1016/0266-7681(94)90180-5
- Bamba, R., Waitayawinyu, T., Nookala, R., Riley, D. C., Boyer, R. B., Sexton, K. W., et al. (2016). A novel therapy to promote axonal fusion in human digital nerves. *J. Trauma Acute Care Surg.* 81, S177–S183. doi: 10.1097/TA.0000000000001203
- Bell-Krotoski, J. A., Fess, E. E., Figarola, J. H., and Hiltz, D. (1995). Threshold detection and Semmes-Weinstein monofilaments. *J. Hand Ther.* 8, 155–162. doi: 10.1016/s0894-1130(12)80314-0

- Bittner, G. D., Ballinger, M. L., and Raymond, M. A. (1986). Reconnection of severed nerve axons with polyethylene glycol. *Brain Res.* 367, 351–355. doi: 10.1016/0006-8993(86)91617-3
- Bittner, G. D., Bushman, J. S., Ghergherehchi, C. L., Roballo, K. C. S., Shores, J. T., and Smith, T. A. (2022). Typical and atypical properties of peripheral nerve allografts enable novel strategies to repair segmental-loss injuries. *J. Neuroinflammation* 19:60. doi: 10.1186/s12974-022-02395-0
- Bittner, G. D., Keating, C. P., Kane, J. R., Britt, J. M., Spaeth, C. S., Fan, J. D., et al. (2012). Rapid, effective, and long-lasting behavioral recovery produced by microsutures, methylene blue, and polyethylene glycol after completely cutting rat sciatic nerves. *J. Neurosci. Res.* 90, 967–980. doi: 10.1002/jnr.23023
- Bittner, G. D., Sengelaub, D. R., Trevino, R. C., Peduzzi, J. D., Mikes, M., Ghergherehchi, C. L., et al. (2016). The curious ability of polyethylene glycol fusion technologies to restore lost behaviors after nerve severance. *J. Neurosci. Res.* 94, 207–230. doi: 10.1002/jnr.23685
- Brushart, T. (2011). *Nerve repair*. New York, NY: Oxford University Press.
- Campbell, W. W. (2008). Evaluation and management of peripheral nerve injury. *Clin. Neurophysiol.* 119, 1951–1965. doi: 10.1016/j.clinph.2008.03.018
- Donaldson, J., Shi, R., and Borgens, R. (2002). Polyethylene glycol rapidly restores physiological functions in damaged sciatic nerves of guinea pigs. *Neurosurgery* 50, 147–156; discussion 156–147. doi: 10.1097/00006123-200201000-00023
- Dworkin, R. H., Backonja, M., Rowbotham, M. C., Allen, R. R., Argoff, C. R., Bennett, G. J., et al. (2003). Advances in neuropathic pain: Diagnosis, mechanisms, and treatment recommendations. *Arch. Neurol.* 60, 1524–1534. doi: 10.1001/archneur.60.11.1524
- Ghergherehchi, C. L., Hibbard, E. A., Mikes, M., Bittner, G. D., and Sengelaub, D. R. (2019). Behavioral recovery and spinal motoneuron remodeling after polyethylene glycol fusion repair of singly cut and ablated sciatic nerves. *PLoS One* 14:e0223443. doi: 10.1371/journal.pone.0223443
- Johnson, A. J., Karparkin, M. H., and Newman, J. (1971). [Clinical investigation of intermediate- and high-purity antihemophilic factor (factor VIII) concentrates]. *Br. J. Haematol.* 21, 21–41. doi: 10.1111/j.1365-2141.1971.tb03414.x
- Jones, P. E., Meyer, R. M., Faillace, W. J., Landau, M. E., Smith, J. K., McKay, P. L., et al. (2018). Combat injury of the sciatic nerve—an institutional experience. *Mil. Med.* 183, e434–e441. doi: 10.1093/milmed/usy030
- Krause, T. L., and Bittner, G. D. (1990). Rapid morphological fusion of severed myelinated axons by polyethylene glycol. *Proc. Natl. Acad. Sci. U.S.A.* 87, 1471–1475. doi: 10.1073/pnas.87.4.1471
- Lore, A. B., Hubbell, J. A., Bobb, D. S. Jr., Ballinger, M. L., Loftin, K. L., Smith, J. W., et al. (1999). Rapid induction of functional and morphological continuity between severed ends of mammalian or earthworm myelinated axons. *J. Neurosci.* 19, 2442–2454.
- Lundborg, G. (2005). *Nerve injury and repair: Regeneration, reconstruction, and cortical remodeling*, 2nd Edn. London: Churchill Livingstone.
- Mallander, P., Berger, A., Schaller, E., and Ruhe, K. (1989). Results of primary nerve repair in the upper extremity. *Microsurgery* 10, 147–150. doi: 10.1002/micr.1920100218
- Mikes, M., Ghergherehchi, C. L., Hastings, R. L., Ali, A., Ramesh, S., Jagannath, K., et al. (2018a). Polyethylene glycol solutions rapidly restore and maintain axonal continuity, neuromuscular structures, and behaviors lost after sciatic nerve transections in female rats. *J. Neurosci. Res.* 96, 1223–1242. doi: 10.1002/jnr.24225
- Mikes, M., Ghergherehchi, C. L., Ramesh, S., Jagannath, K., Ali, A., Sengelaub, D. R., et al. (2018b). Polyethylene glycol treated allografts not tissue matched nor immunosuppressed rapidly repair sciatic nerve gaps, maintain neuromuscular functions, and restore voluntary behaviors in female rats. *J. Neurosci. Res.* 96, 1243–1264. doi: 10.1002/jnr.24227
- Pan, D., Mackinnon, S. E., and Wood, M. D. (2020). Advances in the repair of segmental nerve injuries and trends in reconstruction. *Muscle Nerve* 61, 726–739. doi: 10.1002/mus.26797
- Roos, D. S., Robinson, J. M., and Davidson, R. L. (1983). Cell fusion and intramembrane particle distribution in polyethylene glycol-resistant cells. *J. Cell Biol.* 97, 909–917. doi: 10.1083/jcb.97.3.909
- Rosberg, H. E., Carlsson, K. S., Hojgard, S., Lindgren, B., Lundborg, G., and Dahlin, L. B. (2005). Injury to the human median and ulnar nerves in the forearm—analysis of costs for treatment and rehabilitation of 69 patients in southern Sweden. *J. Hand Surg. Br.* 30, 35–39. doi: 10.1016/j.jhsb.2004.09.003
- Ruijs, A. C., Jaquet, J. B., Kalmijn, S., Giele, H., and Hovius, S. E. (2005). Median and ulnar nerve injuries: A meta-analysis of predictors of motor and sensory recovery after modern microsurgical nerve repair. *Plast. Reconstr. Surg.* 116, 484–494; discussion 495–486. doi: 10.1097/01.prs.0000172896.86594.07
- Silva, P. G., Jones, A., Araujo, P. M., and Natour, J. (2014). Assessment of light touch sensation in the hands of systemic sclerosis patients. *Clinics (Sao Paulo)* 69, 585–588. doi: 10.6061/clinics/2014(09)02



OPEN ACCESS

EDITED BY

George Davis Bittner,
The University of Texas at Austin, United States

REVIEWED BY

Cameron Ghergherehchi,
Johns Hopkins Medicine, United States
Shengyou Li,
Fourth Military Medical University, China

*CORRESPONDENCE

Fei Yu
✉ yufei89@pku.edu.cn
Jun Peng
✉ slp_1972@163.com

†These authors have contributed equally to this work and share first authorship

SPECIALTY SECTION

This article was submitted to
Neurotrauma,
a section of the journal
Frontiers in Neurology

RECEIVED 03 November 2022

ACCEPTED 20 March 2023

PUBLISHED 06 April 2023

CITATION

Li D, Yang Q, Liu X, Jia J, Liu G, Bai K, Jia S, Peng J and Yu F (2023) Experimental study on the repair of peripheral nerve injuries *via* simultaneously coapting the proximal and distal ends of peripheral nerves to the side of nearby intact nerves. *Front. Neurol.* 14:1088983. doi: 10.3389/fneur.2023.1088983

COPYRIGHT

© 2023 Li, Yang, Liu, Jia, Liu, Bai, Jia, Peng and Yu. This is an open-access article distributed under the terms of the [Creative Commons Attribution License \(CC BY\)](https://creativecommons.org/licenses/by/4.0/). The use, distribution or reproduction in other forums is permitted, provided the original author(s) and the copyright owner(s) are credited and that the original publication in this journal is cited, in accordance with accepted academic practice. No use, distribution or reproduction is permitted which does not comply with these terms.

Experimental study on the repair of peripheral nerve injuries *via* simultaneously coapting the proximal and distal ends of peripheral nerves to the side of nearby intact nerves

Dongdong Li^{1†}, Qi Yang^{2†}, Xin Liu¹, Jing Jia¹, Guangbo Liu¹, Kewen Bai¹, Shicheng Jia³, Jun Peng^{1*} and Fei Yu^{4,5*}

¹Department of Orthopedics, Strategic Support Force Medical Center, Beijing, China, ²Department of Ultrasonography, Peking University Shenzhen Hospital, Shenzhen, China, ³Department of Sports Medicine, Peking University Shenzhen Hospital, Shenzhen, China, ⁴Department of Bone and Joint Surgery, Peking University Shenzhen Hospital, Shenzhen, China, ⁵National and Local Joint Engineering Research Center of Orthopaedic Biomaterials, Peking University Shenzhen Hospital, Shenzhen, China

Introduction: Peripheral nerve defect is a difficult disease to treat in clinical practice. End-to-side anastomosis is a useful method to treat it. At present, the end-to-side anastomosis method does not involve the proximal nerve, which results in a waste of proximal donor nerves, and even the formation of traumatic neuromas at the proximal end. The patients suffer from traumatic neuralgia and the curative effect is unsatisfactory.

Methods: In this study, an improved end-to-side anastomosis technique was proposed in this study: both the proximal and distal ends of the damaged common peroneal nerve were sutured to an adjacent normal tibial nerve. Moreover, the possible role and mechanism of the proposed technique were explained at the physiological and anatomical levels. In this study, a 10 mm common peroneal nerve defect was made in SD rats, and the rats were randomly divided into three groups. In Group I, the distal end of the common peroneal nerve was attached end-to-side to the fenestrated tibial nerve adventitia, and the proximal end was ligated and fixed in the nearby muscle. In Group II, the tibial nerve adventitia was fenestrated and the epineurial end-to-end anastomosis surgery was performed to suture the proximal and distal ends of the common peroneal nerve. Rats in Group III were taken as control and received sham operation. Twelve weeks after the operation, the recovery of the repaired nerve and distal effector functions were examined by the sciatic functional index, electrophysiology, osmic acid staining, the muscle wet weight ratio, and the muscle fiber cross-sectional area.

Results: It was found that these results in Group II were similar to those in Group III, but better than those in Group I. Through retrograde tracing of neurons and Electrophysiological examination in Group II, the study also found that the proximal common peroneal nerve also could establish a connection with tibialis anterior, even gastrocnemius.

Discussion: Therefore, it is inferred that fostering both the proximal and distal ends of defective peripheral nerves on normal peripheral nerves using the end-to-side anastomosis technique is a more effective approach to repairing injured nerves.

KEYWORDS

peripheral nerve defect, end-to-side anastomosis, functional recovery, effective approach, repair mechanism

Introduction

Peripheral nerve injury can cause sensory and motor dysfunction, and delayed treatment will lead to poor prognosis and even lifelong disability (1). According to the severity and nature, peripheral nerve injury can be divided into nerve conduction dysfunction, nerve axon interruption and nerve rupture. After the peripheral nerve ruptures, pathological changes occur in nerve fibers, neuronal bodies and target organs (1–3). At present, common methods for repairing peripheral nerve injuries include neurolysis, nerve suture, nerve transplantation, nerve transfer and nerve implantation. With the development of orthopedics and microsurgery technology, progress has been made toward repairing peripheral nerve injuries (4, 5). However, further improvement of the repair effect is required, especially for large segmental peripheral nerve defects. The interrupted connection between the injured proximal and distal nerve fibers makes the repair more difficult in clinical treatment (6, 7).

One method to repair peripheral nerve injuries is end-to-side anastomosis, which sutures the distal end of the injured nerve to the side wall of the adjacent healthy nerve trunk. In this way, the injured nerve can regenerate and the function of the target organ can restore. Since it was proposed, end-to-side anastomosis has attracted increasing attention (8, 9). However, this repair method has some demerits. The disuse of the injured proximal peripheral nerve gives rise to a waste of donor nerves and proximal traumatic neuromas. The neuromas further result in pain and discomfort, and worsen the repair effect (10). To solve this issue, some scholars have modified the end-to-side anastomosis method, and fostered the injured proximal peripheral nerve on the side wall of an adjacent normal nerve. The updated method was proven effective in repairing injured peripheral nerves (11). Nevertheless, there are few studies on the improved method, so its specific repair effect and possible mechanism require further elaboration.

In view of this, an SD rat model with a large segmental common peroneal nerve defect was established in this paper. Besides, the improved end-to-side anastomosis technique was used to suture both the proximal and distal ends of the damaged common peroneal nerve to an adjacent normal tibial nerve. The functional recovery of the injured common peroneal nerve and its effector 12 week after repairing, and the connection between the repaired nerve and motor neurons in the anterior horn of the spinal cord were examined. The purpose of this study is to preliminarily explain the possible role and mechanism of this method at physiology and anatomy levels.

Materials and methods

Animal models

Eight-week-old 150–180 g SD rats were purchased from Beijing Vital River Laboratory Animal Technology Co., Ltd. The operation was carried out following the Guidelines for Ethical Review of Animal Welfare in China (GB/T 35892-2018). All experiments were approved by the Medical Ethics Committee of Peking University People's Hospital (Permit Number: 2020PHC015, 3/1/2019). The rats were anesthetized with sodium pentobarbital intraperitoneally (Merck, Darmstadt, Germany; 30 mg/kg) before random grouping.

In Group I ($n = 9$), the distal end of the common peroneal nerve was coapted end-to-side to the fenestrated tibial nerve adventitia, and the proximal end was ligated and fixed in the nearby muscle. In Group II ($n = 9$), the tibial nerve adventitia was fenestrated and epineurial end-to-end anastomosis was performed to anastomose the proximal and distal ends of the common peroneal nerve. Rats in Group III ($n = 9$) were taken as control and underwent sham operation. After awakening, the rats were fed in groups, and food and drinking water were automatically supplied. A 12:12 light/dark natural circle was adopted in the feeding environment.

Sciatic functional index test

The motor function of rats was measured by the CatWalk XT gait analysis system (Nodus, Netherlands), which can automatically record the motion parameters. The camera was placed at the correct position and corresponding rat parameters were setup. Before recording, the rats were trained to be familiar with the running environment. All rats in different groups were recorded automatically. The calculation formula of sciatic functional index (SFI) is $SFI = 109.5 (ETS-NTS)/NTS - 38.3 (EPL-NPL)/NPL + 13.3 (EIT-NIT)/NIT - 8.8$. SFI is a reliable method for the assessment of the extent of injury and the degree of recovery of the sciatic nerve of the rat. E: experimental; N: normal; PL: print length from heel to longest toe; TS: total spread, or the transverse distance between the 1st and the 5th toes; IT: intermediate toes, or the transverse distance between the 2nd and 4th toes.

Neuroelectrophysiological detection

The compound action potential of gastrocnemius and tibialis anterior muscles was detected by the Medlec synergy electrophysiological system (Oxford Instruments Inc., Oxford, UK) in each group. After the rats in each group were anesthetized with sodium pentobarbital, the repaired nerves were exposed. Then the stimulation electrodes were placed at positions A, B, C, D, and E of the nerve (Figure 1), and the electrical signals of gastrocnemius and tibialis anterior muscles were recorded through receiver electrode, separately. In the meantime, the action potentials of gastrocnemius and tibialis anterior muscles recorded at point A were taken as the maximum action potentials of Group I and Group II. The action potential of the gastrocnemius muscle recorded at point A and the action potential of the tibialis anterior muscle recorded at point B were adopted as the maximum action potentials of Group III. Statistical analysis was subsequently made to evaluate the size of the compound muscle action potential (CMAP) of each group. Rectangular pulse (0.1 ms duration, 0.06 mA intensity, 5 Hz frequency) was used to acquire the CMAP.

Histological observation of the repaired nerve

The tibial nerve and common peroneal nerve 2 mm away from the anastomosed common peroneal nerve were collected. The nerve sample was soaked in 4% paraformaldehyde for 12 h and then

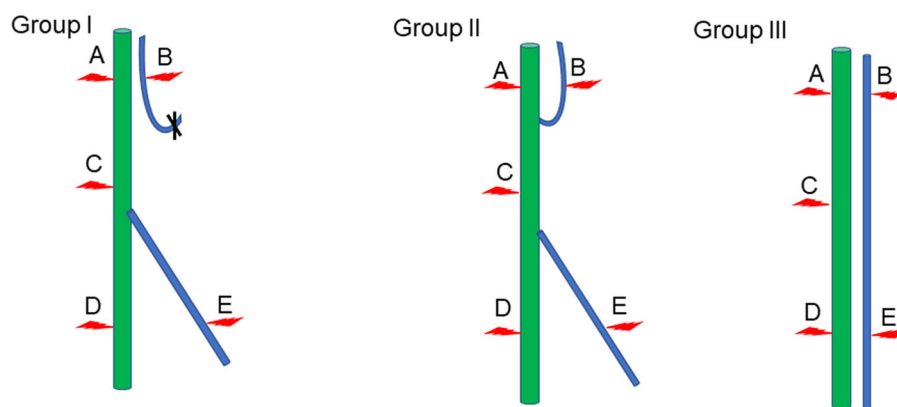


FIGURE 1

Schematic diagram of electrophysiological detection. Green represents the tibial nerve, blue indicates the common peroneal nerve, and the red arrow denotes the location of the stimulation electrode.

died with 1% osmic acid for another 12 h. After the sample was dehydrated with 50, 70, 90, and 100% ethanol successively, it was embedded in paraffin, and sliced into a 2 μm -thick piece (Leica RM2135, Wetzlar, Germany). The piece was placed on the glass slide. After sealing the slide, it was observed under the microscope [Leica DM4B with Leica Application Suite X (LAS X) software, Wetzlar, Germany]. The number of myelinated nerve fibers per unit area in each group was manually counted.

Weighing and histological observation of the effector muscle

The gastrocnemius and tibialis anterior muscles of the model and opposite sides were collected from SD rats and weighed. The ratio of the wet weight of the model side muscle to that of the opposite side muscle was calculated. After trimming, the muscle was placed in 4% paraformaldehyde for fixation overnight, and then dehydrated successively with 50, 70, 90, and 100% ethanol. The muscle was embedded in paraffin, and sliced into a 7 μm -thick piece. Then Masson staining was performed. Those for Masson staining were treated with Weigert stain for 8 min and rinsed with distilled water. The sections were then treated with spring red acid complex red for 5 min, immersed in acetic acid for 1 min, treated with phosphomolybdic acid for 2 min, and immersed in acetic acid for 1 min. Next, the sections were treated with aniline blue for 2 min, immersed in acetic acid for 1 min, and rinsed with water. After sealing the slide, it was imaged under a microscope [Leica DM4B with Leica Application Suite X (LAS X) software, Wetzlar, Germany]. The cross-sectional area of gastrocnemius and anterior tibial muscle fibers was calculated using Image J software. Three visual fields of each sample were selected, and the average value was taken as the ultimate muscle fiber cross-sectional area of the sample.

Retrograde tracing of neurons

Three SD rats were taken from each group for the tracing and labeling experiment, and the method proposed in (12) was adopted.

The regenerated sciatic nerve of rats was re-exposed and cut off. The distal ends of the common peroneal nerve and tibial nerve were immersed in 5% Fluoro-Ruby (FR, Life Technologies) and 4% Fluoro-Gold (FG, Life Technologies) for 2 h, respectively. The wound was washed and sutured layer by layer. Then rats were fed for 7 days so that the retrograde tracer could label the spinal cord neurons. After anesthetizing, the heart of rats was isolated and perfused. L4–L6 lumbar spinal cord segments containing sciatic nerves were cut off and fixed in 4% paraformaldehyde for 12 h. The sample was dehydrated in 10, 20, and 30% sucrose for 12 h, and then sliced to a 40 μm -thick piece by a frozen slicer (Leica CM 1950, Germany). Subsequently, the sample was placed on the glass slide and sealed, and the slice was imaged by the 20 \times microscope objective. The excitation wavelength was FG330nm and FR561nm. Finally, the acquired fluorescence image was analyzed using Image J software to detect the neurons labeled by FG only, FR only, and both FG and FR.

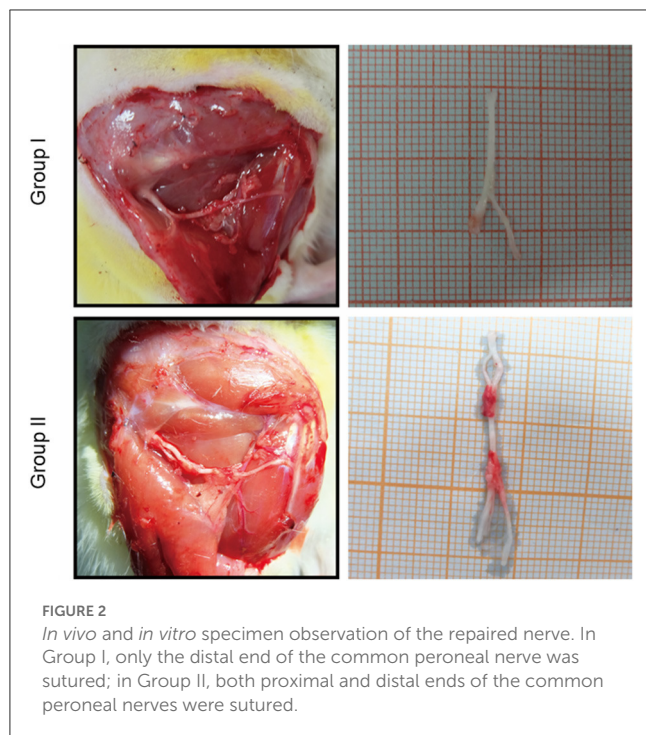
Data analysis

All measurement data were expressed by (mean \pm standard deviation). One-way ANOVA was employed to analyze data in different groups, followed by Tukey's *post-hoc* multiple comparison test. SPSS 18.0 was used for statistical processing. $P < 0.05$ meant that the difference was statistically significant.

Results

Gross observation of nerve repair

The proximal and distal common peroneal nerves at the repair site were observed *in vivo* and *in vitro*. In Group I, only the distal common peroneal nerve remained intact, while in Group II, both the proximal and distal ones were complete (Figure 2).



Sciatic functional index for nerve repair detection

Since the common peroneal nerve and tibial nerve constitute the sciatic nerve, the sciatic functional index can be used to detect the recovery of nerve function. In this paper, the regeneration and repair of the common peroneal nerve were analyzed using the sciatic functional index. The results showed that the sciatic functional indexes of Group I, Group II and Group III were $(-30.09 \pm 5.9, n = 6)$, $(-11.64 \pm 5.12, n = 6)$, and $(-0.05 \pm 4.09, n = 6)$, respectively. Significant statistical difference was found ($p < 0.05$). The sciatic functional index of Group II was better than that of Group I and closer to that of Group III (Figure 3).

Electrophysiological detection of functional recovery of repaired nerves and their innervating effectors

In clinical practice, electromyography is often used to record the electrophysiological characteristics of nerves and muscles. In this study, the functional recovery of the repaired nerves and their innervating effectors were detected by electrophysiology. The CMAP size depends on the number of functional muscle fibers. The detection results suggested that the waveforms of gastrocnemius and tibialis anterior muscles in Group I, Group II, and Group III were not different. The CMAP amplitudes of the gastrocnemius muscle in Group I, Group II and Group III were (26.80 ± 3.10) mV, (27.30 ± 1.80) mV, and (29.00 ± 3.20) mV, respectively, and no significant difference was found ($p > 0.05$). The CMAP amplitude of the tibialis anterior muscle in Group I, Group II and Group III was (8.70 ± 1.60) mV, (12.20 ± 2.10) mV, and (19.70 ± 1.90)

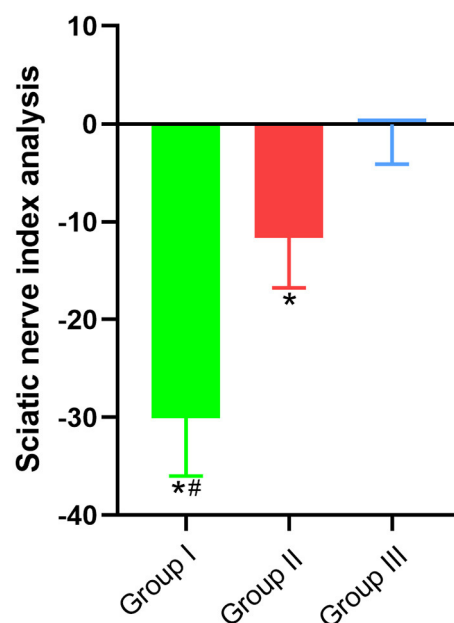


FIGURE 3
Sciatic functional index. In Group I, only the distal end of the common peroneal nerve was fostered; in Group II, both proximal and distal ends of the common peroneal nerve were fostered; Group III was sham operated normal group. Data are expressed as mean \pm SD ($n = 6$ in Group I, 6 in Group II and 6 in Group III). * $P < 0.05$, vs. Group III; # $P < 0.05$, vs. Group II.

mV, respectively, and there was significant statistical difference ($p < 0.05$). The CMAP amplitude of the tibialis anterior muscle in Group II is closer to Group III than Group I is to Group III (Figure 4).

Stimulation electrodes were placed at different positions to check whether the proximal end of the common peroneal nerve was fostered on the tibial nerve, and whether the proximal common peroneal nerve could control the anterior tibial muscle or even the gastrocnemius muscle. According to the results, stimulating point A could cause the contraction of gastrocnemius and anterior tibial muscles in Group I and Group II. When stimulating point B, the gastrocnemius and anterior tibial muscles in Group II tightened. The gastrocnemius and anterior tibial muscles in Group I and Group II constricted as the point C was stimulated. Stimulating point D could lead to the contraction of the gastrocnemius muscle in Group I, Group II and Group III. When the point E was stimulated in Group I, Group II and Group III, the anterior tibial muscle tightened (Table 1).

Osmium acid staining for detecting the recovery of peripheral nerves at the repair site

The numbers of myelinated tibial and common peroneal nerve fibers per unit area were calculated using osmium acid staining in each group. The number of myelinated tibial nerve fibers per unit area in Group I, Group II and Group III was $(14,883 \pm 835)$ mm²/piece, $(14,783 \pm 1,091)$ mm²/piece and $(15,017 \pm 608)$

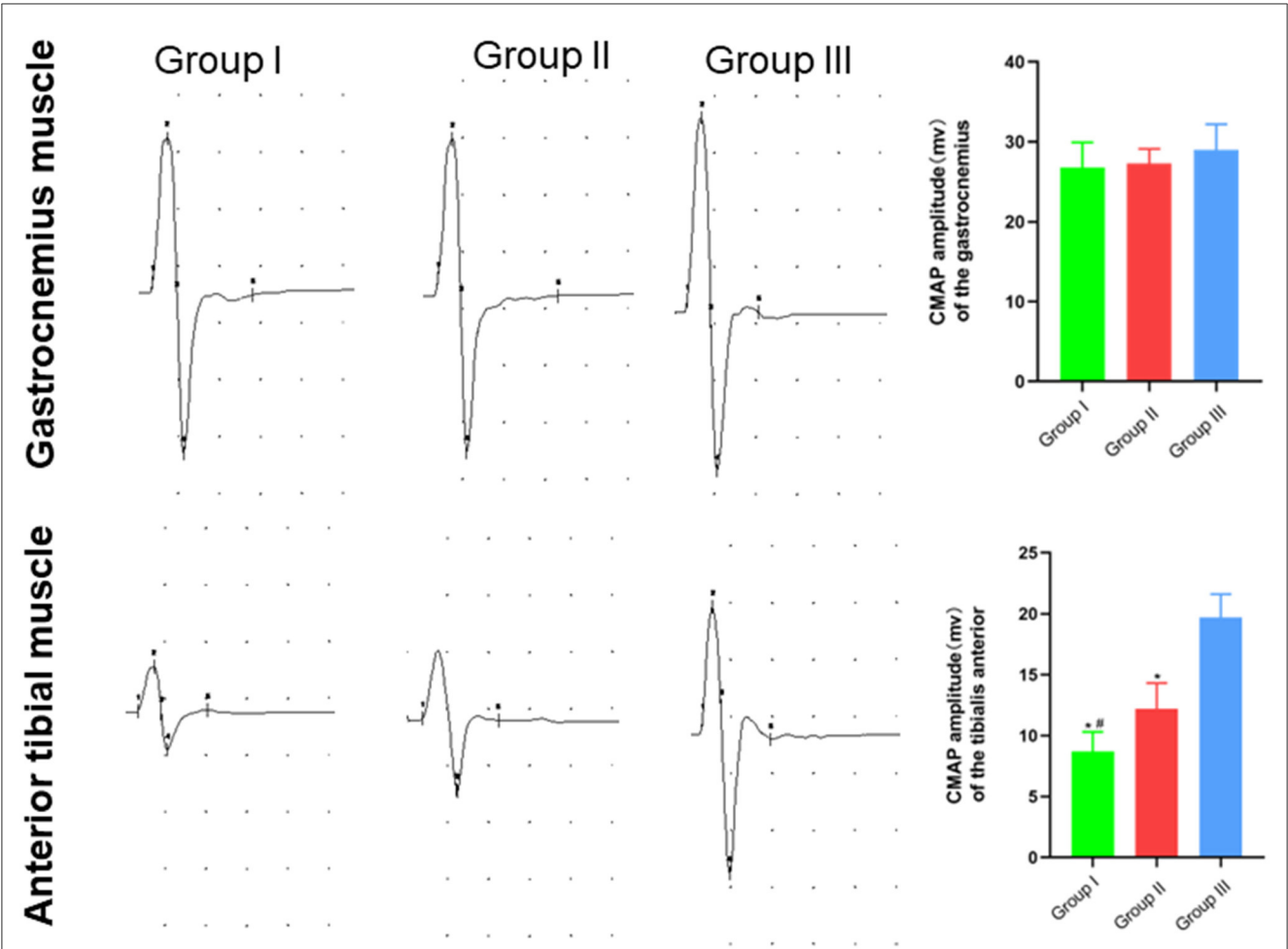


FIGURE 4 Waveform and amplitude of the compound action potential of gastrocnemius and tibialis anterior muscles detected by electrophysiology. In Group I, only the distal end of the common peroneal nerve was fostered; in Group II, both proximal and distal ends of the common peroneal nerves were fostered; Group III was sham operated normal group. Data are expressed as mean \pm SD ($n = 6$ in Group I, 6 in Group II and 6 in Group III). * $P < 0.05$, vs. Group III; # $P < 0.05$, vs. Group II.

TABLE 1 Contraction of gastrocnemius/tibialis anterior muscles after stimulation of different positions of nerves.

Position	A	B	C	D	E
Group I	+/+	-/-	+/+	+/-	-/+
Group II	+/+	+/+	+/+	+/-	-/+
Group III	+/+	-/+	+/+	+/-	-/+

“+” means there is muscle contraction activity, and “-” means no muscle contraction activity; The front of “/” stands for the contraction of the gastrocnemius muscle, and the back of “/” represents the contraction of the tibialis anterior muscle.

mm²/piece, respectively, and no significant difference is observed ($p > 0.05$). The number of myelinated common peroneal nerve fibers per unit area in Group I, Group II and Group III was (6,750 \pm 903) mm²/piece, (8,967 \pm 1,269) mm²/piece, and (14,917 \pm 488) mm²/piece, respectively, and there was significant statistical difference ($p < 0.05$). The number of myelinated common peroneal nerve fibers per unit area in Group II is closer to Group III than Group I to Group III (Figure 5).

Macroscopic and microscopic observation and detection of effector muscle function

The wet weight ratio and the cross-sectional area of gastrocnemius and tibialis anterior muscle fibers were measured using gross specimen and Masson staining methods. The wet weight ratio of gastrocnemius muscle in Group I, Group II and Group III was (0.99 \pm 0.02), (0.99 \pm 0.02), and (1.00 \pm 0.02), respectively. The cross-sectional area of gastrocnemius muscle fibers was (2,025 \pm 121) μ m², (2,011 \pm 76) μ m², and (2,061 \pm 107) μ m², respectively. Both the wet weight ratio and fiber cross-sectional area of gastrocnemius muscle were not significantly different between Group I and Group II ($p > 0.05$). The wet weight ratio of tibialis anterior muscle in Group I, Group II and Group III was (0.46 \pm 0.08), (0.64 \pm 0.08), and (0.99 \pm 0.02), respectively. The cross-sectional area of tibialis anterior muscle fibers was (1,131 \pm 130) μ m², (1,325 \pm 103) μ m², and (1,971 \pm 90) μ m², respectively. Significant statistical difference was found between Group I and Group II in the wet weight ratio and fiber cross-sectional area of gastrocnemius muscle ($p < 0.05$). The wet weight ratio and fiber

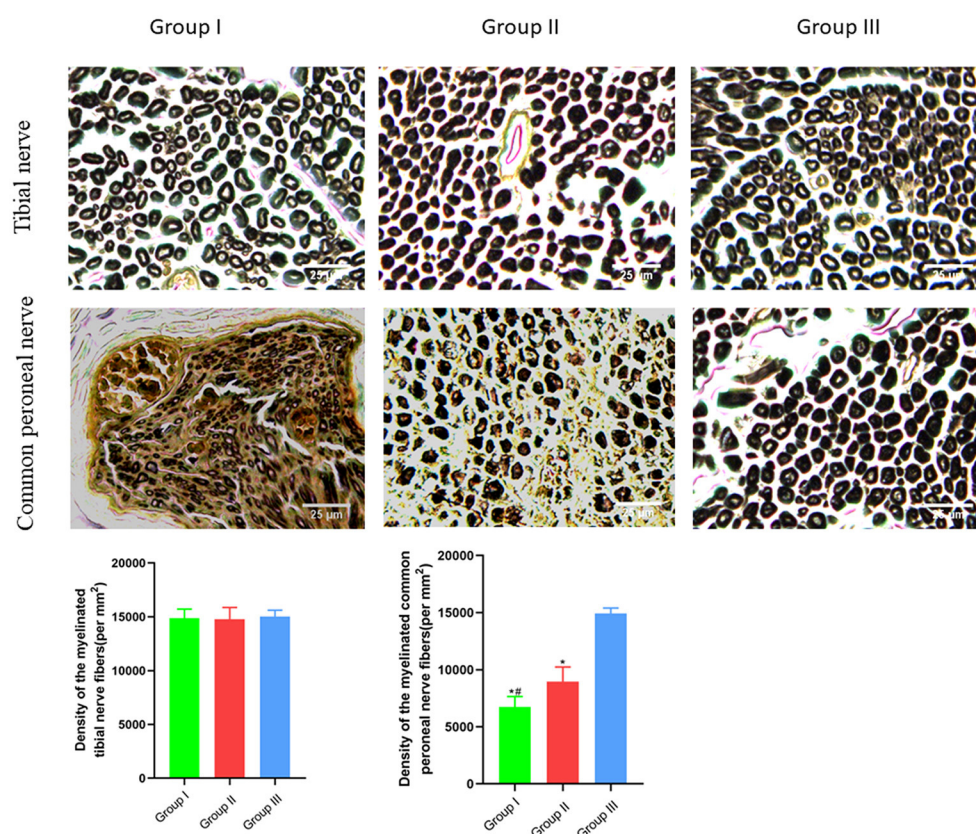


FIGURE 5

Observation of myelinated tibial and common peroneal nerve fibers per unit area. Osmic acid staining, scale bar = 25 µm. In Group I, only the distal end of the common peroneal nerve was sutured; in Group II, both proximal and distal ends of the common peroneal nerve were repaired; Group III was sham operated normal group. Data are expressed as mean ± SD ($n = 6$ in Group I, 6 in Group II and 6 in Group III). * $P < 0.05$, vs. Group III; # $P < 0.05$, vs. Group II.

cross-sectional area of tibialis anterior muscle in Group II is closer to Group III than Group I is to Group III (Figures 6, 7).

Analysis of the relationship between the repair nerve and motor neurons in the anterior horn of the spinal cord by retrograde tracing of neurons

Retrograde tracing of neuron was carried out to explore the reinnervation connection between neurons and effectors. There were only FG-labeled, both FG- and FR-labeled fluorescent neurons in the spinal cord of Group I. But there were no only FR-labeled fluorescent neurons. In Group II, only FG-labeled, only FR-labeled and both FG- and FR-labeled fluorescent neurons were observed in the spinal cord. In Group III, only FG-labeled and only FR-labeled fluorescent neurons were found in the spinal cord, but there were no fluorescent neurons labeled by both FG and FR (Figure 8).

Discussion

Cut, pull and compression induced peripheral nerve injuries can bring about motor, sensory and nutritional dysfunction in

the innervated area, and patients may be disabled as a result of delayed treatment (13, 14). The clinical treatment effect for a large segmental peripheral nerve defect is poor, which has become a thorny problem for orthopedic doctors (15, 16). End-to-side anastomosis, first proposed by foreign scholars in 1901, is one method to repair peripheral nerve injuries. This method anastomoses the distal end of the injured nerve with an adjacent normal nerve (17, 18), while the injured proximal end is left open to restore the function of effectors. However, the application of this method is restricted because it wastes the injured proximal peripheral nerve and is prone to cause neuromas and other complications. To overcome the above shortcomings, both the proximal and distal ends of injured nerves should be attached to normal peripheral nerves. In this study, an SD rat model with a large segmental common peroneal nerve defect was established, and end-to-side anastomosis was employed to suture the proximal and distal stumps of the damaged common peroneal nerve to an adjacent tibial nerve. Twelve weeks after repair, the functional recovery of the injured nerve and its effector was assessed, and the connection between the repaired nerve and motor neurons in the anterior horn of the spinal cord was analyzed.

The functions and mechanisms were explored at neuroanatomy and physiology levels. The analysis results showed that when the proximal and distal stumps of the injured common peroneal

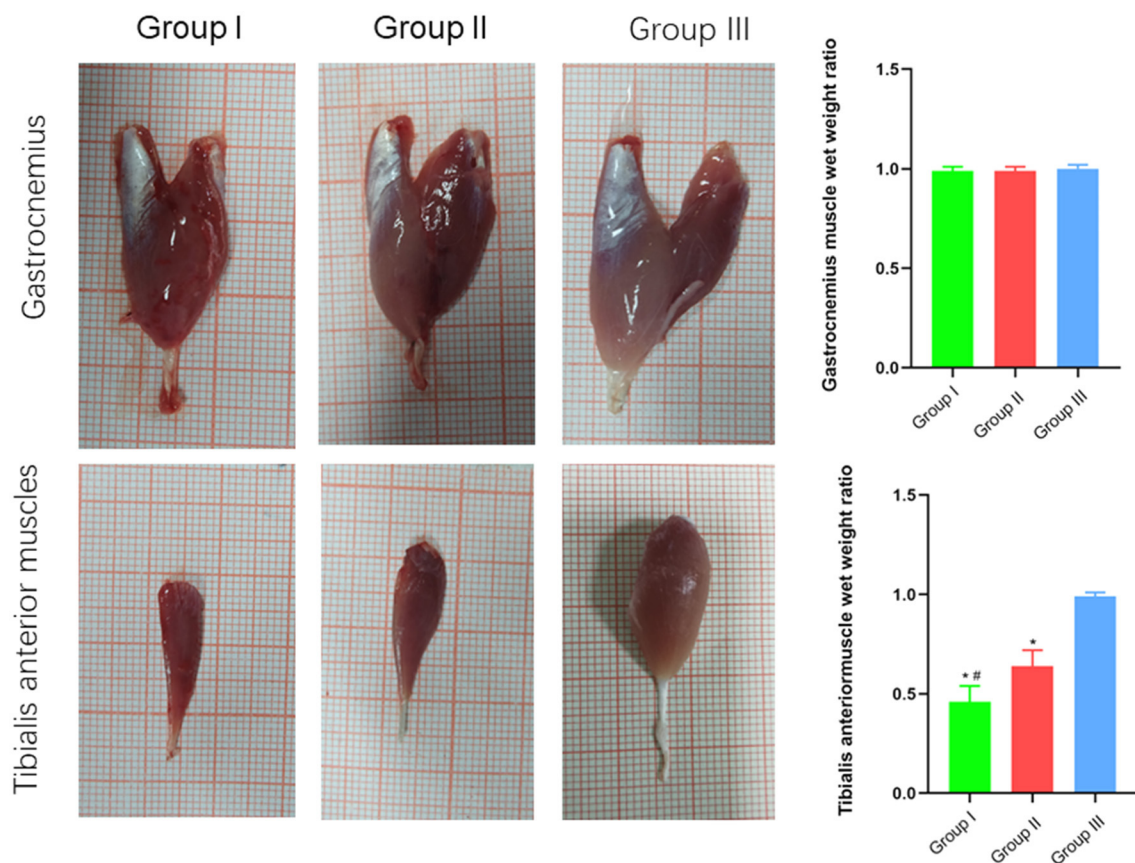


FIGURE 6

Macroscopic specimen observation of gastrocnemius and tibialis anterior muscles. In Group I, only the distal end of the common peroneal nerve was repaired; in Group II, both proximal and distal ends of the common peroneal nerve was repaired; Group III was sham operated normal group. Data are expressed as mean \pm SD ($n = 6$ in Group I, 6 in Group II and 6 in Group III). ^{*} $P < 0.05$, vs. Group III; [#] $P < 0.05$, vs. Group II.

nerve were simultaneously coapted to the adjacent normal tibial nerve, both ends remained intact without neuromas detected. This finding suggests that to repair the proximal common peroneal nerve is better than to keep the proximal common peroneal nerve open. The tibialis anterior muscle and gastrocnemius muscle are innervated by the common peroneal nerve and tibial nerve, respectively. According to the experimental results of this study, no matter whether the proximal end of the common peroneal nerve was fostered or not, the ipsilateral tibialis anterior muscle and gastrocnemius muscle constricted when the tibial nerve near the distal foster point of the common peroneal nerve was stimulated. When the proximal end of the common peroneal nerve was sutured, stimulating the proximal end of the common peroneal nerve could also make the ipsilateral tibialis anterior and gastrocnemius muscles contract. However, when the distal end of the common peroneal nerve was open, two muscles did not tighten. As for the CMAP, it was found that the compound action potential of the gastrocnemius muscle when stimulating the distal foster point of the common peroneal nerve or the open proximal end was not significantly different from that when stimulating the normal nerve at the same level. This result remains true no matter whether the proximal end of the common peroneal nerve was repaired or not. The compound action potential of the tibialis anterior muscle

in the foster group was higher than that in the open group and closer to that in the normal group. The wet weight ratio and cross-sectional area of the gastrocnemius muscle in the three groups had no significant difference. The wet weight ratio and cross-sectional area of the tibialis anterior muscle in the foster group were greater than those in the open group and closer to those in the normal group. Similar results were obtained in detecting the recovery of the tibial nerve and the common peroneal nerve 2 cm below the distal foster nerve of the same height in the three groups. There was no significant difference in the number of myelinated tibial nerve fibers per unit area among the three groups. The number of myelinated common peroneal nerve fibers per unit area in the foster group was more than that in the open group and closer to that in the normal group. Previous studies have confirmed (19, 20) the importance of repairing proximal nerves in the treatment of peripheral nerve injuries. The reason may be that more nerves are available for attracting peripheral repair materials, and donor nerve epineuria act as a bridge for axon regeneration. In this process, proximal nerve endings can grow directly to the distal end, and serve as a catheter to allow the peripheral repair materials to reach the distal injury site through the donor nerve adventitia (11). A similar effect was observed in the present research. When the proximal and distal common peroneal nerves were injured and sutured simultaneously

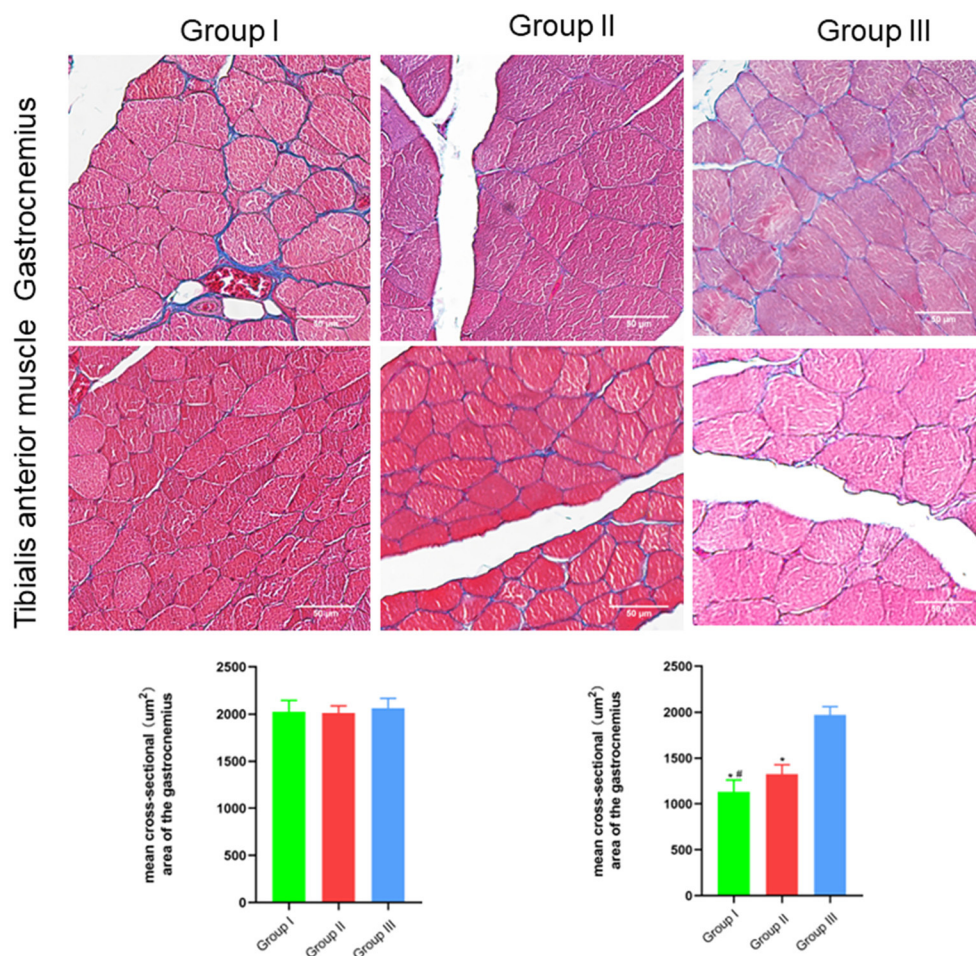


FIGURE 7

Microscopic specimen observation of gastrocnemius and tibialis anterior muscle. Masson stain, scale bar = 50 μm . In Group I, only the distal end of the common peroneal nerve was repaired; in Group II, both proximal and distal ends of the common peroneal nerve were repaired; Group III was sham operated normal group. Data are expressed as mean \pm SD ($n = 6$ in Group I, 6 in Group II and 6 in Group III). * $P < 0.05$, vs. Group III; # $P < 0.05$, vs. Group II.

to the peripheral normal tibial nerve, the conditions of injured nerves and corresponding effectors after repair were better than those when only the injured distal common peroneal nerve was sutured. This may be due to the secretion of such endogenous substances as nerve growth factors (21), basic fibroblast growth factors (22), and glial cell derived neurotrophic factors (23) around the injured nerve through relevant signaling pathways (e.g., PI3K/AKT, Notch, TAK1-MAPK/NF- κ B etc.) (24–26). These factors affect the function of Schwann cells (27) or macrophages (28) and promote the repair of injured peripheral nerves. During the proximal foster caring process, abundant endogenous factors can further regulate relevant signaling pathways and act on cells around the injured proximal and distal nerves through the bridge between the outer membrane of the donor and the distal end. A benign cycle is thus formed, which helps accelerate the repair process and promote the protection and recovery of effector functions. Bontioti et al. (29) believed that fostering both the proximal and distal stumps on peripheral normal nerves was not beneficial to the recovery of the injury effector function, but this does not affect the interpretation of the results of this research. In

the study of Bontioti, the rat model of brachial plexus injury was used. Since the rat's forepaw has more complex functions than its hind paw, damage repair is more difficult. However, the specific mechanism deserves further investigation.

The axon has the ability of collateral regeneration (30–32). In this paper, the axon was also proven capable of reinnervating the recipient nerve and effector through collateral sprouting during end-to-side anastomosis. Especially when both the proximal and distal ends were anastomosed, the proximal common peroneal nerve could reinnervate the distal common peroneal nerve, tibial nerve and effector. The improved end-to-side anastomosis method proposed in this paper provides more donor nerves, so the nerve function recovers better. This research has some limitations. Firstly, previous studies have confirmed that with the extension of repair time, only one axon sprouting from the lateral branch can be retained (12, 33). In this study, when both the injured proximal and distal nerves are hosted on the peripheral nerves, the axons sprouting from the lateral branch and especially, the neurons with multiple axons, can maintain their functions. Nevertheless, this result requires further validation. Secondly, in this paper, the

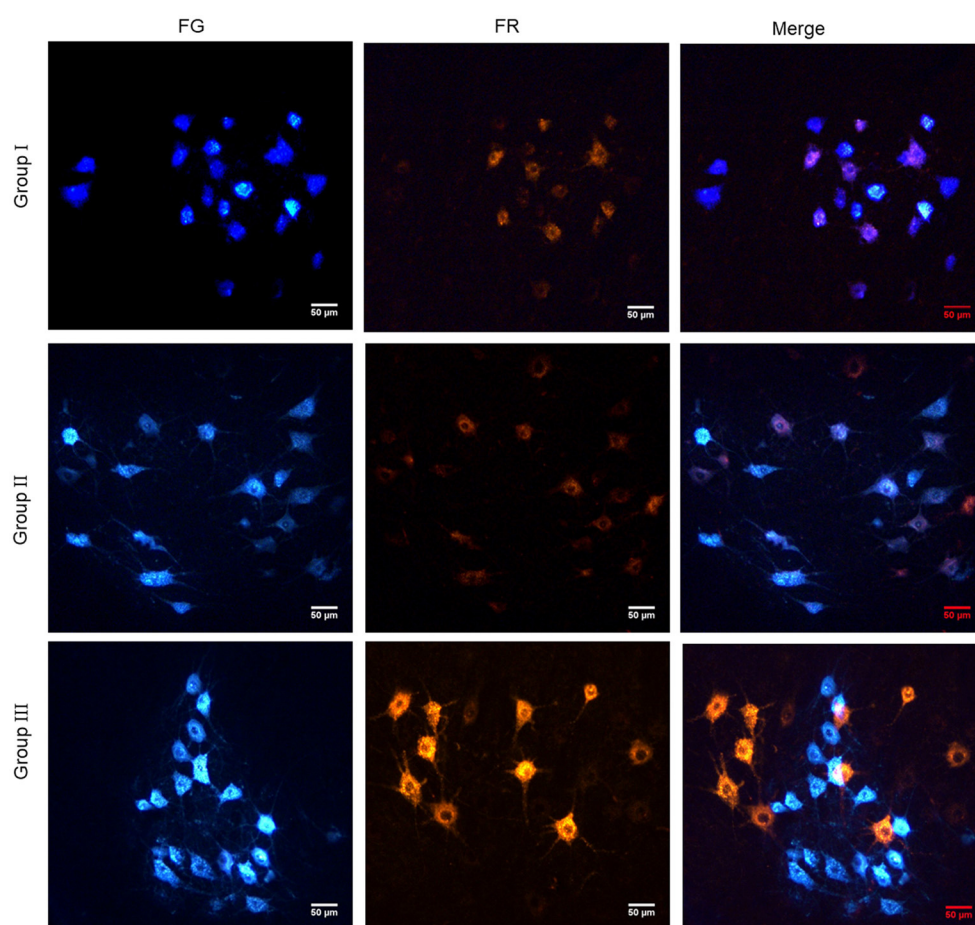


FIGURE 8

Retrograde tracing of neurons showed the reinnervation connection between neurons and effectors. In Group I, only the distal end of the common peroneal nerve was fostered; in Group II, both proximal and distal ends of the common peroneal nerve were fostered; Group III was sham operated normal group.

molecular mechanism for injured distal nerve and effector repair by coapting the injured proximal and distal nerves simultaneously to the peripheral nerves is analyzed based on only previous study findings. The specific mechanism needs to be verified through molecular biology experiments.

Conclusion

An effective method to repair injured peripheral nerves with a large segmental defect is to anastomose both the injured proximal and distal ends to the normal peripheral nerve. To repair the injured proximal peripheral nerve is also an important factor to recover the function of injured nerve. The injured nerves can be innervated by establishing a connection with the distal effector through the fostered nerve.

Data availability statement

The original contributions presented in the study are included in the article/supplementary material, further inquiries can be directed to the corresponding authors.

Ethics statement

The animal study was reviewed and approved by Medical Ethics Committee of Peking University People's Hospital.

Author contributions

DL, QY, FY, and JP designed the experiments. DL, QY, FY, XL, JJ, GL, KB, and SJ carried out the experiments. FY and JP supervised the whole experimental process and revised the manuscript. XL, JJ, GL, KB, and SJ analyzed the data. DL and QY wrote the manuscript. All authors contributed to the article and approved the submitted version.

Funding

This research was continuously funded by the National Natural Science Foundation of China (Nos. 82102568, 82102076, 82172432, and 82001319), National and Local Joint Engineering Research Center of Orthopaedic Biomaterials (No. XMHT20190204007), Shenzhen High-level Hospital Construction Fund, Shenzhen Key

Medical Discipline Construction Fund (No. SZXK023), Shenzhen San-Ming Project of Medicine (No. SZSM201612092), Research and Development Projects of Shenzhen (Nos. Z2021N054 and JCYJ20210324110214040), Guangdong Basic and Applied Basic Research Foundation (No. 2021A1515012586), Bethune Charitable Foundation and CSPC Osteoporosis Research Foundation Project (No. G-X-2020-1107-21), and the Scientific Research Foundation of Peking University Shenzhen Hospital (No. KYQD2021099).

Conflict of interest

The authors declare that the research was conducted in the absence of any commercial or financial relationships

that could be construed as a potential conflict of interest.

Publisher's note

All claims expressed in this article are solely those of the authors and do not necessarily represent those of their affiliated organizations, or those of the publisher, the editors and the reviewers. Any product that may be evaluated in this article, or claim that may be made by its manufacturer, is not guaranteed or endorsed by the publisher.

References

- Heinzel JC, Dadun LF, Prahm C, Winter N, Bressler M, Lauer H, et al. Beyond the knife-reviewing the interplay of psychosocial factors and peripheral nerve lesions. *J Pers Med*. (2021) 11:1200. doi: 10.3390/jpm11111200
- Qu S, Ma N, Wang W, Chen S, Wu Q, Li Y, et al. Human adipose-derived stem cells delay muscular atrophy after peripheral nerve injury in rats. *Cell Biochem Biophys*. (2022) 80:555–62. doi: 10.1007/s12013-022-01082-4
- Cintron-Colon AF, Almeida-Alves G, VanGyseghe JM, Spitsbergen JM. GDNF to the rescue: GDNF delivery effects on motor neurons and nerves, and muscle re-innervation after peripheral nerve injuries. *Neural Regen Res*. (2022) 17:748–53. doi: 10.4103/1673-5374.322446
- Nuelle JAV, Bozynski C, Stoker A. Innovations in peripheral nerve injury: current concepts and emerging techniques to improve recovery. *Mo Med*. (2022) 119:129–35.
- Adidharma W, Khouri AN, Lee JC, Vanderboll K, Kung TA, Cederna PS, et al. Sensory nerve regeneration and reinnervation in muscle following peripheral nerve injury. *Muscle Nerve*. (2022) 66:384–96. doi: 10.1002/mus.27661
- Mao R, Wei Z, Li W, Zhu X, Du D, Xu W. Analysis of influencing factors of repair effect after peripheral nerve injury. *Comput Math Methods Med*. (2021) 2021:8294267. doi: 10.1155/2021/8294267
- Lopes B, Sousa P, Alvites R, Branquinho M, Sousa AC, Mendonca C, et al. Peripheral nerve injury treatments and advances: one health perspective. *Int J Mol Sci*. (2022) 23:918. doi: 10.3390/ijms23020918
- Viterbo F, Magnani LV, Nunes HC. Zygomatic muscle neurotization with nerve grafts and end-to-side neurorrhaphies: a new technique for facial palsy. *Plast Reconstr Surg Glob Open*. (2022) 10:e4288. doi: 10.1097/GOX.00000000000004288
- Braga Silva J, Busnello CV, Becker AS, Moriguchi CA, de Melo RO, Waichel VB. End-to-side neurorrhaphy in peripheral nerves: Does it work? *Hand Surg Rehabil*. (2022) 41:2–6. doi: 10.1016/j.hansur.2021.08.010
- Fagotti de Almeida CE, Farina Junior JA, Colli BO. Morphometric and functional analysis of axonal regeneration after end-to-end and end-to-side neurorrhaphy in rats. *Plast Reconstr Surg Glob Open*. (2015) 3:e326. doi: 10.1097/GOX.0000000000000280
- Hosseini MA, Gharibi Loron A, Nemati B, Khandaghy M. Comparison of a distal end-to-side neurorrhaphy with a proximal-distal end-to-side neurorrhaphy: in a rat model. *Eur J Orthop Surg Traumatol*. (2015) 25:1261–4. doi: 10.1007/s00590-015-1699-x
- Yu Y, Zhang P, Han N, Kou Y, Yin X, Jiang B. Collateral development and spinal motor reorganization after nerve injury and repair. *Am J Transl Res*. (2016) 8:2897–911.
- Frostadottir D, Ekman L, Zimmerman M, Dahlin LB. Cold sensitivity and its association to functional disability following a major nerve trunk injury in the upper extremity-A national registry-based study. *PLoS ONE*. (2022) 17:e0270059. doi: 10.1371/journal.pone.0270059
- Yao X, Yan Z, Li X, Li Y, Ouyang Y, Fan C. Tacrolimus-induced neurotrophic differentiation of adipose-derived stem cells as novel therapeutic method for peripheral nerve injury. *Front Cell Neurosci*. (2021) 15:799151. doi: 10.3389/fncel.2021.799151
- Sarcon AK, Li NY, Houdek MT, Moran SL. Restoration of hamstring function following sciatic nerve resection at the greater sciatic foramen with reconstruction involving acellular nerve allograft and vascularized sural nerve autograft: a case report. *Microsurgery*. (2022) 42:824–8. doi: 10.1002/micr.30970
- Matsumoto T, Banda CH, Kondo E, Yoshida K, Hirata T, Ikeda T, et al. Laparoscopic repair of segmental obturator nerve injury defect using an artificial nerve conduit: a case report. *J Obstet Gynaecol Res*. (2021) 47:4118–21. doi: 10.1111/jog.14920
- de Barros RSM, Brito MVH, de Brito MH, de Aguiar Ledo Coutinho JV, Teixeira RKC, Yamaki VN, et al. Morphofunctional evaluation of end-to-side neurorrhaphy through video system magnification. *J Surg Res*. (2018) 221:64–8. doi: 10.1016/j.jss.2017.08.003
- Chen Y, Yuan W, Zeng X, Ma Y, Zheng Q, Lin B, et al. Combining reverse end-to-side neurorrhaphy with rapamycin treatment on chronically denervated muscle in rats. *J Integr Neurosci*. (2021) 20:359–66. doi: 10.31083/j.jin2002035
- Jung JM, Chung MS, Kim MB, Baek GH. Contribution of the proximal nerve stump in end-to-side nerve repair: in a rat model. *Clin Orthop Surg*. (2009) 1:90–5. doi: 10.4055/cios.2009.1.2.90
- Nepomuceno AC, de Faria JC, Politani EL, Silva EG, Salomone R, Longo MV, et al. Convergent end-to-end neurorrhaphy: an alternative technique for dual innervation of the gastrocnemius muscle in rats. *Microsurgery*. (2019) 39:535–42. doi: 10.1002/micr.30433
- Zhang S, Zhou Y, Xian H, Shi Y, Liu Y, Li Z, et al. Nerve regeneration in rat peripheral nerve allografts: an assessment of the role of endogenous neurotrophic factors in nerve cryopreservation and regeneration. *Eur J Neurosci*. (2022) 55:1895–916. doi: 10.1111/ejn.15655
- Ahmed MN, Shi D, Dailey MT, Rothermund K, Drewry MD, Calabrese TC, et al. Dental pulp cell sheets enhance facial nerve regeneration via local neurotrophic factor delivery. *Tissue Eng Part A*. (2021) 27:1128–39. doi: 10.1089/ten.tea.2020.0265
- Fang X, Zhang C, Yu Z, Li W, Huang Z, Zhang W, et al. Pretreatment overcomes Schwann cell phenotype mismatch to promote motor axon regeneration via sensory graft. *Exp Neurol*. (2019) 318:258–66. doi: 10.1016/j.expneurol.2019.05.011
- Yao Y, Wen Y, Li Y, Zhu J, Tian T, Zhang Q, et al. Tetrahedral framework nucleic acids facilitate neurorestoration of facial nerves by activating the NGF/PI3K/AKT pathway. *Nanoscale*. (2021) 13:15598–610. doi: 10.1039/D1NR04619E
- Wang W, Gu MF, Wang ZF, Shen XM, Zhang J, Yang L. Let-7a-5p regulated by lncRNA-MEG3 promotes functional differentiation to Schwann cells from adipose derived stem cells via directly inhibiting RBPJ-mediated Notch pathway. *Apoptosis*. (2021) 26:548–60. doi: 10.1007/s10495-021-01685-x
- Dai WL, Yan B, Bao YN, Fan JF, Liu JH. Suppression of peripheral NGF attenuates neuropathic pain induced by chronic constriction injury through the TAK1-MAPK/NF-kappaB signaling pathways. *Cell Commun Signal*. (2020) 18:66. doi: 10.1186/s12964-020-00556-3
- Li R, Li D, Wu C, Ye L, Wu Y, Yuan Y, et al. Nerve growth factor activates autophagy in Schwann cells to enhance myelin debris clearance and to expedite nerve regeneration. *Theranostics*. (2020) 10:1649–77. doi: 10.7150/thno.40919
- Chen CC, Chang LC, Yao CH, Hsu YM, Lin JH, Yang TY, et al. Increased calcitonin gene-related peptide and macrophages are involved in astragalus membranaceus-mediated peripheral nerve regeneration in rats. *Am J Chin Med*. (2018) 46:69–86. doi: 10.1142/S0192415X18500040
- Bontioti E, Kanje M, Dahlin LB. End-to-side nerve repair: attachment of a distal, compared with a proximal and distal, nerve segment. *Scand J Plast Reconstr Surg Hand Surg*. (2006) 40:129–35. doi: 10.1080/02844310600574056

30. Qi Z, Li D, Li L, Meng D, Deng J, Jin B, et al. Studies on the manner of collateral regeneration from nerve stem to motor endplate. *Front Physiol.* (2021) 12:795623. doi: 10.3389/fphys.2021.795623
31. Batty NJ, Torres-Espin A, Vavrek R, Raposo P, Fouad K. Single-session cortical electrical stimulation enhances the efficacy of rehabilitative motor training after spinal cord injury in rats. *Exp Neurol.* (2020) 324:113136. doi: 10.1016/j.expneurol.2019.113136
32. Adula KP, Shorey M, Chauhan V, Nassman K, Chen SF, Rolls MM, et al. The MAP3Ks DLK and LZK direct diverse responses to axon damage in zebrafish peripheral neurons. *J Neurosci.* (2022) 42:6195–210. doi: 10.1523/JNEUROSCI.1395-21.2022
33. Brushart TM. Motor axons preferentially reinnervate motor pathways. *J Neurosci.* (1993) 13:2730–8. doi: 10.1523/JNEUROSCI.13-06-02730.1993

Frontiers in Cellular Neuroscience

Leading research in cellular mechanisms
underlying brain function and development

Part of the world's most cited neuroscience
journal series that advances our understanding of
the cellular mechanisms underlying cell function
in the nervous system across all species.

Discover the latest Research Topics

[See more →](#)

Frontiers

Avenue du Tribunal-Fédéral 34
1005 Lausanne, Switzerland
frontiersin.org

Contact us

+41 (0)21 510 17 00
frontiersin.org/about/contact

